NOTICE

The quality of this microform is heavily dependent upon the quality of the original thesis submitted for microfilming. Every effort has been made to ensure the highest quality of reproduction possible.

If pages are missing, contact the university which granted the degree.

Some pages may have indistinct print especially if the original pages were typed with a poor typewriter ribbon or if the university sent us an inferior photocopy.

Reproduction in full or in part of this microform is governed by the Canadian Copyright Act, R.S.C. 1970, c. C-30, and subsequent amendments.

AVIS

La qualité de cette microforme dépend grandement de la qualité de la thèse soumise au microfilmage. Nous avons tout fait pour assurer une qualité supérieure de reproduction.

S'il manque des pages, veuillez communiquer avec l'université qui a conféré le grade.

La qualité d'impression de certaines pages peut laisser à désirer, surtout si les pages originales ont été dactylographiées à l'aide d'un ruban usé ou si l'université nous a fait parvenir une photocopie de qualité inférieure.

La reproduction, même partielle, de cette microforme est soumise à la Loi canadienne sur le droit d'auteur, SRC 1970, c. C-30, et ses amendements subséquents.

Deuterium NMR and High-Pressure FT-IR Studies of Membranes:

Anesthetic-Lipid Interactions

and

Molecular Dynamics in Lipid Bilayers

by
Michèle Auger

Thesis submitted to the School of Graduate Studies, University of Ottawa,
in partial fulfillment of the requirements of the
Degree of Doctor of Philosophy

ISBN 0-315-60085-3

UNIVERSITÉ D'OTTAWA
UNIVERSITY OF OTTAWA

Tard, très tard, j'ai découvert la véritable nature de la science, de sa démarche, des hommes qui la produisent. J'ai compris que, contrairement à ce que j'avais pu croire, le cheminement de la science ne consiste pas en une suite de conquêtes inéluctables; qu'elle ne parcourt pas la voie royale de la raison humaine; qu'elle n'est pas le résultat nécessaire, le produit inévitable d'observations sans appel imposées par l'expérimentation et le raisonnement. J'ai découvert là un monde de jeu et d'imagination.

François Jacob, La statue intérieure

ABSTRACT

The interactions of the local anesthetic tetracaine with multilamellar dispersions of dimyristoylphosphatidylcholine (DMPC) containing cholesterol have been investigated by deuterium nuclear magnetic resonance (^{2}H NMR). ^{2}H NMR spectra of tetracaine indicate that the location of the anesthetic in the cholesterol-containing DMPC bilayers differs from that in pure phosphatidylcholine bilayers, the anesthetic being located closer to the lipid-water interface in the former system. Moreover, the incorporation of the anesthetic into DMPC bilayers with or without cholesterol results in a reduction of the lipid order parameters both in the plateau and in the tail regions of the acyl chains, but does not significantly affect the cholesterol ordering. The interactions of tetracaine with the glycolipid 1,2-di-*O*-tetradecyl-3-*O*-(β-D-glucopyranosyl)-*sn*-glycerol (β-DTGL) and with β-DTGL (20 mole%) in DMPC have also been investigated by ^{2}H NMR. The stability of the lamellar structure of the pure glycolipid system is very sensitive to the presence of anesthetic while the interaction of tetracaine with the mixed glycolipid-phospholipid system does not trigger the formation of non-lamellar phases but leads to a slight reduction in molecular ordering.

The location of tetracaine in different lipid bilayers and in nerves has been studied by high-pressure Fourier transform infrared (FT-IR) spectroscopy. The results reveal a correlation between the location of the anesthetic in model membranes and that in nerves. They also indicate that tetracaine is expelled by pressure from both model and nerve membranes, and that for model membrane systems, low pH or cholesterol will assist pressure in squeezing the anesthetic out of the bilayer. On the other hand, high-pressure

FT-IR has also been used to study the effects of tetracaine on the structural and dynamic properties of lipids in model membrane systems.

A combination of ^2H spin-lattice relaxation and lineshape analysis has been used to demonstrate that a simple model involving two motions is sufficient to describe the spectral and relaxation features of the glycerol-labelled glycolipid β-DTGL. The lineshape and relaxation features of this lipid in the gel phase are best simulated using a three-site jump model with relative site populations of 0.46, 0.34 and 0.20, and a correlation time of 6.7×10^{-10} s . A second motion, namely rotation about the long axis of the molecule as a whole, is needed to account for the observed variation in the quadrupolar echo amplitude and the spectral lineshape over the temperature range of 25 to 60°C. Similar results have been obtained for several phospholipid and glycolipid bilayers, which suggest that the glycerol backbone dynamics in all these systems can be described in terms of common fast internal motions and a slower whole molecule axial motion.

Two-dimensional solid-state deuteron NMR spectroscopy has been used to confirm the presence of a slow whole molecule motion in the gel phase of the glycolipid β-DTGL at 35°C, with an associated correlation time of the order of milliseconds. Comparison of the experimental and simulated two-dimensional ridge patterns suggest that a large angle jump about the long molecular axis can best account for the 2D exchange spectra of β-DTGL in the gel phase in comparison to small step Brownian diffusion. On the other hand, it is demonstrated that lateral diffusion over curved membrane surface of dipalmitoylphosphatidylcholine bilayers in the liquid-crystalline phase can be detected by 2D deuteron NMR, with an associated correlation time of the order of $\approx$ 100 ms.

RÉSUMÉ

L'interaction d'un anesthésique local, la tétracaïne, avec des dispersions multilamellaires de dimyristoylphosphatidylcholine (DMPC) contenant du cholestérol a été étudiée par résonance magnétique nucléaire du deutérium (RMN ^{2}H). Les spectres RMN ^{2}H de la tétracaïne indiquent que la position de l'anesthésique dans ce système est différente de celle dans les bicouches de lipide pur, l'anesthésique étant situé plus près de l'interface lipide-eau en présence de cholestérol. De plus, l'incorporation de l'anesthésique dans des bicouches de DMPC en absence et en présence de cholestérol amène une réduction des paramètres d'ordre du lipide sur toute la longueur des chaînes d'acides gras mais n'affecte pas de façon significative l'ordre du cholestérol. L'interaction de la tétracaïne avec le glycolipide 1,2-di-*O*-tetradecyl-3-*O*-(β-D-glucopyranosyl)-*sn*-glycerol (β-DTGL) et avec des bicouches mixtes de DMPC et de β-DTGL (en proportions molaires 8:2, respectivement) a aussi été étudiée par RMN ^{2}H. La stabilité de la structure lamellaire du glycolipide pur est très sensible à la présence de l'anesthésique tandis que l'interaction de la tétracaïne avec le système mixte n'entraîne pas la formation de phases non-lamellaires mais conduit à une faible réduction de l'ordre moléculaire.

La position de la tétracaïne dans différentes bicouches lipidiques et dans des nerfs a été étudiée par spectroscopie infra-rouge à haute pression. Les résultats indiquent que la tétracaïne est expulsée à la fois des membranes modèles et des nerfs suite à l'application d'une pression hydrostatique et suggèrent une position similaire de l'anesthésique dans ces différents systèmes. D'autre part, la spectroscopie infra-rouge à haute pression a aussi été utilisée pour étudier l'effet de la tétracaïne sur les propriétés structurales et dynamiques

des lipides dans des membranes modèles.

La dynamique du glycolipide β-DTGL marqué à la position C3 du glycérol a été étudiée par RMN ^2H. Il est démontré qu'un simple mouvement de saut entre trois sites avec des populations relatives de 0.46, 0.34 and 0.20 et un temps de corrélation de 6.7×10^{-10} s peut adéquatement rendre compte des temps de relaxation T_{1Z} et des formes de spectres observés pour le glycolipide dans la phase gel. Un second mouvement de rotation axiale est nécessaire pour expliquer la variation de l'amplitude de l'écho quadrupolaire et de la forme des spectres en passant de la phase gel à la phase cristal-liquide, en variant la température de 25 à 60°C. Des résultats similaires ont été obtenus pour différentes bicouches de phospholipides et de glycolipides, suggérant que la dynamique du glycérol dans ces différents systèmes peut être décrite en termes d'un mouvement interne rapide et d'un mouvement plus lent de rotation axiale.

La spectroscopie RMN ^2H à deux dimensions a été utilisée pour confirmer la présence d'un mouvement moléculaire lent dans la phase gel du glycolipide β-DTGL à 35°C, avec un temps de corrélation de l'ordre de la milliseconde. La comparaison entre les spectres expérimentaux et simulés suggère que ce mouvement est mieux décrit par un saut entre trois sites plutôt que par un mouvement de diffusion autour de l'axe long de la molécule. D'autre part, il est démontré que la diffusion latérale des lipides dans des bicouches de dipalmitoylphosphatidylcholine (DPPC) dans la phase cristal-liquide peut être détectée par RMN ^2H à deux dimensions, et que le temps de corrélation de ce mouvement est d'environ 100 ms.

ACKNOWLEDGEMENTS

Doing a Ph.D. in Ottawa presents numerous advantages, and for me, one of them has been to improve my knowledge of the English language. I therefore had the pleasure, during the past four years, to meet and work with many exceptional persons, both francophone and anglophone. Therefore, in order that everyone is acknowledged in the language of his choice, this acknowledgment section will be available in both official languages.

I would first like to express my gratitude and friendship to my supervisor, Dr. Ian Smith. Ian has been much more than a scientific director for me, and his enthusiasm and constant desire to learn have been a great source of inspiration. Thank you Ian.

I would also like to thank my co-supervisor, Dr. Harold Jarrell, who has been closely involved in every aspect of this Ph.D. degree. Through long and numerous discussions, he shared with me his knowledge and vision of science, and his interest and patience have shown no limit. His help has been very precious. Thank you Harold.

I had the pleasure, during my Ph.D., to work in collaboration with the Molecular Spectroscopy group of the Chemistry Division at NRC. I would first like to thank the director, Dr. Henry Mantsch, who has always been very enthusiastic about our common projects. I would also like to thank Dr. Patrick Wong, the high-pressure infrared spectroscopy expert, for his judicious advice and support, as well as Dr. David Siminovitch, who has closely contributed to many aspects of these projects.

Beside collaborating in the infrared spectroscopy projects, David Siminovitch, with his great knowledge of NMR spectroscopy, has been very helpful in my learning and understanding of this technique. Thank you David.

I would also like to thank all the graduate students, John Baenziger, Sylvain Lareau, Myrna Monck, Eva Princz, Laura Stewart, Marie-Rose Van Calsteren and Beatrice Winsborrow, and post-doctoral fellows, Drs. Jean-Marc Bonmatin, Danielle Carrier and David Fenske, for sharing with me the past four years at NRC. Thank you for personal contributions.

I would like to thank especially Dr. Pierre Tancrède from the Université du Québec à Trois-Rivières, who first initiated me into biophysics and who judiciously guided me in the choice of a Ph.D project. For your friendship and for everything else, thank you Pierre.

I would also like to thank my family, as well as all my friends, and especially Jean Larose, for their support and encouragement during this Ph.D. degree. Thanks to everyone.

Finally, I would like to acknowledge the Natural Sciences and Engineering Research Council (NSERC) and the University of Ottawa for their financial.

REMERCIEMENTS

Poursuivre des études de doctorat à Ottawa comporte de nombreux avantages, et pour moi, un d'eux fut de pouvoir améliorer ma connaissance de la langue de Shakespeare. J'ai donc eu la chance, durant les quatre dernières années, de rencontrer et de travailler avec plusieurs personnes formidables, autant de langue française qu'anglaise. Ainsi, afin que chacun et chacune puisse être remerciés dans la langue de son choix, cette section remerciement sera disponible dans les deux langues offielles. A vous de choisir...

Je tiens d'abord à exprimer ma plus profonde gratitude et amitié à mon superviseur, le Dr Ian Smith. Ian fut pour moi beaucoup plus qu'un directeur scientifique et il a su avant tout me communiquer son enthousiasme et son désir d'apprendre, et ce, toujours dans la langue de Molière. Merci pour tout Ian.

Je voudrais aussi remercier sincèrement mon co-superviseur, le Dr Harold Jarrell, qui a collaboré étroitement à toutes les étapes de ce doctorat. A travers de nombreuses et longues discussions, il m'a fait partager ses connaissances et sa vision des sciences, et a toujours fait preuve d'une patience infinie. Son aide fut des plus précieuses. Merci Harold.

J'ai aussi eu le plaisir, durant mon doctorat, de travailler en collaboration avec le groupe de Spectroscopie Moléculaire de la Division de Chimie du CNRC. J'aimerais d'abord en remercier le directeur, le Dr Henry Mantsch, qui a toujours démontré un grand enthousiasme à nos projets communs. Je voudrais aussi remercier le Dr Patrick Wong,

l'expert en spectroscopie infra-rouge à haute pression, pour ses judicieux conseils et son encouragement, ainsi que le Dr David Siminovitch, qui a collaboré étroitement à différentes phases de ces projets. Merci à tous.

En plus d'avoir collaboré aux projets en spectroscopie infra-rouge, David Siminovitch, par sa grande connaissance de la spectroscopie RMN, a aussi été une aide précieuse dans mon apprentissage de cette technique. Merci David.

J'aimerais aussi remercier tous les étudiants gradués, John Baenziger, Sylvain Lareau, Myrna Monck, Eva Princz, Laura Stewart, Marie-Rose Van Calsteren et Beatrice Winsborrow, et les post-docs, Jean-Marc Bonmatin, Danielle Carrier et David Fenske, qui ont partagé avec moi ces quatre dernières années au CNRC. Merci à tous pour vos contributions respectives.

Je tiens aussi à accorder un merci tout spécial au Dr Pierre Tancrède de l'Université du Québec à Trois-Rivières, qui m'a donné le goût à la biophysique et qui m'a si judieusement guidée dans le choix de mon doctorat. Pour ton amitié et pour tout le reste, merci Pierre.

J'aimerais aussi remercier ma famille, ainsi que tous mes amis, et tout particulièrement Jean Larose, pour leur support et encouragement durant ces études de doctorat. Merci à tous.

Finalement, je voudrais remercier le Conseil de Recherches en Sciences Naturelles et en Génie (CRSNG) et l'Université d'Ottawa pour leur support financier.

TABLE OF CONTENTS

Part one: Generalities

Chapter 1. Introduction

Chapter 2. Theory of deuterium NMR

Chapter 3. Experimental methods

Part two: ^{2}H NMR studies of anesthetic-lipid interactions

Chapter 4. Interactions of tetracaine with phosphatidylcholine and cholesterol bilayers

Chapter 5. Interactions of tetracaine with glycoglycerolipid bilayers

Part three: High-pressure FT-IR studies of anesthetic-lipid interactions

Part four: Lipid dynamics as viewed by ^{2}H NMR

Part five: General conclusion

LIST OF FIGURES

LIST OF TABLES

ABBREVIATIONS

α-DTML	1,2-di-*O*-tetradecyl-3-*O*-(α-D-mannopyranosyl)-*sn*-glycerol
β-DTGL	1,2-di-*O*-tetradecyl-3-*O*-(β-D-glucopyranosyl)-*sn*-glycerol
BPC	borate phosphate citrate buffer
CSA	chemical shift anisotropy
DHAEPn	1,2-di-*O*-hexadecyl-*sn*-glycero-3-(2-aminoethyl)phosphonate
DHPC	1,2-di-*O*-hexadecyl-*sn*-glycero-3-phosphocholine
DMPC	1,2-dimyristoyl-*sn*-glycero-3-phosphocholine
DMPS	1,2-dimyristoyl-*sn*-glycero-3-phosphoserine
DMS	dimethyl sulfone
DOPC	1,2-dioleoyl-*sn*-glycero-3-phosphocholine
DOPE	1,2-dioleoyl-*sn*-glycero-3-phosphoethanolamine
DOPS	1,2-dioleoyl-*sn*-glycero-3-phosphoserine
DPPC	1,2-dipalmitoyl-*sn*-glycero-3-phosphocholine
EFG	electric field gradient
ESR	electron spin resonance
FT-IR	Fourier-transform infrared
K_p	Partition coefficient
NMR	nuclear magnetic resonance
NPGS	N-palmitoylgalactosyl sphingosine
PC	*sn*-3-phosphatidylcholine
PE	*sn*-3-phosphatidylethanolamine
PS	*sn*-3-phosphatidylserine

rf	radio-frequency
S_{CD}	carbon deuterium bond order parameter
S_{mol}	molecular (or segmental) order parameter
T_c	gel to liquid-crystalline phase transition temperature
T_1	spin-lattice (or longitudinal) relaxation time
T_2	spin-spin (or transverse) relaxation time
TLC	thin layer chromatography
TTC	tetracaine

PART ONE: GENERALITIES

CHAPTER 1

Introduction

1.1 The biological membrane

All living creatures are made of cells. One cellular component, the membrane, plays a crucial role in almost all cellular activity. The primary function of all cell membranes is to act as a barrier between the intra and extracellular environments and as a site for diverse biochemical activities. The cell itself is encapsulated by its own membrane, the plasma membrane. The plasma membrane is the best understood membrane and most of the following discussion will be devoted to it.

Among several possible stable arrangements of protein and lipid molecules in plasma membranes, the bilayer model has dominated for over 50 years. This arrangement was originally proposed by E. Gorter and F. Grendel in 1925 (Gorter & Grendel, 1925). An important feature of this model was that the hydrophilic groups of the lipids were oriented at the surface of the bilayer and hydrophobic groups at its interior. Subsequent models also based on the lipid bilayer have taken the proteins into consideration, such as the early model proposed by Danielli and Davson (1935). In 1972, S. Jonathan Singer and Garth Nicolson postulated a unified theory of membrane structure called the *fluid-mosaic model* (Figure 1.1) (Singer & Nicolson, 1972). They proposed that the matrix, or continuous part of membrane structure, is a fluid lipid bilayer and that globular

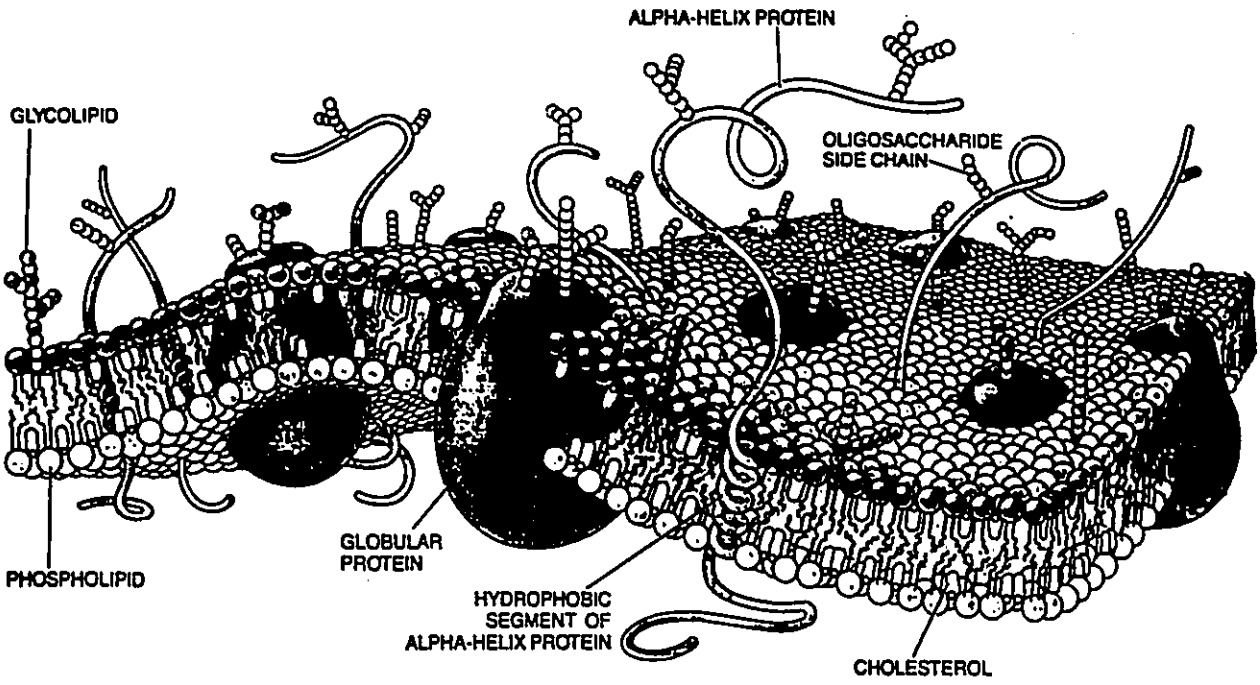

Figure 1.1 The fluid mosaic model of cell membranes (from Bretscher, 1985).

amphiphilic proteins are embedded in one or the other monolayer, with some proteins spanning the thickness of the bilayer. Both proteins and lipids are mobile and thus, as a first approximation, the membrane is viewed as a two-dimensional solution of proteins in lipids.

With few exceptions, all membranes contain proteins and various amounts of lipids, and often small amounts of carbohydrates, covalently bound to proteins and lipids. The major class of lipid in plasma membranes is phospholipid. They consist of a glycerol backbone with fatty acid esters at the first two positions and a phosphate at the third. Different groups can be esterified to the phosphate, thus defining the different classes of phospholipids. Figure 1.2 shows the general structure of the phospholipids and the more common head groups. The fatty acids can have varying chain lengths and degrees of unsaturation. However, in natural lipids, it is most common for the unsaturated lipids to occupy the 2 position of the glycerol backbone. The presence of the non-polar acyl chain region and the polar head group gives the phospholipid its amphipathic character, which allows the lipid to form the bilayer arrangement in membranes. In addition to phospholipids, two other kinds of lipids are found in the membranes of animal cell: glycolipids and cholesterol. The glycolipid molecule has a hydrophobic tail similar to that of sphingomyelin while the hydrophilic end is composed of a variety of simple sugars joined to form a linear or branching structure called an oligosaccharide. Glycolipids usually make up only a small fraction of the lipids in the membrane but have been shown to assume many biological roles, one of which is their capacity to function as recognition sites. On the other hand, cholesterol is also an important component of plasma membranes and has been shown to play a role in the control of membrane fluidity.

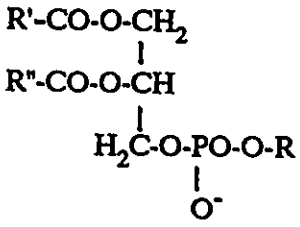

In natural lipids, R' and R" are saturated and unsaturated chains, respectively

R group	Name of phospholipid	Abbreviation
$-H$	Phosphatidic acid	PA
$-CH_2CH(NH_2)-COOH$	Phosphatidylserine	PS
$-CH_2CH_2NH_2$	Phosphatidylethanolamine	PE
$-CH_2CH_2N(CH_3)_3$	Phosphatidylcholine	PC

Figure 1.2 Structure of the major phospholipids in plasma membranes.

1.2 Model membranes

In many studies of membrane structure and function, it is desirable to simplify the system by making model membranes of one or a few lipids. Dispersions of lipids in water can take several forms depending on geometrical and thermodynamic considerations. The most common form is the multilamellar dispersion, in which the lipids are arranged in concentric layers. Fully hydrated bilayers of lipids usually undergo a well-defined thermotropic phase transition in which the lipid chains change from an ordered or gel state to a fluid or liquid-crystalline state. For the well characterized phosphatidylcholine bilayers, the liquid-crystalline phase is conventionally designated L_α and the gel phase is designated $L_{\beta'}$. In addition, an intermediate phase, $P_{\beta'}$, in which the bilayer is rippled, is found in the gel phase of certain phospholipids. The phase diagram of hydrated dimyristoylphosphatidylcholine bilayers, together with the representations of the $L_{\beta'}$, $P_{\beta'}$, and L_α phases, are shown in Figure 1.3.

1.3 The molecular mechanism of local anesthesia

1.3.1 Introduction

Local anesthetics are chemicals that reversibly block action potentials in excitable membranes. The generation and propagation of action potentials depend on the opening and closing of ionic sodium channels that span excitable nerve and muscle membranes (Hodgkin & Huxley, 1952; Hille, 1970). Two general theories have been proposed to explain the action of local anesthetics on sodium channels; one considers the general

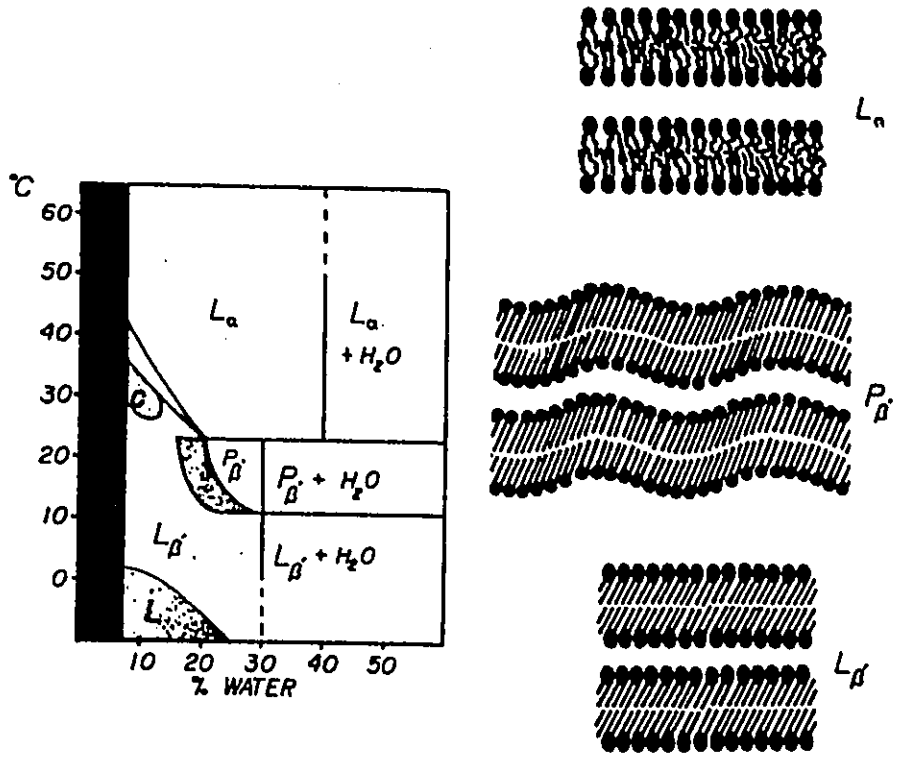

Figure 1.3 Phase diagram of hydrated dimyristoylphosphatidylcholine bilayers, together with representations of the $L_{\beta'}$, $P_{\beta'}$, and L_α phases (from Cevc & Marsh, 1987).

perturbation of the bulk membrane structure by anesthetics and its consequences for channel function (Seeman, 1972) and the other considers a direct binding of local anesthetic molecules to specific receptors on the sodium channel (Strichartz, 1973). During the past decade, much evidence has accumulated to support the latter specific receptor hypothesis (Hille, 1980), although general membrane perturbation may still provide part of the explanation for anesthetic actions. It is indeed doubtful that local anesthetic action can be accounted for solely in terms of an action at a single receptor site.

1.3.2 Previous ^{2}H NMR studies

Many techniques have been used to study the interactions of local anesthetics with model and biological membranes, including high-resolution nuclear magnetic resonance (Cerbon et al., 1972), electron spin resonance (Butler et al., 1973; Neal et al., 1976; Giotta et al., 1974) and neutron diffraction (Coster et al., 1981). All these studies suggested that the anesthetic intercalates partially into the lipid bilayer. On the other hand, information about the effects of the local anesthetic tetracaine (Figure 1.4A) on the order and dynamics of the lipid acyl chains has been obtained by ^{2}H NMR spectroscopy. The results of these studies suggested that tetracaine interacts differently with different phospholipids such as phosphatidylcholine (PC), phosphatidylethanolamine (PE), and phosphatidylserine (PS), depending mostly on the charge and the shape of the lipid studied (Smith & Butler, 1985). Moreover, it has been shown that the charged and uncharged forms of the anesthetic have different partition coefficients in the lipid bilayer. In PC and PE bilayers, the uncharged form is more lipid-soluble due to hydrophobic interactions between the anesthetic and the lipid molecule (Kelusky & Smith, 1984). For PS, which is negatively

A

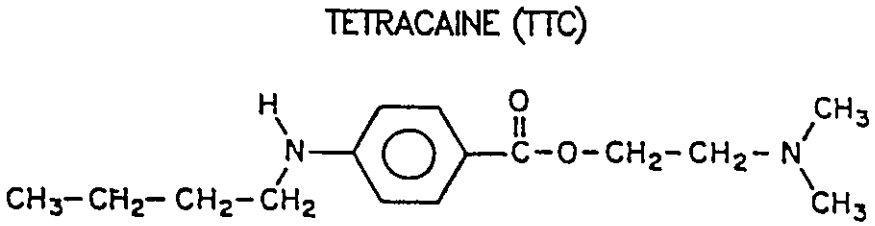

B

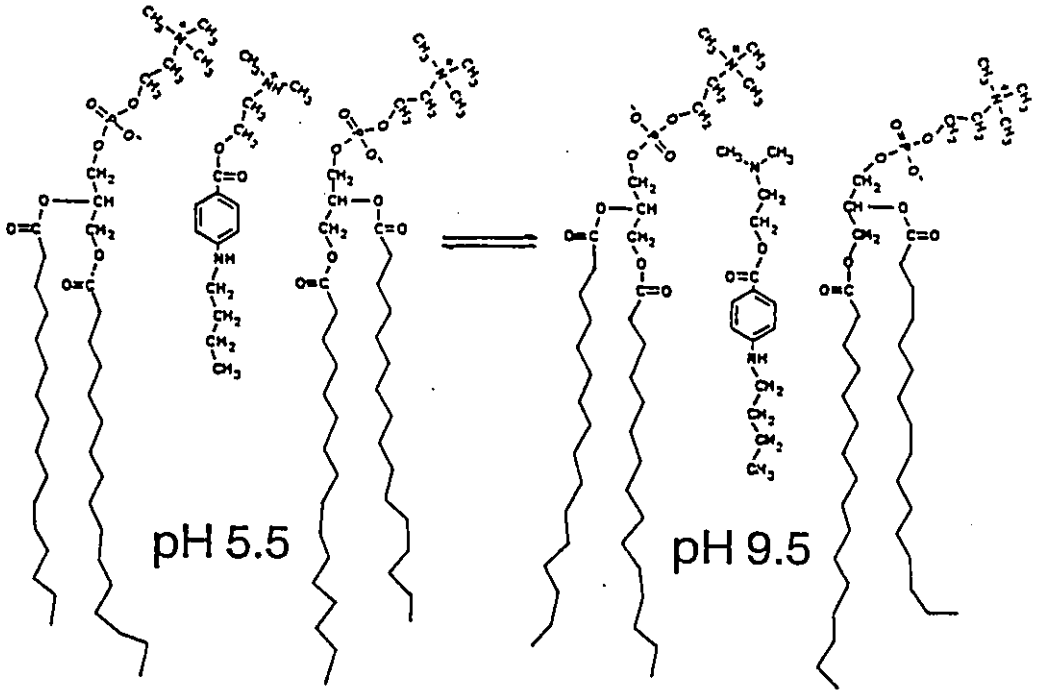

Figure 1.4 **A.** Structure of the local anesthetic tetracaine. **B.** Proposed location of tetracaine in phosphatidylcholine bilayers at low (5.5) and high (9.5) pH. The neutral tetracaine is located lower in bilayer than is the charged form (from Boulanger et al., 1981).

charged at the pH studied, the charged form of the anesthetic is more soluble in the lipid bilayer due to electrostatic interactions between the two opposite charges (Kelusky et al., 1986). From the ^2H NMR studies of both labelled anesthetic and phosphatidylcholine, the location of tetracaine in bilayers of phosphatidylcholine at low (5.5) and high (9.5) pH has been proposed (Figure 1.4B) (Boulanger et al., 1981). Note on this figure that neutral tetracaine is located lower in the bilayer than is the charged form. Moreover, these studies suggested two binding sites for tetracaine: one site is within the bilayer, is highly ordered, and is exchanging slowly ($< 1{,}000\ s^{-1}$) with anesthetic in the aqueous medium whereas the other site is probably on the surface of the bilayer, is weakly ordered, and is exchanging rapidly with aqueous anesthetic. On the other hand, the anesthetic has been shown to decrease the degree of order of the lipid acyl chains but to increase the degree of order in the head group region.

1.3.3 Aim of the research

Most plasma membranes, and especially most excitable plasma membranes, contain a relatively large amount of cholesterol. For example, the cholesterol concentration of the excitable membranes of nerve-ending particles (synaptosomes) is about 29% of the total lipids (Breckenridge et al., 1972). Moreover, it has been shown that cholesterol acts as a regulatory agent with respect to the amplitude of the C-^2H angular fluctuations of the lipid acyl chains: it orders the lipid above the gel to liquid-crystalline phase transition temperature and disorders it below (Dufourc et al., 1984b). Therefore, the interactions of the local anesthetic tetracaine with phosphatidylcholine membranes containing a physiological concentration (30 mole%) of cholesterol will first be investigated by ^2H NMR

from the anesthetic, the lipid and the cholesterol points of view.

An important clue in elucidating the molecular mechanism of anesthetic action and in discriminating between lipid and protein as the primary site of anesthetic action is the antagonistic effect of hydrostatic pressure against anesthesia in vivo (Lever et al., 1971; Wann & Macdonald, 1980). A particularly convenient way of monitoring changes in the structural and dynamic properties of lipid bilayers induced by pressure is Fourier transform infrared (FT-IR) spectroscopy (Wong, 1987a-c). This technique will first be used to investigate the pressure-induced expulsion of tetracaine from model and nerve membranes and to confirm the location, indirectly deduced from deuterium NMR results, of the anesthetic in different model systems. On the other hand, high-pressure FT-IR will be used to monitor the effects of tetracaine on the structural and dynamic properties of lipids in different model membranes.

1.4 Molecular dynamics in lipid bilayers

1.4.1 Introduction

Until the late 1960's, lipid bilayers were often perceived to be static structures. However, the application of spectroscopic techniques capable of monitoring molecular motion over a broad range of time scales has changed this naive conception of membrane structure and dynamics. Electron spin resonance (ESR), nuclear magnetic resonance (NMR) and fluorescence depolarization have been used extensively to examine molecular motions in lipid bilayers. In pioneering experiments in the late 1960's, Hubbell and

McConnell first showed that synthetic phospholipid vesicles undergo rapid anisotropic motions (Hubbell & McConnell, 1969).

Since that pioneering ESR work, considerable effort has been expended over the last twenty years on probing dynamic properties of lipid bilayers. The principle motive behind most of these studies has been to achieve a better understanding of the physical properties of biological membranes. However, although there have been numerous studies of molecular motion in lipid membranes (Seelig, 1977; Griffin, 1981; Brown, 1982; Marsh, 1981), frequently experimental results can not be interpreted unambiguously in terms of rates and modes of molecular motion. Recent studies have begun to unravel the complex dynamics of these systems (Bonmatin et al., 1988, 1989; Griffin et al., 1988; Meier et al., 1986; Siminovitch et al., 1985, 1988; Speyer et al., 1989). Interest in characterizing the types and rates of motions of the constituent molecules in bilayers has focussed not so much on their absolute nature and values, respectively, but more so on how they change as a function of membrane composition, temperature and other factors. With such information, a more complete understanding of the nature of membrane systems should be forthcoming.

1.4.2 ^{2}H NMR studies of lipid dynamics

Since membrane systems often exhibit complex motions, it is important to characterize molecular motion over a broad frequency range in order to achieve as complete a description of bilayer dynamics as possible. Establishing the time scales and amplitudes of molecular motions in the anisotropic environment of lipid bilayers is a

problem well suited to solid state ^2H NMR spectroscopy (Seelig, 1977; Griffin, 1981; Davis, 1983, 1986; Bloom & Smith, 1985; Smith, 1984), which provides observation windows in the range where the frequencies of most molecular motions occur ($1\text{-}10^{10}$ s^{-1}, for lipid bilayers) (Kimmich et al., 1983), as summarized in Table 1.1. Lineshape studies can elucidate motions on the $10^3\text{-}10^6$ s^{-1} time scale while spin-lattice relaxation data are a source of information about molecular dynamics on time scales near the Larmor frequency ($10^7\text{-}10^{10}$ s^{-1}). The observation of anisotropic relaxation is significant in that it puts severe constraints on the motional descriptions that may be considered to explain relaxation in these systems. Anisotropic spin-lattice relaxation has been used in biomolecular systems to extract details of molecular motion in proteins (Batchelder et al., 1983; Beshah et al., 1987), DNA (Vold et al., 1986) and lipids (Siminovitch et al., 1988; Jarrell et al., 1988; Bonmatin et al., 1988, 1989; Speyer et al., 1989). On the other hand, measurement of transverse relaxation times T_{2e}, which have been shown to be sensitive to slow motions (Jeffrey, 1981), has been used to obtain correlation times of slow motions. However, in general, such measurements do not provide information about the nature of the slow motions. An alternative method of gaining information about the rates and nature of slow molecular motions is the two-dimensional exchange technique, which has recently been applied to deuteron NMR, and shown to extend the frequency range over which motions may be probed to the ms or longer time scales (Schmidt et al., 1986, 1987, 1988; Wefing & Spiess, 1988; Wefing et al., 1988).

1.4.3 Aim of the research

Glycosphingolipids constitute a class of biomolecules which can assume many

Table 1.1

Investigation of molecular dynamics in lipid bilayers by ^2H NMR

Frequency of motion	Example of motion	^2H NMR measurement
10^7-10^{10} s^{-1}	Chain isomerization Internal conformational changes	Spin-lattice relaxation times, T_{1Z}, T_{1Q} Fast-limit lineshape analysis
10^4-10^6 s^{-1}	Whole molecule axial motion (liquid crystalline phase) Chain isomerization (gel phase)	Quadrupolar echo amplitude Quadrupolar echo lineshape analysis
10^0-10^3 s^{-1}	Whole molecule axial motion (gel phase), lateral diffusion over curved surface	Transverse relaxation times 2D exchange methods

biological roles, of which their capacity to function as recognition sites may be most important. In view of the important roles played by the glycolipid head group, it is clear that a knowledge of the dynamics of the carbohydrate moiety is of considerable importance for a complete understanding of cell surface recognition at the molecular level. Previous studies have focused on glycoglycerolipids as models of glycosphingolipids in order to elucidate the orientation, conformation and dynamics of the carbohydrate head groups at a bilayer surface and to probe the factors influencing these spatial and motional parameters (Jarrell et al., 1986; 1987a-b; Carrier et al., 1989; Renou et al., 1989). During the course of these studies, two observations were common to all systems studied: anisotropic ^2H spin-lattice relaxation (dependent on the orientation of the director with respect to the magnetic field direction) in the liquid-crystalline phase, and a dramatic reduction in the ^2H quadrupolar echo signal intensity at temperatures just below the gel to liquid-crystalline phase transition temperature.

In this thesis, the dynamics of the glycolipid 1,2-di-*O*-tetradecyl-3-*O*-(β-D-glucopyranosyl)-*sn*-glycerol (β-DTGL) will first be studied in the gel phase by ^2H spin-lattice relaxation and analysis of quadrupolar echo lineshapes. The principal objective of this study is to probe the lipid dynamics in the ordered gel state, where molecular motion is expected to be less complicated, in order to develop a basis for describing molecular motion in the more complex but biologically more relevant liquid-crystalline phase. The results will then be compared with those obtained for different glycolipid and phospholipid systems, in order to investigate if the simple motional model elucidated for the glycolipid β-DTGL can be extrapolated to other lipid systems. As mentioned earlier, a combination of lineshape and spin-lattice relaxation analysis can elucidate motions of intermediate (10^4-10^6 s^{-1}) and fast (10^7-10^{10} s^{-1}) rates but are not effective for slower motions. In the last

part of this thesis, 2D exchange deuteron NMR will be applied to the study of slow motions (with rates < 10^3 s^{-1}) in lipid bilayers. This technique will first be used to confirm the presence of a slow whole molecule axial motion in the gel phase of the glycolipid β-DTGL and to suggest its nature. On the other hand, slow lateral diffusion over the curved membrane surface of dipalmitoylphosphatidylcholine bilayers in the liquid-crystalline phase will be also investigated.

1.5 Outline of the thesis

The thesis will be divided in five major parts. The introduction will first present a general outline of deuterium NMR theory (chapter 2), followed by the materials and methods section (chapter 3). The second part of the thesis will discuss deuterium NMR studies of the interactions of the local anesthetic tetracaine with model lipid bilayers. The study of the interactions between the local anesthetic tetracaine and cholesterol-containing phosphatidylcholine bilayers will be presented in chapter 4, followed in chapter 5 by the study of the interactions between tetracaine and glycolipid bilayers. The third part of this thesis will be devoted to the study of anesthetic-membrane interactions by high-pressure Fourier transform infrared-spectroscopy. Two major aspects will be discussed, namely the pressure-induced expulsion of the local anesthetic tetracaine from model and nerve membranes (chapter 6) and the study of the effects of tetracaine on the structural and dynamic properties of lipids by high-pressure FT-IR (chapter 7). The study of molecular dynamics in lipid bilayers will be presented in the fourth part of this thesis. The elucidation of motional modes in the glycolipid β-DTGL by lineshape and spin-lattice relaxation analysis will first be discussed (chapter 8) and the results compared with those obtained

with other lipid systems (chapter 9). Finally, chapter 10 will present how two-dimensional exchange NMR can be used to study slow motions in lipid bilayers (chapter 10). In the last part (chapter 11), the main conclusions of the thesis research will be presented and some suggestions for future work given.

CHAPTER 2

Theory of deuterium NMR

2.1 Introduction

"Many atomic nuclei in their ground state have a non-zero spin angular momentum Ih (integer or half integer in units of ħ) and a dipolar magnetic moment μ colinear with it...It is these moments that give rise to nuclear magnetism."

It is very common in NMR discussions to hear "it's taken from Abragam". The first sentence of this NMR theory section was therefore taken, without any originality, from page 1 of Abragam, the so-called "NMR Bible" (Abragam, 1961). It describes, in a clear and simple way, the basis of nuclear magnetic resonance (NMR).

The spin angular momentum of a nuclei and the magnetic moment are linked by the following relationship:

$$\mu = \gamma \hbar \cdot I \qquad (2.1)$$

where γ is a scalar, the magnetogyric ratio, whose value is intrinsic to each nucleus. The magnetic moment of a nuclear spin within a sample may interact with magnetic fields. The magnetic coupling can be external (applied magnetic field), which allows the detection of

NMR signals, or they can be internal (local fields within the sample), giving information on the chemical environment around the nucleus and on molecular motions. For nuclei with spin $I > 1/2$ (quadrupolar nuclei, *vide infra)*, the nuclear spins may also interact with electric fields, this coupling being also internal.

The best way to describe the couplings of the nuclear spins with their surroundings is to use the concept of the nuclear spin Hamiltonian (Abragam, 1961). The general nuclear spin Hamiltonian will be discussed in section 2.3 of this chapter while the quadrupolar Hamiltonian will be discussed in more detail in section 2.4. Before doing so, some properties of the ^2H nucleus will be given in the following section.

2.2 The ^2H nucleus

The nuclear properties of ^2H are summarized in Table 2.1. A feature of nuclei with $I > 1/2$ is an non-spherically symmetric charge distribution in the nucleus, and therefore an electric quadrupole moment, Q. However, the deuterium quadrupole moment is relatively small (second smallest after ^6Li). The dominance of ^2H relaxation by the relatively simple quadrupolar mechanism facilitates the analysis of T_1 values. The magnetogyric ratio of ^2H is considerably smaller than that of ^1H or ^3H, leading to lower sensitivity. The low natural abundance of ^2H is an advantage, since labelling to 100% is relatively accessible, and the negligible background signals at natural abundance will not complicate the overall spectrum. This property makes deuterium an ideal probe for the study of membrane lipids.

Table 2.1

Properties of the ^{2}H nucleus

Spin	1
Quadrupole moment (m^2)	2.73×10^{-31}
Frequency, 4.7 T (MHz)	30.7
Sensitivity referred to ^{13}C [a]	0.6
Natural abundance (%)	0.015
Receptivity referred to ^{13}C [a]	8.21×10^{-3}

[a] Values for ^{13}C set equal to 1 (from Smith ,1983).

2.3 The nuclear spin Hamiltonian

The nuclear spin Hamiltonian for nuclei with spin I > 1/2, such as deuterium, can be described by:

$$H = H_0 + H_1 + H_D + H_{CSA} + H_J + H_Q \qquad (2.2)$$

where H_0 and H_1 represent the Hamiltonian describing the coupling of the magnetic dipole moment of the nucleus, μ, with the externally applied static magnetic field H_0 and the applied radio-frequency (rf) field $H_1(t)$, respectively. The interaction energy between the magnetic moment, μ, and the externally applied static field and the time-dependent rf field can be represented by one Hamiltonian, the Zeeman Hamiltonian H_Z:

$$\begin{aligned} H_Z &= -\mu\,(H_0 + H_1(t)) \\ H_Z &= -\gamma\hbar\, I\,(H_0 + H_1(t)) \end{aligned} \qquad (2.3)$$

H_D describes the internal dipolar couplings with other neighboring spins, H_{CSA} is the chemical shielding Hamiltonian and H_J is the scalar coupling Hamiltonian. The quadrupolar Hamiltonian H_Q describes the interaction between the quadrupole moment of the nuclei and the internal electric field gradient (EFG) at the nucleus. The quadrupolar Hamiltonian will be discussed in more detail in the following section (2.4).

In a large magnetic field, for example H_0 = 4.7 T, the ^2H Larmor frequency , ν_0 = 30.7 MHz. This frequency is much larger than the ^2H quadrupolar coupling constant e^2qQ/h = 170 kHz, which gives rise to a maximum quadrupolar splitting (*vide infra*) of

about 250 kHz for ^2H in C-^2H bonds. The quadrupolar interaction can therefore be treated as a first-order perturbation of the Zeeman interaction (Davis, 1983), as discussed in the next section. Due to the low magnetogyric ratio of the ^2H nucleus ($\gamma^1H/\gamma^2H=6.5$), the dipolar interaction leads to a maximum dipolar splitting of only about 4 kHz. The range of chemical shifts for ^2H is also very small, i.e. about 500 Hz at 4.7 T. The dipolar and chemical shift interactions, as well as scalar coupling, though not entirely negligible, are much smaller than the quadrupolar interaction and can therefore usually be neglected in the discussion of the ^2H spectra.

2.4 The electric quadrupolar coupling

We have seen earlier that a nucleus with spin $I > 1/2$, like the ^2H nucleus, may possess an electric quadrupole moment which can interact with an electric field gradient (EFG) at the nucleus. The Hamiltonian describing this interaction may be written as the scalar product of two second-rank irreducible tensors:

$$H_Q = \frac{eQ}{4I\,(2I-1)} \sum_{M=-2}^{2} (-1)_M\, V_M\, T_{-M} \qquad (2.4)$$

where V_M are the irreducible spherical components of the electrostatic field gradient tensor and T_M are the irreducible tensor components of the spin angular momentum operators. The tensor V_M is given by:

$$V_0 = V_{ZZ}$$
$$V_{\pm 1} = \mp (2/3)^{1/2} (V_{XZ} \pm iV_{YZ}) \qquad (2.5)$$
$$V_{\pm 2} = (2/3)^{1/2} [1/2(V_{XX} - V_{YY}) \pm iV_{XY}]$$

where V_{ij} are the Cartesian components of the electrostatic field gradient tensor at the nucleus. The irreducible components of the spin angular momentum operators are:

$$T_0 = (3I_Z^2 - I^2)$$
$$T_{\pm 1} = \mp (3/2)^{1/2} (I_Z I_{\pm} + I_{\pm} I_Z) \qquad (2.6)$$
$$T_{\pm 2} = I^2_{\pm}$$

The field gradient tensor V is symmetric and traceless in the principal coordinate system of the molecule of interest. In this case:

$$V_P = \begin{bmatrix} V_{XX} & 0 & 0 \\ 0 & V_{YY} & 0 \\ 0 & 0 & V_{ZZ} \end{bmatrix} \qquad (2.7)$$

with: $$V_{XX} + V_{YY} + V_{ZZ} = 0 \qquad (2.8)$$

It is also convenient to define the asymmetry parameter, η, of the EFG tensor, assuming that $V_{ZZ} > V_{XX} > V_{YY}$:

$$\eta = (V_{XX} - V_{YY})/V_{ZZ} \qquad (2.9)$$

Referred to the principal coordinate system, the irreducible tensor elements V_K^P are determined according to equation 2.5:

$$\begin{aligned} V_0^P &= V_{ZZ} = eq \\ V_{\pm 1}^P &= 0 \\ V_{\pm 2}^P &= (1/6)^{1/2} (V_{XY} - V_{YY}) = (1/6)^{1/2} \eta eq \end{aligned} \tag{2.10}$$

On the other hand, the spin angular momentum I is quantized in the laboratory coordinate system (L) defined by the direction of the applied magnetic field H_0. By an appropriate rotation of either V_M or T_M, it is possible to evaluate the various components of the quadrupolar Hamiltonian in a single coordinate system. This is most easily accomplished using Wigner rotation matrices (Rose, 1957). To calculate H_Q in the laboratory frame (L), it is therefore necessary to express the V_M elements in the frame L:

$$V_M^L = \sum_{K=-2}^{2} D_{KM} (\alpha,\beta,\gamma)\, V_K^P \tag{2.11}$$

where α, β and γ are the Euler angles as defined by Rose (1957) and D_{KM} are the elements of the Wigner rotation matrix, which can be found elsewhere (Rose, 1957; Seelig, 1977). Using equation 2.11, equation 2.4 becomes:

$$H_Q = \frac{eQ}{4I(2I-1)} \sum_{M=-2}^{2} (-1)_M T_{-M} \sum_{K=-2}^{2} D_{KM} (\alpha,\beta,\gamma)\, V_K^P \tag{2.12}$$

To first order, we can keep only the terms in T_0 (Davis, 1983), so that:

$$H_Q = \frac{eQ}{4I\,(2I-1)} \; T_0\,[D_{0,0}(\alpha,\beta,0)V_0^{\,P} + D_{\pm 2,0}(\alpha,\beta,0)V_{\pm 2}^{\,P}] \qquad (2.13)$$

where the symmetric and traceless properties of V^P have been used ($V_{\pm 1}^{\,P}=0$) and $\gamma=0$ since when $M=0$, the $D_{K,0}(\alpha,\beta,\gamma)$ elements are independent of γ. It should be noted at this point that the Euler angles α and β correspond to the usual spherical polar angles (θ,ϕ) defining the orientation of the principal component V_{ZZ} of the EFG tensor (along the C-^{2}H bond) with respect to the magnetic field H_0. Substituting the values of the Wigner rotation matrix elements and the values of $V_0^{\,P}$and $V_{\pm 2}^{\,P}$ into equation 2.13, the quadrupolar Hamiltonian becomes:

$$H_Q = \frac{eQ}{4I\,(2I-1)}(3I_Z^{\,2}-I^2) \; \frac{1}{2}[(3\cos^2\theta-1) + (\eta\sin^2\theta\cos 2\phi)] \qquad (2.14)$$

The energy levels of this Hamiltonian are given by (including the Zeeman term $-h\omega_0 m$):

$$E_m = -h\omega_0 m + \frac{eQ}{4I\,(2I-1)}\,(3m^2-I(I+1)) \; \frac{1}{2}[(3\cos^2\theta-1)+(\eta\sin^2\theta\cos 2\phi)] \qquad (2.15)$$

where $m=1,0,-1$ (since $I=1$ for deuterium). The Zeeman term of equation 2.15 gives three equally spaced energy levels and leads to a single absorption line at the frequency ν_0 (Larmor frequency). The effect of the quadrupolar term is therefore to remove the degeneracy and split that single line by the value $\Delta\nu_Q$, called the quadrupolar splitting:

$$\Delta\nu_Q = \frac{3}{2}\frac{e^2qQ}{h}\frac{1}{2}[(3\cos^2\theta - 1 + (\eta \sin^2\theta\cos 2\phi)] \qquad (2.16)$$

where e^2qQ/h is generally referred to as the quadrupolar coupling constant. For a monocrystalline sample, in which all the nuclei have the same orientation with respect to H_0, two lines will be obtained, with frequency separation $\Delta\nu$. This is illustrated in Figure 2.1.

2.5 Lineshape of polycrystalline samples

In the previous section, the expression of the quadrupolar splitting has been derived for homogeneously oriented samples, in which all deuterium sites were assumed to have the same orientation with respect to the magnetic field. However, most biological membranes do not orient in a magnetic field and therefore, the nuclear sites are randomly oriented with respect to the field. The shape of this "powder-type" spectrum is the superposition of the resonances arising from all possible orientations of the nuclear spins.

A polycrystalline sample can be pictured as a multiple of microcrystals where the EFG tensor principal axes (z in this case) are distributed over the surface of a sphere (Figure 2.2A). Their probability distribution $P(\theta)$ is $1/2 \sin\theta$. Therefore, in a randomly dispersed sample, we will observe all the resonance lines due to the variation of θ from 0° to 90° with respect to H_0, weighted by the probability $P(\theta)$. The shapes of the powder pattern for several values of the asymmetry parameter η are shown in Figure 2.2B. In the

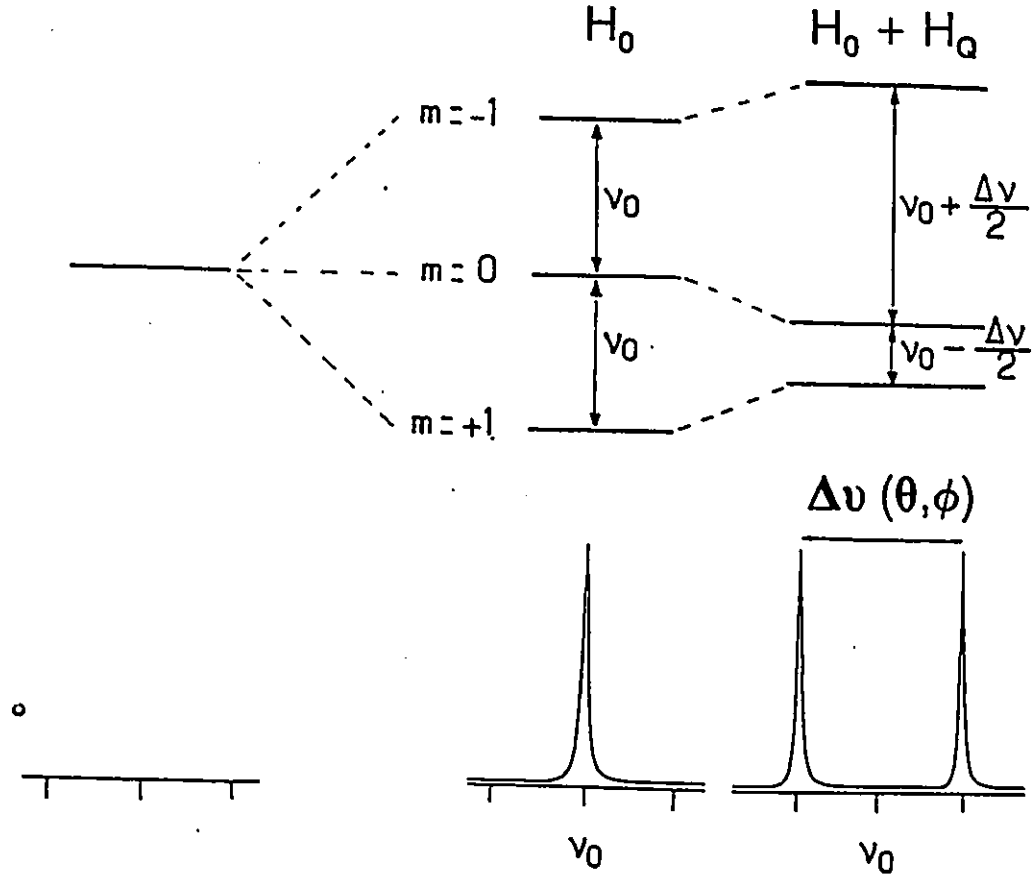

Figure 2.1 Energy levels for a spin-1 in a high magnetic field. The quadrupolar interaction gives rise to two transitions at frequencies $\nu_0 \pm \nu_Q$.

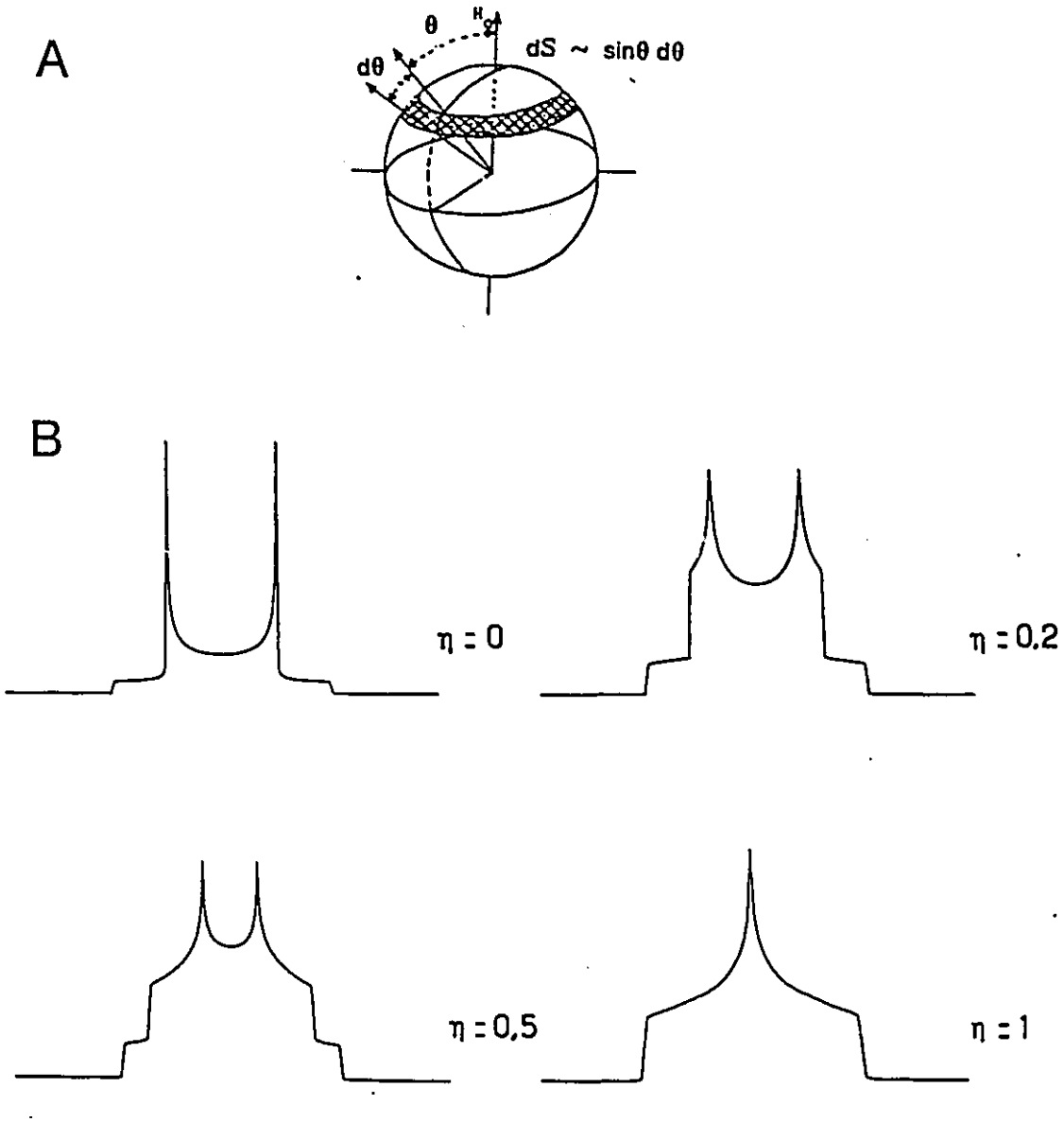

Figure 2.2 Theoretical spin-1 quadrupolar powder patterns. **A.** Random distribution over the surface of a sphere. **B.** Theoretical spectral shapes for several values of the asymmetry parameter η.

case of C-^{2}H bond, it has been shown theoretically (Hoyland, 1968) and experimentally (Derbyshire et al., 1969; Barnes & Bloom, 1973) that the asymmetry parameter is less than 0.05. However, as will be seen later, although the static EFG tensor has axial symmetry, the motionally averaged tensor elements may not (*vide infra*). This occurs when the motions averaging the EFG tensor have less than three fold symmetry.

2.6 Effects of molecular motions on ^{2}H lineshapes

2.6.1 Introduction

The equation giving the value of the quadrupolar splitting as a function of the angles θ and ϕ defining the orientation of the principal component of the EFG tensor with respect to H_0 is only valid in the case of rigid molecules. If there are molecular motions, equation 2.16 has to take into account the time-dependence of the quadrupolar interaction, which is reflected by a time-averaging of the Euler angles. In an isotropic medium, the Wigner matrix elements are averaged to zero. In this case, the time-averaged value of H_Q vanishes and will no longer perturb the Zeeman energy levels. A single resonance line is therefore obtained. However, the quadrupolar interaction still exists but only affects relaxation (*vide infra*). In anisotropic media, such as model membranes, the Euler angles are still time-averaged but not necessarily to zero.

In the following sections, the effects of fast axially symmetric motions on ^{2}H NMR lineshapes and how these effects can be described in terms of order parameters will be discussed. We will then discuss the lineshapes obtained for fast axially asymmetric motions

and finally the case of motions of intermediate rate relative to the quadrupolar interaction.

2.6.2 Fast axially symmetric motions

The maximum quadrupolar splitting that is possible for C-^{2}H bonds is of about 250 kHz ($\eta=0$, $\theta=0$, equation 2.16). Anisotropic motion with correlation times τ_i such that $\tau_i << 1/250$ kHz $\approx 4 \times 10^{-6}$ s will therefore be considered as fast on the ^{2}H NMR lineshape time scale. In order to take into account these molecular motions, one has to replace the initial transformation of the EFG principal axis system to the laboratory frame L by several transformations necessary to describe the contribution of each motion to the averaged EFG tensor. If we consider for example that the lipid molecule in a bilayer undergoes two types of axially symmetric motions, i.e. a rotation about the long axis of the molecule, as well as an angular fluctuation of this axis with respect to the bilayer normal, the evaluation of the averaged EFG tensor is performed by transforming stepwise from (1) the coordinate system of the EFG tensor to the rotational diffusion axis of the molecule n(t), (2) from n(t) to n, the local bilayer normal and (3) from n to the z axis of the laboratory frame. Each of these coordinate system transformations are accomplished using Wigner rotation matrices, as described previously. Assuming fast axially symmetric motions, the quadrupolar splitting then becomes:

$$\Delta\nu_Q = \frac{3}{2}\frac{e^2qQ}{h}\frac{3\cos^2\theta-1}{2}\left\langle\frac{3\cos^2\beta-1}{2}\right\rangle\left\langle\frac{3\cos^2\gamma-1}{2}\right\rangle \qquad (2.17)$$

where the angles θ, β, and γ are illustrated in Figure 2.3 and the angular brackets denote an ensemble average. In the case of multilamellar lipid dispersions, the angle θ is not time-dependent since the rotational diffusion of the system is normally too slow to average the EFG tensor. The effects of axial rotation and angular fluctuations or "wobbling" on the ^2H powder spectrum are illustrated in Figure 2.4.

2.6.3 The order parameter approach

When using spectroscopic techniques for the study of ordered, anisotropic systems in the presence of molecular motions, one must often deal with the "orientational averages" of second rank tensor interactions, as discussed in the previous section. In such cases, it can be useful to describe the average orientational order in terms of an order parameter tensor (Davis, 1983). The concept of order parameter, S, was originally introduced by Saupe to describe in a general way the fluctuations of second rank tensors (Saupe, 1964).

If we attach a cartesian coordinate system x,y,z to the lipid molecule and consider the average fluctuations of these axes around the director axis z', a convenient way to measure these fluctuations is the order parameter S_{ii}, defined as (Seelig, 1977):

$$S_{ii} = (1/2)\,(3\langle\cos^2\theta_i\rangle - 1) \quad (i=1,2,3=x,y,z) \tag{2.18}$$

where the angular brackets denote the time average of the angular fluctuations of the ith coordinate axis with respect to the director axis z'. If the molecule fixed tensor is axially symmetric, with for example the z axis as its symmetry axis, then it is only necessary to

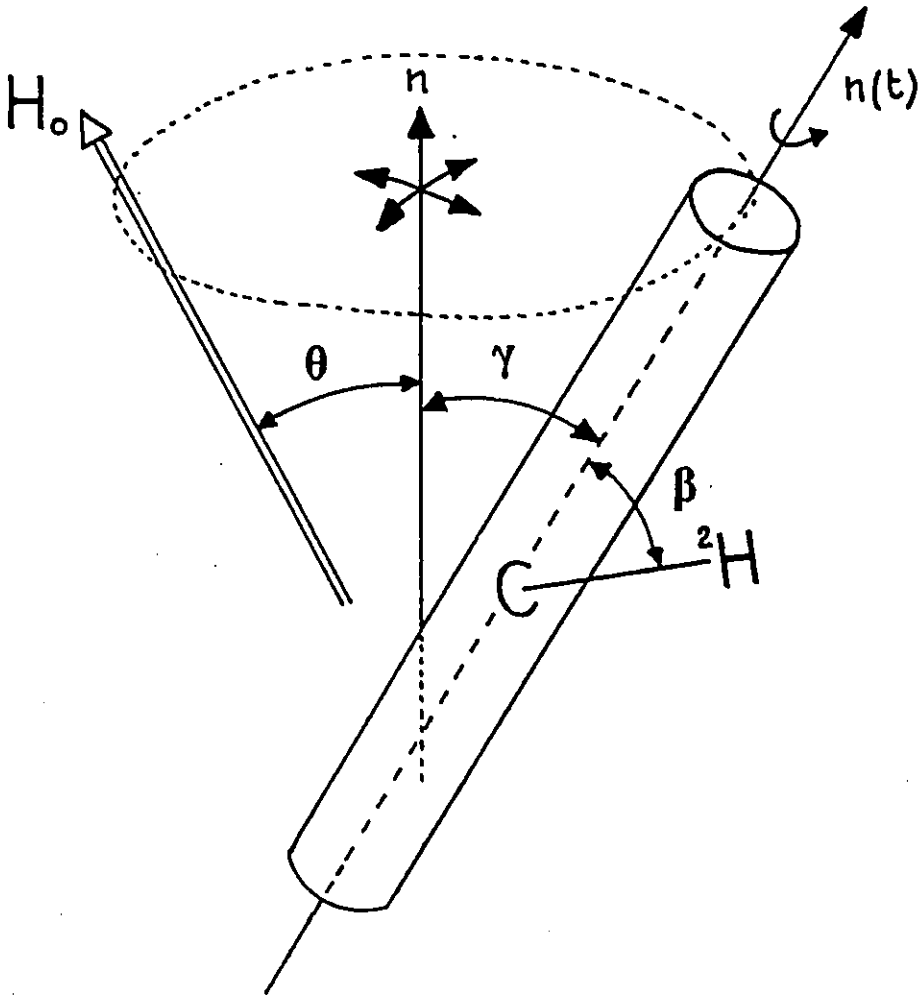

Figure 2.3 Axially symmetric motions of a rigid molecule in a lamellar phase. γ, β and θ are the angles relating the C-^{2}H bond vector to the laboratory frame (H_0).

specify the order parameter S_{ZZ} of this axis. The two other axes (x,y) are physically indistinguishable and have the same order parameter such that:

$$S_{ZZ} = -(1/2)S_{XX} = -(1/2)S_{YY} \tag{2.19}$$

If we consider only one motion, i.e. the axial rotation of the molecule, the angle γ of equation 2.17 becomes 0 and the direction cosines $\cos\theta_Z$ of equation 2.18 is in fact $\cos\beta$, according to the notation of Figure 2.3. In this case, equation 2.17 can be written as:

$$\Delta\nu_Q = \frac{3}{2}\,\frac{e^2qQ}{h}\,\frac{1}{2}(3\cos^2\theta-1)\,S_{ZZ} \tag{2.20}$$

The quadrupolar splitting can be directly obtained from the separation between the two most intense peaks ($\theta=90°$) of the powder spectrum:

$$\Delta\nu\,(\theta=90°)=\Delta\nu_Q=3/4(e^2qQ/h)\,S_{ZZ} \tag{2.21}$$

The consequence of the axis rotation is therefore to reduce the quadrupolar splitting by $(3\cos^2\beta-1/2)$, as indicated in Figure 2.4. If another axially symmetric motion is added, for example the angular fluctuation of the molecular rotation axis, the quadrupolar interaction is further reduced and the quadrupolar splitting can be expressed as:

$$\Delta\nu\,(\theta=90°)=\Delta\nu_Q=3/4(e^2qQ/h)\,S_1\,S_2 \tag{2.22}$$

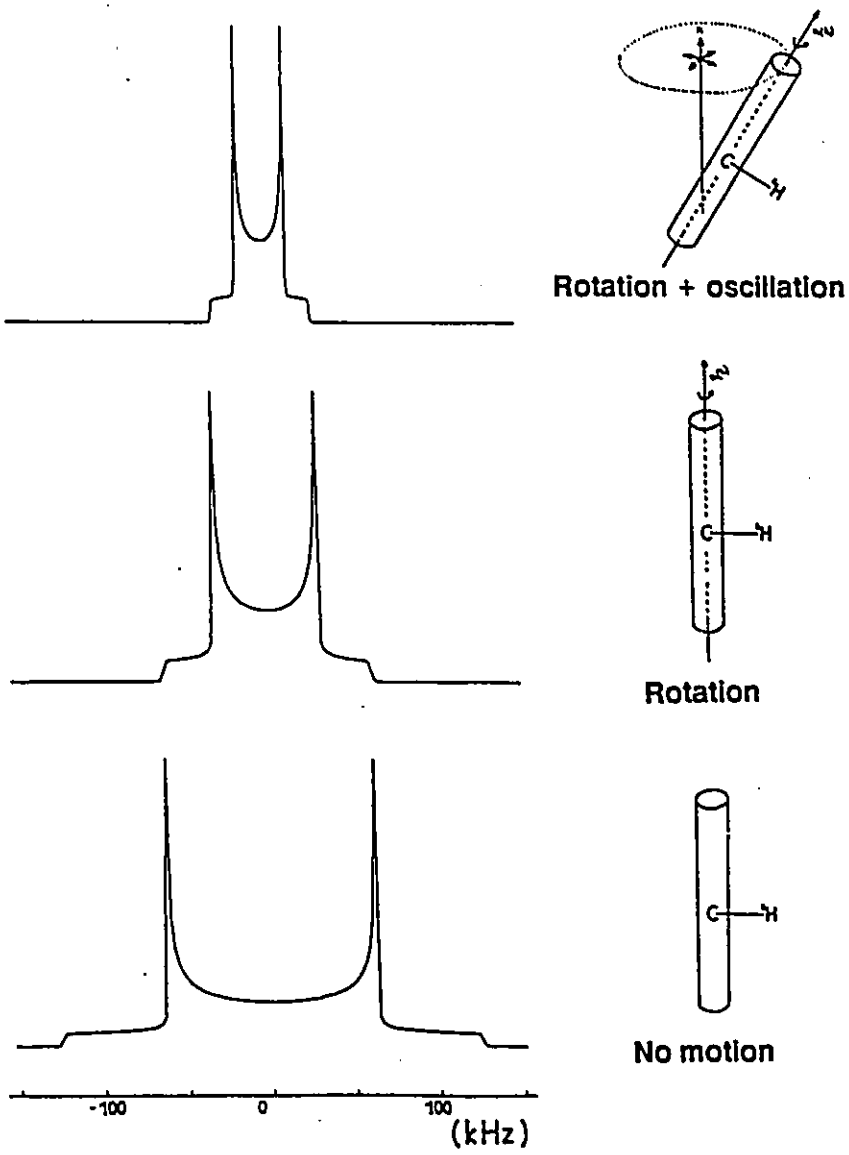

Figure 2.4 Effects of different axially symmetric motions on the deuterium powder spectrum.

where S_1 and S_2 represent the order parameter S_{ZZ} of the first and second motion (rotation and angular fluctuation, respectively). In a general way, if there exists N axially symmetric motions such that the ith motion reduces the residual quadrupolar interaction (already reduced by the motions i-1, i-2 etc...) by a quantity $S_i = (1/2<3\cos^2\beta_i-1>)$, the quadrupolar splitting can be written as :

$$\Delta\nu\,(\theta=90°)=\Delta\nu_Q=3/4(e^2qQ/h)\,S_{CD} \qquad (2.23)$$

where S_{CD}, the orientational order parameter is defined by:

$$S_{CD} = \prod_{i=1}^{N} S_i \qquad (2.24)$$

S_{CD} can therefore be considered as a general measure of the order in the system, with respect to the bilayer normal. In the particular case discussed previously, where the molecule undergoes two types of motion, rotation and angular excursion, the location of the C-^{2}H bonds are fixed relative to each other. The order parameter S_1 of equation 2.22 is therefore not time-dependent, but is in fact a geometrical factor. The measurement of the order parameter S_{CD} can therefore give information about the orientation of C-^{2}H bonds within a molecule relative to the rotation axis and on the amplitude of the angular fluctuations of this axis relative to the bilayer normal.

Although strictly rigorous, order parameters do not necessarily provide a physical picture of the motional processes leading to the averaged spin interaction. The observation of fast axially symmetric lineshapes is indicative of motion with axial symmetry

and with rates fast compared to the quadrupolar interaction. However, the exact nature and rate of this (these) motions(s) cannot be fully determined by an order parameter analysis. It will be shown in section 2.7 that the measurement of longitudinal relaxation times T_1 can give information on the rate of fast motion (with rate comparable to the Larmor frequency). Moreover, the study of the orientation (θ) dependence of longitudinal relaxation time can give very useful information about the type of molecular motion present in a system. However, before discussing spin-lattice relaxation times, we will briefly discuss the case of fast-limit axially asymmetric motions and in section 2.6.5 how information can be obtained from lineshape analysis in the case of intermediate-regime motions, occurring at rates comparable to the quadrupolar interaction.

2.6.4 Fast axially asymmetric motions

Observation of axially asymmetric ^2H NMR spectra requires that the motion(s) giving rise to such spectra has twofold or lower symmetry. The simplest way to satisfy this requirement is to have a two-site exchange process, but other ways are also possible. For example, a threefold reorientation mechanism with unequal populations of the sites will result in axially asymmetric lineshapes (Griffin, 1981). While twofold or lower symmetry is necessary for the observation of axially asymmetric spectra, the lineshapes will depend strongly on the details of the motion, the populations of the sites and the rate constant associated with the process. When the rate of motion is fast compared to the quadrupolar coupling constant, the problem is in the "fast-exchange" limit and the spectra will depend only on the equilibrium distribution of molecular orientations $P(\Omega)$. In this case, the frequency can be expressed as:

$$\Delta\nu = (3/2)^{1/2} \quad (eQ/2h) \quad \sum_{j=1}^{N} p_{eq}(j) \quad \sum_{K} D_{KM}(\Omega_{PC})\, D_{K0}(\Omega_{CL}) \qquad (2.25)$$

where rotation through the Euler angles Ω_{PC} brings the principal axis coordinate system, P, into coincidence with the crystal-fixed (or molecular) coordinate system, C. Similarly, rotation through Ω_{CL} brings the C system into coincidence with the laboratory system, L (Torchia & Szabo, 1982). In equation 2.25, it is assumed that the P system has N discrete orientations, and $p_{eq}(j)$ is the equilibrium probability orientation.

As an example of axially asymmetric motion resulting in axially asymmetric lineshapes ($\eta \neq 0$), let us consider the ^{2}H-labelled aromatic ring shown in Figure 2.5, which can potentially undergo two types of motion about the C_ξ-C_γ bond. In the rigid lattice, the separation between the perpendicular edges (90°) of the spectrum is D=135 kHz. The total breath of the spectrum will therefore be of $\approx$ 270 kHz. The first motion, which was discussed in the previous section, is continuous diffusion, and results in a dramatic narrowing (by a factor of $(3\cos^2 60\text{-}1/2)=1/8$) of the ^{2}H spectrum, as shown in Figure 2.5. In contrast, fast discrete diffusion by 180° twofold flips about C_ξ-C_γ results in a dramatically different spectrum. Since the two ring orientations are equally probable, the motionally averaged tensor will have its principal axes along the xyz coordinate system shown in Figure 2.5. The frequency perpendicular to the plane of the ring (x) is unaffected by the motion and remains equal to 135 kHz whereas the frequency along the jump axis (y) is that evaluated previously (-D/4). Since the tensor must remain traceless, the third component (z) must be of 5D/4. Thus, fast twofold reorientation yields an $\eta = 0.6$ spectrum with a breath about half that of the rigid spectrum.

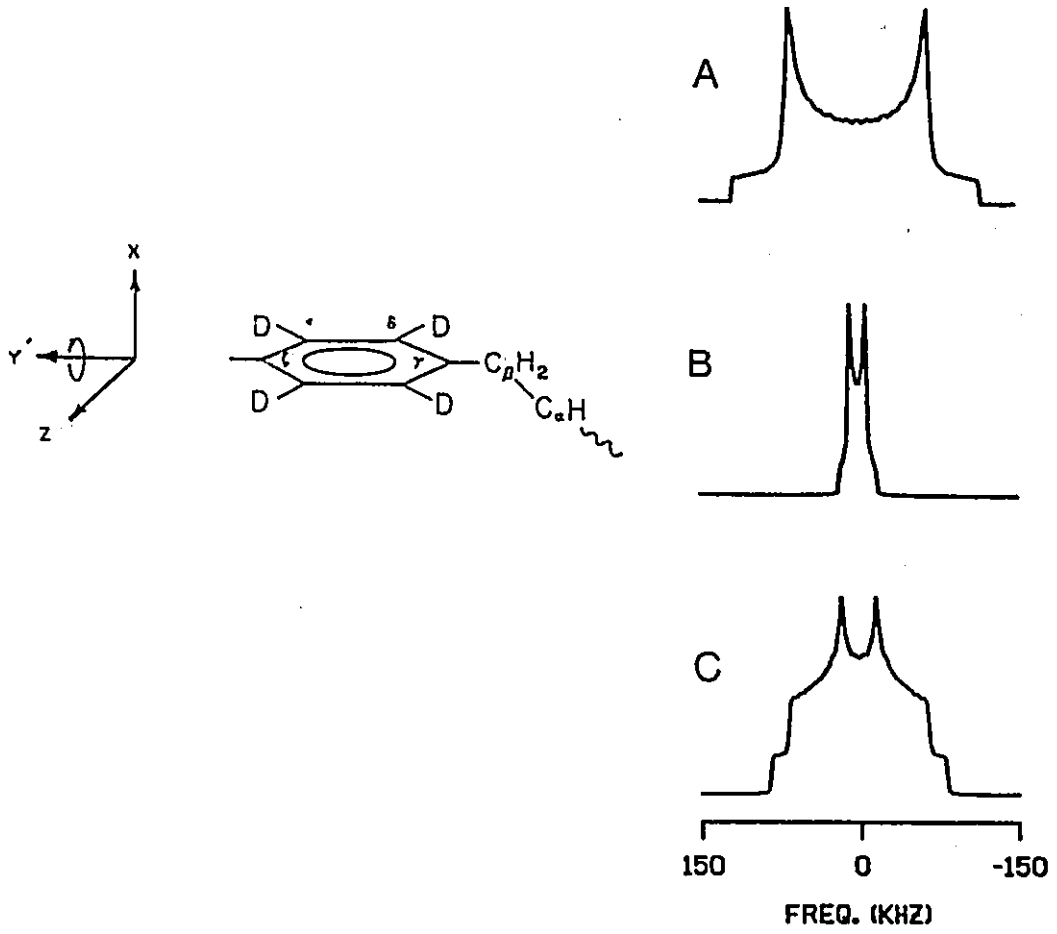

Figure 2.5 Theoretical ^2H NMR lineshapes for a ^2H labelled aromatic ring. A. Rigid lattice spectrum exhibiting a splitting of 135 kHz. B. Spectrum resulting from fast continuous diffusion about the Y axis, with a splitting between the perpendicular edges of D=17 kHz. C. Axially asymmetric spectrum arising from fast 180° ring flip about the Y axis (from Griffin et al., 1988).

2.6.5 Intermediate lineshape analysis

The current method of choice for recording rather wide (up to ≈ 250 kHz) ^2H NMR spectra involves Fourier transformation of a two-pulse quadrupolar echo (discussed in section 3.6.1), $90°_x$-τ-$90°_y$-τ-acq. In the slow ($\omega_Q\tau_C >> 1$) or fast ($\omega_Q\tau_C << 1$) limit motion regions, quadrupolar echo lineshapes are identical to those obtained by continuous wave (CW) NMR techniques. However, for intermediate exchange rate ($\omega_Q\tau_C \approx 1$) (rate ≈ 10^3-10^5 s^{-1}), CW and quadrupolar echo lineshapes differ considerably.

In the slow or fast limit, the transverse relaxation time T_{2e}, which describes the decay of the quadrupolar echo amplitude, is much larger than τ in the echo sequence and the magnetization is completely refocused by the second pulse. In contrast, for intermediate exchange, T_{2e} is anisotropic and $< \tau$ for many orientations in the powder, so that some of the signal decays irreversibly and is not refocused. This effect is manifested in several ways in the quadrupolar echo lineshapes. First, the lineshapes are distorted due to anisotropic T_{2e} in the powder sample. The second effect is the dependence of the lineshapes on τ, which can be used to discriminate amongst various models for molecular motion. Moreover, a unique final feature of quadrupolar echo spectra is that the overall spectral intensity declines dramatically when passing through the intermediate exchange region. Examples of lineshape distortion obtained using the quadrupolar echo sequence compared to the "Bloch" lineshape in the intermediate exchange regime are shown in Figure 2.6 for a two-site jump process. The evaluation of intermediate-exchange lineshape obtained by the quadrupolar echo sequence is of importance since the attempt to analyze such spectra quantitatively, not realizing that they are distorted because of finite τ, can lead to incorrect conclusions about the rate and nature of the motion giving rise to such

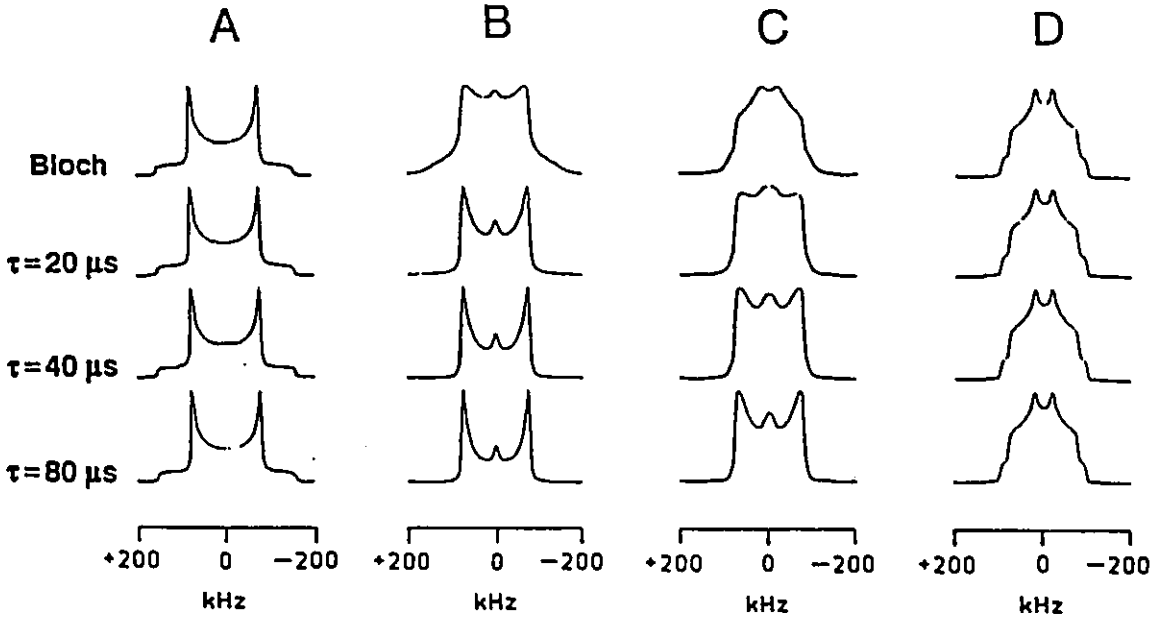

Figure 2.6 Lineshapes for a two-site diamond lattice jump process (P_1=0.7 and P_2=0.3) as a function of the echo delay time τ for various jump rates. The jump rates are A. $k=10^3\ s^{-1}$, E. $k=10^5\ s^{-1}$, C. $k=10^6\ s^{-1}$ and D. $k=10^7\ s^{-1}$ (from Wittebort et al., 1987).

spectra (Spiess & Sillescu, 1981; Griffin et al., 1988).

Quite generally, intermediate exchange spectra are calculated by solving the usual exchange modified Bloch equation (Abragam, 1961; Spiess & Sillescu, 1981; Wittebort et al., 1987; Griffin et al., 1988):

$$dM/dt = [i\omega + R]M \tag{2.26}$$

The two terms in the operator $[i\omega + R]$ correspond to the Larmor precession and the random dynamics, respectively. For continuous dynamics in isotropic fluids, R is typically taken as a diffusion operator while for discrete jump processes, R becomes a jump matrix R_{ij}. For an N-site jump process, equation 2.26 therefore becomes:

$$\frac{dM_i}{dt} = \sum_{k=1}^{N} [i\omega_i d_{ij} + R_{ij}]M_j \tag{2.27}$$

where R_{ij} is the rate matrix describing the dynamics among the N jump site and ω_i (β_i, α_i, θ, ϕ) is the quadrupolar frequency corresponding to the orientation of V_{ZZ} for site i, specified by β_i and α_i, and θ and ϕ specifies the orientation of the molecule with respect to the external magnetic field. The solution of the desired quadrupolar echo conditions gives the frequency domain lineshape $I(\omega,\theta,\phi)$:

$$I(\omega,\theta,\phi,\tau) = \mathrm{Re}\sum_{k=1}^{N} b_k/(\lambda_k - i\omega) \tag{2.28}$$

$$b_k = a_k \sum_m a_m^* \left(\sum_n X_n^{(k)} X_n^{(m)*}\right) \exp(\lambda_m^* + \lambda_k)\tau$$

$$a_k = \sum (P_i)^{(1/2)} X_i^{(k)}$$

where $X^{(k)}$ and λ_k are the N complex eigenvectors and eigenvalues of the symmetrized matrix $[i\omega_i\delta_{ij} + (R_{ij}R_{ji})^{(1/2)}]$. Thus, for a given crystal orientation, the spectrum is the sum of N Lorentzians. Intensity distortions of the quadrupolar echo spectrum ($\tau \neq 0$) are contained in the b_k terms. For powder spectra, the single crystal spectrum (fixed θ and ϕ) is numerically integrated over all possible orientations (θ and ϕ).

2.7 ^{2}H spin-lattice relaxation

2.7.1 Introduction

In the previous section, we have focused on the motional narrowing of the quadrupolar echo lineshapes. It was demonstrated that these lineshapes are affected by motions in the range 10^3-10^7 s^{-1}. However, most biological systems exhibit faster motions and these motions with rates comparable to the Larmor frequency are most easily investigated by ^{2}H spin-lattice relaxation.

For the case of spin I=1 nuclei like deuterium, where there is a non-vanishing electric quadrupolar interaction, the dominant relaxation mechanism is quadrupolar relaxation (Jeffrey, 1981). The spin-lattice (or longitudinal) relaxation time T_{1Z} is associated with the return of the Zeeman energy to its equilibrium value, while T_{1Q} is

associated with the decay of the quadrupolar energy. One can also measure three spin-spin (or transverse) relaxation times T_2 for spin I=1 nuclei. A complete description of the relaxation times in a spin I=1 system, as well as their derivation from the time dependence of the density matrix, has been given by Jeffrey (1981). Solving the master equation for the time evolution of the density matrix, the theoretical expression for T_{1Z}, T_{1Q} and T_{2e} are given by:

$$\begin{aligned} 1/T_{1Z} &= 1/3\,(\omega_Q{}^2)\,[J_1(\omega_0) + 4J_2(2\omega_0)] \\ 1/T_{1Q} &= 1/3\,(\omega_Q{}^2)\,[3J_1(\omega_0)] \\ 1/T_{2e} &= 1/3\,(\omega_Q{}^2)\,[3J_0(0) + 3J_1(\omega_0) + 2J_2(2\omega_0)] \end{aligned} \qquad (2.29)$$

where $\omega_Q = 3e^2qQ/4h$ and $J_m(m\omega_0)$ (m=0,1,2) are the spectral density functions which will be discussed in more detail in the following section.

The main difference between the spin-lattice relaxation times T_{1Z} and T_{1Q} and the spin-spin relaxation time T_{2e} resides in the presence of the $J_0(0)$ term in the equation for the transverse relaxation rate. This spectral density monitors the motions occurring at low frequencies and therefore T_{2e} is more sensitive to slow motions than T_{1Z}. In the following sections, the discussion will be focused on spin-lattice relaxation times, which are sensitive to motions with rates comparable to the Larmor frequency.

2.7.2 Spectral densities and autocorrelation functions

Let us consider a spin system characterized by eigenstates a, b and c and corresponding energies E_a, E_b and E_c. A perturbation, time-dependent Hamiltonian H(t), acts on this system. H(t) corresponds in our case to the coupling of the spin system with the lattice. If A is an operator acting on the spin variables of the system, time-dependent perturbation theory leads to (Abragam, 1961):

$$\omega_{ab} = 1/\hbar^2 \; | (a | A | b) |^2 J(\omega_0) \qquad (2.30)$$

which relates the average transition probability per second, ω_{ab} to $J(\omega_0)$, the spectral density value for a process which involves the states a and b of the spin system exposed to fluctuations with frequency components $\omega = \omega_0 = | E_a - E_b |$ (Reisse, 1983).

The spectral density functions $J(\omega)$ are related to the Fourier transform of the autocorrelation functions $G(\tau)$ by the Wiener-Khintchine theorem (Wiener, 1930; Khintchine, 1934):

$$J(\omega) = \int G(\tau)\, e^{-i\omega\tau}\, d\tau \qquad (2.31)$$

The autocorrelation function itself is defined as:

$$G(\tau) = \langle f(t) \bullet f(t+\tau) \rangle_t \qquad (2.32)$$

in which the brackets imply an ensemble average taken over the time t (Reisse, 1983). The

correlation function describes how long some given property of a system persists until it is averaged out by the microscopic motion of the molecules in the system.

The choice of a correct analytical form for the spectral density and the autocorrelation function is a very difficult task. Measurements of NMR relaxation times as a function of both frequency and sample orientation can provide much useful information for developing detailed models of molecular motion in such systems, as discussed in the following section.

2.7.3 Frequency and orientation dependence of spin-lattice relaxation times

The spectral densities of motion for lipid bilayers are often frequency dependent due to the presence of different kinds of motion. In such cases, it is often necessary to carry out the relaxation experiments at different field strengths in order to determine both $J_1(\omega_0)$ and $J_2(2\omega_0)$ (in the case of T_{1Z}) as a function of frequency. In practice however, the limited number of ^2H resonance frequencies available does not allow one to distinguish unequivocally among various motional models. Therefore, in addition to getting information about the frequency dependence of individual spectral densities of motion from field dependent relaxation measurements, it is also possible to exploit the sensitivity of the relaxation expressions to angular factors, by measuring the angular dependence of the spin-lattice relaxation rates, i.e. the dependence of the relaxation rates on the angles between the bilayer normal (director) and the magnetic field direction. This point will be further discussed in chapter 8, section 8.3.3.2.

2.8 Two-dimensional deuteron NMR

We have shown in sections 2.6 and 2.7 that lineshape studies can elucidate motions on the 10^3-10^6 s^{-1} timescale while spin-lattice relaxation measurements are sensitive to motions occurring at the timescale of the Larmor frequency (10^7-10^{10} s^{-1}). These techniques can also provide motional discrimination but are not effective for slower motions, with rates $< 10^3$ s^{-1}. For these motions, two-dimensional solid-state deuteron NMR techniques (Schmidt et al., 1986, 1987, 1988; Wefing & Spiess, 1988; Wefing et al., 1988) have extended the frequency range over which motions may be probed to the ms or longer timescales. This technique is sensitive to both the rate and type of slow motion and in the case of tensorial interactions with axial symmetry, such as the quadrupole coupling of deuterons, the singularities of the 2D exchange signals give rise to simple geometric ridges from which the angles through which the molecules reorient can be read directly. A detailed description of this technique, including the pulse sequence and phase cycling used to record the two-dimensional deuteron spectra, will be given in chapter 10, section 10.2.

CHAPTER 3

Experimental methods

3.1 Materials

Dimyristoylphosphatidylcholine (DMPC) and tetracaine hydrochloride were obtained from Sigma Chemical Co. (St-Louis, MO). Dihexadecylphosphatidylcholine (DHPC) was purchased from Calbiochem Behring Corp. (La Jolla, CA). Dioleoylphosphatidylcholine (DOPC), dipalmitoylphosphatidylcholine-$^2H_{62}$ (DPPC-$^2H_{62}$) and the sodium salts of both dimyristoylphosphatidylserine (DMPS-Na^+) and dioleoylphosphatidylserine (DOPS-Na^+) were purchased from Avanti Polar Lipids (Birmingham, AL). Cholesterol was purchased from Steraloids Inc. (Pawling, NY). The deuteriated tetracaines [$^2H_2$]TTC, [$^2H_3$]TTC and [$^2H_6$]TTC were the generous gift of Dr. Y. Boulanger (NRC, Ottawa) and the multiply labelled [2,2,4,4,6-$^2H_5$] cholesterol was the generous gift of Dr E.J. Parish (Auburn University, Auburn AL). 1,2-di-*O*-tetradecyl-3-*O*-(β-D-[1-$^2H_1$]glucopyranosyl)-*rac*-glycerol and 1,2-di-*O*-tetradecyl-3-*O*-(β-D-glucopyranosyl)-*sn*-[3,3-$^2H_2$]glycerol were the generous gift of Dr. H.C. Jarrell (NRC, Ottawa) and were prepared as described previously (Jarrell et al., 1986, 1987a). 1,2-di-*O*-tetradecyl-3-*O*-(α-D-mannopyranosyl)-*sn*-[3,3-$^2H_2$]glycerol was a generous gift of Dr. H.C. Jarrell (NRC, Ottawa) and prepared as described previously (Ogawa & Beppu, 1982, Jarrell et al., 1987b). 1,2-di-*O*-hexadecyl-*sn*-[2-$^2H_1$]glycero-3-(2-aminoethyl)phosphonate and 1,2-di-*O*-hexadecyl-*sn*-[3-$^2H_1$]glycero-3-(2-aminoethyl)phosphonate were the generous gift of M.R.

Van Calsteren (NRC, Ottawa) and were prepared as described elsewhere (Van Calsteren, 1989). Dimethyl sulfone-$^2H_6$ was purchased from Cambridge Isotope Laboratories (Cambridge, MA). Deuterium-depleted water used for ^2H NMR all samples was obtained from Aldrich Chemical Co. (Milwaukee, WI) and D_2O was obtained from MSD Isotopes (Montreal, Que.); all other materials were analytical grade.

3.2 Synthesis of specifically deuteriated DMPC

The specifically deuteriated DMPC were prepared by a modification (Perly et al., 1983) of a reported procedure (Gupta et al., 1974). The fatty acid anhydride of specifically labelled myristic acid was obtained by a standard procedure (Selinger & Lapidot, 1966). [4,4-$^2H_2$] myristic acid and [4,4,14,14,14-$^2H_5$] myristic acid were the generous gift of Dr. H.C. Jarrell (NRC, Ottawa). 1-myristoyl-*sn*-3-glycero-phosphocholine (0.25 mmole) (Sigma Chemical Co., St-Louis MO) was dispersed in 5 ml of distilled water and lyophilized overnight. The fatty acid anhydride (0.30 mmole) and N,N-dimethyl-4-aminopyridine (0.32 mmole) (Aldrich Chemical Co., Milwaukee WI) were added to lyso-PC, solubilized in carbon tetrachloride (6.5 ml) distilled from phosphorus pentoxide. The reaction mixture was protected from light and stirred for 2 hours.

Completion of reaction was verified by thin layer chromatography (TLC) on silica gel plates in the solvent system chloroform:methanol:water 65:25:4 (v/v/v), by comparison with a DMPC standard using a stain made of 10% $CuSO_4$ in 8% H_3PO_4 (Bitman & Wood, 1982). The reaction mixture was diluted with chloroform:methanol 1:1 (v/v) (10 ml) and the mixture washed with cold 0.9% KCl in 1N HCl (10 ml). The lower phase was washed

with H_2O:MeOH 1:1 (v/v) (3 × 5 ml) and chromatographed on silica gel (Bio-sil A (100-200 mesh) (Bio-Rad Laboratories, Richmond CA). The unused fatty acid was quantitatively eluted with chloroform (100 ml). Elution with $CHCl_3$:CH_3OH:H_2O 45:25:2.5 (v/v/v) afforded the product. The filtered eluate was concentrated under reduced pressure. The residue was dispersed in water (2 ml) and freeze-dried overnight to give the PC as a white hydroscopic powder. The yields based upon lyso-PC were about 60%.

3.3 Determination of partition coefficients

The partition coefficient K_p is the ratio of the local anesthetic concentration in the lipid phase to that in the buffer (expressed in grams of anesthetic per gram of each phase). Because the partition coefficients for positively charged anesthetic decrease at higher free anesthetic concentration and at higher ionic strength (Roth & Seeman, 1972), K_p were determined on samples as close in composition as possible to the NMR samples. K_p were measured by dispersing the lipid mixture (100 mg total) and the anesthetic (10 mg) in the BPC buffer (1 ml) at the pH of interest. The buffer (BPC) consisted of sodium citrate (0.02 N), sodium phosphate (0.02 N), sodium borate (0.017 N) and sodium chloride (0.1 N) (Boulanger et al., 1980). The samples were heated to about 10°C above the gel to liquid-crystalline phase transition temperature of the lipid, freeze-thawed, and centrifuged. The concentration of anesthetic in the supernatant was determined spectrophotometrically (λ_{max} for TTC = 285 nm), and the partition coefficient was calculated (Miller & Yu, 1977).

3.4 Preparation of ^{2}H NMR samples

The lipid mixture of interest was dissolved in chloroform/methanol (2:1, v/v). The sample was dried under a stream of nitrogen and the solvent completely removed under vacuum. The resulting residue was dispersed in 1 ml of deuterium-depleted water and lyophilized overnight. The residue which appeared as a fluffy white powder was hydrated with ^{2}H-depleted water. Hydrated samples were heated cyclically to a temperature about 10°C above the gel to liquid-crystalline phase transition temperature of the lipid system, with vortex mixing and freeze-thawed to homogeneity (four to five cycles). When the local anesthetic was used, the solid was hydrated with 1 ml of BPC buffer (section 3.3) made with deuterium-depleted water and containing about 10 mg of anesthetic. The sample was then subjected to at least 10 freeze-thaw cycles to ensure complete equilibration of the anesthetic (Westman et al., 1982). Samples prepared in this manner gave very reproductible results. The samples were checked for degradation by thin layer chromatography after the NMR experiments.

3.5 Preparation of oriented samples

For the preparation of oriented samples, the required amount of each lipid (30-60 mg, total lipid) was dissolved in chloroform-methanol (2:1, v/v). The lipid mixture was dropped on 22 × 7 × 0.15 mm glass plates and allowed to dry. The plates were stacked in a 10-mm (o.d.) NMR tube and dried under vacuum for 3 hours. The sample was then hydrated overnight at a temperature about 5°C above the gel to liquid-crystalline phase transition temperature of the lipid system, under a humid atmosphere of ^{2}H-depleted

water. A drop of ^2H-depleted water was added and the tube sealed. The NMR tube was placed in a 10-mm solenoid coil (section 3.6.1) and manually rotated. The accuracy of the orientation was estimated to be about ± 2°, from multiple settings at one orientation. For each sample, the degree of orientation was checked by ^{31}P NMR spectroscopy (section 3.8).

3.6 ^2H NMR spectroscopy

3.6.1 Spectral acquisition: the quadrupolar echo

The ^2H NMR data were acquired at 30.7 MHz on a "home-built" Fourier-transform spectrometer operated by a Nicolet 1280 computer or on a Bruker MSL 300. Spectra were recorded by means of the quadrupolar echo sequence (Davis et al., 1976):

$$90_x - \tau - 90_y - \tau - \text{acquire} \qquad (3.1)$$

The basic quadrupolar echo sequence consists of an initial $\pi/2$ pulse applied along the x-axis of the rotating frame, followed by a $\pi/2$ pulse along the y direction after a time τ. The echo signal occurs at a time τ after the second pulse. Quadrature detection and full phase cycling (Griffin, 1981) were used to record the echo signals. Pulse spacing was typically 60 μs, unless indicated otherwise, the $\pi/2$ pulse length was about 3.8 μs (10-mm solenoid coil) or 2.3 μs (5-mm solenoid coil) and the recycle time was always greater than $5T_{1Z}$, assuring that the spectra were fully relaxed with respect to T_{1Z}. The frequency of the spectrometer was carefully set at the center of the quadrupolar powder pattern. Samples

were enclosed in a glass jacket where the temperature was regulated to within ± 0.5°C. Proton-decoupled ^2H NMR spectra were acquired at 46.1 MHz on a Bruker MSL-300 using the quadrupolar echo sequence with proton decoupling using the WALTZ pulse sequence (Shaka et al., 1983).

3.6.2 Longitudinal relaxation times T_{1Z}

Longitudinal relaxation times (T_{1Z}) were obtained by the standard inversion recovery sequence coupled with the quadrupolar echo sequence (Dufourc et al., 1984a):

$$180°\text{-}T\text{-}90°_x\text{-}\tau\text{-}90°_y\text{-}\tau\text{-acquire} \qquad (3.2)$$

Spectra were acquired in a way similar to that described in section 3.6.1, the only variable was the time T between the 180° inverting pulse and the first 90° pulse of the echo sequence.

If the spin-lattice relaxation can be described by a single exponential process, then the longitudinal magnetization, M(T), as a function of T is given by:

$$M(T) = M_0 [1\text{-}2\exp(-T/T_{1Z})] \qquad (3.3)$$

where M_0 is the equilibrium magnetization. To correct for imperfect 180° pulse, equation 3.3 may be modified to:

$$M(T) = M_0 [1-Aexp(-T/T_{1Z})] \quad (3.4)$$

where the parameter A is substituted for the 2 which appears in equation 3.3. Equation 3.4 was used to fit the experimental data.

3.6.3 Transverse relaxation times T_{2e}

The rate of transverse relaxation by T_{2e} was measured by monitoring the decay of the quadrupolar echo as a function of the spacing τ between the two pulses of the quadrupolar echo sequence. If the transverse relaxation process can be described by a simple exponential decay, the dependence of the transverse magnetization $M_y(2\tau)$ on τ is given by:

$$M_y(2\tau) = M_y(0)exp(-2\tau/T_{2e}) \quad (3.5)$$

where $M_y(0)$ is the transverse magnetization at $2\tau=0$. T_{2e} was obtained by fitting the above equation using the integrated intensities of each spectrum.

3.6.4 2D exchange spectra

Two-dimensional time functions were obtained by the pulse sequence: 90_y-t_1-54_ϕ-t_{mix}-54_ϕ-Δ-90_x-Δ-t_2 described by Schmidt et al. (1988) and discussed in more detail in section 10.2.2. This pulse sequence is an adaptation for solid-state deuteron NMR of the

classical two-dimensional three-pulse sequence (Jeener et al., 1979). Data were collected during the period t_2, while t_1 was incremented successively through the set of values covered by t_2. The fourth pulse serves to refocus the signal following the third pulse in order to circumvent the dead time of the receiver. The phase ϕ of the second and third pulses was set to ϕ=y for measurement of the $<\cos(\omega_1 t_1) \times \cos(\omega_2 t_2)>$ correlation function probing Zeeman order during the mixing time t_{mix} and to ϕ=x for measurement of the $<\sin(\omega_1 t_1) \times \sin(\omega_2 t_2)>$ correlation function probing quadrupolar order during t_{mix} (Schmidt et al., 1988). The Zeeman and quadrupolar order spectra were stored in separate data files. The angle 54° for the second and third pulses is used in order to obtain two signals of equal intensities, providing that relaxation effects are negligible.

3.6.5 Data treatment

The ^2H NMR data treatment was performed on a Nicolet 1280 data processor. The NMR data collected on the MSL-300 were transferred from the Bruker ASPECT-3000 computer to the Nicolet 1280 data processor. The data points before the top of the echo were discarded and the Fourier transformation was applied to this resulting FID, giving rise to undistorted spectra. Spectra which approximated axially symmetric lineshapes were "dePaked" according to Bloom et al. (1981) to obtain the 90°-oriented sample spectra from which the quadrupolar splittings were estimated. For two-dimensional spectra, zero filling to 256 values as well as a Gaussian apodization function were applied in both dimensions.

3.7 ^{2}H NMR simulations

Lineshape and longitudinal relaxation time simulations were performed on a μ-Vax or on a Sun 4-260 computer using a lineshape simulation program (Wittebort et al., 1987) based on the general formalism of Torchia and Szabo (Torchia & Szabo, 1982). The program was a generous gift of Dr. R.G. Griffin (MIT, Cambridge MA) and was modified for simulations of oriented sample spectra. Simulated lineshapes were corrected for the finite pulse width of the experimental 90° pulse in the quadrupolar echo sequence (Bloom et al., 1980) and the partially recoved T_{1Z} spectra were further corrected for the finite width of the 180° pulse (Hiyama et al., 1986). Two-dimensional spectral simulations were performed on a Sun 4-260 computer using a modification of a deuteron 2D exchange simulation program (H.C. Jarrell, unpublished results). Details of these simulations are given in chapter 10, section 10.4, and a copy of the simulation program can be found in appendix. Zero filling and a Gaussian apodization function were used in both dimensions.

3.8 ^{31}P NMR spectroscopy

^{31}P NMR spectra were obtained on a Bruker MSL-300 specrometer operating at 121.47 MHz using a 10 mm home-built probe. Spectra were acquired by the Hahn spin-echo technique (Hahn, 1950; Rance & Byrd, 1983):

$$90°_x\text{-}\tau\text{-}180°_y\text{-}\tau\text{-acquire} \qquad (3.6)$$

with full phase cycling of the radiofreqeuncy pulse (Rance & Byrd, 1983). Pulse spacings

were typically 40-50 μs, the 90° pulse length was 5-6 μs and the recycle time was always greater than $5T_{1Z}$. Proton-decoupling was achieved using the WALTZ pulse sequence (Shaka et al., 1983).

3.9 Preparation of FT-IR samples

3.9.1 Model membranes

To prepare lipid dispersions for study by FT-IR, the lipids were hydrated with 50 wt% of D_2O. When the local anesthetic tetracaine was used, the lipids were hydrated with 50 wt% of a borate-phosphate-citrate buffer (section 3.3), made with D_2O and containing about 10 wt% of tetracaine. To ensure complete equilibration of the anesthetic in the lipid bilayers, the dispersions were subjected to at least 5 freeze-thaw cycles (Kelusky & Smith, 1984). Small amounts (typically 0.01 mg) of the homogeneous dispersions resulting from the freeze-thaw cycles were then placed at room temperature, together with powdered α-quartz, in a 0.37 mm diameter hole in a 0.23 mm thick stainless steel gasket mounted on a diamond anvil cell, described in section 3.10.1.

3.9 2 Nerve systems

After dissection, nerves were soaked for two hours in physiological solutions made with D_2O in the absence and in the presence of the local anesthetic (1% tetracaine). The composition of the physiological solutions in millimoles per liter were the following: (a)

Loke's solution for the frog sciatic nerve: NaCl, 154; KCl, 5.6; $CaCl_2$, 2.2; $MgCl_2$, 1; dextrose, 5; Tris, 8 (pH 7.4); (b) artificial sea water for the lobster nerve: NaCl, 400; $CaCl_2$, 11; $MgCl_2$, 55; Tris, 5 (pH 7.4) (Pézolet & Georgescauld, 1985).

3.10 High-pressure Fourier transform infrared spectroscopy

3.10.1 The diamond anvil cell

To obtain infrared spectra at high pressure, a high-pressure optical cell and its optical link to the spectrophotometer are required. The high-pressure optical device is an opposed anvil cell, which is schematically shown in Figure 3.1. Samples are placed in the hole of the gasket (diameter = 0.3 mm) between the parallel faces of two opposed anvils and are pressurized when the two opposed anvils are pushed toward each other. The most common material for anvils is diamond due to its hardness. For infrared and far infrared measurements, type IIa diamond is commonly used.

3.10.2 Spectral acquisition

Infrared spectra were measured at 28°C on a Bomem model DA3.02 Fourier transform spectrophotometer with a liquid nitrogen-cooled mercury cadmium telluride detector. The infrared beam was condensed by a sodium chloride lens system onto the diamond anvil cell. For each spectrum, 512 scans were co-added, at a spectral resolution of

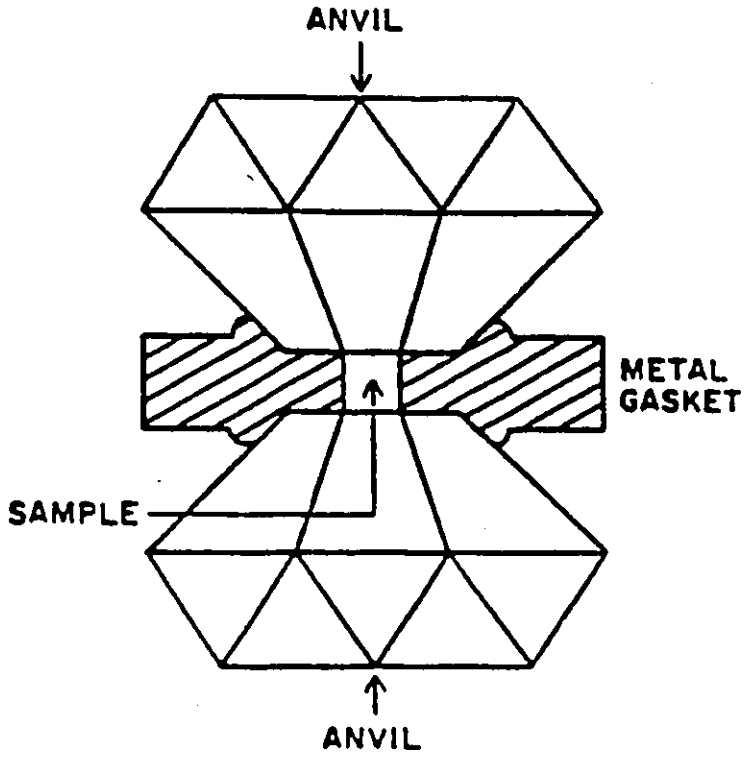

Figure 3.1 The diamond anvil cell.

4 cm^{-1} (corresponding to a total measuring time/spectrum of about 10 min).

3.10.3 Pressure calibration

Pressures were determined from the 695 cm^{-1} phonon band of α-quartz (Wong et al., 1985). The frequency of this band was obtained from third-order derivative spectra (section 3.10.4) using a breakpoint of 0.3 in the Fourier domain, and pressures were calculated according to the equation:

$$P = 1.2062\,\Delta\upsilon + 0.015164\,\Delta\upsilon^2 \qquad (3.7)$$

where $\Delta\upsilon$ is the difference in the frequency of the α-quartz band at atmospheric pressure ($\upsilon \approx 695.2$ cm^{-1}) and its frequency at a given pressure P.

3.10.4 Data reduction techniques

In order to separate unresolvable infrared band contours, Fourier derivation techniques (Moffatt et al., 1986; Mantsch et al., 1988) were applied. Frequencies associated with the methylene scissoring and rocking modes were obtained from third order derivative spectra, using a breakpoint of 0.95 in the Fourier domain. Frequencies associated with carbonyl and carboxylate stretching bands were obtained from third order derivative spectra, using a breakpoint of 0.3 in the Fourier domain.

PART TWO: ^{2}H NMR STUDIES OF ANESTHETIC-LIPID INTERACTIONS

CHAPTER 4

Interactions of tetracaine with phosphatidylcholine and cholesterol bilayers

4.1 Introduction

The location of the local anesthetic tetracaine in model membranes of phospholipids and its effects on the order and dynamics of the lipids have been the subject of several studies. Results obtained by ^2H NMR suggest that tetracaine interacts differently with different phospholipids such as phosphatidylcholine (PC), phosphatidylethanolamine (PE), and phosphatidylserine (PS), depending mostly on the charge and the shape of the lipid studied (Smith & Butler, 1985). Moreover, it has been shown that the charged and uncharged forms of the anesthetic have different partition coefficients in the lipid bilayer. In PC and PE bilayers, the uncharged form is more lipid-soluble due to hydrophobic interactions between the anesthetic and the lipid molecules (Kelusky & Smith, 1983, 1984). For PS, which is negatively charged at the pH studied, the charged form of the anesthetic is more soluble in the lipid bilayer due to electrostatic interactions between the two opposite charges (Kelusky et al., 1986).

However, most plasma membranes, especially most excitable plasma membranes, contain a relatively large amount of cholesterol. For example, the cholesterol concentration of the excitable membranes of the garfish (*Lepisosteus osseus*) olfactory

nerve is about 27% of the total lipids (Chacko et al., 1976). In the plasma membranes of nerve-ending particles (synaptosomes), the cholesterol concentration is about 29% of the total lipids (Breckenridge et al., 1972). Moreover, it has been shown that cholesterol acts as a regulatory agent with respect to the amplitude of the C-^{2}H angular fluctuations of the lipid fatty acyl chains: it orders the lipid above the transition temperature (T_c) and disorders it below T_c (Dufourc et al., 1984b). In this study, the interactions of the local anesthetic tetracaine with phosphatidylcholine membranes containing a physiological concentration of cholesterol have been investigated by ^{2}H NMR spectroscopy from the anesthetic, the lipid and the cholesterol points of view.

4.2 Review of theoretical background

For lipids in lamellar liquid-crystalline phases, in which the bilayer normal is an axis of motional averaging, the ^{2}H NMR spectra of C-^{2}H fragments often have the shape corresponding to axially symmetric motion. In this case, the quadrupolar splitting, $\Delta\upsilon_Q$, between the peaks of the powder spectrum is related th the orientation order parameter, S_{CD}, according to Seelig (1977):

$$\Delta\upsilon_Q = (3/4)\, A_Q\, S_{CD} \qquad (4.1)$$

The static deuterium quadrupolar coupling constant, $A_Q = e^2qQ/h$ is 170 kHz for aliphatic C-^{2}H bonds (Burnett & Muller, 1971). Assuming axially symmetric motions of a given molecular subunit of the lipid, the S_{CD} order parameter can be separated according to Seelig (1977) and Dufourc et al. (1983):

$$S_{CD} = \frac{3\cos^2\gamma - 1}{2} \frac{3\cos^2\beta - 1}{2} = S_\gamma S_\beta \qquad (4.2)$$

where S_β relates the average orientation of a given C-^{2}H bond of the subunit with respect to the axis of motional averaging and S_γ monitors the angular fluctuations of the axis of motional averaging of the subunit with respect to the main axis of motion (usually the bilayer normal). In the present study, the segmental order parameter S_γ will be referred to as S_{mol}. For a highly ordered environment, S_{mol} is 1, and it decreases to 0 for an isotropic environment.

4.3 Partition coefficients

The partition coefficient K_p is the ratio of the anesthetic concentration in the lipid phase to that in the buffer (expressed in grams of anesthetic per gram of each phase). The measured partition coefficients of tetracaine between DMPC/cholesterol (7:3, molar ratio) and the buffer at pH 5.5 and 9.5 are 8 and 110, respectively. For pure DMPC and egg PC bilayers (Boulanger et al., 1980), the partition coefficients are 21 and 22 at pH 5.5, respectively, and 200 and 600 at pH 9.5, respectively. For PC bilayers with and without cholesterol, the higher partition coefficients at pH 9.5 reflect the strong hydrophobic interactions between the primarily uncharged tetracaine and the hydrocarbon region of the lipids. For the cholesterol-containing systems, the smaller partition coefficients at both pH values indicate that cholesterol, which increases the order of the lipid acyl chains at temperatures above that of the gel to liquid-crystalline phase transition, T_c, decreases the solubility of tetracaine in the bilayer. These smaller K_p values are closer, however, to those

found for tetracaine partitioned in bovine spinal cord and in nerves from the walking legs if lobster ($K_p \approx$ 40 and 55, respectively).

4.4 ^{2}H NMR of specifically deuteriated tetracaines

4.4.1 The order parameter approach

The ^{2}H NMR spectra for [$^2H_2$]TTC and [$^2H_3$]TTC (Figure 4.1) in multilamellar dispersions of DMPC/cholesterol (7:3, molar ratio) at pH 9.5 are shown in Figure 4.2. At high temperature, the spectra are characterized by a superposition of a quadrupolar pattern resulting from tetracaine in the bilayer and the narrow line from tetracaine in solution. These spectra are characteristic of axially symmetric motions, and the quadrupolar splittings can be obtained from the dePaked spectra. However, at low temperature, the lineshapes for the spectra of both [$^2H_2$]TTC and [$^2H_3$]TTC do not reflect axial symmetry. This can result from several possibilities, such as axially asymmetric motions, or from an intermediate exchange between tetracaine in solution and tetracaine in the bilayer (exchange rate comparable to the difference in the quadrupolar splittings). However, the spectra do not show a pulse spacing dependence for τ values from 40 to 300 μs in the quadrupolar echo sequence, indicating that the exchange between tetracaine in solution and in the bilayer is not intermediate (Wittebort et al., 1987). The dynamics of tetracaine in DMPC/cholesterol bilayers will be further discussed in section 4.4.2

Quadrupolar splittings for the spectra at low temperature have been estimated

TETRACAINE (TTC)

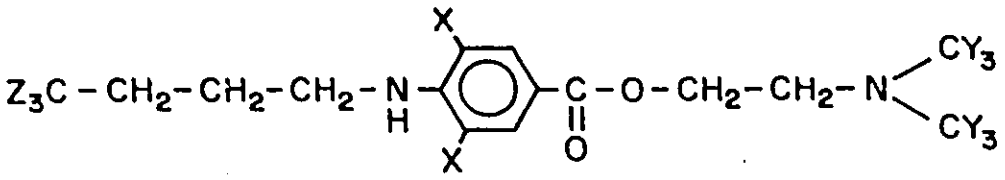

TTC–$^2H_2$: X=^{2}H, Y= H, Z= H

TTC–$^2H_3$: X= H, Y= H, Z=^{2}H

TTC–$^2H_6$: X= H, Y=^{2}H, Z= H

Figure 4.1 Structure of the specifically deuteriated tetracaines.

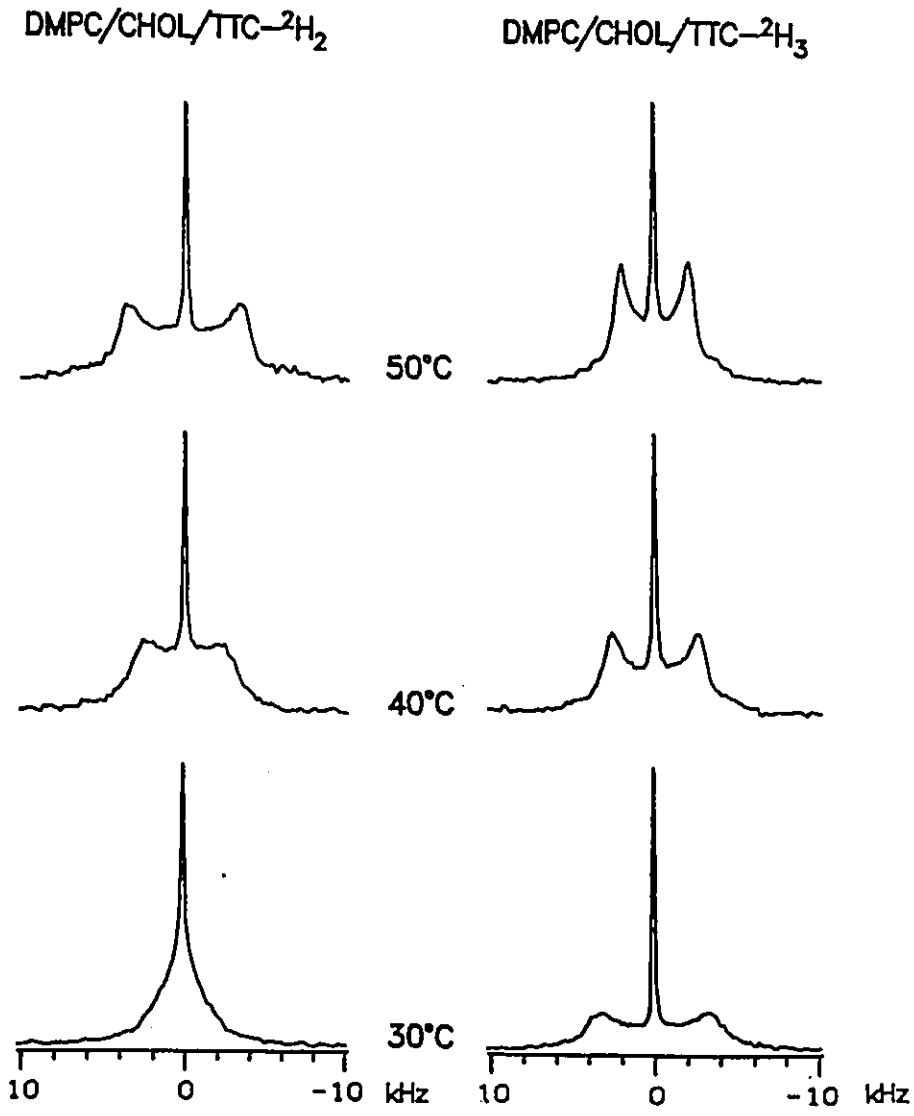

Figure 4.2 Temperature dependence of ^2H NMR spectra of [$^2H_2$]TTC and [$^2H_3$]TTC in multilamellar dispersions of DMPC/cholesterol (7:3, molar ratio), pH 9.5.

from the simulated spectra. Spectral simulations were done using a narrow central resonance and a quadrupolar pattern. From these spectral simulations, it appeared that the intensity of the central resonance needed to reproduce the experimental spectra is too large to result only from tetracaine in the surrounding buffer, according to the partition coefficients (*vide supra*). However, because of the different spin-lattice relaxation times (T_{1Z}) for the isotropic peak and the quadrupolar pattern (about 30 and 4 ms, respectively, at 30°C), we have been able to use partially relaxed spectra of [$^2H_2$]TTC in DMPC/cholesterol bilayers at pH 9.5 (Figure 4.3) to determine that the intensity of the isotropic peak is about 10% of the total spectrum, which corresponds to the amount of tetracaine in solution, as predicted by the partition coefficient.

The temperature dependence of the quadrupolar splittings observed at pH 5.5 and 9.5 for [$^2H_2$]TTC in DMPC/cholesterol (7:3, molar ratio), is illustrated in Figure 4.4. The quadrupolar splittings for [$^2H_2$]TTC at pH 9.5 in pure DMPC bilayers are also shown. The quadrupolar splittings observed at both pH values in cholesterol-containing system are relatively small and *increase* with an increase of temperature. For pure DMPC bilayers at pH 9.5, the quadrupolar splittings are much larger and *decrease* slightly with an increase of temperature. The decrease of the quadrupolar splittings for the cholesterol-containing system can be related to a change in the orientational order parameter S_{CD}, according to equation 4.1. In order to get such a change, two possibilities must be considered. The first implies a change in the angle β between the C-^{2}H bond and the axis of motional averaging. Since the portion of the tetracaine molecule from the ester carbonyl to the *p*-amino group is essentially rigid, only one quadrupolar splitting is observed for [$^2H_2$]TTC in both systems, which confirms that the angle between the C-^{2}H bond and the axis of motional averaging is equivalent for both deuterons (Boulanger et al., 1980; Johanson & Lindblom,

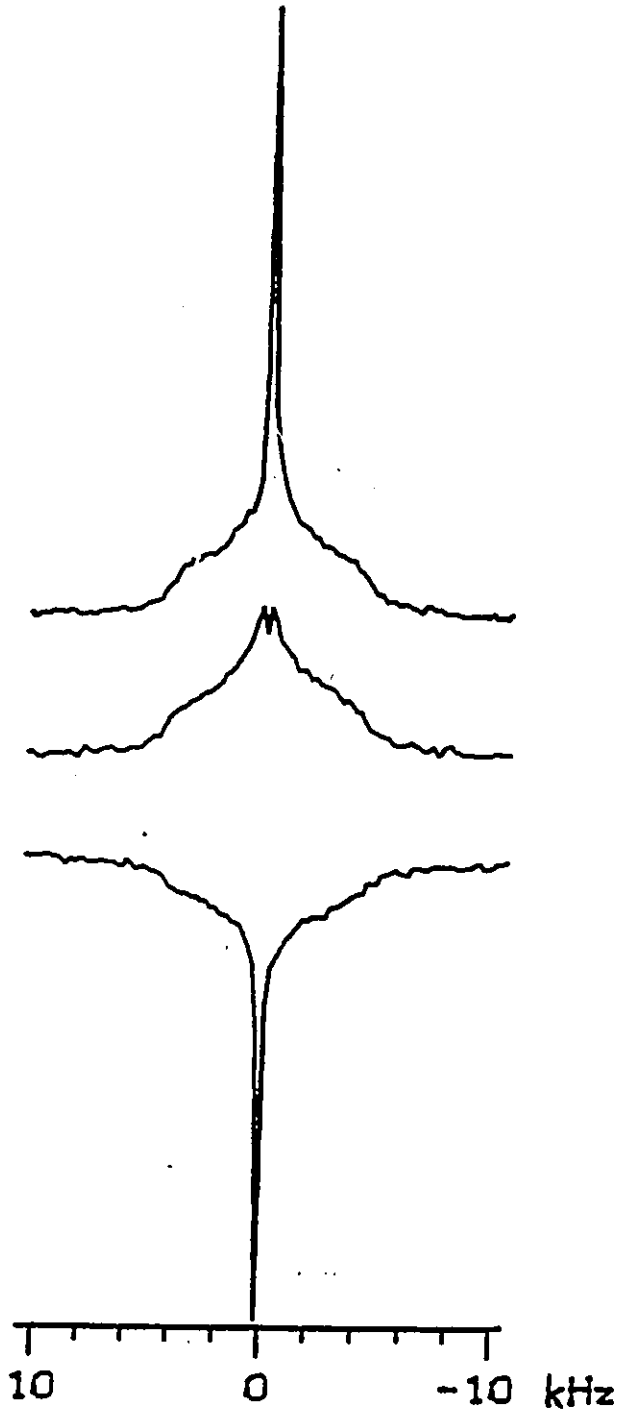

Figure 4.3 ^2H NMR spectra of [$^2H_2$]TTC in DMPC/cholesterol bilayers at pH 9.5, 30°C, as a function of T in the inversion recovery sequence.

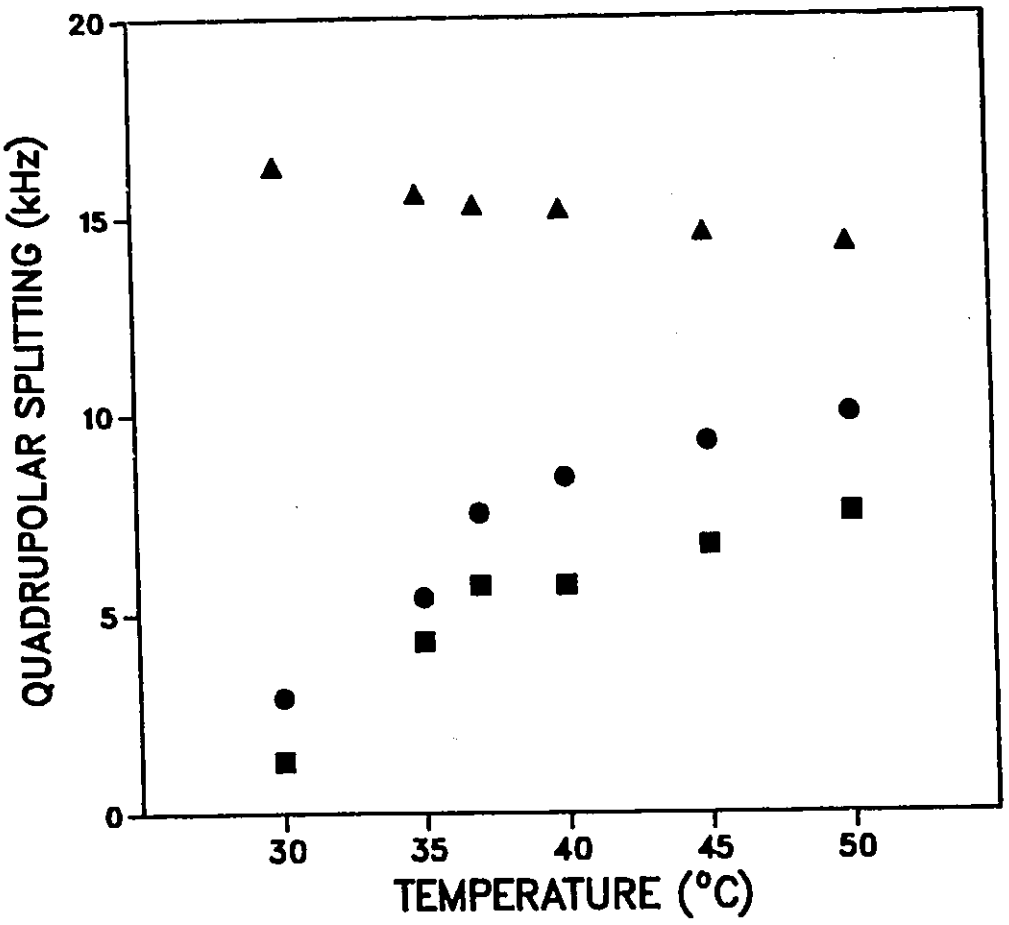

Figure 4.4 Temperature dependence of the quadrupolar splittings for $[^2H_2]$TTC in multilamellar dispersions of (▲) DMPC, pH 9.5, (●) DMPC/cholesterol (7;3. molar ratio), pH 5.5, and (■) DMPC/cholesterol (7:3, molar ratio) pH 9.5.

1981). A reduction in the quadrupolar splittings for [$^2H_2$]TTC in these systems can then be interpreted in terms of a reduction of the segmental order parameter S_{mol}. For physical reasons, it seems reasonable to assume that the axis of motional averaging for tetracaine in lipid bilayers passes through or near the 1,4 direction of the aromatic ring. This assumption has also been made in previous studies on the interaction of tetracaine with different phospholipid bilayers (Boulanger et al., 1980; Kelusky et al., 1986; Kelusky & Smith, 1983, 1984). By making this assumption, we can compare relative order parameter values for the different systems studied. The angle β of equation 4.2 is 120°, and if the static quadrupolar coupling constant is set to 176 kHz (Barnes, 1974), then a combination of equations 4.1 and 4.2 can be rearranged to give:

$$S_{mol} = (0.061)\,\Delta\upsilon_Q \qquad (4.3)$$

where $\Delta\upsilon_Q$ is in kilohertz.

For [$^2H_2$]TTC in pure DMPC bilayers at pH 9.5, the values of S_{mol} calculated according to equation 4.3 vary from 1.00 to 0.86 for temperatures from 30 to 50°C, respectively. These values are very large in part because of the rigid nature of the TTC aromatic ring but are also higher than the value of 0.93 obtained for [$^2H_2$]TTC in egg PC at pH 9.5 (Kelusky & Smith, 1984). This can be explained by the higher degree of saturation of the DMPC acyl chains compared to egg PC. However, for [$^2H_2$]TTC in cholesterol-containing DMPC bilayers, the values of S_{mol} vary from 0.18 to 0.61 at pH 5.5 for temperatures from 30 to 50°C, respectively, and from 0.17 to 0.48 at pH9.5 for the same temperature range. The values at low temperature (30°C) are much smaller than those obtained for all the phospholipids previously studied (Kelusky & Smith, 1983; Kelusky et

al., 1986), which suggests that this portion of the tetracaine molecule is in a less ordered environment in the cholesterol-containing systems. Moreover, an increase of temperature for these systems induces a change in the environment of the aromatic ring of tetracaine, resulting in increased order. These results may be rationalized as follows. At low temperature, the lipid acyl chains are highly ordered in the cholesterol-containing DMPC bilayers (*vide infra*) and thus exclude the tetracaine molecule from the hydrophobic region to one near the aqueous interface. An increase in temperature, which decreases the order of the lipid acyl chains (*vide infra*), would then allow a deeper penetration of the anesthetic in the bilayer, where the aromatic ring of tetracaine would be located closer to the ordered plateau region of the lipid bilayer. According to this hypothesis, comparison of the results at pH 5.5 and 9.5 for [$^2H_2$]TTC in DMPC/cholesterol bilayers suggests that the positively charged form of the anesthetic at pH 5.5 is located slightly deeper in the bilayer than the uncharged form, probably because of electrostatic interaction between the phospholipid head group and the anesthetic dimethylammonium moieties.

In order to confirm these results obtained with [$^2H_2$]TTC, we have monitored the ^2H NMR spectra of [$^2H_3$]TTC in DMPC bilayers in the presence and absence of cholesterol as a function of temperature, from 30 to 50°C. Figure 4.2 displays the ^2H NMR spectra for [$^2H_3$]TTC in the DMPC/cholesterol (7:3, molar ratio) system at pH 9.5 for three temperatures, from 30 to 50°C. The temperature dependence of the quadrupolar splittings observed at pH 5.5 and 9.5 for [$^2H_3$]TTC in this system is also illustrated in Figure 4.5. At both pH values, the quadrupolar splittings are relatively large and decrease with an increase of temperature. For pure PC bilayers at both pH values, no quadrupolar splittings are observed for [$^2H_3$]TTC (Boulanger et al., 1981; Kelusky & Smith, 1984). According to the model proposed by Boulanger et al. (1981) (Figure 1.4), the terminal

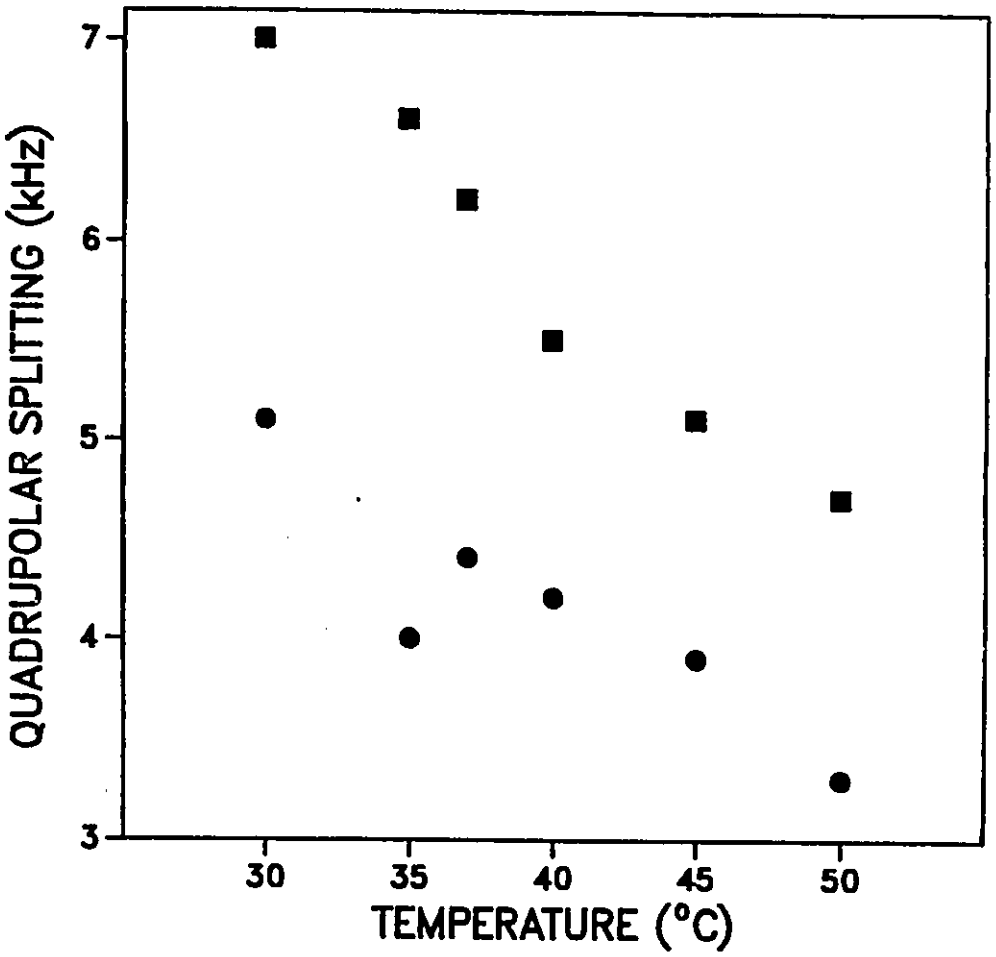

Figure 4.5 Temperature dependence of the quadrupolar splittings for [$^2H_3$]TTC in multilamellar dispersions of (●) DMPC/cholesterol (7:3. molar ratio), pH 5.5 and (■) pH 9.5.

methyl group of the anesthetic would be located close to the plateau region of the lipid bilayer. For the cholesterol-containing system, the plateau region is more ordered (*vide infra*), which could explain the larger quadrupolar splittings obtained for $[^2H_3]$TTC. Moreover, the large decrease in the quadrupolar splittings with increasing temperature suggests a change to a less ordered environment of the terminal methyl group of TTC. This can be explained by a tetracaine molecule sitting higher in the cholesterol-containing bilayers, for which an increase of temperature results in a deeper penetration of the anesthetic in the bilayer into the hydrophobic region which is below the plateau in acyl chain order.

Since the terminal methyl group of tetracaine is in the acyl chain region of the lipid bilayer, an estimate of the molecular order parameter S_{mol} would be of interest. This parameter (S_{mol}) has been calculated by using:

$$S_{mol} = S_{CD}\,[1/2(3\cos^2 109.5-1)]\,[1/2(3\cos^2 35.25-1)] \times [1/2(3\cos^2 24.75-1)] = 8.15S_{CD} \qquad (4.4)$$

according to the convention of Stockton et al. (1976). Values of the S_{CD} can be found from equation 4.1. The values of S_{mol} for $[^2H_3]$TTC calculated from equation 4.4 vary from 0.35 to 0.21 at pH 5.5 for temperatures from 30 to 50°C, respectively, and from 0.44 to 0.29 at pH 9.5 for the same temperature range. The relatively large S_{mol} values reflect the constrained environment of the terminal methyl group of the tetracaine molecule in DMPC/cholesterol bilayers. This confirms that the anesthetic is located higher in cholesterol-containing PC bilayers. The differences in the S_{mol} values for the two pH values also confirm that the charged form of the molecule at pH 5.5 is located slightly

deeper in DMPC/cholesterol bilayers than its uncharged form at pH 9.5.

The values of the quadrupolar splittings obtained for [$^2H_6$]TTC in egg PC and DMPC/cholesterol (7:3, molar ratio) at pH 5.5 and 9.5 are summarized in Table 4.1, together with those obtained in spinal cord at pH 7.0 (Smith & Butler, 1985). These values are very small and are essentially independent of the systems studied. This suggests that there is no significant change in the average orientation of this portion of the tetracaine molecule in PC bilayers in the presence and absence of cholesterol.

The differences in the location of the charged and uncharged form of tetracaine in DMPC bilayers in the presence and absence of cholesterol have been confirmed by high-pressure FT-IR studies on these systems (Auger et al., 1987, 1988b), as discussed in chapters 6 and 7 of this thesis. These studies demonstrate that the local anesthetic is located close to the aqueous interface of the lipid bilayer in cholesterol-containing DMPC bilayers and that in pure DMPC bilayers, the uncharged form of the anesthetic intercalates more deeply than the charged form.

4.4.2 Lineshape and spin-lattice relaxation analysis

As discussed in the previous section, axially asymmetric lineshapes are observed for [$^2H_2$]TTC partitioned into DMPC/cholesterol (7:3, molar ratio) multilamellar dispersions at 30°C. This is best illustrated in the partially relaxed spin-lattice relaxation spectrum (T=20 ms) shown in Figure 4.3. It is interesting to note that similar lineshapes have been obtained for [$^2H_2$]TTC partitioned into the unmyelinated nerve of the lobster walking leg

Table 4.1

Quadrupolar splittings (kHz) for [$^2H_6$]TTC in different systems

	pH	$\Delta\upsilon_Q$
egg PC	5.5	1.8
	9.5	0.0
DMPC/chol (7:3)	5.5	1.4
	9.5	0.8
spinal cord	7.0	1.5

and into other biological membranes, such as *A. laidlawii* and human erythrocytes membranes (Kelusky, 1983). An example is shown in Figure 4.6. It is therefore of interest to try to describe these lineshapes in terms of specific motional models, which could lead to more information on the system dynamics compared to the information obtained from the order parameter analysis.

Observation of axially asymmetric spectra requires that the motions giving rise to such spectra have two fold or lower symmetry (Griffin, 1981). A two-fold flip of the tetracaine aromatic ring could produce such axially asymmetric lineshapes. Such two-fold aromatic ring flips have been widely observed for amino acids in proteins (Griffin et al., 1988; Frey et al., 1985; Gall et al., 1981). Using a lineshape simulation program developed by Wittebort et al. (1987) based on the general formalism of Torchia and Szabo (1982), the [$^2H_2$]TTC powder spectrum was simulated using a composite six-site jump model including a whole molecule axial motion modelled by an equally populated three-site jump and a two-site ring flip. The C-^{2}H bonds of the aromatic ring are oriented at 120° with respect to the axis of motional averaging. The relative rates of the two motions were varied in order to obtain the best fit. The lineshape was best simulated using an axial motional rate k_{axial} of 5×10^6 rad s^{-1} and a two-site jump rate k_{jump} of 5×10^8 rad s^{-1} (Figure 4.7). The spectral lineshapes were found to be very sensitive to changes in the axial motional rate while increasing the two-site jump rate above 5×10^8 rad s^{-1} results in no further change in the lineshape. It is important to notice that the experimental powder spectrum is slightly narrower than the simulated spectrum, which may be due to off-axis motions ("wobbling") that have not been taken into account in the simulations.

We have also measured the ^{2}H NMR spectra of oriented multibilayers (Jarrell et

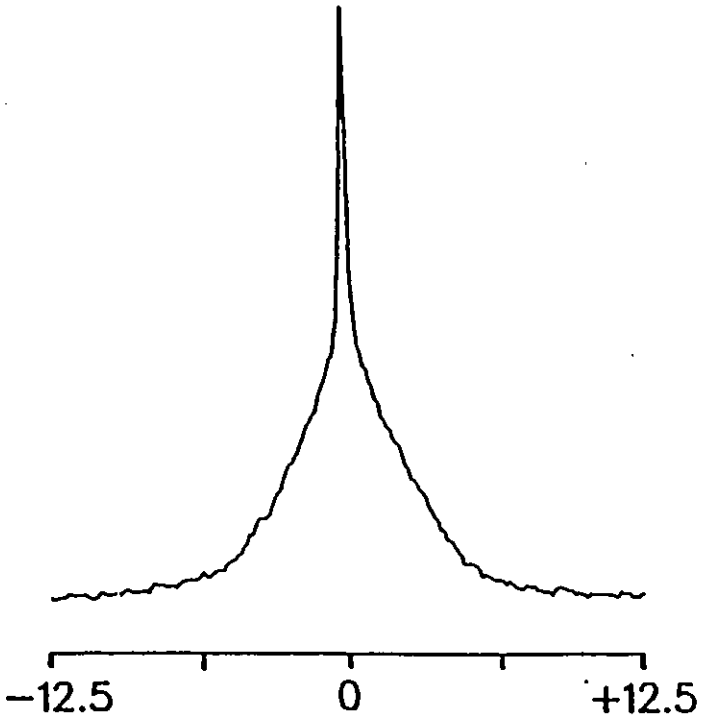

Figure 4.6 ^{2}H NMR spectrum of [$^{2}H_{2}$]TTC incorporated into human erythrocytes (from Kelusky, 1983).

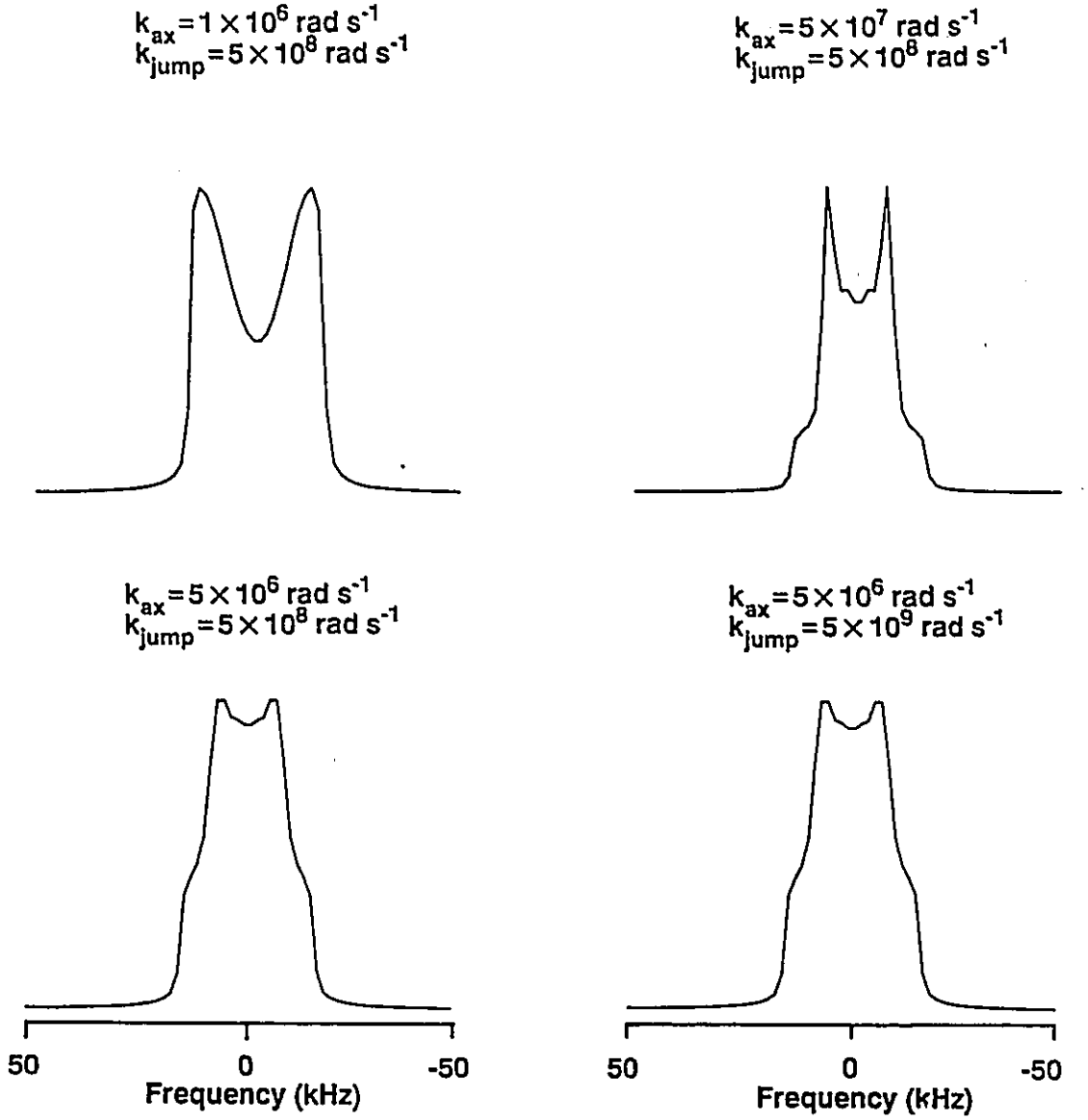

Figure 4.7 Simulated powder spectrum of [$^2H_2$]TTC incorporated into DMPC/cholesterol bilayers, 30°C, pH 9.5. Simulations were performed using a composite six-site jump model including a whole molecule axial motion modelled by an equally populated three-site jump (with rate k_{axial}) and a two-site ring flip (with rate k_{jump}). The C-^{2}H bonds of the aromatic ring are oriented at 120° with respect to the axis of motional averaging.

al., 1987a) of DMPC/cholesterol + [$^2H_2$]TTC as a function of the angle θ between the normal to the glass plates and the magnetic field direction (Figure 4.8). The 0° orientation corresponds to the plane of the glass plates orthogonal to the magnetic field direction. The ^{31}P NMR spectra (Figure 4.9) of the oriented multibilayer samples clearly confirm the orientation of the lipids between the glass plates. The angular dependence of the ^2H NMR spectra of oriented multibilayers of DMPC/cholesterol + [$^2H_2$]TTC differs considerably from that observed for samples giving axially symmetric powder patterns (Jarrell et al., 1987a; chapter 8 of this thesis). Moreover, this angular dependence does not seem to follow that predicted by equation 2.16 for different values of the asymmetry parameter η (simulations not shown). Using a modified version of the lineshape simulation program previously used for the [$^2H_2$]TTC powder spectra, the oriented-sample spectral lineshapes were also simulated using the six-site jump model described above (Figure 4.10). The results indicate that, as was observed for the powder lineshape, the simulated spectra are relatively similar to those observed experimentally, although slightly wider.

So far, we have demonstrated that both the powder and oriented-sample lineshapes of [$^2H_2$]TTC incorporated into DMPC/cholesterol bilayers at 30°C can be relatively well simulated using a combine six-site jump model involving a whole molecule axial motion and a two-site ring flip. However, since the two-site motion appears to be in the fast limit relative to the ^2H NMR lineshape time scale, a unique correlation time τ_c for this motion could not be obtained solely from the spectral lineshape simulations. In such cases, spin-lattice relaxation may provide a way of distinguishing between motional models. For phospholipids in the liquid-crystalline phase, where correlation times for C-^2H motions are shorter than 10^{-7} s, molecular dynamics has been widely studied by ^2H spin-lattice relaxation (Brown, 1982; Brown & Davis, 1981; Brown et al; 1983). Moreover, the

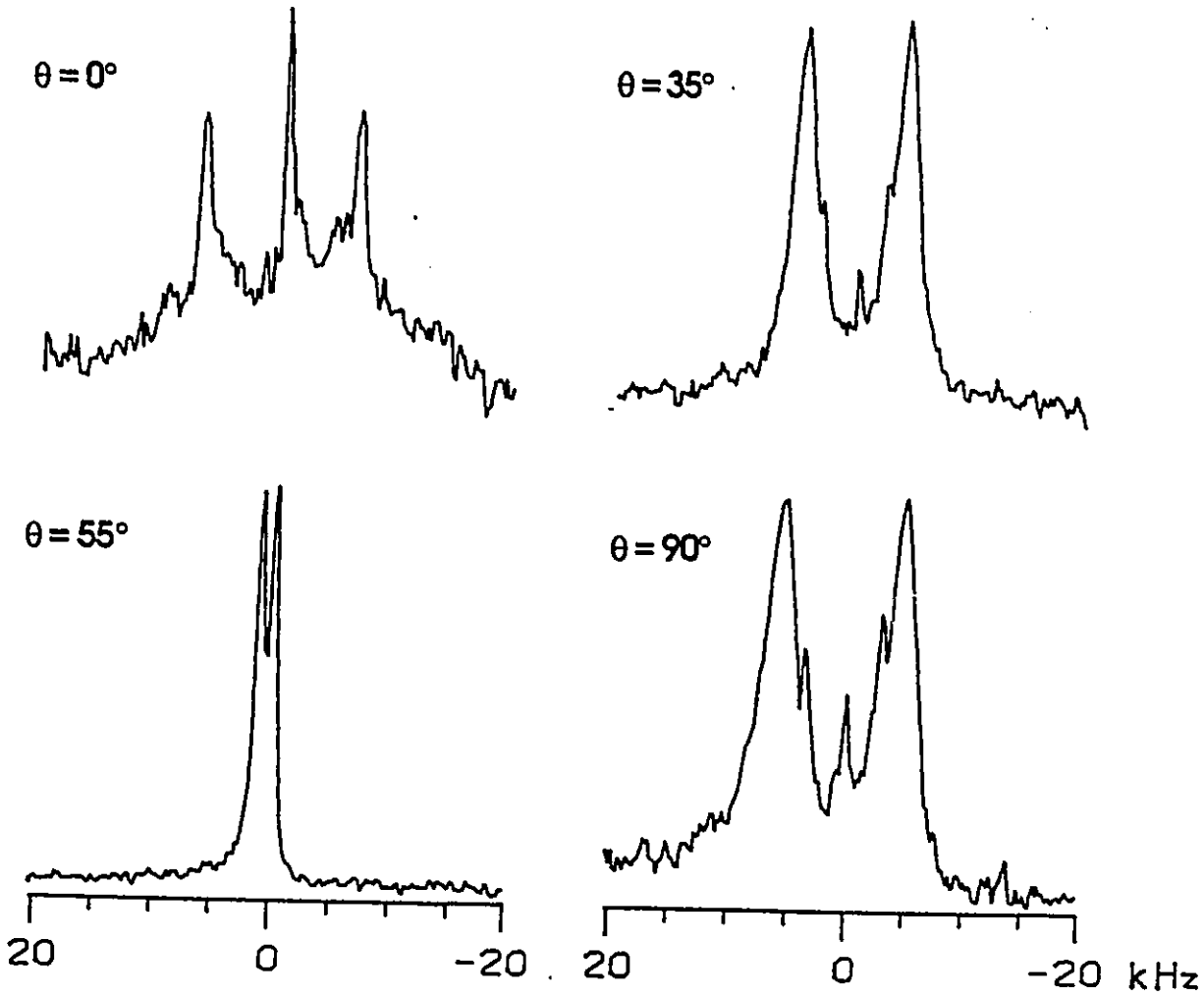

Figure 4.8 ^2H NMR spectra (30.7 MHz) of oriented multibilayers of DMPC/cholesterol + [$^2H_2$]TTC at 30°C as a function of the angle θ between the normal to the glass plates and the magnetic field direction. The 0° orientation corresponds to a parallel orientation of the bilayer normal and the magnetic field direction.

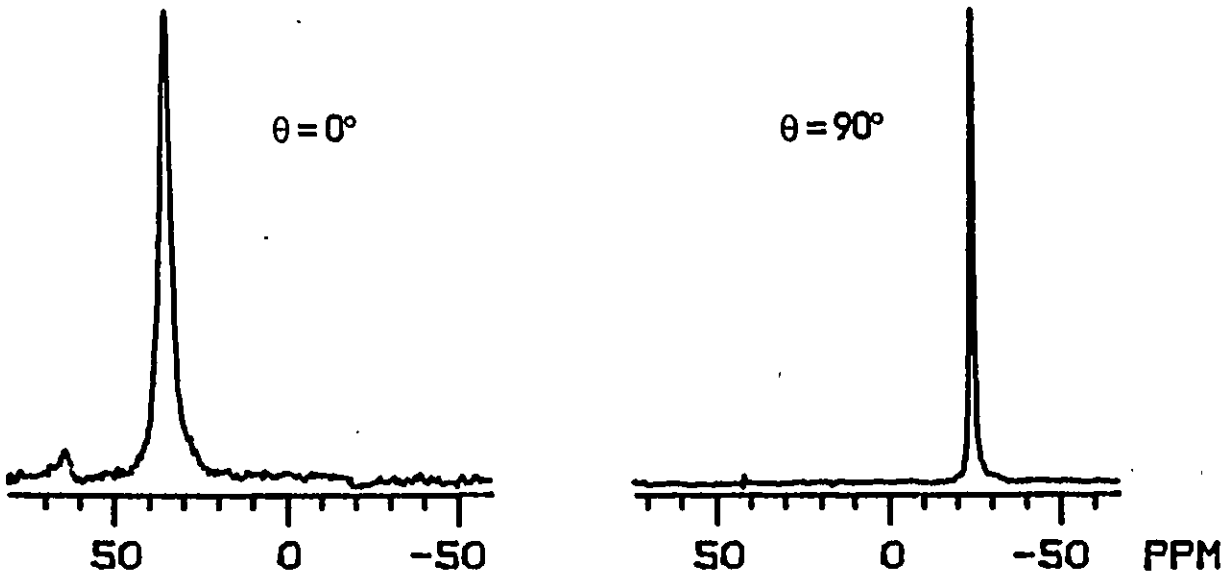

Figure 4.9 ^{31}P NMR spectra (121.5 MHz) of oriented multibilayers of DMPC/cholesterol + [$^{2}H_{2}$]TTC at 30°C as a function of the angle θ between the normal to the glass plates and the magnetic field direction. The 0° orientation corresponds to a parallel orientation of the bilayer normal and the magnetic field direction.

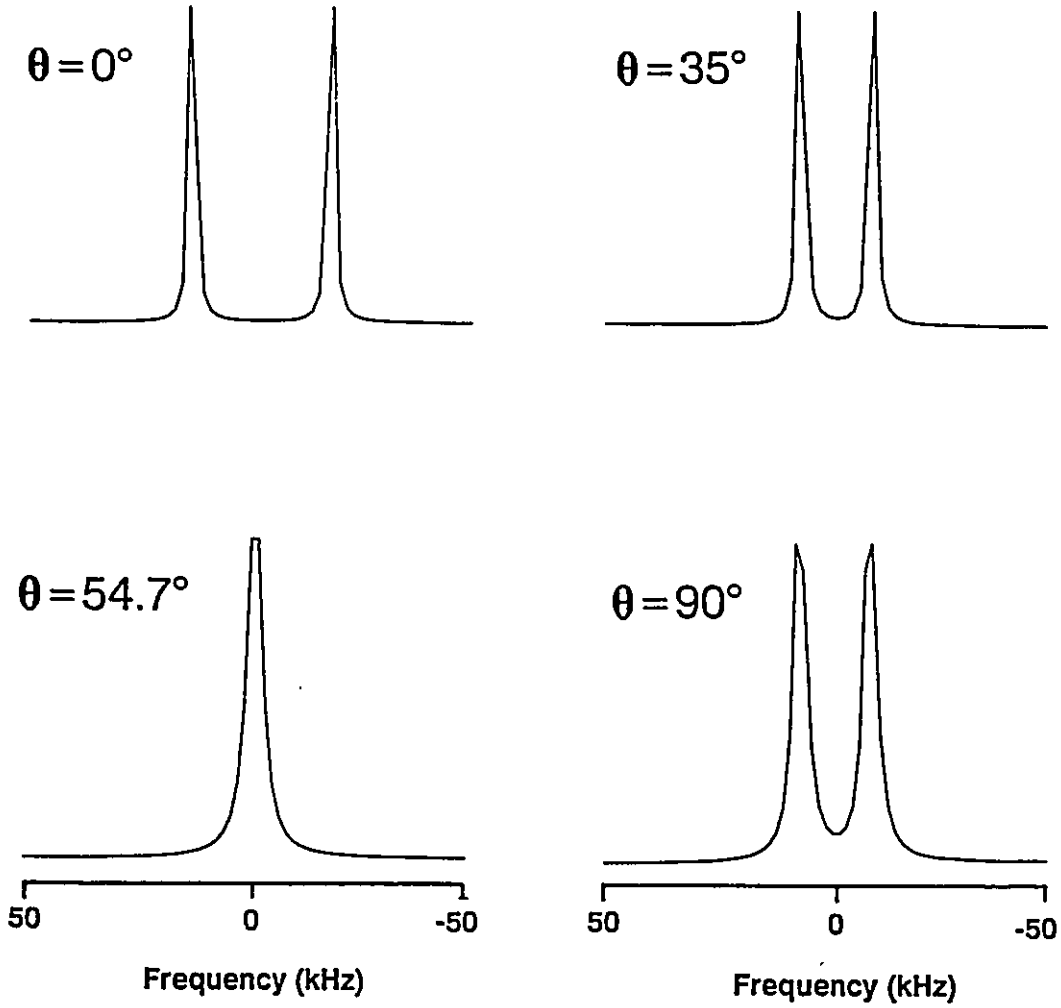

Figure 4.10 Simulated oriented-sample spectra of $[^2H_2]$TTC incorporated into DMPC/cholesterol bilayers, 30°C, pH 9.5. Simulations were performed using a composite six-site jump model including a whole molecule axial motion modelled by an equally populated three-site jump ($k_{ax}=5\times10^6$ rad s^{-1}) and a two-site ring flip ($k_{jump}=5\times10^8$ rad s^{-1}). The C-^{2}H bonds of the aromatic ring are oriented at 120° with respect to the axis of motional averaging.

measurement of orientation-dependent ^2H spin-lattice relaxation times (T_{1Z}) can be very useful in discriminating between different motional models, as discussed in more details in section 8.3.3.2. In the present study, the spin-lattice relaxation times were only measured on the multilamellar dispersions of DMPC/cholesterol + [$^2H_2$]TTC at 30°C, pH 9.5. Values of ≈ 4.5 and 30 ms were obtained for the broad and narrow components of the [$^2H_2$]TTC spectrum, respectively. The spin-lattice relaxation time obtained for tetracaine incorporated in the membrane (broad component) is very short, indicating that the correlation time(s) of the motion(s) dominating the relaxation is(are) very close to the T_1 minimum ($\omega_0\tau_c \approx 0.65$). Using the six-site motional model described above, the spin-lattice relaxation times T_{1Z} were calculated for the 0 and 90° orientations and compared with the average value obtained experimentally for the broad component of the spectrum. The relaxation time values were found to be very sensitive to the two-site jump rate and the best fit was obtained using $k_{jump}=5\times10^8$ rad s^{-1} and $k_{axial}=5\times10^6$ rad s^{-1} (T_{1Z} (0°)= 6.6 ms and T_{1Z} (90°)= 3.5 ms).

We have demonstrated in the present section that both the lineshape and relaxation features of [$^2H_2$]TTC incorporated into DMPC/cholesterol at 30°C, pH 9.5 can be relatively well simulated using a motional model including a whole molecule axial motion and a fast two-site flip of the aromatic ring. Further analysis, such as the measurement of the orientation-dependence of the spin-lattice relaxation times, as well as the oriented-sample lineshapes at different temperatures, would be necessary to confirm and most likely refine that motional model. An example of a detailed lineshape and spin-lattice relaxation analysis in glycolipid bilayers will be presented in chapter 8 of this thesis. However, the preliminary results obtained from the lineshape and relaxation analysis of [$^2H_2$]TTC incorporated into DMPC/cholesterol bilayers indicates that complementary

information to the order parameter approach can be gained from such an analysis.

4.5 ^{2}H NMR of DMPC

4.5.1 Membrane organization

The effects of the local anesthetic tetracaine on the order and the dynamics of the acyl chains of DMPC in DMPC/cholesterol (7:3, molar ratio) and in pure DMPC bilayers have been studied by using DMPC ^{2}H-labelled at positions 4 and 14 on the *sn*-2 chain, [4',4',14',14',14'-$^2H_5$]DMPC. This allows the simultaneous investigation of the effects of the anesthetic on the plateau and the tail regions of the lipid acyl chains. The ^{2}H NMR spectrum and the dePaked spectrum of [$^2H_5$]DMPC (Figure 4.11) exhibit two quadrupolar patterns. On the basis of the spectrum obtained for [4',4'-$^2H_2$]DMPC, the larger quadrupolar pattern is assigned to the 4'-deuterons (plateau region) while the smaller one is assigned to the three deuterons of the terminal methyl group (tail region). The central resonance is due to residual HDO.

For both the plateau and the tail regions, the quadrupolar splittings have been measured at 30 and 50°C for seven different systems. The influence of cholesterol on pure DMPC bilayers was first investigated and compared with previously reported results (Dufourc et al., 1984b). The effects of both the charged and uncharged forms of tetracaine on the order of the plateau and the tails regions of DMPC bilayers in the presence and absence of cholesterol have also been investigated. For the studies with the charged form of the anesthetic at pH 5.5, the same amount of tetracaine ($\approx$ 10 mg) was added to pure

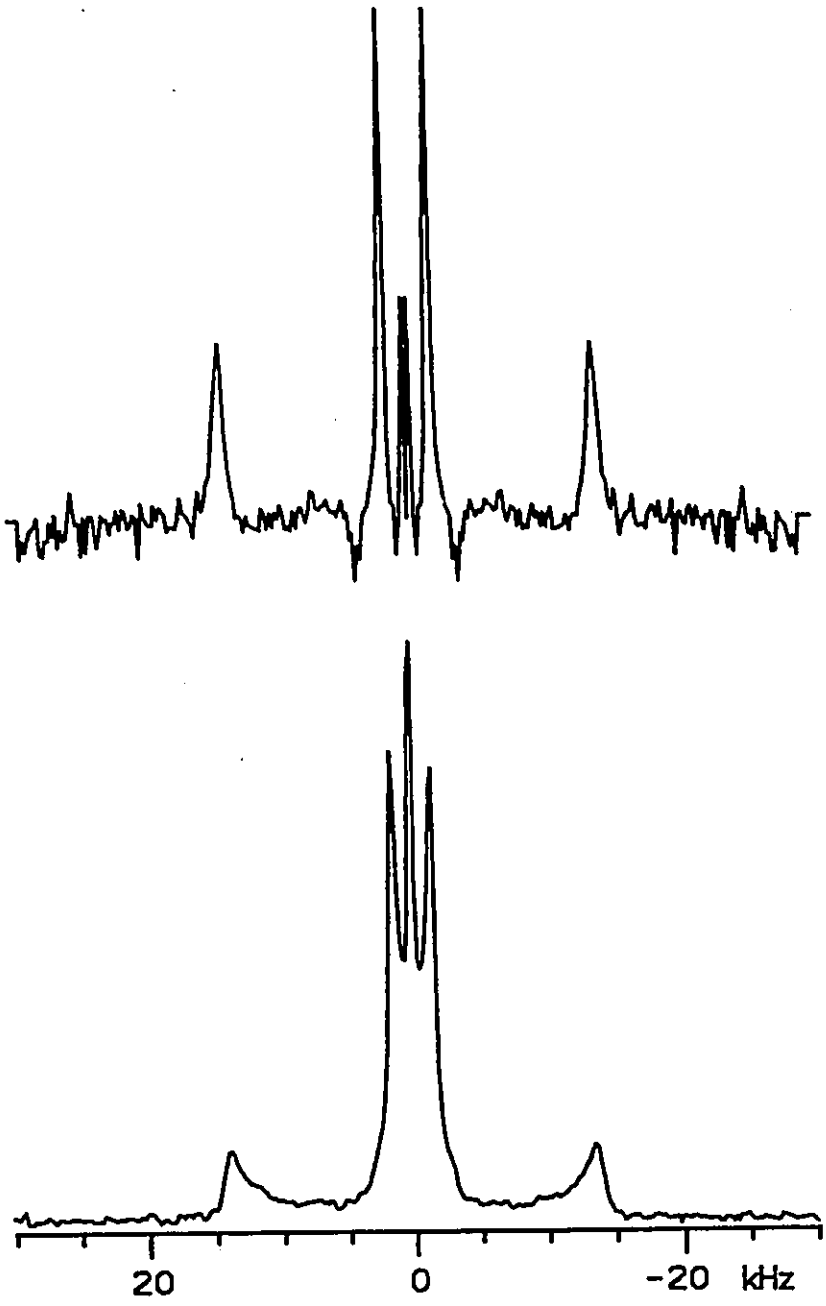

Figure 4.11 ^{2}H NMR spectrum (bottom) and dePaked spectrum (top) of [4',4',14',14',14'-$^{2}H_5$] DMPC at 30°C.

DMPC and to the cholesterol-containing DMPC bilayers. However, because of the differences in the partition coefficients of tetracaine in the two systems (*vide supra*), the experiment for the cholesterol-containing system was repeated under conditions where the equivalent amount of anesthetic was actually partitioned into the lipids. This is referred to as the (DMPC + chol + TTC +) system in Figure 4.12 and 4.13.

For DMPC deuteriated at C-4' (plateau region), the average orientation of a chain methylene C-^{2}H bond with respect to the axis of motional averaging can be taken to be 90°, i.e. the C-^{2}H bond angular reorientations are equiprobable around $\beta = 90°$ (Seelig & Niederberger, 1974). In this case, the segmental order parameter S_{mol} can be expressed as:

$$S_{mol} = -2S_{CD} \qquad (4.5)$$

where the orientational order parameter S_{CD} is calculated from the quadrupolar splitting values, according to equation 4.1. The S_{mol} values for the plateau region of DMPC in the different systems studied as shown in Figure 4.12.

Addition of cholesterol (30 mole%) to pure DMPC bilayers results in a large increase of the molecular order parameter S_{mol} although the temperature dependence remains the same. These results are in agreement with those obtained by Dufourc et al. (1984b) and have been interpreted in terms of a reduction by the cholesterol molecule of the angular fluctuations of the lipids in the plateau region. When tetracaine is added to pure DMPC bilayers at pH 5.5, the S_{mol} values for the C-4' position are reduced by about 10% at 30°C and 5% at 50°C. At pH 9.5, when tetracaine is primarily uncharged, the S_{mol} values are reduced by about 5% at 30°C but do not change at 50°C. The effect of

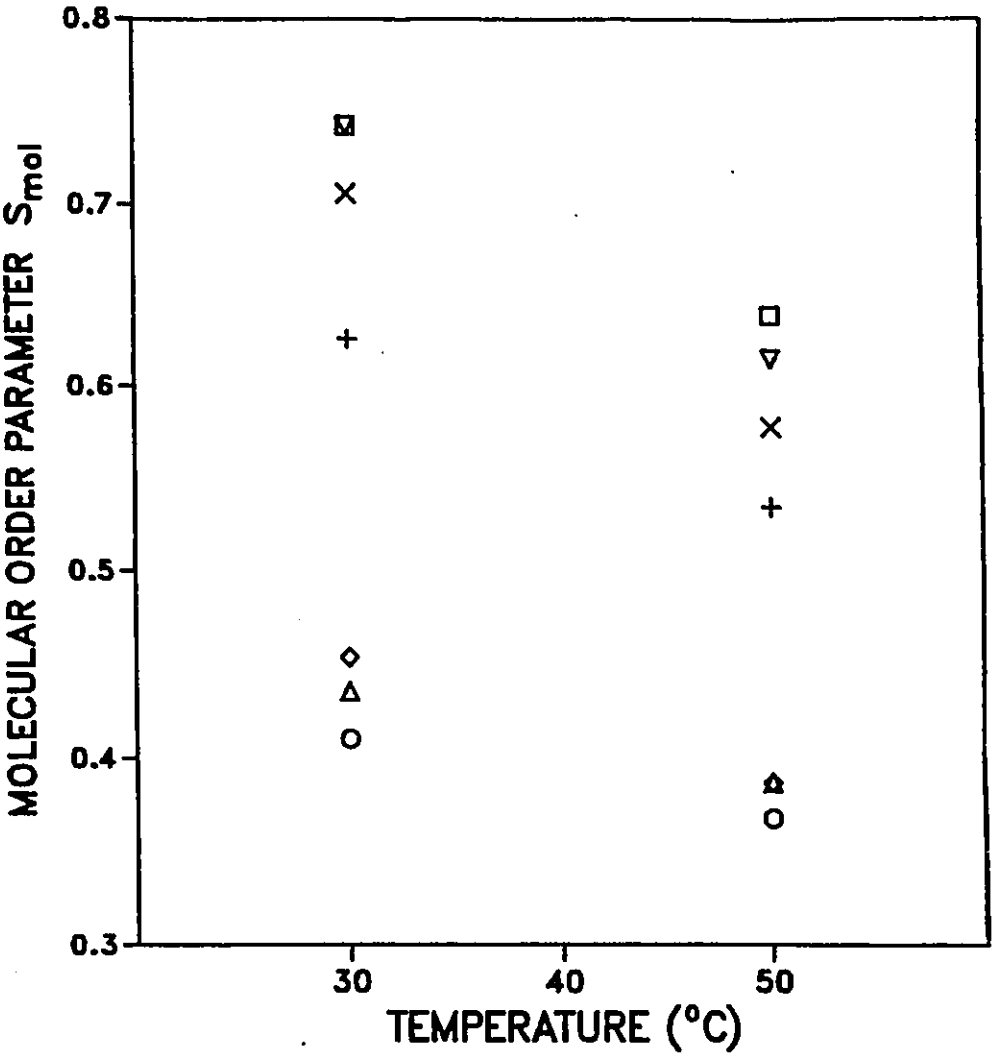

Figure 4.12 Temperature dependence of the molecular order parameter S_{mol} for (◇) [4',4',14',14',14'-$^2H_5$] DMPC (plateau region) alone and in mixtures of (□) DMPC + cholesterol, (○) DMPC + TTC, pH 5.5, (×) DMPC + cholesterol + TTC, pH 5.5, (+) DMPC + cholesterol + TTC +, pH 5.5, (△) DMPC + TTC, pH 9.5, and (▽) DMPC + cholesterol + TTC, pH 9.5.

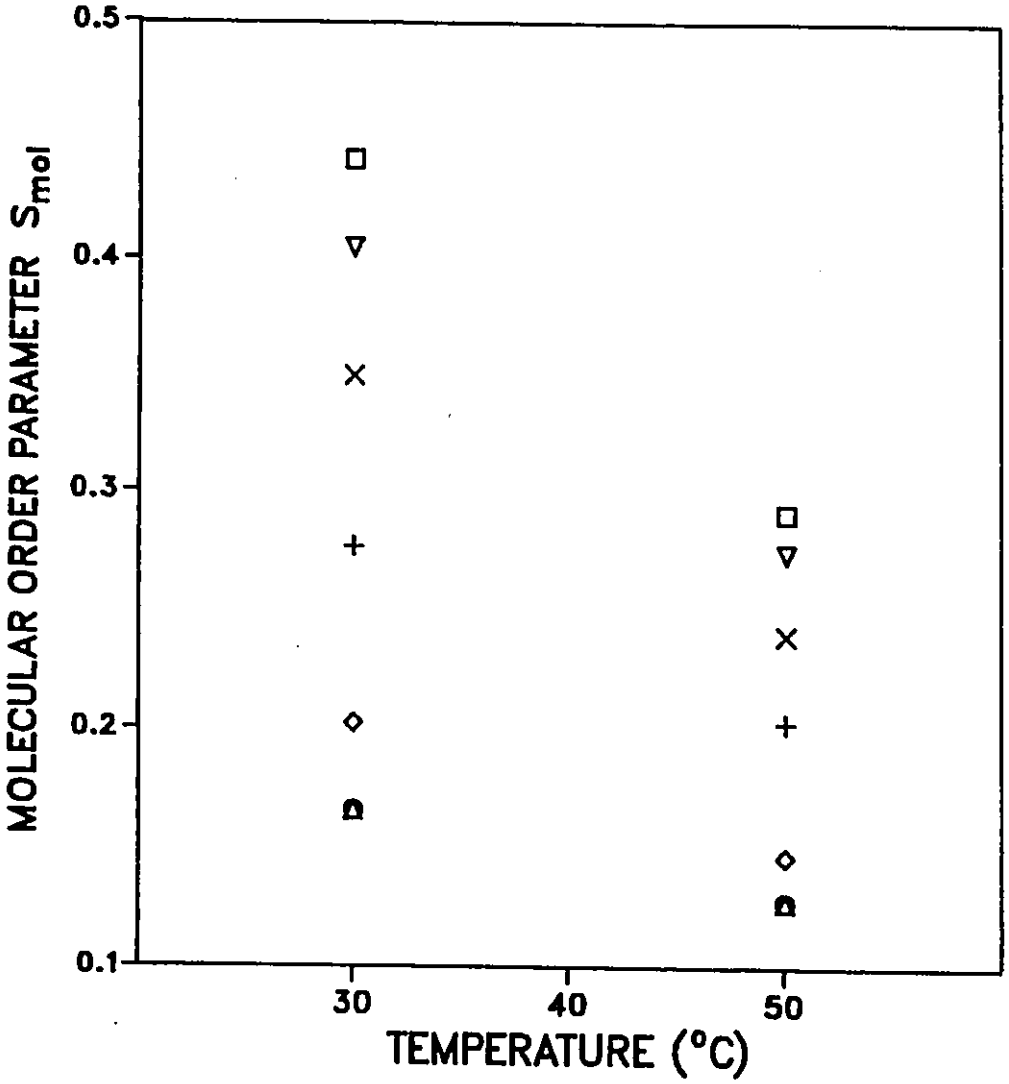

Figure 4.13 Temperature dependence of the molecular order parameter S_{mol} for (◇) [4',4',14',14',14'-$^2H_5$] DMPC (tail region) alone and in mixtures of (□) DMPC + cholesterol, (○) DMPC + TTC, pH 5.5, (×) DMPC + cholesterol + TTC, pH 5.5, (+) DMPC + cholesterol + TTC +, pH 5.5, (△) DMPC + TTC, pH 9.5, and (▽) DMPC + cholesterol + TTC, pH 9.5.

tetracaine on the acyl chain plateau region is then to increase the amplitude of motion of the C-^{2}H segment, which is reflected in a decrease of the order parameter S_{mol}. Moreover, this effect is greater for the charged form of the anesthetic. The same behavior was observed with tetracaine partitioned into deuteriated DPPC bilayers (Boulanger et al., 1981). These results can be rationalized as follows: the electrostatic interaction between the phosphate group of the phospholipid and the dimethylammonium moiety of the anesthetic leads to a higher location of the charged form of tetracaine, greater space between the phospholipid molecules, and a consequent increase in the amplitude of motions for the C-4' position of the acyl chains. At high pH, the tetracaine molecule partitions more deeply into the bilayer (*vide supra*) with a concomitantly smaller effect on the motion of the plateau region.

For cholesterol-containing DMPC bilayers, addition of the same amount of tetracaine results in a reduction of the order parameters, S_{mol}, compared to that of the DMPC/cholesterol system. This effect is of the same order of magnitude as in the absence of cholesterol and is less for the uncharged form of the anesthetic. This again can be explained by the electrostatic interactions between the DMPC headgroup and the charged tetracaine. For the uncharged form of the anesthetic, results obtained with deuteriated tetracaines (*vide supra*) and by high-pressure FT-IR spectroscopy (Auger et al., 1987, 1988b; chapters 6 & 7 of this thesis) suggest that the uncharged tetracaine is located close to the aqueous interface in cholesterol-containing DMPC bilayers. The "condensing" effect of cholesterol prevents a deeper penetration of the anesthetic into the membrane. This higher location can be responsible for the smaller effect of the uncharged form of the anesthetic on the amplitude of motion of the lipid acyl chain. If more tetracaine is added to the DMPC/cholesterol system in order to have the same amount partitioned into the

membrane (compared to pure DMPC bilayers), S_{mol} for the C-4' position of DMPC is reduced by about 15% at pH 5.5, which is greater than the reduction observed in pure DMPC bilayers. For the same ratio of lipid to anesthetic, the effect of the charged form of tetracaine is greater in cholesterol-containing DMPC bilayers. The "ordering" effect of cholesterol is partially compensated by the "fluidizing" effect of the local anesthetic in the plateau region of the bilayer.

For DMPC deuteriated at C-14' (tail region), the S_{mol} values at 30 and 50°C are represented in Figure 4.13. These S_{mol} values have been calculated according to Stockton et al. (1976) where the motions of the chain methylene group and the terminal methyl group are related to the same motional axis, i.e., the bilayer normal. To do so, S_{mol} for [14',14',14'-$^2H_3$]DMPC can be defined as:

$$S_{mol} = 6S_{CD} \qquad (4.6)$$

In the absence of cholesterol, the S_{mol} values for DMPC deuteriated at C-14' are very small and decrease by about 20% at 30°C and 10% at 50°C on addition of both the charged and uncharged form of the anesthetic. The presence of cholesterol results in a large increase of S_{mol}, as was observed in the plateau region. The S_{mol} values obtained for DMPC/cholesterol (7:3, molar ratio) are in agreement with those obtained by Dufourc et al. (1984b) and confirm that cholesterol decreases the amplitude of motion of the DMPC acyl chains, both in the plateau and the tail region.

Addition of tetracaine to the DMPC/cholesterol system results in a reduction of the order parameter S_{mol} at C-14' by about 20% for the charged anesthetic at pH 5.5 and

7% for the uncharged form at pH 9.5. If more charged tetracaine is added in order to have the same amount partitioned into the lipids, the S_{mol} values are reduced by about 35%. The differences observed between the effects of the two forms of the anesthetic in the tail region of the lipid bilayer confirm that the uncharged form is located close to the aqueous interface and does not perturb the acyl chains of DMPC as much as the charged form. Moreover, as observed in the plateau region, the effect of the same amount of charged tetracaine partitioned into the lipids is greater in cholesterol-containing DMPC bilayers. On the other hand, the effect of tetracaine on lipid headgroup conformation has been investigated by Siminovitch et al. (1984) and Browning and Akutsu (1982). These studies suggested that the anesthetic interacts with the polar headgroup of phosphatidylcholine bilayers.

4.5.2 Membrane dynamics

As discussed previously, the deuterium quadrupolar splittings $\Delta\upsilon_Q$ gives structural information on the average orientation of a particular C-^{2}H bond and on the amplitude of the angular fluctuations of that segment. ^{2}H NMR relaxation rates, on the other hand, yield complementary information about the dynamics of the lipid molecule (Jeffrey, 1981; Brown, 1982), as discussed in sections 2.7 and 4.4.2. Longitudinal (spin-lattice) deuterium relaxation times (T_{1Z}) were measured for [4',4',14',14',14'-$^2H_5$]DMPC in DMPC/cholesterol and DMPC/cholesterol/TTC at pH 5.5 and 9.5. Results for the plateau and the tail regions are presented in Table 4.2. Due to the superposition of two powder spectra, the entire set of partially relaxed spectra was dePaked to facilitate spectral integrations.

Table 4.2

Relaxation times (T_{1Z}, ms) of DMPC in DMPC + chol and DMPC + chol + TTC as a function of temperature and position of labelling

		DMPC + chol + TTC at	
Temp.(°C)	DMPC + chol	pH 5.5	pH 9.5
	Plateau Region		
30	18.3 ± 1.5	15.9 ± 0.9	
37	21.6 ± 1.8	20.2 ± 0.6	22.1 ± 1.8
50	25.9 ± 2.3	26.0 ± 0.9	
	Tail Region		
30	189 ± 3	166 ± 4	
37	223 ± 6	196 ± 7	188 ± 6
50	286 ± 8	244 ± 9	

Errors are estimated from the fitting procedure.

For DMPC/cholesterol systems in the presence and absence of tetracaine, the relaxation times T_{1Z} increase with temperature, for both the plateau and the tail regions, suggesting that the relevant molecular motions of DMPC in the temperature range studied are in the short correlation time regime ($\omega_0^2\tau_c^2 << 1$) (Brown et al., 1979). The larger T_{1Z} values obtained for the tail region relative to those of the plateau region can be rationalized in terms of the faster motion of the terminal methyl group of the acyl chain of the lipid. Addition of tetracaine does not induce significant variations in the relaxation times T_{1Z} for the plateau region of cholesterol-containing DMPC bilayers. The T_{1Z} values are, however, slightly decreased in the tail region upon addition of tetracaine.

If T_{1Z} for a specifically deuteriated position of a molecule increases exponentially with temperature, the activation energy E_a^i for the motion dominating the longitudinal relaxation at the frequency and temperature studied can be estimated from the plot of ln T_{1Z}^{-1} as a function of 1/T. The E_a^i values obtained from the data of Table 4.2 are 13.9 ± 2.5 and 16.7 ± 0.8 kJ mol^{-1} for the plateau and the tail regions, respectively, of [$^2H_5$]DMPC/cholesterol and 19.6 ± 2.5 and 15.3 ± 1.5 kJ mol^{-1} for the plateau and the tail regions of [$^2H_5$]DMPC/cholesterol/TTC, pH 5.5. Within the errors of our measurements, there is no dependence of the activation energies on the position of the deuteriated chain segment. This was also observed by Brown et al. (1979) for deuteriated DPPC. The average activation energy obtained for DPPC was 14.6 ± 1.2 kJ mol^{-1}, which is relatively close to the average obtained in this study for DMPC in a cholesterol-containing system. Moreover, the addition of tetracaine to DMPC/cholesterol bilayers does not induce a significant change in the activation energy.

The results presented in sections 4.5.1 and 4.5.2 therefore suggest that tetracaine affects the amplitude of the acyl chain motion of cholesterol-containing DMPC bilayers without causing significant changes in the rates of motions with frequencies close to the Larmor frequency.

4.6 ^{2}H NMR of cholesterol

In order to elucidate the effect of the local anesthetic tetracaine on the orientation and the amplitude of motion of the cholesterol molecule in DMPC/cholesterol (7:3, molar ratio), we have monitored the spectra of [2,2,4,4,6-$^2H_5$]cholesterol in DMPC/cholesterol bilayers in the presence and absence of tetracaine, at pH 5.5 and 9.5, from 30 to 50°C. The ^{2}H NMR spectrum and the dePaked spectrum of [2,2,4,4,6-$^2H_5$]cholesterol/DMPC bilayers are shown in Figure 4.14. For all temperatures studied, the spectra are characteristic of axially symmetric motion. The assignment of each peak has been done according to Taylor et al. (1981). The different quadrupolar splittings associated with deuterons on the rigid sterol nucleus reflect the common molecular order parameter, S_{mol}, of the fused ring system and the inequivalent geometrical orientations of the C-^{2}H bonds within the molecular frame.

The quadrupolar splitting of about 2.7 kHz associated with the C-6 deuteron of cholesterol does not change significantly with temperature or upon addition of tetracaine, at either pH 5.5 or pH 9.5. The small value of this quadrupolar splitting indicates that the angle β between the C-^{2}H bond and the axis of motional averaging is close to the "magic angle" of 54.7° for which the $3\cos^2\beta$-1 dependence of the quadrupolar splitting collapses.

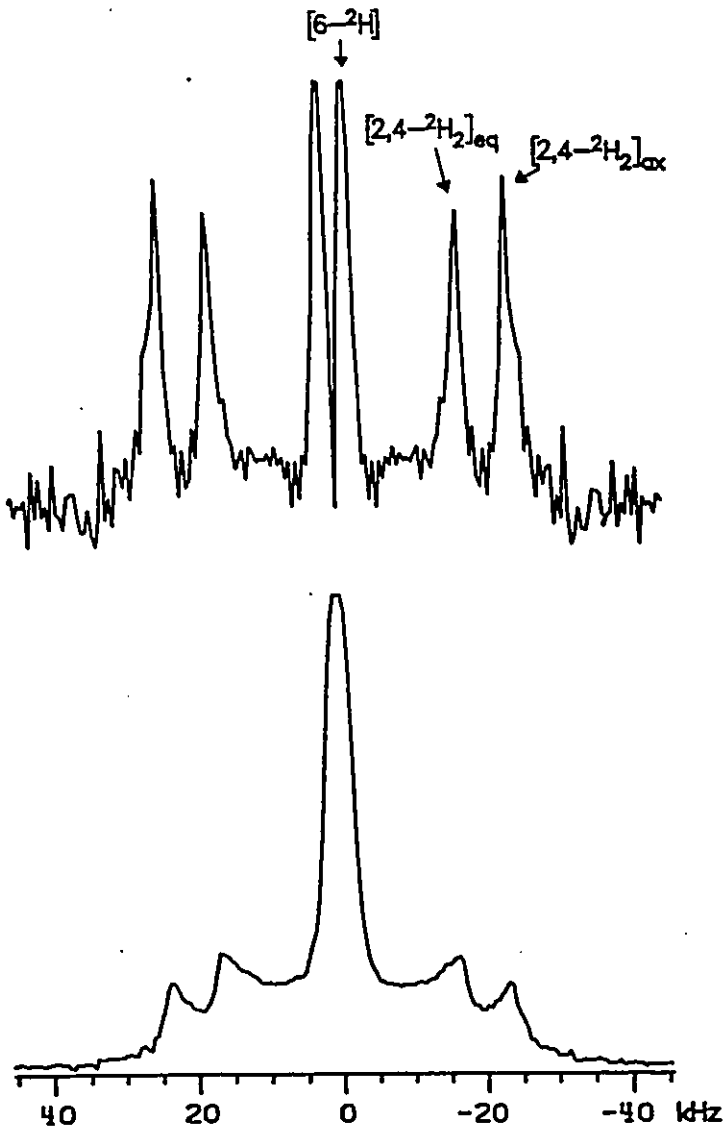

Figure 4.14 ^2H NMR spectrum (bottom) and dePaked spectrum (top) of [2,2,4,4,6-$^2H_5$]cholesterol 30 mole% in DMPC at 30°C.

As a result, a very small variation in the orientation of this C-^{2}H bond with respect to the axis of motional averaging results in a large change of the quadrupolar splitting. Since no significant variation of the quadrupolar splitting for the C-6 deuteron of cholesterol is observed upon addition of tetracaine at both pH values, it seems that intercalation of tetracaine does not induce a change in the orientation of cholesterol in DMPC/cholesterol (7:3, molar ratio) bilayers.

The temperature dependence of the quadrupolar splittings for the $[2,4\text{-}^2H_2]_{eq}$ and $[2,4\text{-}^2H_2]_{ax}$ deuterons is represented in Figure 4.15 for DMPC/cholesterol, DMPC/cholesterol/TTC, pH 5.5, and DMPC/cholesterol/TTC, pH 9.5. These quadrupolar splittings decrease slightly with increasing temperature, reflecting an increase in motional averaging of the quadrupolar interaction. In the presence of tetracaine at both pH values, the splittings are slightly reduced, the effect being greater at pH 5.5 when tetracaine is positively charged. This decrease in the quadrupolar splittings can be related to a change in the orientational order parameter S_{CD}, which according to equation 4.2 may reflect a change in one of both angular terms. One possibility implies a change in the orientation of cholesterol relative to its motional axis, which would then result in a change of the angle β (equation 4.2) for each deuteriated position. However, this possibility is unlikely since no change in the quadrupolar splitting for the C-6 deuteron of cholesterol is observed (*vide supra*). To confirm that the average orientation of cholesterol is unchanged, the ratios of the observed quadrupolar splittings for the $[2,4\text{-}^2H_2]_{eq}$ and $[2,4\text{-}^2H_2]_{ax}$ deuterons were calculated. Since S_{mol} is constant for the rigid steroid nucleus, this ratio, R_k, can be expressed as:

$$R_k = \frac{\Delta\upsilon_i}{\Delta\upsilon_j} = \frac{3\cos^2\beta_i - 1}{3\cos^2\beta_j - 1} \qquad (4.3)$$

assuming equal quadrupolar coupling constants for the various deuterons (Taylor et al., 1981). If the average orientation of the cholesterol molecule remains unchanged upon addition of tetracaine, the ratios R_k should stay constant for the different systems. This is in fact observed for the three systems studied, which confirms the hypothesis that the average orientation of cholesterol is unchanged in DMPC/cholesterol (7:3) bilayers in the presence and absence of tetracaine.

The reduction of the quadrupolar splittings observed in the presence of tetracaine can thus be related to a decrease of the molecular order parameter S_{mol}. In order to quantitate this effect, we will assume that for pure DMPC/cholesterol (7:3) bilayers, the order parameter S_{mol} is equal to 0.79 ± 0.03 at 30°C, as determined by Dufourc et al. (1984b), and decreases to 0.75 ± 0.03 at 45°C. With these S_{mol} values, the angle between the C-^{2}H bond and the axis of motional averaging calculated from equation 4.2 would be approximately 36.3° for the axial deuterons and 41.7° for the equatorial. Assuming no change in the orientation of the cholesterol molecule upon addition of the anesthetic (*vide supra*), the molecular order parameter S_{mol} decreases by about 2% on average at pH 5.5 and by 1% at pH 9.5. These reductions are very small but constant over all the temperature range. The major effect of tetracaine on the cholesterol molecule in DMPC/cholesterol (7:3, molar ratio) bilayers is thus a small increase of the amplitude of angular fluctuations with respect to the bilayer normal.

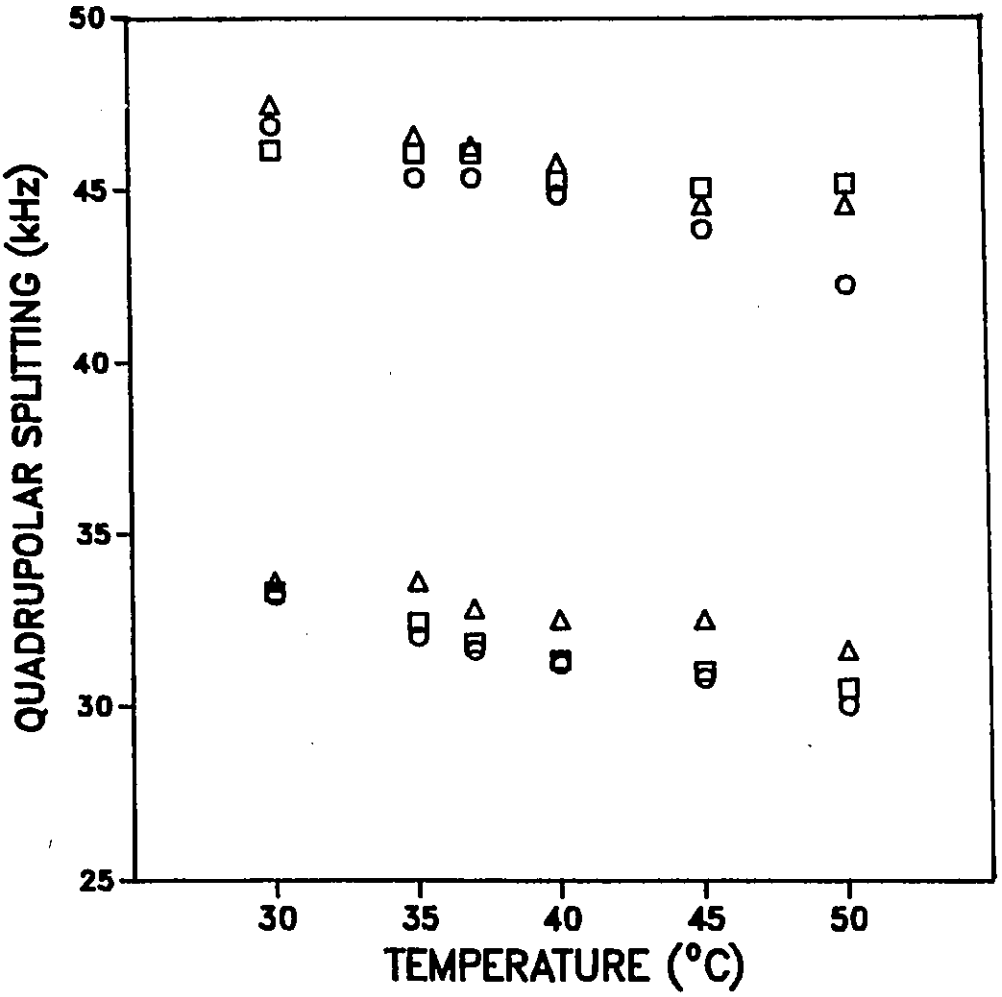

Figure 4.15 Temperature dependence of the quadrupolar splittings for [2,2,4,4,6-$^2H_5$]cholesterol in (△) DMPC + cholesterol, (○) DMPC + cholesterol + TTC, pH 5.5, and (□) DMPC + cholesterol + TTC, pH 9.5

4.7 Conclusions

The results presented in this chapter demonstrate that the location of the local anesthetic tetracaine in DMPC bilayers in the presence and absence of cholesterol is dependent on the charge of the anesthetic. The uncharged form partitions deeply in pure DMPC bilayers while the presence of cholesterol (30 mole%) "squeezes" it closer to the aqueous interface of the bilayer. The charged form may interact electrostatically with the phospholipid headgroup and induce a greater perturbation of the amplitude of motion of the lipid acyl chains than does the uncharged form, both in the presence and in the absence of cholesterol. In contrast to its influence on acyl chain order, intercalation of the anesthetic has little effect on the rates of acyl chain motion, or on ordering of cholesterol, in the DMPC/cholesterol system. These results are in agreement with the view that the charged form of local anesthetic is pharmacologically active at micromolar concentrations, as suggested by Aracava et al. (1984). This approach, in conjunction with other techniques, may afford a better understanding to the mechanism of local anesthesia. It is also applicable to the study of intact nerve systems.

CHAPTER 5

Interactions of tetracaine with glycoglycerolipid bilayers

5.1 Introduction

As discussed in the previous chapter, the ^2H NMR studies of the interactions of tetracaine with phospholipid bilayers (Kelusky & Smith, 1983; Smith & Butler, 1985; Boulanger et al., 1981;) suggest that the anesthetic interacts differently with different phospholipids such as phosphatidylcholine (PC), phosphatidylethanolamine (PE) and phosphatidylserine (PS), depending mostly on the charge and shape of the lipid studied. Moreover, both ^2H NMR and high-pressure Fourier-transform infrared (FT-IR) studies (Boulanger et al., 1981; Auger et al., 1987,1988a-b; chapter 4, 6 & 7 of this thesis) have shown that the charged form of the local anesthetic tetracaine at pH 5.5 is located close to the aqueous interface of pure phospholipid bilayers while the uncharged form at pH 9.5 penetrates deeper into the bilayer. In the case of the charged form of tetracaine, several NMR studies have also shown that the anesthetic interacts with phospholipid head groups (Boulanger et al., 1981; Siminovitch et al., 1984).

A natural extension of these studies with model systems is the study of the interactions of local anesthetics with unmyelinated and myelinated nerves (Smith & Butler, 1985; Auger et al., 1987). In the case of myelinated nerves, the myelin sheath surrounding the nerve assumes considerable importance in maintaining proper nerve function. Thus in

addition to probing the direct effect of agents on nerves, it is of interest to ask if it is possible that the same agents can lead to indirect effects through perturbation of the organization and physico-chemical properties of myelin.

Glycolipids are common components of the myelin sheath, in particular a glycosphingolipid, galactocerebroside is present. The influence of various agents on the physico-chemical properties of phospholipids, also components of myelin, has been studied extensively. However, the glycolipid components have received much less study. Thus, it is of interest to probe the effects of these agents on other components of myelin. The orientational and motional properties of an analog of the neutral myelin glycolipid, the glycoglycerolipid 1,2-di-*O*-tetradecyl-3-*O*-β-D-glucopyranosyl-*sn*-glycerol (β-DTGL) (Figure 5.1), have been studied by ^{2}H NMR spectroscopy (Jarrell et al., 1986, 1987a-b) and are well characterized. Since this glycolipid has been shown to be a reasonable model for the corresponding glycocerebroside (Skarjune & Oldfield, 1982), we have examined the effect of the local anesthetic tetracaine on the physical properties of the β-DTGL head group. We have studied the interaction of the local anesthetic with pure β-DTGL and with the glycolipid (20 mole%) in dimyristoylphosphatidylcholine (DMPC), a situation which more closely resembles that in the myelin sheath.

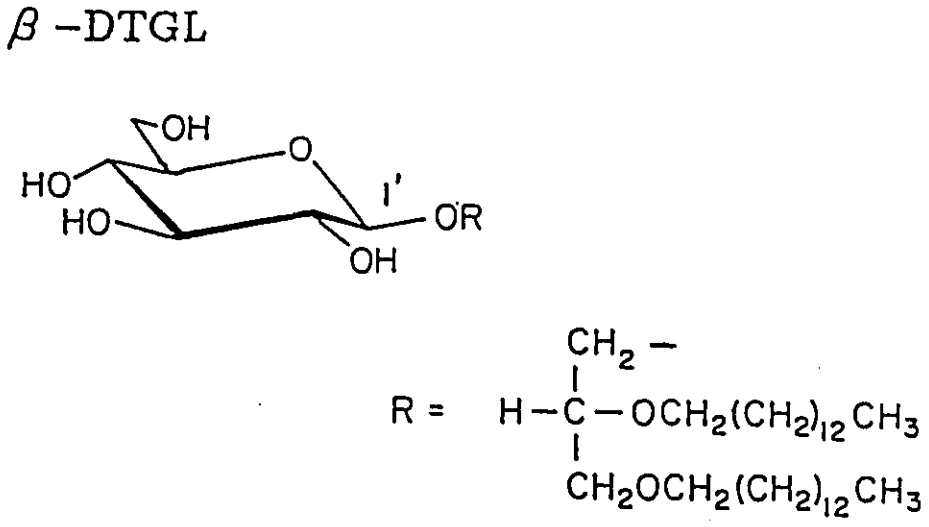

Figure 5.1 Structure of 1,2-di-*O*-tetradecyl-3-*O*-β-D-glucopyranosyl-*sn*-glycerol (β-DTGL).

5.2 Interactions of tetracaine with pure β-DTGL bilayers

5.2.1 Formation of non-lamellar phases

The ^2H NMR spectra of β-DTGL, labelled at C1' of the glucosyl moiety and C3 of the glycerol backbone, at 52°C in the presence and absence of tetracaine at pH 9.5, where the anesthetic is primarily uncharged, are shown in Figure 5.2. Previous studies have shown that β-DTGL exhibits a transition from a gel- to a liquid-crystalline phase at 52°C and from a lamellar to a hexagonal phase at 58°C (Jarrell et al., 1986). In the absence of tetracaine at 52°C, the spectrum is characteristic of axially symmetric motion attributable to the lamellar phase. This spectrum persists up to 58°C. At 60°C (results not shown), the ^2H NMR spectra retain the shape characteristic of axially symmetric motion but the quadrupolar splittings are reduced by more than a factor of two, suggesting a hexagonal aggregate structure for the lipid. If all motional and orientational parameters remain the same as in the lamellar phase, the quadrupolar splitting is expected to be reduced by a factor of two for the hexagonal phase lipid relative to that of the lamellar phase (Seelig, 1977; Davis, 1983; Smith, 1984). The fact that the quadrupolar splittings at 60°C are reduced by more than one-half the values at 52°C suggests that the orientation of the sugar ring is changed relative to that in the lamellar phase.

In the presence of uncharged tetracaine, and for temperatures from 52 to 60°C, the quadrupolar splitting of β-DTGL labelled at C1' of the carbohydrate head group is also reduced by more than a factor of two, suggesting that, as with pure β-DTGL at higher temperature (58°C), the lipid is in the hexagonal phase. However, with these data alone, one cannot discount a conformational change in the head group. To establish which of the

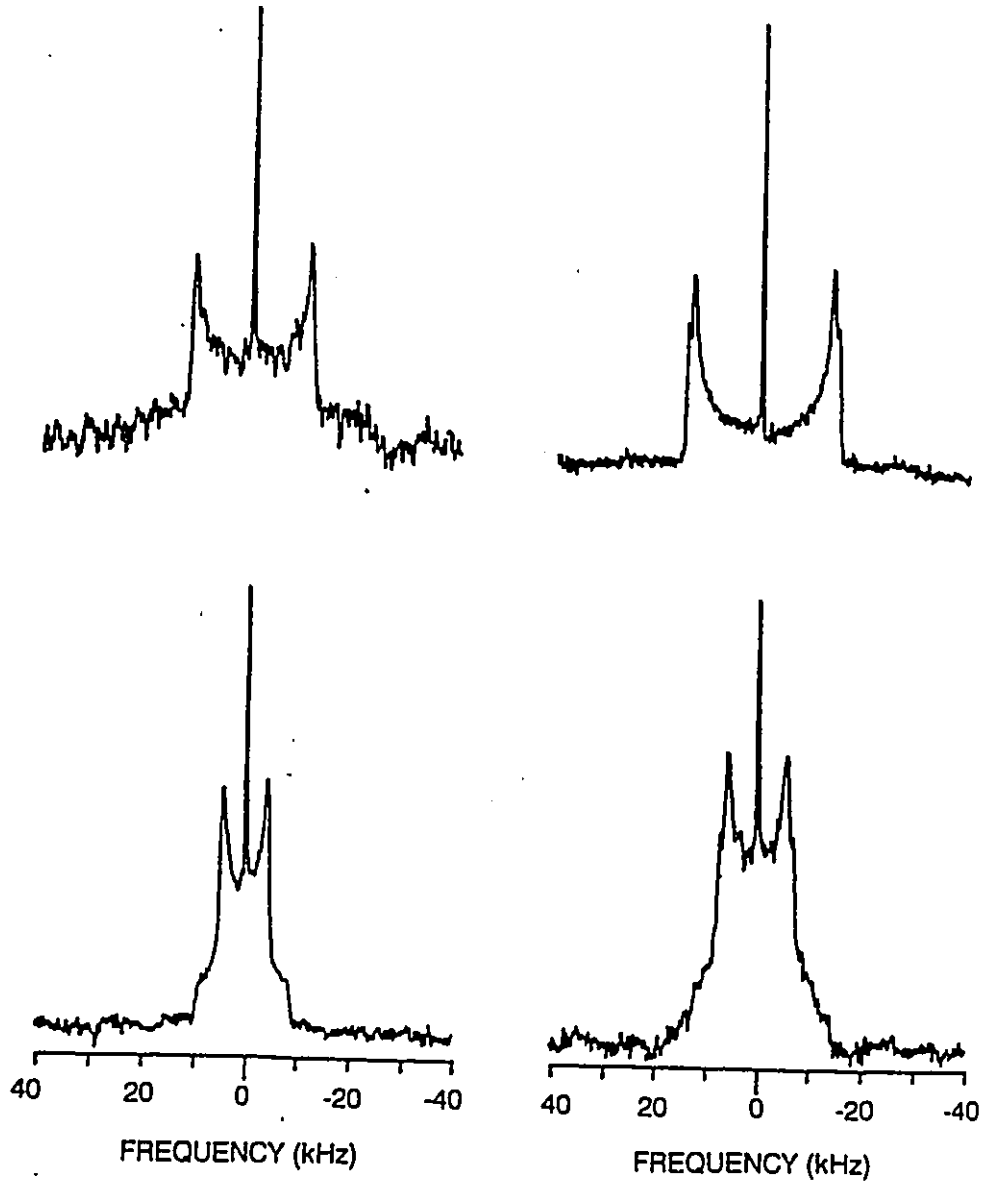

Figure 5.2 ^{2}H NMR spectra (30.7 MHz) of β-DTGL labelled at C1' of the carbohydrate head group (left) and at C3 of glycerol (right) in the absence (top spectra) and presence of tetracaine (bottom spectra) at pH 9.5, 52°C.

two possibilitites is occuring, β-DTGL labelled at the C3 position of the glycerol backbone was examined (Figure 5.2, right). A reduction in the quadrupolar splitting of the system in the presence of tetracaine is seen. The parallel behavior of two very different positions in the lipid is consistent with a hexagonal aggregate structure of the lipid, which is stable from 52 to 58°C. Such destabilization of the lamellar phase of a glycolipid by exogenous molecules has previously been demonstrated (Wieslander et al., 1986; Rilfors et al., 1984).

It has been shown that the transition between lamellar and non-lamellar phases in lipid-water model systems is affected by temperature, hydration, cations, pH and additions of exogenous molecules such as steroids, alcohols, local anesthetics and detergents, as well as the structure of the lipid molecules (Rilfors et al., 1984). The formation of different lipid aggregate structures is dependent on the cross-sectional area of lipid at the hydrocarbon-water interface, the hydrophobic volume and the hydrocarbon chain length of the participating molecules. Lamellar phases are built-up of cylindrical-like molecules. However, a decrease in the interfacial area of the lipid, and an increase in the hydrophobic volume, gives the lipid molecules the effective shape of a truncated cone. This shape favors the formation of non-lamellar aggregates of the reverse type (water in oil), such as the hexagonal H_{II} phase.

Previous ^{2}H NMR (Boulanger et al., 1981; Auger et al., 1988a) and high-pressure FT-IR (Auger et al., 1987, 1988b) studies have shown that the uncharged form of the local anesthetic tetracaine at pH 9.5 partitions deeply into pure phospholipid multilamellar dispersions, whereas the charged form at pH 5.5 remains close to the head group region. If the uncharged form of tetracaine partitions relatively deeply into the hydrocarbon region of the glycolipid bilayer, as it does for pure phospholipid bilayers, the requirement for the

formation of a hexagonal phase is satisfied. This is supported by the fact that nonpolar organic solvents that partition more or less deeply into the hydrophobic interior of the bilayer (McIntosh et al., 1980; White et al., 1981) are able to transform a lamellar phase into non-lamellar phases of the reversed type. For example, the presence of n-dodecane in the systems egg phosphatidylethanolamine-water (Hornby & Cullis, 1981) and dioleoyl-PE (DOPE) - dioleoylphosphatidylcholine (DOPC) - water (Kirk & Gruner, 1985), which normally form a L_α phase, induces the formation of a H_{II} phase. These results are therefore in agreement with the induction of a hexagonal phase of the reverse type in β-DTGL by the addition of the uncharged form of the local anesthetic tetracaine.

At lower pH (5.5), where the anesthetic is primarily charged, a dramatically different picture is obtained, as shown in Figure 5.3. At 52°C, the ^2H NMR spectrum is very similar to that obtained for the β-glucolipid alone, labelled in either the head group or the glycerol positions, and is attributable to a lipid in a lamellar phase. This contrasts with the corresponding system at pH 9.5 in which a non-lamellar structure occurs at the same temperature. As the temperature is elevated to 60°C, the spectra indicate a transition from an axially symmetric to a nearly isotropic state for the lipids. The total integrated intensity of the spectra remains constant, within experimental error, indicating that the observed changes are not attributable to the effects of very short transverse relaxation times, T_{2e}. The spectrum due to isotropic behavior may result from several possibilities, including formation of vesicles, micelles, or macroscopic structures having high symmetry. Visual inspection of the sample at 60°C clearly indicates that micelles or small vesicles are not the dominant structures present. It has been shown that in addition to forming hexagonal phases, glycolipids can form macroscopic structures of high symmetry, such as cubic and rhombic, and that exogenous molecules can facilitate the formation of such structures

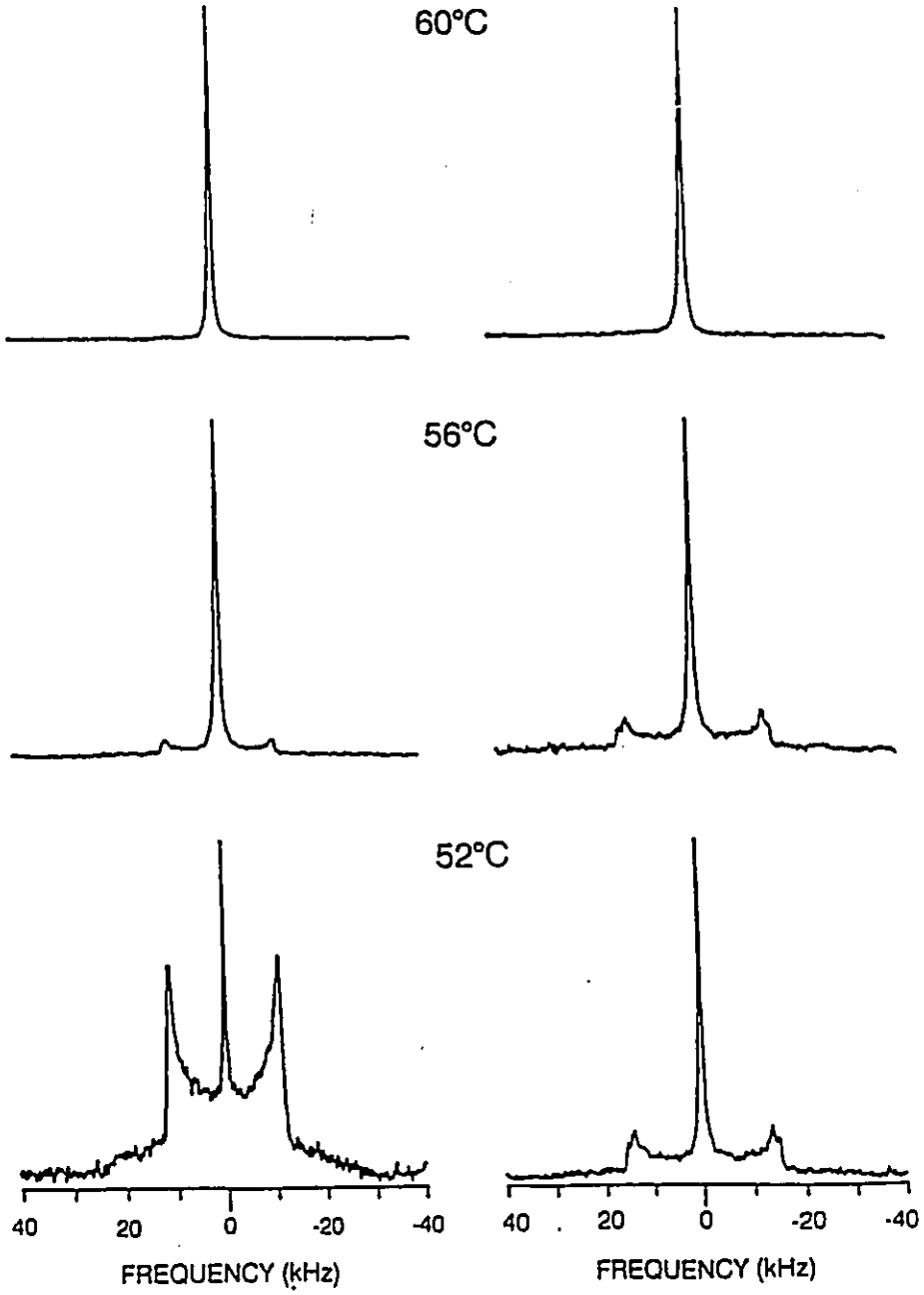

Figure 5.3 Temperature dependence of ^2H NMR spectra (30.7 MHz) of [1'-$^2H_1$] β-DTGL (left) and [3,3-$^2H_2$] β-DTGL (right) in the presence of tetracaine at pH 5.5.

(Wieslander et al., 1986; Lindblom & Rilfors, 1989). It appears that for the β-glucolipid, the presence of tetracaine close to the aqueous interface of the bilayer induces, over the temperature range of 52 to 58°C, the formation of a cubic or rhombic phase.

Several cubic phases have been encountered in lipid and lipid-water systems. Two fundamentally different types have been proposed, namely structures with continuous regions of both water and hydrocarbon chains and structures composed of closed aggregates of "oil-in water" or "water-in-oil" type (Rilfors et al., 1984, 1986; Siegel, 1986; Lindblom et al., 1979). Measurements of the self-diffusion coefficients of both lipid and water using the NMR pulsed field gradient technique (Stejskal & Tanner, 1965) provide a means to differentiate between these possibilities (Lindlom et al., 1979). The cubic phases formed by biological membrane lipid-water systems seem to be located between the lamellar and H_{II} (hexagonal of the reversed type) phases (Rilfors et al., 1986) and from NMR diffusion coefficient measurements, it has been suggested that the cubic phase in such systems is a bicontinuous structure (Siegel, 1986).

The transition from lamellar to a continous cubic structure has been rationalized by Lindblom and co-workers (Lindblom et al., 1979) in the following way. In a sample of fixed composition, an increase in temperature will increase the chain mobility toward the chain end, resulting in a tendency to form a structure where the cross-sectional area per molecule at the methyl end groups is larger than at the polar head groups. The continuous cubic structure proposed by these authors would result in a larger cross-sectional area per molecule at the methyl end group compared to the cross-section of the polar head group. ^2H NMR (Boulanger et al., 1981; Auger et al., 1988a) and high-pressure FT-IR (Auger et al., 1987, 1988b) studies have shown that the local anesthetic tetracaine, primarily charged

at pH 5.5, is located close to the aqueous interface of pure phospholipid bilayers. If this is so for tetracaine partitioned into β-DTGL bilayers, then the presence of tetracaine close to the aqueous interface of the bilayer may induce, over the temperature range of 52 to 58°C, the formation of a continuous cubic phase. In this system, the cross-sectional area at the methyl end group would be greater than that for the pure β-DTGL molecule, since tetracaine would act as a spacer between the lipid head groups. A transition from a lamellar to a cubic phase has also been observed by Cullis and co-workers (Cullis et al., 1978a) for a diphosphatidylglycerol system in the presence of the local anesthetic dibucaine. An additional feature of the transition from a lamellar to an isotropic phase for β-DTGL in the presence of charged tetracaine is that, on cooling the sample from 60 to 52°C, the formation of a lamellar phase does not readily occur. Such a hysteresis effect has been reported for other systems undergoing aggregate structural changes (Cullis et al., 1978b).

5.2.2 Effects on head group orientation

While the spectral changes presented in Figures 5.2 and 5.3 for β-DTGL in the presence of both the charged and uncharged forms of tetracaine may be attributed to lamellar-to-non-lamellar transitions, information on head group orientation may also be sought. For a C-^{2}H bond executing axially symmetric motion, the quadrupolar splitting is related, according to equation 2.12, to the angle β between the C-^{2}H bond vector and the axis about which the molecular segment undergoes rotation and to the segmental order parameter, S_{mol} describing the anisotropic motion of the entire rigid structure.

The quadrupolar splittings for deuterium in both the head group and glycerol

moieties at pH 9.5 in the presence of tetracaine at 52°C, are very similar to those of β-DTGL alone at 58°C (hexagonal phase). This indicates that both molecular ordering and head group orientation are essentially the same for both of these systems. For β-DTGL in the presence of charged tetracaine at 52°C, the quadrupolar splittings for both labelled positions are nearly identical to those obtained for the pure glycolipid at 52°C (lamellar phase), again reflecting similar orientational and motional properties of the glycolipid head group. The head group orientation of β-DTGL is therefore not significantly altered by the presence of the local anesthetic tetracaine. In contrast, the lamellar structure of the glycolipid system becomes less stable in the presence of tetracaine.

The behavior of the glycolipid system in the presence of anesthetics is very different from that of phospholipids. ^{2}H, ^{31}P and ^{14}N NMR studies (Boulanger et al., 1981; Siminovitch et al., 1984) have shown that the charged form of the local anesthetics tetracaine and dibucaine interacts with phospholipid head group. Specifically, the absolute magnitude of the ^{31}P chemical shift anisotropy increases from a value of 48 ppm to 58 ppm in the presence of tetracaine while the ^{14}N quadrupolar splitting decreases. The ^{2}H quadrupolar splittings of the C_{α} and C_{β} positions of the phosphatidylcholine head group are also changed in the presence of charged anesthetic, the binding of tetracaine or dibucaine decreasing the C_{α} splitting and increasing the C_{β} position splitting. Similar effects have been observed with metal cation binding to the phosphatidylcholine head group (Brown & Seelig, 1977; Akutsu & Seelig, 1981), although the magnitude of the effects caused by anesthetics is much larger. However, at higher pH (9.0), the magnitude of the effect of tetracaine on phosphatidylcholine head group is much smaller than that at low pH (Boulanger et al., 1981). This demonstrates the deeper penetration of the uncharged form of tetracaine in PC bilayers.

The interactions of phospholipid polar groups with charged or dipolar molecules have recently been rationalized in terms of the electrical properties of the membrane surfaces (Seelig et al., 1987; Roux et al., 1989). These studies demonstrated that phospholipid head groups are sensitive to electric surface charges and that the conformational change of the phosphocholine dipole with positive charges is inverse to that occuring with negative surface charges. For a given charged molecule, the quadrupolar splitting is linearly related to the amount of bound/adsorbed molecules and only small bond rotations are sufficient to induce large variations in the quadrupolar splittings (Akutsu & Seelig, 1981; Seelig et al., 1987). In the case of the neutral glycolipid investigated in this study, the electrical properties of the membrane surface will be different than those of zwitterionic phospholipid membranes; as a result, conformational changes in the β-DTGL head group in the presence of charged tetracaine are negligible.

5.3 Interaction of tetracaine with β-DTGL (20 mole%) in DMPC

In contrast to the pure glycolipid system, the interaction of tetracaine with β-DTGL (20 mole%) in dimyristoylphosphatidylcholine (DMPC) at both pH 5.5 and 9.5 does not lead to the formation of non-lamellar phases. The ^{2}H NMR spectra of β-DTGL, labelled in both head group and glycerol positions, in the presence of tetracaine closely resemble those obtained in its absence. Specifically, the quadrupolar splitting for the C1' labelled positions of the glucose ring is about 20 kHz, both in the absence and presence of tetracaine (spectra not shown).

The ^2H NMR spectra of [3,3-$^2H_2$] β-DTGL (20 mole%) in DMPC in the absence and presence of tetracaine (pH 5.5 and pH 9.5) are shown in Figure 5.4, together with the corresponding dePaked spectra. These spectra exhibit two quadrupolar splittings, indicating that the two C-^2H bonds at this positions make different angles with respect to the axis of motional averaging (Jarrell et al., 1987a). In the presence of both the charged (pH 5.5) and uncharged (pH 9.5) form of tetracaine, there is a small decrease of the quadrupolar splittings associated with the two inequivalent deuterons, this effect being slightly more pronounced at pH 5.5. The results are shown in Figure 5.5. This decrease in the quadrupolar splittings can be related to a change in one or both angular term of equation 2.17. One possibility implies a change in the orientation of the glycerol backbone relative to its motional axis, which would then result in a change of the angle β (equation 2.17) for the two deuteriated positions. On the other hand, a small reduction of the segmental order parameter S_{mol} can also account for the decrease in the quadrupolar splittings. In order to discriminate between the two possibilities, the ratios of the observed quadrupolar splittings for the two deuterons of the glycerol backbone were calculated. Since S_{mol} is constant for this segment of the molecule, this ratio is sensitive to changes in the angle β for each deuteron (Taylor et al., 1981).

If the average orientation of the C3 position of glycerol remains unchanged upon addition of tetracaine, the ratio should stay constant for the different systems. This is in fact observed for the three systems studied, which indicates that the average orientation of the C3 position of glycerol is unchanged by the presence of tetracaine in DMPC : β-DTGL (4:1) bilayers. The reduction of the quadrupolar splittings observed in the presence of tetracaine can thus be related to a decrease of the segmental order parameter S_{mol} by 5%.

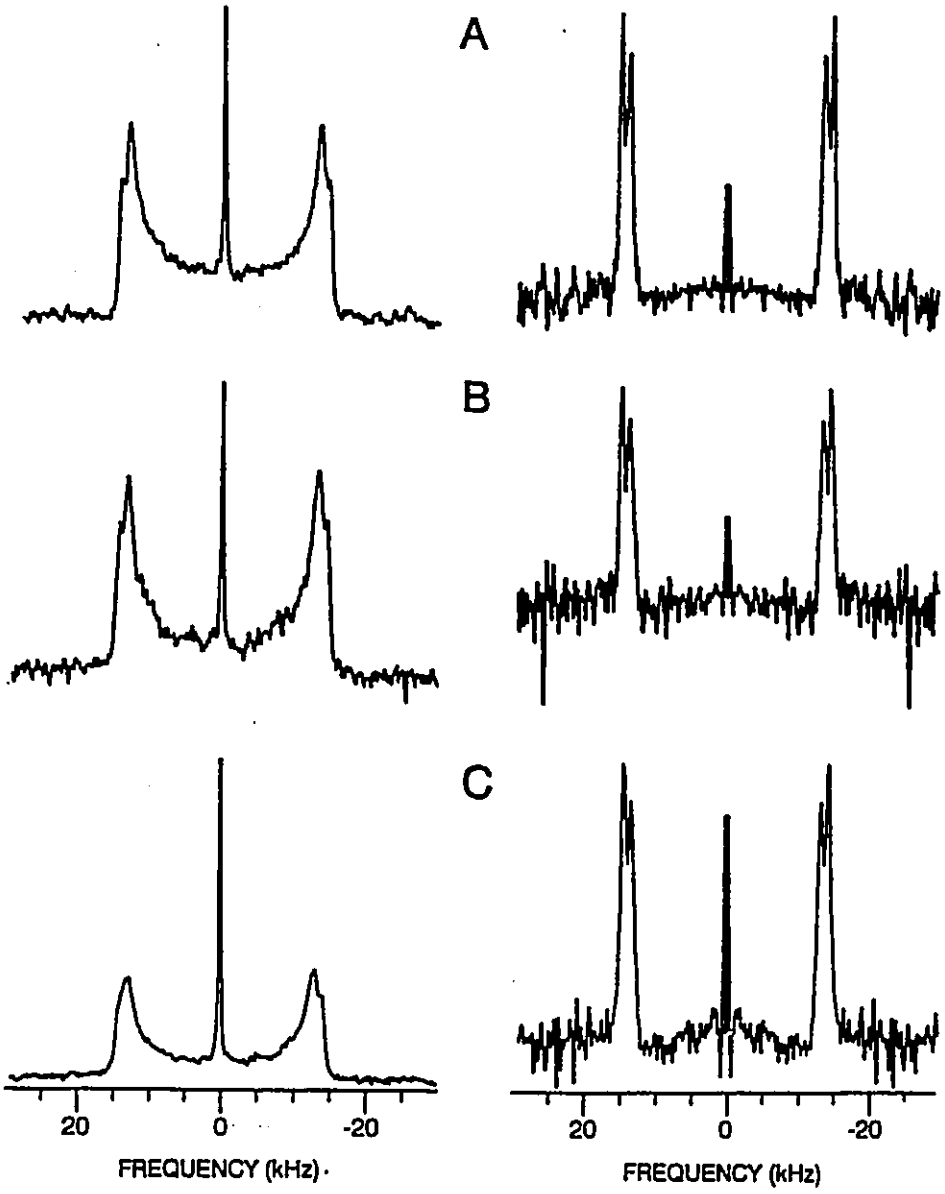

Figure 5.4 ^2H NMR spectra (30.7 MHz) (left) and dePaked counterparts (right) of [3,3-$^2H_2$] β-DTGL in A. DMPC:β-DTGL, B. DMPC:β-DTGL + TTC, pH 9.5 and C. DMPC:β-DTGL + TTC, pH 5.5, all at 50°C.

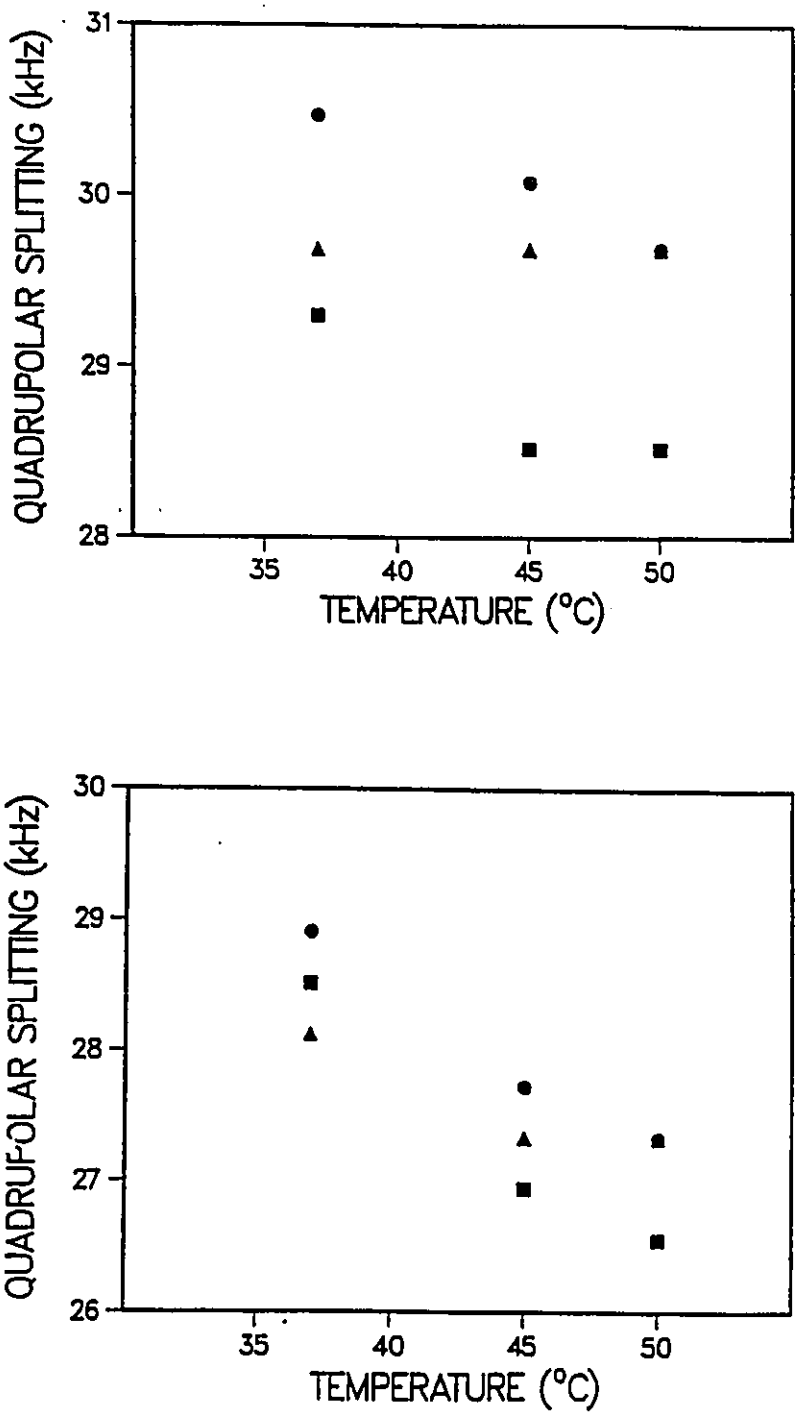

Figure 5.5 Temperature dependence of the quadrupolar splittings for the inequivalent deuterons of [3,3-$^2H_2$]β-DTGL in (●) DMPC:β-DTGL, (▲) DMPC:β-DTGL + TTC, pH 9.5 and (■) DMPC:β-DTGL + TTC, pH 5.5.

These reductions are small but constant over the temperature range studied and indicate that the presence of tetracaine causes a small reduction in segmental order.

Inspection of the dePaked spectra in Figure 5.4 reveals that the two quadrupolar patterns for the C3 position in β-DTGL have different component widths. Previous studies from this laboratory (Jarrell et al., 1987a) have demonstrated that this additional line broadening is due to ^{1}H-^{2}H dipolar coupling between the proton at C2 and the two deuterons at C3. If the C2-C3 segment of glycerol is considered, this dipolar coupling is dependent on the conformation about the C2-C3 bond. Oriented sample spectra of [3,3-$^{2}H_{2}$] β-DTGL obtained with ^{1}H decoupling showed that the two quadrupolar splittings have the same linewidth (Jarrell et al., 1987a). From these results, the conformation about the C2-C3 bond of glycerol was estimated.

In the presence of uncharged tetracaine at pH 9.5 (Figure 5.4B), the width of the two quadrupolar splittings for the C3 position in β-DTGL are very close to that obtained for pure β-DTGL, the inner doublet being slightly broader than the outer one. This suggests that the conformation about the C2-C3 bond is not significantly changed by the addition of the uncharged anesthetic. However, in the presence of charged tetracaine at pH 5.5 (Figure 5.4C), the outer doublet appears to be slightly broader than the inner one. With ^{1}H decoupling, the widths of the two doublets for this system become essentially equal, as was observed for the pure glycolipid system (Jarrell et al., 1987a). These results suggest different couplings $^{1}H2$-$^{2}H3$ (S) and $^{1}H2$-$^{2}H3$ (R) (S and R referring to the pro-S and pro-R deuterons of C3) for β-DTGL in the presence of charged tetracaine. The conformation about the C2-C3 bond of the glycerol for β-DTGL (20 mole%) in DMPC may therefore be altered by the presence of charged tetracaine. Since the charged form of

tetracaine in phosphatidylcholine bilayers interacts relatively strongly with the phospholipid head group (Boulanger et al., 1981), it is of interest to note that a change in the DMPC head group orientation induced by charged tetracaine may cause the change in the conformation about the C2-C3 bond of the glycerol backbone of β-DTGL, a change that is not observed at higher pH. These results are further supported by the fact that unlike the orientation of the C2-C3 bond of the glycerol backbone which is relatively invariant from lipid to lipid, the conformation about this bond appears to vary significantly (Jarrell et al., 1987a; Pearson & Pasher, 1979). Additional labelling of the glycerol moiety would however be required to enable a more precise definition of the glycerol conformation for β-DTGL (20 mole%) in DMPC in the absence and presence of tetracaine.

5.4 Conclusions

The present study demonstrates that unlike the interaction of tetracaine with phospholipids , there is no large change in the head group orientation of β-DTGL. The stability of the lamellar structure of the pure glycolipid system is very sensitive to the presence of anesthetic while the mixed glycolipid-phospholipid systems exhibit only a lamellar structure.

PART THREE: HIGH-PRESSURE FT-IR STUDIES OF ANESTHETIC-LIPID INTERACTIONS

CHAPTER 6

Pressure-induced exclusion of the local anesthetic tetracaine from model and nerve membranes

6.1 Introduction: High-pressure vibrational spectroscopy in membranes

Vibrational spectra of membrane systems consist of bands arising from the transition between vibrational levels of various types of intramolecular and intermolecular vibrations in the ground electronic state. They are observed experimentally as infrared and Raman spectra. Many infrared and Raman spectral parameters, such as the frequencies, widths, intensities, shapes, and splittings of the infrared and Raman bands are very sensitive to the structural and dynamic properties of membrane lipid molecules, as well as functional groups in the molecule (Wong, 1984; Wong & Mantsch, 1985a). Therefore, vibrational spectroscopy is a very powerful physical technique in the study of biomembranes. It provides not only macroscopic but also microscopic information on the structural and dynamic properties of biomembranes at the molecular level, as well as the functional group level. Table 6.1 summarizes some of the most useful correlations between vibrational spectroscopic parameters and properties related to structure and dynamics in these systems.

Table 6.1

Correlations between spectral parameters and structural and dynamic properties

Spectral parameters	Structural and dynamic properties
Spectral parameter discontinuities (IR and R)	phase transition and critical pressure
H_{2930}/H_{2880} (R)	*gauche* conformer population
H_{1080}/H_{1130} (R)	*gauche* conformer population
Widths of anisotropic components (R)	reorientational fluctuations
Widths of isotropic components (R)	interchain interactions
H_{2880}/H_{2850} (R)	interchain interactions
$\nu_s CH_2$ band shape (R)	interchain packing
Correlation-field splitting (IR and R)	interchain packing
νC=O frequency (IR and R)	hydrogen bond and conformation in interfacial region
νCN and νPO_2^- frequency (IR and R)	hydrogen bond and conformation in head group region
$I\gamma' CH_2/I\gamma CH_2$ (IR)	orientation of neighboring chains
νC=C frequency and I_νC=C (R)	nature of C=C double bonds
$I\delta$=CH/$I\tau CH_2$ (IR)	degree of unsaturation
$H\delta' CH_2/H\delta CH_2$ (IR)	interdigitation packing

H_a/H_b, peak height ratio between band a and b; I_a/I_b, integrated intensity ratio between band a and b; ν, stretching mode; δ and δ', bending mode and its correlation-field component; γ and γ', rocking mode and its correlation-field component; τ, twisting mode; (R) Raman spectrum; and (IR), infrared spectrum (from Wong et al., 1988).

The study by vibrational spectroscopy of biologically important materials that are subjected to high-pressure has long been neglected. The reasons for this were difficulties in obtaining high-pressure vibrational spectra in the aqueous media in which biological molecules are frequently investigated. The recent development of high-pressure infrared and Raman optical cells suitable for aqueous systems (discussed in section 3.10 of this thesis) has considerably increased the amount of activity in this area (Wong, 1981, 1985, 1987a-c; Wong & Mantsch, 1985a; Wong et al., 1985). A number of high-pressure vibrational spectroscopic studies of aqueous multilamellar dispersions of phospholipid membranes and more recently proteins have been reported in the literature since the first one appeared in 1982 (Wong et al., 1982). Vibrational spectroscopy is now a relatively sensitive technique, requiring small sample sizes to obtain spectra with a favorable signal-to-noise ratio and a high information content.

High-pressure investigations of biological systems or their models are usually motivated by one of the two factors: (1) a desire to understand the biological effects of pressure (*piezobiology*), including such diverse phenomena as the adaptation of marine organisms to extreme depths, the sensitivity of excitable cell membranes to pressure and the antagonistic action of pressure to anesthetic action (Wong et al., 1988); or (2) a desire to understand the behavior of these systems under the perturbation of extreme pressure at a molecular level (*piezobiophysics*), including their dynamic properties, dynamical structure and phase behavior (Wong, 1984, 1986, 1987a-c). The latter aspect also includes the use of high pressure as a tool to answer specific biophysical questions which are difficult, if not impossible, to answer under ambient conditions of pressure. In order to exaggerate the effects of intermolecular interactions, or to study specific molecular associations which are pressure-sensitive, the high-pressure experiments often require pressures well above those

found anywhere in the biosphere. However, by illuminating the molecular mechanism of barotropic phenomena in model systems, the knowledge gained from these experiments is often directly applicable to the problems of piezobiology.

6.2 Pressure reversal of anesthesia

It is nearly a century since Regnard (1887) made the first observations of the effects of high hydrostatic pressure on the excitability of nerve, but only recently has there been a concerted attempt to understand these effects at molecular level (Wann & Macdonald, 1980). An important clue in elucidating the molecular mechanism of anesthetic action and in discriminating between lipid and protein as the primary site of anesthetic action is the well-established effect of hydrostatic pressure on anesthesia in vivo (Halsey & Wardley-Smith, 1975; Kendig & Cohen, 1977; Lever et al., 1971; Roth, 1979; Wann & Macdonald, 1980). This phenomenon has been attributed to the effects of pressure on membrane fluidity (Trudell et al., 1973) or membrane-bound proteins (Jaenicke, 1983), although the possibility that anesthetics are simply expelled from the membrane by pressure, or squeezed away from their target sites (Franks & Lieb, 1982) (be they lipid or protein), has been suggested but never directly confirmed (Trudell et al., 1973; Seelig, 1987).

In order to see if pressure can induce the expulsion of a local anesthetic, tetracaine, from model phospholipid bilayers and from nerves, we have monitored the carbonyl stretching infrared band of tetracaine as a function of pressure from 0.001 (1 atm) to 25 kbar. Since the frequency and shape of an ester carbonyl stretching band are sensitive to

its environment, this band can be used to probe environmental changes (Mushayakarara et al., 1986). In this study, high pressure is used to modulate the depth of penetration of the anesthetic into the bilayer and FT-IR is used to monitor the changes in the environment of specific functional groups in the molecule under high pressure. It should be emphasized however that in the present context, the results obtained at high pressure reflect the nature of the system at low pressure, which is of biological interest.

6.3 Pressure-induced exclusion of tetracaine from model membranes

6.3.1 Neutral phospholipid membranes

Figure 6.1 shows the effect of a physiological concentration of cholesterol on the pressure dependence of the infrared spectra of an ester-linked (DMPC) and an ether-linked (DHPC) phospholipid. In both lipid systems, the local anesthetic tetracaine was partitioned into the lipid bilayers in the uncharged form (pH 9.5). The partition coefficient K_p, which is the ratio of the anesthetic concentration in the lipid phase to that in the buffer, is about 600 for uncharged tetracaine in phosphatidylcholine bilayers (Boulanger et al., 1980). Previous ^2H NMR studies of tetracaine in egg phosphatidylcholine bilayers have suggested that the uncharged form at high pH penetrates more deeply into the bilayer that the charged form at low pH (Boulanger et al., 1981). This model is entirely consistent with the pressure dependence of the DMPC infrared spectra shown in Figure 6.1A. In the spectral region between 1650 and 1800 cm^{-1}, and over the pressure range from 0.001 to 25 kbar, the spectra of this system are dominated by the relatively intense ester C=O stretching mode band at 1735 cm^{-1} (Mushayakarara et al., 1986). The shoulder on the low-

Figure 6.1 Stacked plots of infrared spectra of 1,2-dimyristoylphatidylcholine (DMPC) and 1,2-di-*O*-hexadecylphosphatidylcholine (DHPC) in the C=O stretching region as a function of hydrostatic pressure at high pH (pH 9.5). Note that the abrupt appearance of the well-defined tetracaine (TTC) C=O band at approximately 1685 cm^{-1} in the spectra of the DMPC/TTC and DHPC/TTC systems occurs only in the presence of cholesterol (right column). To the right of each stacked plot, the lowest and highest pressures in kilobars are indicated and, when appropriate, the pressure of the spectrum that first reflects the bandwidth change of tetracaine C=O band. **A.** DMPC + TTC; **B.** DMPC + cholesterol + TTC; **C.** DHPC + TTC; **D.** DHPC + cholesterol + TTC.

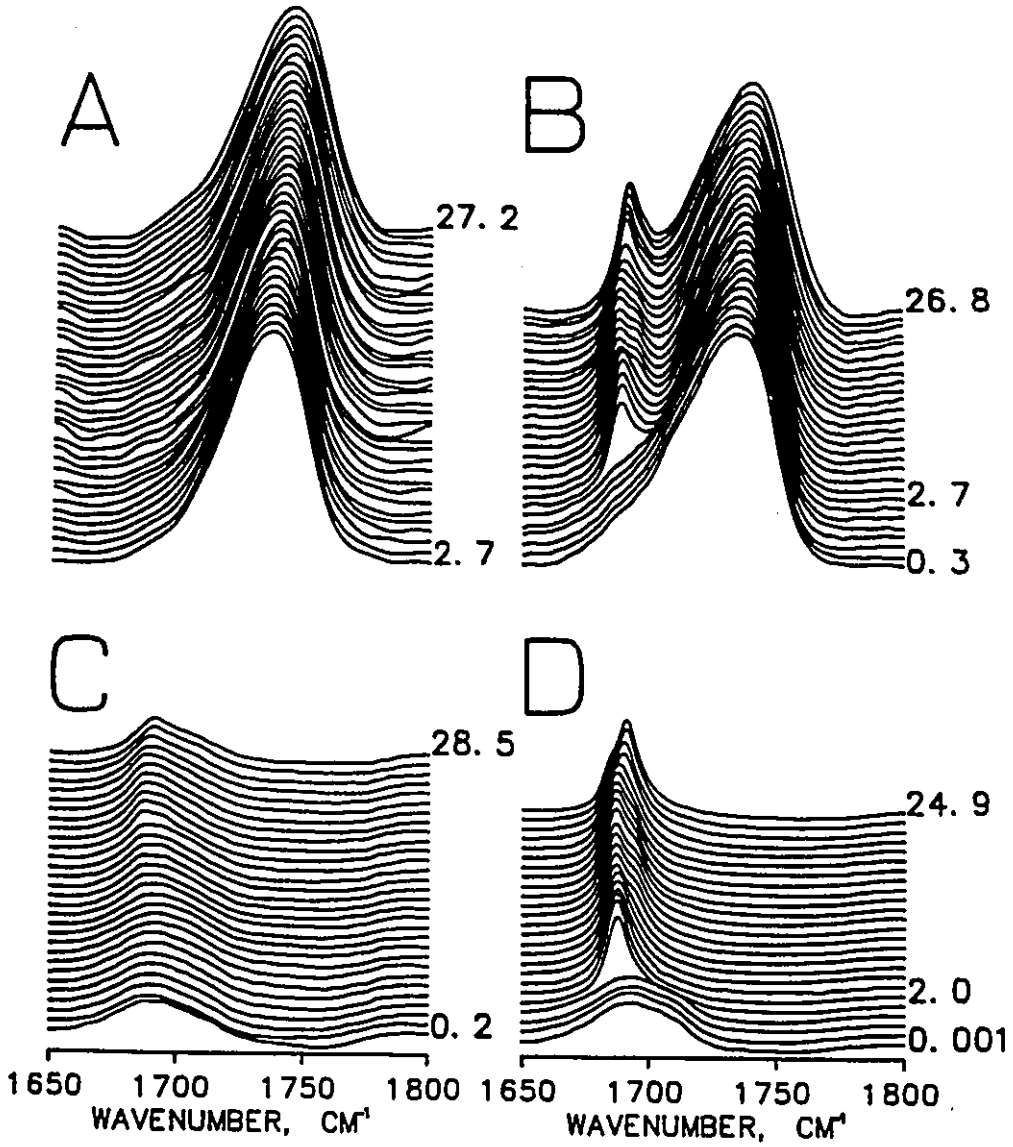
A
27. 2
2. 7
B
26. 8
2. 7
0. 3
C
28. 5
0. 2
D
24. 9
2. 0
0. 001
1650
1700
1750
1800
WAVENUMBER, CM⁻¹
1650
1700
1750
1800
WAVENUMBER, CM⁻¹

frequency side of the lipid C=O band is due to the very broad C=O band of tetracaine in the disordered environment of the lipid bilayer (*vide infra*), a spectral feature that undergoes no apparent change with increasing pressure. Thus, except for the slight increase in the lipid C=O band frequency with increasing pressure, there are no pressure-induced changes in this spectral region, indicating that, in the absence of cholesterol, the relatively deep penetration of tetracaine into the bilayer at high pH cannot be modified by pressures up to 25 kbar. Note that just the presence of gel phase lipid (pressure induced (Wong, 1987a)) is not sufficient to exclude the anesthetic.

^{2}H NMR studies of systems containing cholesterol suggest that, even at high pH, local anesthetic may be "squeezed" into a hydrophobic site closer to the lipid-water interface and that the partition coefficient is reduced compared to the obtained for the pure lipid (110 vs. 600) (Auger et al., 1988a, chapter 4 of this thesis). If tetracaine is closer to the interface in the presence of cholesterol, could pressure expel the anesthetic completely out of the bilayer, taking its C=O group from a disordered hydrophobic to an isotropic aqueous environment? To address this question, DMPC/TTC containing 30 mole % cholesterol was examined as a function of pressure. The FT-IR spectra of this system are shown in Figure 6.1B. By comparison of the stacked plots of parts A and B of Figure 6.1, it is readily apparent that a striking change occurs at 2.7 kbar in the spectra of the system containing cholesterol. The broad band at 1696 cm^{-1}, which we have attributed to the tetracaine C=O group, undergoes an abrupt decrease in band width.

To demonstrate that this C=O band arises from tetracaine, we have examined the DHPC/TTC system under the same conditions as those used for the DMPC/TTC system. With the spectral region between 1650 and 1800 cm^{-1} now free of the intense C=O band of

the ester-linked DMPC (Siminovitch et al., 1987a), it is evident from the spectra of the DHPC/TTC system shown in parts C and D of Figure 6.1 that the band at 1696 cm^{-1} must originate from tetracaine. It is important to note that without cholesterol (Figure 6.1C), this band at approximately 1696 cm^{-1} remains very broad, whereas with cholesterol (Figure 6.1D), a sudden decrease in bandwidth occurs at 2.0 kbar, similar to that observed in the DMPC/TTC system. Not only do these DHPC/TTC spectra (Figure 6.1C, D) prove that the band at 1696 cm^{-1} is due only to the carbonyl group of tetracaine but also, by showing that the influence of cholesterol on the pressure behavior of this band is very similar in both ester- and ether-linked lipids, they rule out any specific role of the lipid ester carbonyl groups.

The dramatic change in the bandwidth of the tetracaine C=O band at a particular critical pressure in the lipid/tetracaine systems containing cholesterol is due to the complete exclusion of the anesthetic from the lipid bilayer, since above the critical exclusion pressure, the shape of the tetracaine band and its response to increasing pressure duplicate those observed from pure tetracaine in solution, as shown in Figure 6.2. Moreover, it is interesting to note that the tetracaine C=O band frequency in solution (or, equivalently, above the critical exclusion pressure) is about 1685 cm^{-1} whereas in the lipid bilayer, or in a similar hydrocarbon environment such as hexane, this frequency is about 1696 cm^{-1}.

For tetracaine partitioned into DMPC bilayers in its charged form ($K_p \approx 22$ at pH 5.5), the application of pressure eventually does expel the anesthetic even without cholesterol, as shown in Figure 6.3A. Previous ^2H NMR studies suggested that the charged form of tetracaine at low pH is located near the lipid-water interface (Boulanger et al.,

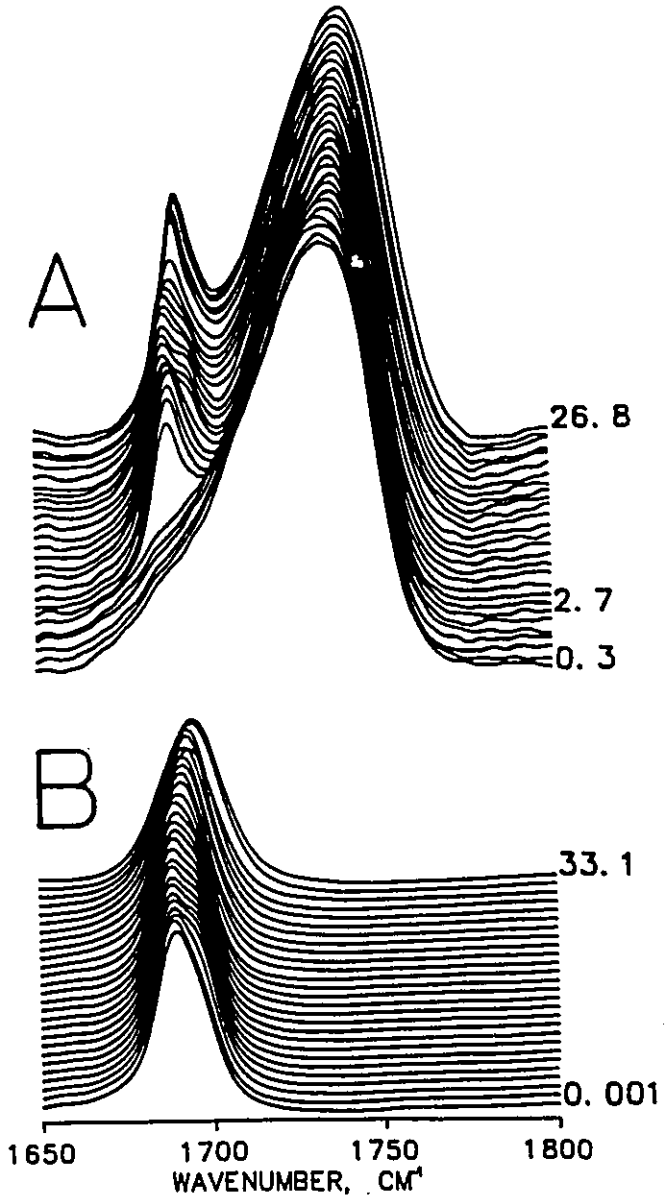

Figure 6.2 A comparison of the pressure-dependent behavior of the C=O band of tetracaine in lipid bilayers and in solution: A. DMPC + cholesterol + TTC, pH 9.5; B. TTC in D_2O, pH 9.5.

1981, Figure 1.4). In the presence of cholesterol (Figure 6.3B), the anesthetic ($K_p \approx 8$, Auger et al., 1988a) is squeezed even closer to the lipid-water interface, and therefore the critical pressure required for this expulsion is significantly lower. To summarize, Figures 6.1 and 6.3 demonstrate that low pH or cholesterol will assist pressure in squeezing the anesthetic out of the bilayer, since in either case the anesthetic molecule is closer to the lipid-water interface.

6.3.2 Charged phospholipid membranes

High phosphatidylserine (PS) levels are found in several preparations of excitable membranes (Camejo et al., 1969; Chacko et al., 1976); data obtained from different tissues suggest that PS is present in greater proportion in excitable tissues (Ritchie & Rogart, 1977) than in nonexcitable ones (Lazdunski et al., 1980). The structure and thermotropic properties of phosphatidylserine bilayers have been shown to be sensitive to the presence of divalent cations such as Ca^{2+} and Mg^{2+} (Hauser et al., 1982; Papahadjopoulos et al., 1977). In fact, it has been suggested that negative groups of phospholipid molecules might serve as binding sites for Ca^{2+} as well as for local anesthetics on membranes (Papahadjopoulos, 1970). Interactions between phosphatidylserine bilayers and monovalent and divalent ions have recently been studied by Fourier-transform infrared spectroscopy (Casal et al., 1987a-c). However, these studies have concentrated on the thermotropic behavior of the phosphatidylserine bilayers but with the addition of high pressure as a variable, new information on lipid structure and dynamics can be gained from studies of their barotropic behavior. In the present study, we have examined the pressure-induced expulsion of the local anesthetic tetracaine from fully hydrated phosphatidylserine

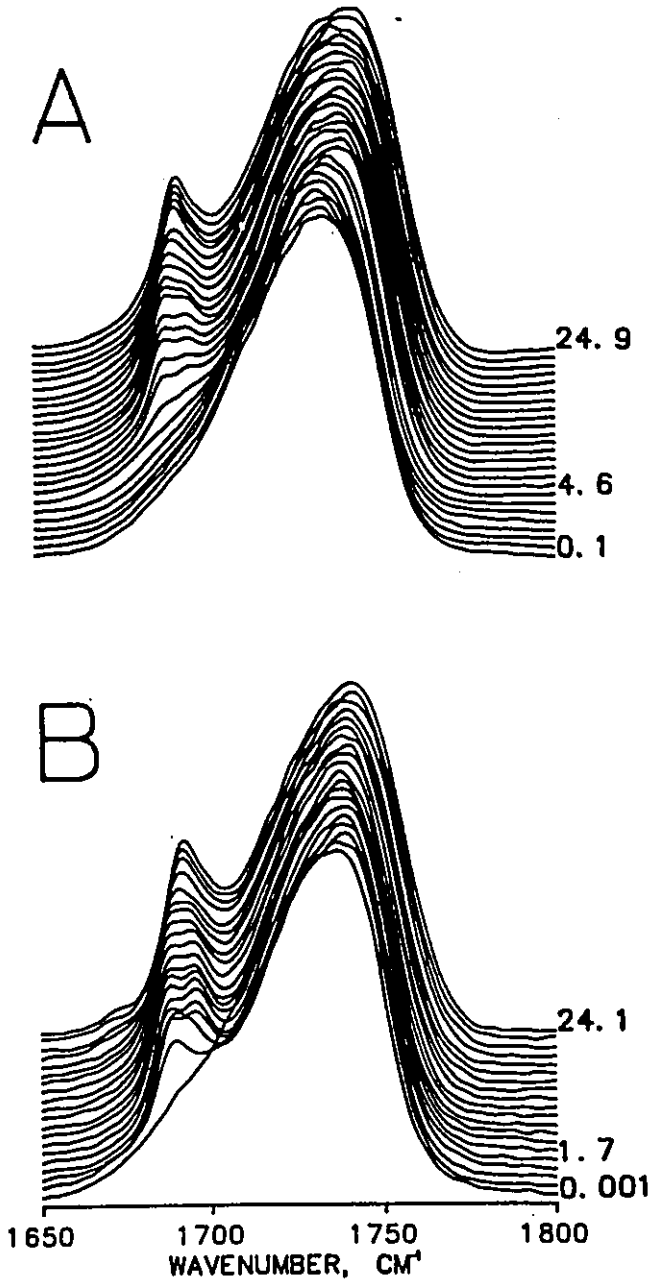

Figure 6.3 Stacked plots of infrared spectra of DMPC/TTC in the C=O stretching region as a function of hydrostatic pressure at low pH (5.5): **A.** without cholesterol; **B.** with cholesterol (30 mole%).

bilayers containing saturated (dimyristoylphosphatidylserine (DMPS)) and unsaturated (dioleoylphosphatidylserine (DOPS)) acyl chains and compared the results with those obtained previously for the zwitterionic lipid phosphatidylcholine in the absence and presence of cholesterol. Finally, the results are compared with those obtained for tetracaine incorporated into the mixed system DOPS:DOPC (1:4, molar ratio), a situation more relevant to that encountered in excitable membranes.

We have monitored the pressure-induced expulsion of tetracaine from pure DMPS and DOPS bilayers, for both the charged (pH 5.5) and uncharged form (pH 9.5) forms of the local anesthetic. The comparison of the infrared spectra in the spectral region 1550-1800 cm^{-1} for pure DMPS and DMPS in the presence of charged tetracaine at pH 5.5 is shown in Figure 6.4. Two phospholipid bands are present in this spectral region, at approximately 1740 and 1620^{-1}. The first band is associated with the ester-carbonyl stretching mode of the lipid acyl chains while the band at 1620 cm^{-1} is associated with the antisymmetric stretching vibration of the serine carboxylate (CO_2^-) group (Casal et al., 1987a-c). The results presented in Figure 6.4 indicates that at a pressure of 2.1 kbar, the anesthetic is expelled by pressure from the bilayer. This is indicated by the abrupt increase in spectral intensity of the anesthetic carbonyl band at 1685 cm^{-1}. Moreover, it appears from this figure that another infrared band, namely the tetracaine aromatic band at $\approx$ 1605 cm^{-1}, can be used to monitor the pressure-induced expulsion of the local anesthetic. Specifically, the frequency of this aromatic band is shifted from $\approx$ 1605 cm^{-1} to $\approx$ 1600 cm^{-1} when tetracaine goes from a hydrophobic to an aqueous environment. Whereas the shift in frequency observed for the anesthetic carbonyl stretching band was accompanied by a dramatic change in shape and intensity, the shape and intensity of the tetracaine aromatic band do not vary significantly as a function of pressure. A similar behavior is

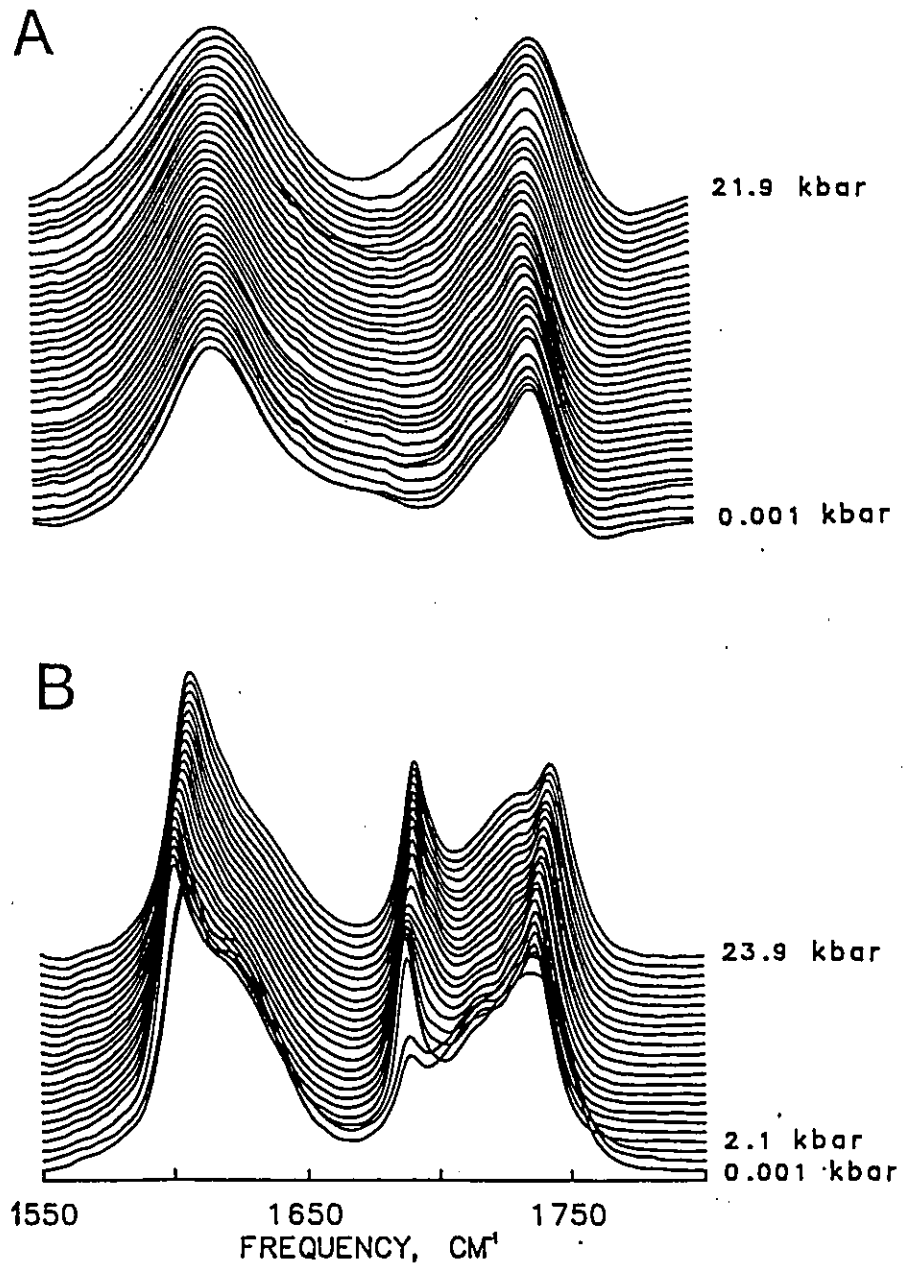

Figure 6.4 Stacked plots of infrared spectra recorded at increasing hydrostatic pressure of DMPS in **A.** the absence and **B.** the presence of charged tetracaine at pH 5.5 in the region of C=O and $\upsilon_{as}CO_2^-$ stretching bands.

observed at higher pH (pH 9.5), in which case the expulsion pressure is 2.7 kbar (results not shown). At pH 9.5, the local anesthetic tetracaine (pKa ≈ 8.5) is mostly in the uncharged form. For uncharged tetracaine incorporated into DMPC bilayers, it was shown in the previous section that application of pressure up to ≈ 25 kbar could not expel the anesthetic from the bilayer. These results were interpreted in terms of location of the uncharged form deeper in the membrane than the charged form.

The expulsion of tetracaine from DMPS bilayers at relatively low pressure is somewhat surprising since it was expected that the interaction between the negatively charged lipid and the positively charged anesthetic would result in a higher expulsion pressure compared to those obtained for tetracaine in phosphatidylcholine bilayers. However, if the electrostatic interactions between the anesthetic and the serine head group result in location of the anesthetic close to the aqueous interface of the bilayer, a relatively low expulsion pressure could result. The similarities between the pressure-induced expulsion of the charged and uncharged forms of the anesthetic can be rationalized by the fact that the uncharged form can most likely still interact via hydrogen bonding with the serine head group. In fact, it was demonstrated that the partition coefficient of the uncharged anesthetic in PS bilayers is still very high, although smaller than that of the charged form (Kelusky et al., 1986), suggesting strong lipid-anesthetic interactions.

At ambient temperature and pressure in the diamond anvil cell, DOPS is in the liquid-crystalline phase, as opposed to DMPS which is in the gel phase. Inspection of the infrared spectra in the region 1550-1800 cm^{-1} for DOPS in the presence of charged tetracaine (Figure 6.5) clearly reveals that at atmospheric pressure, tetracaine is incorporated into the bilayer. A similar behavior was observed for the uncharged form of

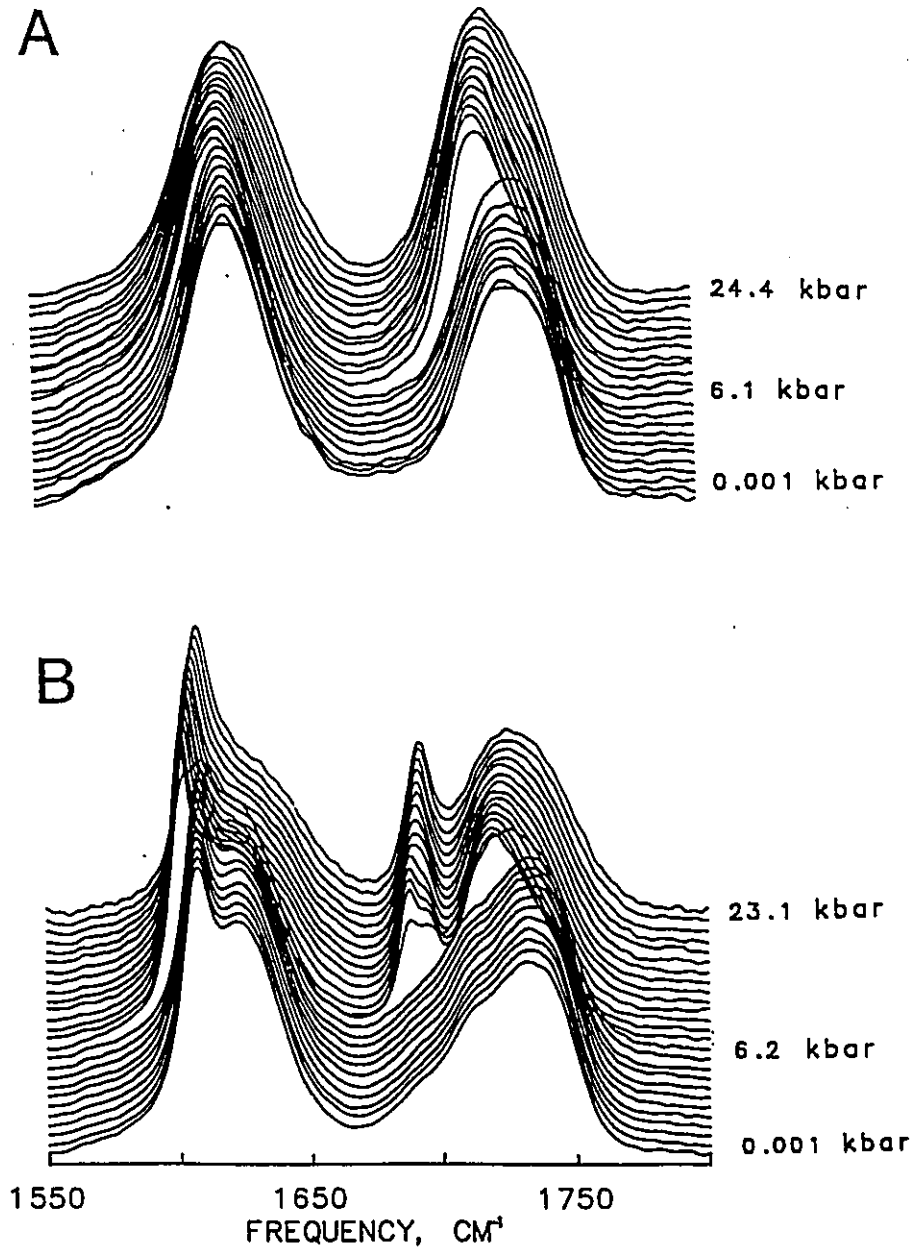

Figure 6.5 Stacked plots of infrared spectra recorded at increasing hydrostatic pressure of DOPS in **A.** the absence and **B.** the presence of charged tetracaine at pH 5.5 in the region of C=O and $\upsilon_{as}CO_2^-$ stretching bands.

the anesthetic (results not shown). Spectral features characteristic of the pressure-induced expulsion of the anesthetic only become apparent at much higher pressure. For the charged form of tetracaine, it appears that the expulsion pressure is in fact the liquid-crystalline to gel phase transition pressure (6.2 kbar vs 6.1 kbar for the expulsion and phase transition pressure, respectively). In the case of the uncharged form at pH 9.5, the expulsion pressure is also very close to the critical pressure, although slightly smaller (5.6 kbar vs 6.1 kbar).

As discussed previously, the presence of gel phase lipid (pressure-induced (Wong, 1987a)) is not sufficient to exclude the anesthetic, the uncharged form of tetracaine not being expelled from DMPC bilayers at pressures up to 25 kbar. However, the pressure-induced gel phase of DOPS is highly ordered. It therefore appears that this highly ordered phase cannot accommodate the presence of the local anesthetic molecule and that the liquid-crystalline to gel phase transition thus results in the complete expulsion of the anesthetic from the bilayer.

6.3.3 Mixed phospholipid membranes

We have discussed in the previous section the interactions of the local anesthetic tetracaine with bilayers of pure phosphatidylserine. However, the concentration of phosphatidylserine found in excitable membranes is usually near 20 mole% of the total lipids (Camejo et al., 1969; Chacko et al., 1976). We have thus examined the interactions of the charged form of tetracaine at pH 5.5 with DOPS:DOPC (1:4, molar ratio) bilayers, a situation which more closely resembles that observed in biological membranes. The

unsaturated phosphatidylserine was examined since high levels of unsaturated lipid are also found in excitable membranes.

The infrared spectra of DOPS:DOPC (1:4, molar ratio) bilayers in the absence and in the presence of charged tetracaine are shown in Figure 6.6 as a function of the hydrostatic pressure applied on the systems. From this figure, it is clear that, as was observed in the pure DOPS system, the anesthetic is expelled by pressure from the bilayer at the phase transition pressure of the lipid system. The fact that the expulsion pressure still corresponds to the liquid-crystalline to gel phase transition pressure even in the presence of only 20 mole% of phosphatidylserine indicates that chain unsaturation rather than negative head group charge is responsible for the high expulsion pressure in this system.

6.4 Nerve membranes

The expulsion of local anesthetic by pressure from model membrane systems described above would assume a much larger significance if the same phenomenon was also observed in nerve membranes. We have therefore performed the infrared experiments on myelinated (frog sciatic) and unmyelinated (lobster) nerves as a function of pressure. The results indicate that the application of hydrostatic pressure also leads to an expulsion of the anesthetic from these nerve membranes. The pressure dependence of the infrared spectra of frog sciatic nerve in the absence and in the presence of tetracaine is compared in parts A and B of Figure 6.7, respectively. Similar to the model systems, the tetracaine C=O band at low pressures is very broad (Figure 6.7B) but undergoes an abrupt

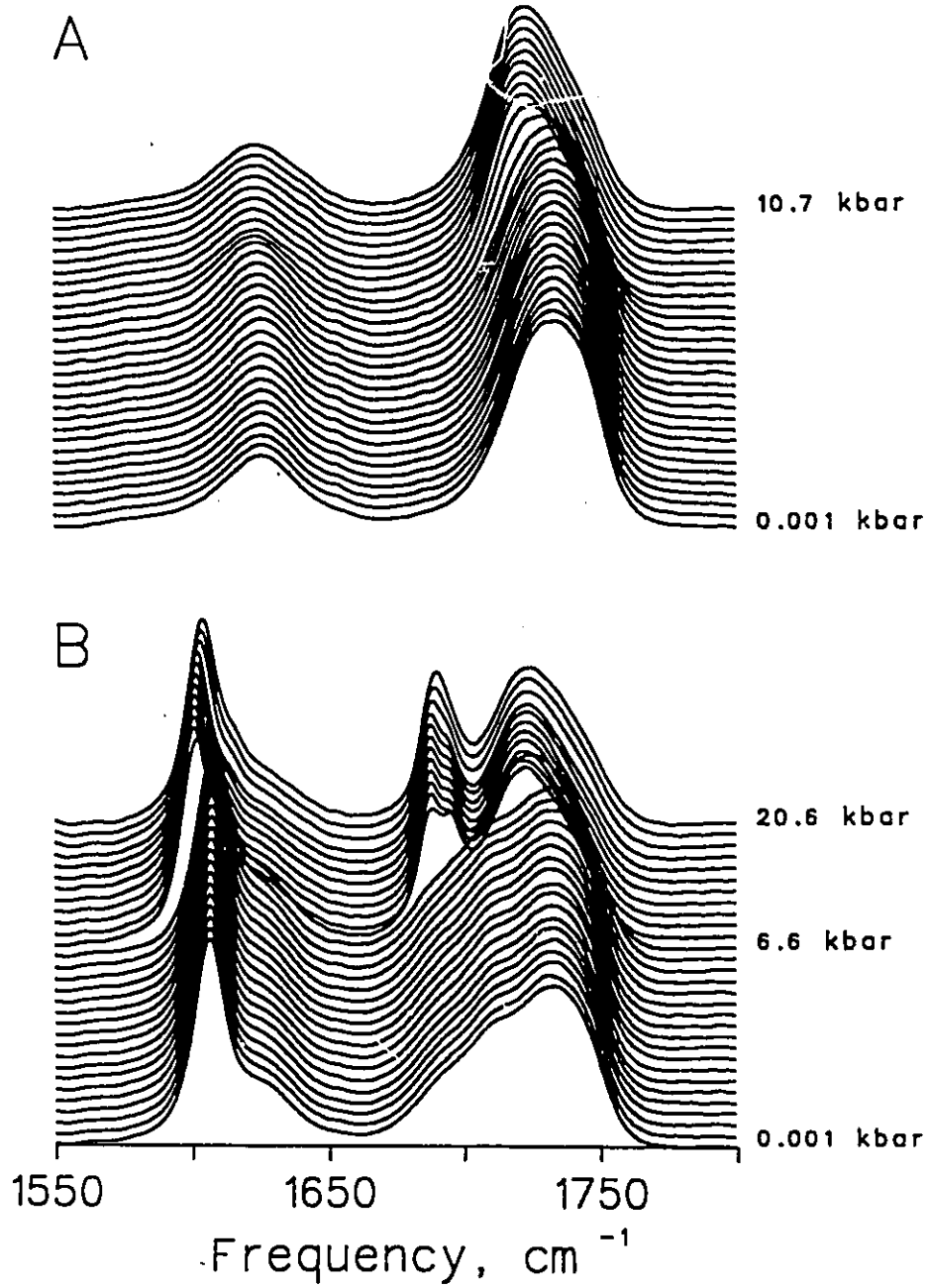

Figure 6.6 Stacked plots of infrared spectra in the 1550-1800 cm^{-1} region of **A.** DOPS:DOPC (1:4, molar ratio) and **B.** DOPS:DOPC (1:4, molar ratio) + TTC, pH 5.5.

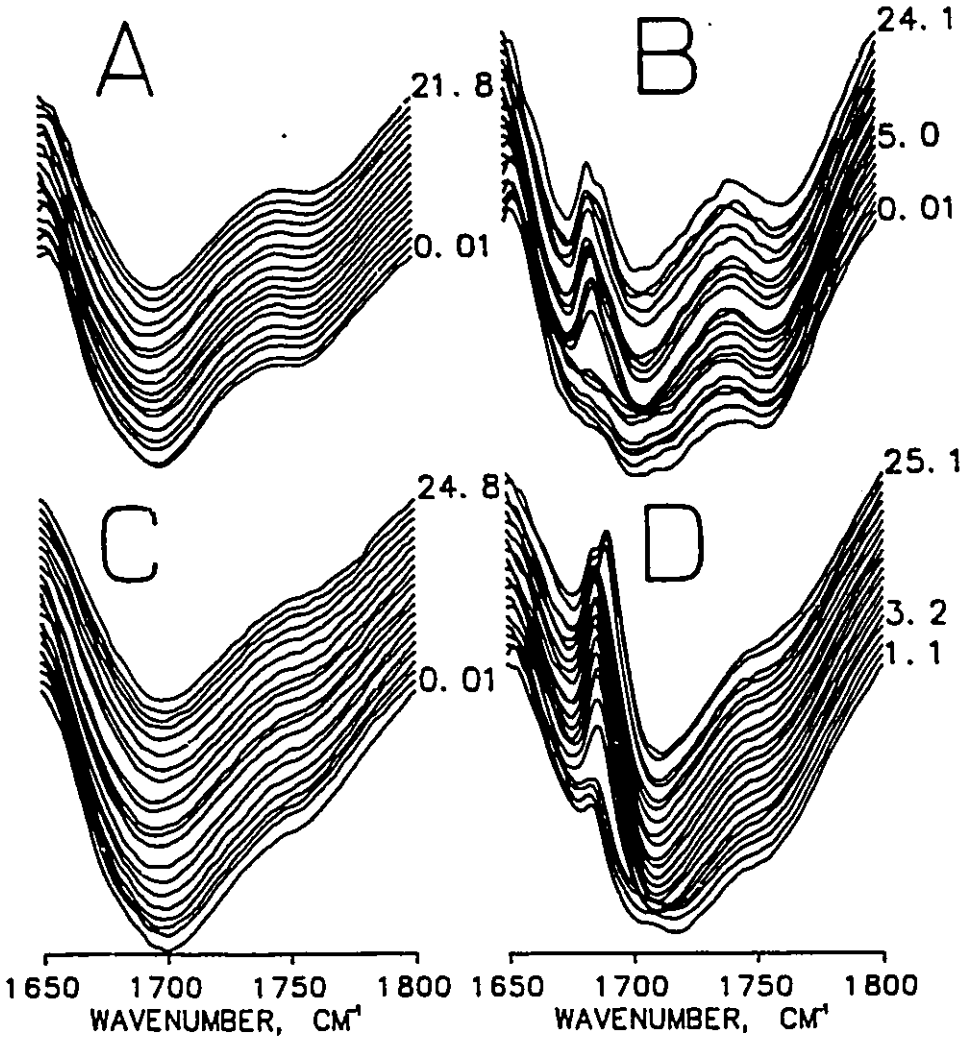

Figure 6.7 Pressure dependence of infrared spectra in the C=O stretching region of nerves at physiological pH (pH 7.4) in the absence (left column) and in the presence (right column) of tetracaine: **A.** frog sciatic nerve; **B.** frog sciatic nerve + TTC; **C.** lobster nerve; **D,** lobster nerve + TTC.

reduction in bandwidth at a critical pressure of approximately 5 kbar. Since these changes mimic those observed in the model systems, we can conclude that tetracaine, partitioned into the nerve membrane at atmospheric pressure and located close to the lipid-water interface, is expelled by pressure.

Since the myelin membrane is approximately 75% lipid (Norton, 1984; Morell, 1984), a large proportion of which (about 40 mole %) is cholesterol (Norton, 1981), it is not unreasonable to suggest that, in this system, cholesterol may also play a role in assisting pressure to squeeze out the anesthetic. As shown in parts C and D of Figure 6.7, over the same pressure range, the p. sure behavior of the C=O band of tetracaine partitioned into lobster nerve membranes is similar to that observed in either the frog sciatic nerve spectra (Figure 6.7A,B) or those of the model systems. Thus, even though the lobster nerves have a lower proportion of membrane (Pézolet & Georgescauld, 1985), it is evident from the comparison of parts C and D of Figure 6.7 that tetracaine does partition into the nerve and that pressure will also expel the anesthetic from this system. Moreover, for both model and nerves, the pressure-induced exclusion of tetracaine was found to be reversible.

In this study, we have simply demonstrated that pressure can exclude anesthetics from membranes. The fact that the exclusion pressure can be as much as an order of magnitude larger than that required in vivo for pressure reversal of anesthesia may indicate that this phenomenon requires only a pressure-induced change in anesthetic location within the membrane, and not complete exclusion.

6.5 Conclusions

In model systems, it is clear that pH, the presence of cholesterol, the degree of chain unsaturation and the charge of the phospholipid head group play important roles in determining the ability of pressure to exclude the anesthetic, but in the heterogeneous environment found in the lipid bilayers of nerve membranes, other factors may predominate. Nevertheless, the unity of the pressure-induced phenomenon observed in both model and biological membranes demonstrated in this study is significant and indicates that further experiments using this novel high-pressure vibrational spectroscopic technique on nerve membranes may lead to a better understanding of barotropic phenomenon in these tissues, and of the mechanism of anesthesia.

CHAPTER 7

Effects of the local anesthetic tetracaine on the structural and dynamic properties of phosphatidylcholine and cholesterol membranes

7.1 Introduction

In the last chapter, it was demonstrated that the local anesthetic tetracaine is located close to the aqueous interface of the lipid bilayer in model membrane systems containing a physiological concentration (30 mole%) of cholesterol (Auger et al., 1987). This study also demonstrated that tetracaine, in both myelinated and unmyelinated nerves, is located in an environment similar to that in model systems. On the other hand, information about the effects of the local anesthetic tetracaine on the order and dynamics of the lipid acyl chains have been obtained by deuterium NMR spectroscopy. These studies indicated that the anesthetic reduces the order parameter of the entire lipid acyl chains in the liquid-crystalline phase. This disordering effect is larger in the presence of cholesterol (30 mole%) and for the charged form of the anesthetic (Boulanger et al.; 1981, Auger et al., 1988a). By comparing ^2H spin-lattice relaxation times, these studies also showed that tetracaine alters only slightly the dynamics of DMPC acyl chains in cholesterol-containing systems.

Nevertheless, little is known about the effects of local anesthetics on the structural

and dynamic properties of phospholipid bilayers in the gel state. We have therefore examine the effects of tetracaine on 1,2-dimyristoyl-*sn*-glycero-3-phosphocholine (DMPC) and 1,2-di-*O*-hexadecyl-*sn*-glycero-3-phosphocholine (DHPC) bilayers in the presence and absence of 30 mole% of cholesterol, by using high pressure FT-IR spectroscopy. This technique has proven to be very powerful in the study of structural and dynamic properties of phospholipid bilayers (Wong, 1987a-c). In particular, the correlation field splitting of the methylene scissoring mode, δCH_2, in both Raman and infrared spectra is very useful for the characterization of interchain packing (Wong, 1984; Boerio & Koenig, 1970).

7.2 Effects of tetracaine on pure DMPC bilayers

Figure 7.1 compares the pressure dependence of the methylene scissoring mode δCH_2 of DMPC multilamellar dispersions in the presence and absence of tetracaine. The anesthetic was incorporated in either its charged form at pH 5.5 or its uncharged form at pH 9.5. For pure DMPC bilayers, the pressure dependence of the methylene scissoring mode band is very similar to that observed for 1,2-dipalmitoyl-*sn*-glycero-3-phosphocholine (DPPC) in multilamellar aqueous dispersions (Wong & Mantsch, 1985a; Siminovitch et al., 1987a). As the pressure is increased, one observes a pressure-induced correlation field splitting of the δCH_2 mode, which at low pressure gives rise to only one band at $\approx$ 1470 cm^{-1}. The first manifestation of this splitting with increasing pressure is a shoulder on the high frequency side of δCH_2, which steadily gains intensity until a well-defined correlation field component is apparent. The observation of only a single CH_2 scissoring band at atmospheric pressure reflects the fact that under these conditions of temperature and pressure, the orientation of the methylene chains is highly disordered due to significant

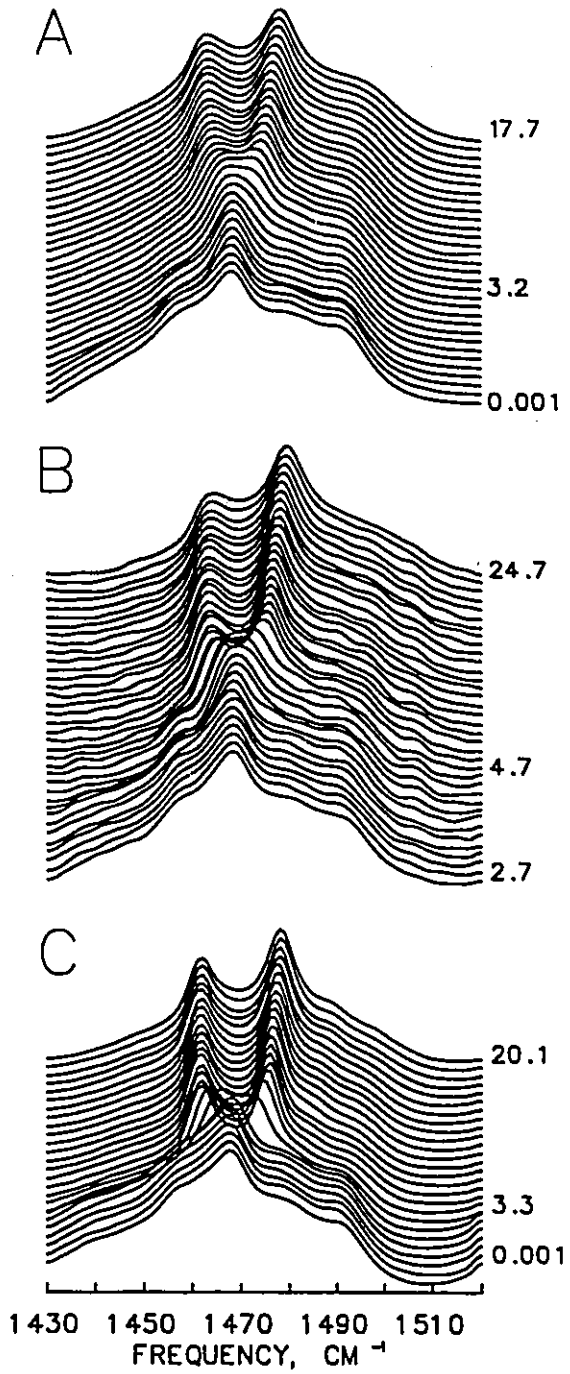

Figure 7.1 Stacked plots of the infrared spectra at increasing hydrostatic pressures of aqueous DMPC dispersions in the CH_2 scissoring region for **A.** DMPC, **B.** DMPC + TTC, pH 9.5, and **C.** DMPC + TTC, pH 5.5.

reorientational fluctuations of the acyl chains. Increasing pressure leads to a damping of these reorientational fluctuations, and an increase in interchain interactions, which gives rise to the observed correlation field splitting.

The gel (L_{β}') to liquid-crystalline (L_{α}) phase transition temperature for DMPC is 23.5°C (Silvius, 1982), which means that at ambient temperature (28°C) and at atmospheric pressure, DMPC is in the liquid-crystalline phase. Assuming that the gel to liquid-crystalline phase transition for DMPC is a first-order transition, as it is in DPPC, the critical temperature T_m can be raised by applying external pressure (the Clausius-Clapeyron relationship). Elevation of pressure should therefore induce the transition to the gel phase. This pressure-induced increase in T_m has been described in detail (Wong et al., 1982; Wong & Mantsch, 1985b). The critical pressure for the transition from the liquid-crystalline phase to the gel phase in DMPC is 0.15 kbar at 28°C (Wong & Mantsch, 1985b). Therefore, application of a very small pressure to DMPC in the liquid-crystalline phase in the diamond anvil cell will induce a transition to the gel state.

When uncharged tetracaine (pH 9.5) is incorporated into DMPC bilayers, high pressure FT-IR (Auger et al., 1987, chapter 6 of this thesis) and ^2H NMR studies (Auger et al., 1988a; Boulanger et al., 1981, chapter 4 of this thesis) have shown that the anesthetic intercalates deeply into the bilayer. In order to elucidate the effects of the incorporation of uncharged tetracaine on the acyl chain interactions in DMPC, the pressure dependence of the CH_2 scissoring mode bands for DMPC in the presence of uncharged tetracaine at pH 9.5 (Figure 7.1B) was first compared with that observed for pure DMPC (Figure 7.1A). The pressure dependences of the frequencies of the methylene scissoring mode components for DMPC in the absence and presence of uncharged tetracaine were also

examined (Figure 7.2A). From this figure, the pressures at which the pressure-induced correlation field splittings become apparent can easily be determined. A well-defined correlation field component band $\delta'CH_2$ becomes apparent at 3.2 kbar for pure DMPC and at 4.7 kbar for DMPC+TTC, pH 9.5. Further increase in pressure then results in a relatively rapid, non-linear increase in the magnitude of this splitting. The pressure at which the correlation field component band becomes apparent is much higher for DMPC in the presence of uncharged tetracaine compared to pure DMPC, while the magnitude of the correlation field splitting is smaller for the former system.

The pressure-induced correlation field splittings of CH_2 scissoring bands are the result of interchain interactions between the lipid hydrocarbon chains (Snyder, 1961). These interactions can be intramolecular or intermolecular, the former being predominant at lower pressure. For DMPC in the presence of uncharged tetracaine, the smaller correlation field splitting indicates smaller interchain interactions due to the increase in both the orientational and conformational disorder as a result of the intercalation of the anesthetic between the lipid acyl chains. Moreover, the higher pressure at which this splitting becomes apparent compared to that obtained for pure DMPC bilayers also indicates that in the presence of uncharged tetracaine, the DMPC acyl chains are orientationally more disordered, and thus a higher pressure is necessary to stop the acyl chain reorientational fluctuations and induce a correlation field splitting.

The pressure dependence of the CH_2 scissoring mode bands for DMPC in the presence of charged tetracaine at pH 5.5 (Figure 7.1C) was also examined and compared with that obtained for pure DMPC (Figure 7.1A). A visual inspection of these spectra shows that the "valley" between the two component bands of the pressure-induced

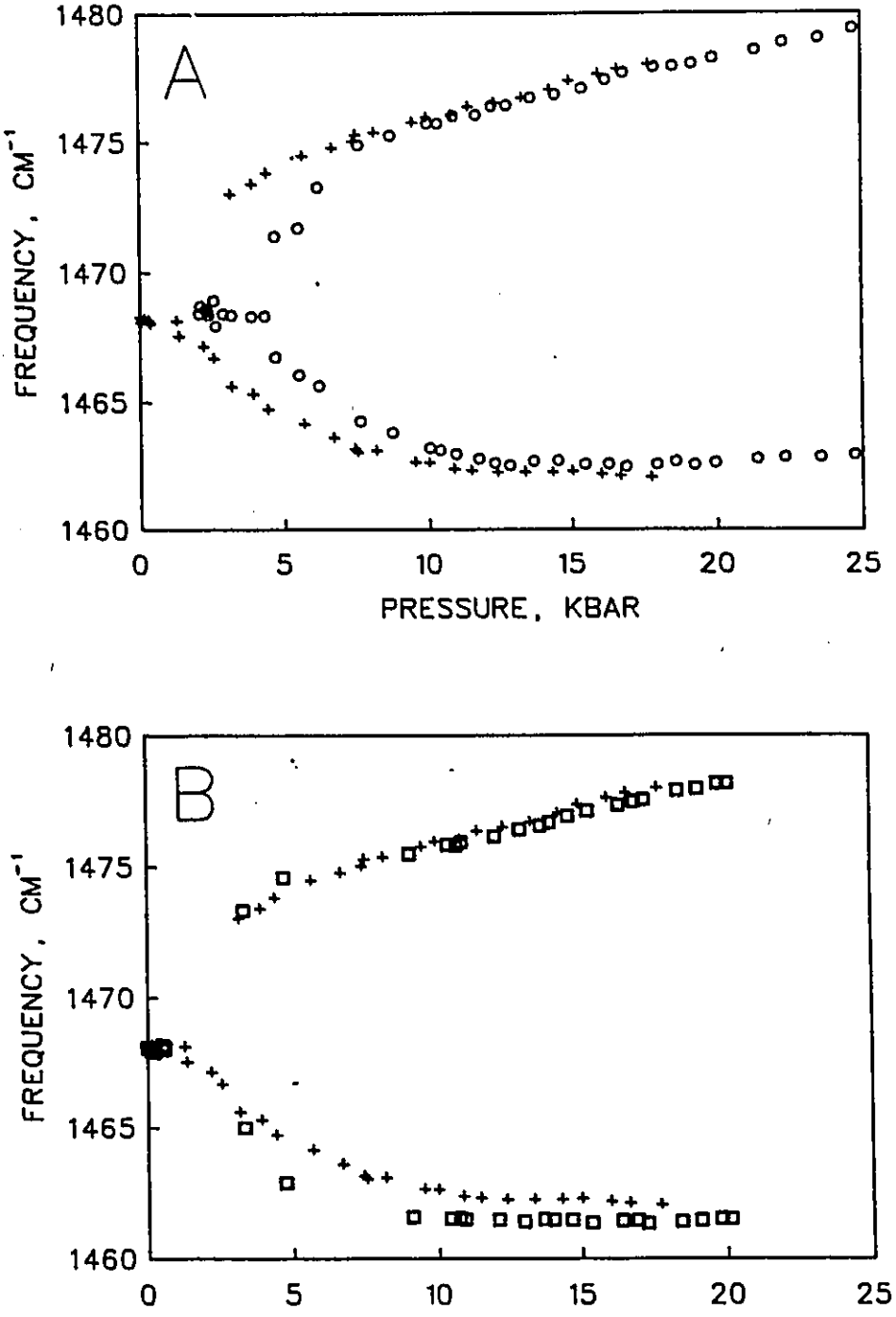

Figure 7.2 Comparison of the pressure dependence of the frequencies of the δCH_2 mode for (+) DMPC with that of A. (o) DMPC+TTC, pH 9.5 and B. (□) DMPC+TTC, pH 5.5.

correlation field splitting is particularly pronounced for DMPC in the presence of charged tetracaine, but much less so for pure DMPC. A pressure dependence of the δCH_2 mode similar to that observed for DMPC in the presence of charged tetracaine has been observed for various lipid bilayer systems, such as 1,2-DHPC, 1-palmitoyl-*sn*-glycero-3-phosphocholine (lyso PC) and 1,3-dipalmitoyl-*sn*-glycero-2-phosphocholine (1,3-DPPC) (Siminovitch et al, 1987a-b). These systems are known to form a lamellar phase with complete interdigitation of the hydrocarbon chains under the conditions of temperature and pressure at which the correlation field splitting is observed. The pressure dependence of the methylene scissoring mode obtained for DMPC in the presence of the charged anesthetic therefore suggests that the incorporation of charged tetracaine in DMPC bilayers induces the formation of an interdigitated lamellar gel phase.

The induction of an interdigitated gel phase in phospholipids by exogeneous agents such as glycerol (McDaniel et al., 1983; McIntosh et al., 1983; O'Leary & Levin, 1984), protein (Boggs & Moscarello, 1982), ions (Cunningham & Lis, 1986) and tetracaine (McIntosh et al., 1983) has been extensively studied. It has been demonstrated that the ability to induce an interdigitated phase does not depend on the presence or absence of a charge on the molecule (Simon et al., 1986). However, Simon et al. (1986) suggested that the one requirement for the induction of the interdigitated phase is that the guest molecule must reside at the membrane-water interface and must not extend too deeply into the acyl chain region. This explains why there is no interdigitation in the presence of uncharged tetracaine, which penetrates too deeply into the hydrophobic region to allow a stable interdigitated phase.

High pressure FT-IR (Auger et al., 1987, chapter 6 of this thesis) and ^2H NMR

studies (Auger et al., 1988a; Boulanger et al., 1981, chapter 4 of this thesis) have demonstrated that charged tetracaine is located close to the aqueous interface of DMPC bilayers. Moreover, X-ray diffraction studies have shown that with incorporation of tetracaine into DPPC liposomes at 20°C, the bilayer thickness is only 30 Å, which is about 20 Å smaller than two fully-extended DPPC molecules (McIntosh et al., 1983). From these observations, we can therefore conclude that because charged tetracaine is located close to the aqueous interface of DMPC bilayers, the DMPC acyl chains in the pressure-induced gel phase are interdigitated. The stability of the interdigitated phase can be rationalized as follows. The intercalation of the charged anesthetic in DMPC bilayers tends to separate the lipid head groups. Since the gel state acyl chains are rigid under the present conditions, this will tend to form defects between the chains which are energetically unfavorable (Israelachvili et al., 1980). The lowest energy phase is therefore the interdigitated phase (Simon et al., 1986).

The pressure dependences of the frequencies of the CH_2 scissoring mode components for pure DMPC and DMPC in the presence of charged tetracaine at pH 5.5 (Figure 7.2B) are very similar, the magnitude of the correlation field splitting being however slightly larger in the presence of tetracaine. These results support the conclusion of the formation of an interdigitated lamellar gel phase in DMPC in the presence of charged tetracaine.

It has been shown that at a pressure of 4.6 kbar, the charged form of the anesthetic is expelled from DMPC bilayers (Auger et al., 1987). However, above that pressure, the pressure dependence of the methylene scissoring region remains characteristic of lipids in an interdigitated gel phase. This can be explained by the fact that under high hydrostatic

pressure, the energy required to revert to a non-interdigitated phase after the expulsion of the anesthetic would be very large. The mismatch between the lipid headgroup and the hydrocarbon region created by the expulsion of the anesthetic can however be compensated by a complete interdigitation of the lipid acyl chains.

The pressure dependences of the methylene rocking mode γCH_2 of DMPC multilamellar dispersions in the absence and presence of tetracaine, both in its charged and uncharged form, have also been examined (data not shown). In the presence of charged tetracaine at pH 5.5, the pressure dependence of the CH_2 rocking mode is similar to that observed for systems known to form an interdigitated lamellar gel phase (Siminovitch et al., 1987a-b) which therefore supports the conclusion that the pressure-induced gel phase for DMPC bilayers in the presence of charged tetracaine is an interdigitated lamellar gel phase.

7.3 Effects of tetracaine on DHPC bilayers.

Recent studies using differential scanning calorimetry (DSC) , X-ray diffraction, ^{14}N, ^{31}P, and ^{2}H NMR and high pressure FT-IR spectroscopy (Ruocco et al., 1985a-b; Siminovitch et al., 1983, 1987a) have shown that the replacement of the fatty acyl chains with the corresponding alkyl chains has a significant effect on the structure and dynamics of lipids in the low temperature gel phase. As mentioned previously, it has been demonstrated that 1,2-di-*O*-hexadecyl-*sn*-glycero-3-phosphocholine (DHPC) forms an interdigitated lamellar gel phase at temperatures below the pretransition at 35°C, whereas DPPC does not.

From the pressure dependence of the carbonyl stretching band of tetracaine incorporated in DHPC multilamellar dispersions at pH 9.5, it has been shown that the uncharged anesthetic intercalates deeply into DHPC bilayers in the gel state (Auger et al., 1987). In order to see the effects of the incorporation of uncharged tetracaine on the alkyl chain packing of DHPC in the gel phase, we have monitored the pressure dependence of the methylene scissoring and rocking mode bands for DHPC in the presence of uncharged tetracaine and compare the results with those obtained by Siminovitch et al. (1987a) for pure aqueous DHPC multilamellar dispersions. The results are presented in Figure 7.3.

The pronounced "valley" between the methylene scissoring and rocking mode bands and their correlation field components for pure DHPC has been interpreted in terms of the formation of an interdigitated lamellar gel phase (vide supra) . The DHPC headgroup surface area in the gel state is 79 $Å^2$ compared to 48 $Å^2$ for that of DPPC in non-interdigitated bilayers at 20°C (Janiak et al., 1979). For both phospholipids however, the hydrocarbon chain cross-sectional area is approximatively 40 $Å^2$ per molecule (i.e. 20 $Å^2$ per acyl chain). The mismatch between the DHPC headgroup and hydrocarbon chain surface area (79 $Å^2$ vs. 40 $Å^2$, respectively) therefore favors the formation of an interdigitated bilayer phase.

The pressure dependences of the CH_2 scissoring and rocking mode bands for DHPC in the presence of uncharged tetracaine are very similar to those obtained for pure DHPC and are characteristic of lipids in an interdigitated gel phase. Moreover, the pressure dependences of the frequencies of the methylene scissoring mode band and its correlation field component (Figure 7.4) for DHPC do not vary significantly upon addition

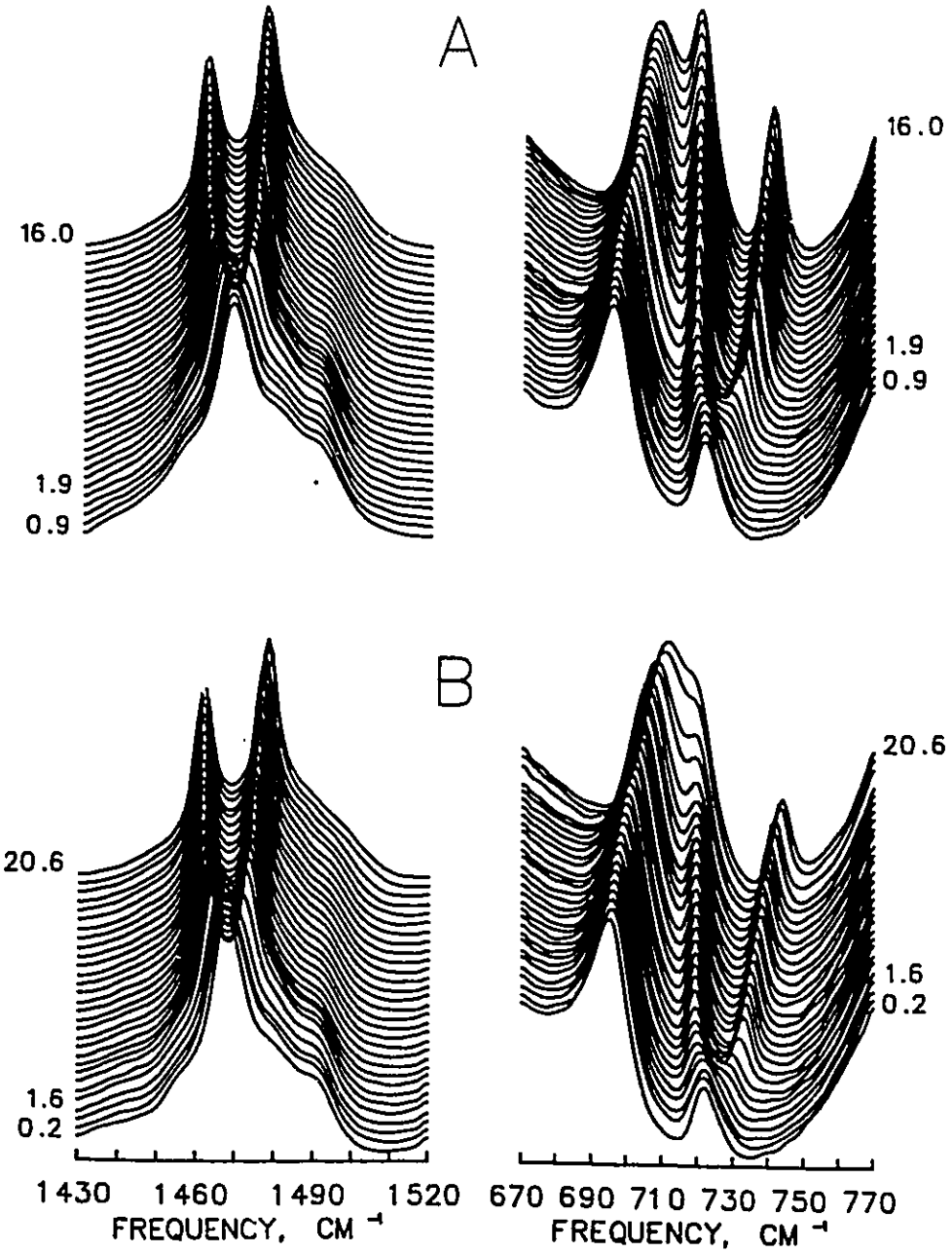

Figure 7.3 Stacked plots of the infrared spectra of aqueous DHPC dispersions in the CH_2 scissoring region (left spectra) and in the CH_2 rocking region (right spectra) for **A.** DHPC, and **B.** DHPC+TTC, pH 9.5. The band at 695 cm^{-1} (right spectra) is the phonon band of α-quartz used for the pressure calibration.

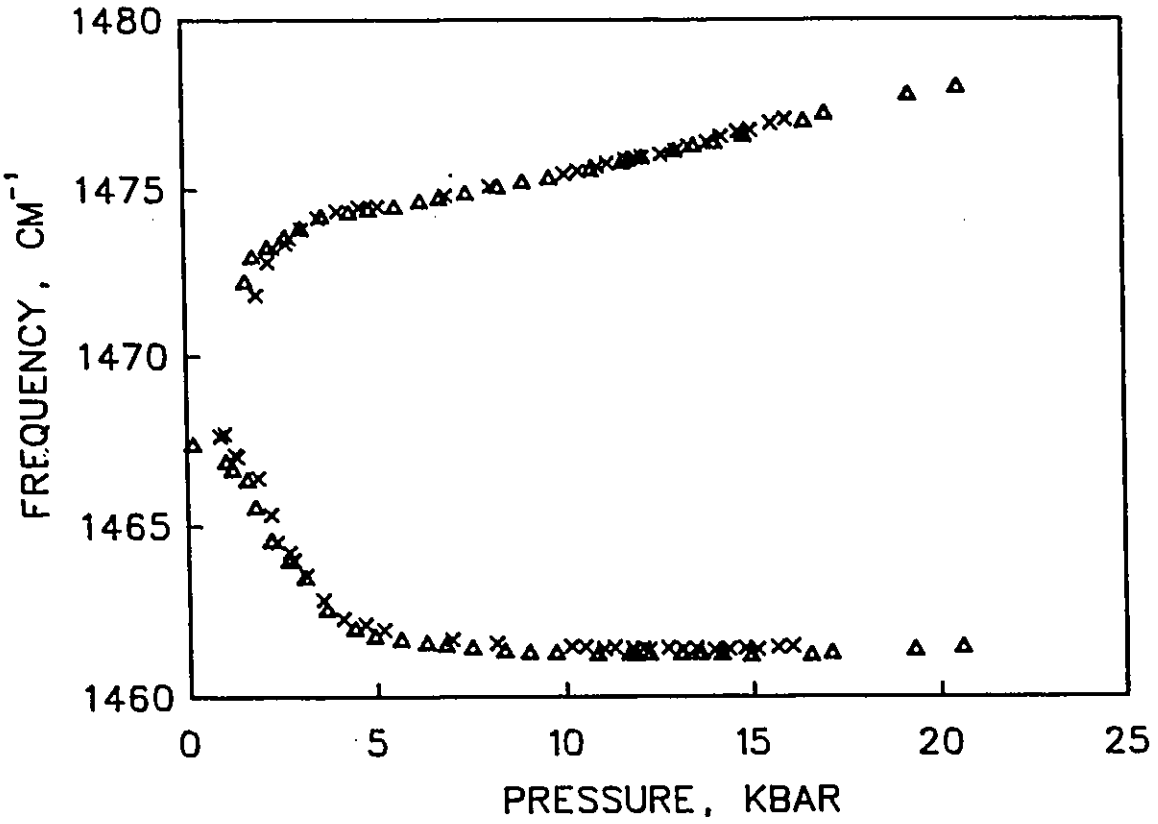

Figure 7.4 Pressure dependence of the frequencies of the δCH_2 mode for (×) DHPC and (△) DHPC+TTC, pH 9.5.

of uncharged tetracaine. The results therefore suggest that the incorporation of uncharged tetracaine into DHPC does not prevent the formation of an interdigitated lamellar gel phase.

The effects of the incorporation of an equimolar concentration of cholesterol on the lipid packing, conformation and dynamics of DHPC multilamellar dispersions have been studied by X-ray diffraction and ^2H NMR spectroscopy (Siminovitch et al., 1987c). The results of these studies indicate that the addition of 50 mole% cholesterol to DHPC prevents the formation of an interdigitated phase at 22°C since the introduction of cholesterol (surface area $\approx$ 38 $Å^2$ (Pethica, 1955; Small, 1977)) into the hydrophobic hydrocarbon portion of the bilayer creates a more favorable match between the head group and hydrocarbon surface areas (Siminovitch et al., 1987c). Moreover, the thermal phase behavior and structure of hydrated mixtures of DPPC and DHPC have been investigated by DSC and X-ray diffraction techniques (Lohner et al., 1987; Kim et al., 1987), and indicate that at temperatures below the subtransition of DHPC, the incorporation of 50 mole% of DPPC to DHPC prevents the formation of an interdigitated gel structure. However, when less than 50 mole% DPPC is added, DHPC remains in the interdigitated gel phase and shows full solubility for DPPC up to equimolarity without major structural changes.

The amount of uncharged tetracaine incorporated in the DHPC bilayers corresponds to about 20 mole% of the total lipids, according to the very large partition coefficients determined for uncharged tetracaine in phosphatidylcholine bilayers (Boulanger et al., 1980). This amount is therefore less than the amount of cholesterol or DPPC (50 mole%) required to prevent the formation of interdigitated DHPC bilayers.

This could explain why upon addition of 20 mole% of uncharged tetracaine, DHPC bilayers maintain an interdigitated gel structure. However, the hydrophobic portion of the tetracaine molecule is much shorter than that of cholesterol and DPPC. Moreover, in the model proposed by Boulanger et al. (1981) (Figure 1.4) for the location of uncharged tetracaine in phosphatidylcholine bilayers, the anesthetic penetrates relatively deeply in the bilayer but, because of the shortness of the butyl tail, the last few CH_2 segments of the phospholipid molecules are not in contact with the anesthetic. This model could also explain why DHPC maintains an interdigitated structure upon addition of uncharged tetracaine. However, whether the shorter hydrophobic portion of tetracaine or the concentration of anesthetic used in this study are responsible for this effect is still to be determined.

The pressure dependence of the methylene scissoring bands for DHPC:cholesterol + TTC, pH 9.5 (Figure 7.5A) was also examined in order to see if the presence of 30 mole% of cholesterol can prevent the interdigitation of the DHPC alkyl chains in the presence of uncharged tetracaine. Upon addition of cholesterol, the "valley" between the two component bands of the pressure-induced correlation field splitting in DHPC is less pronounced than it is for the pure lipid in the absence and presence of uncharged anesthetic. Moreover, comparison of the pressure dependence of the frequencies of the CH_2 scissoring mode components for DHPC+TTC, pH 9.5 and DHPC:cholesterol+TTC, pH 9.5 (Figure 7.5B) shows that the magnitude of the correlation field splitting is smaller for the latter system and that the pressure at which the splitting becomes apparent is 4.4 kbar in the presence of cholesterol compared to 1.6 kbar for the system without cholesterol. These results indicate that the presence of cholesterol does prevent, to a certain extent, the interdigitation of DHPC alkyl chains in the presence of uncharged

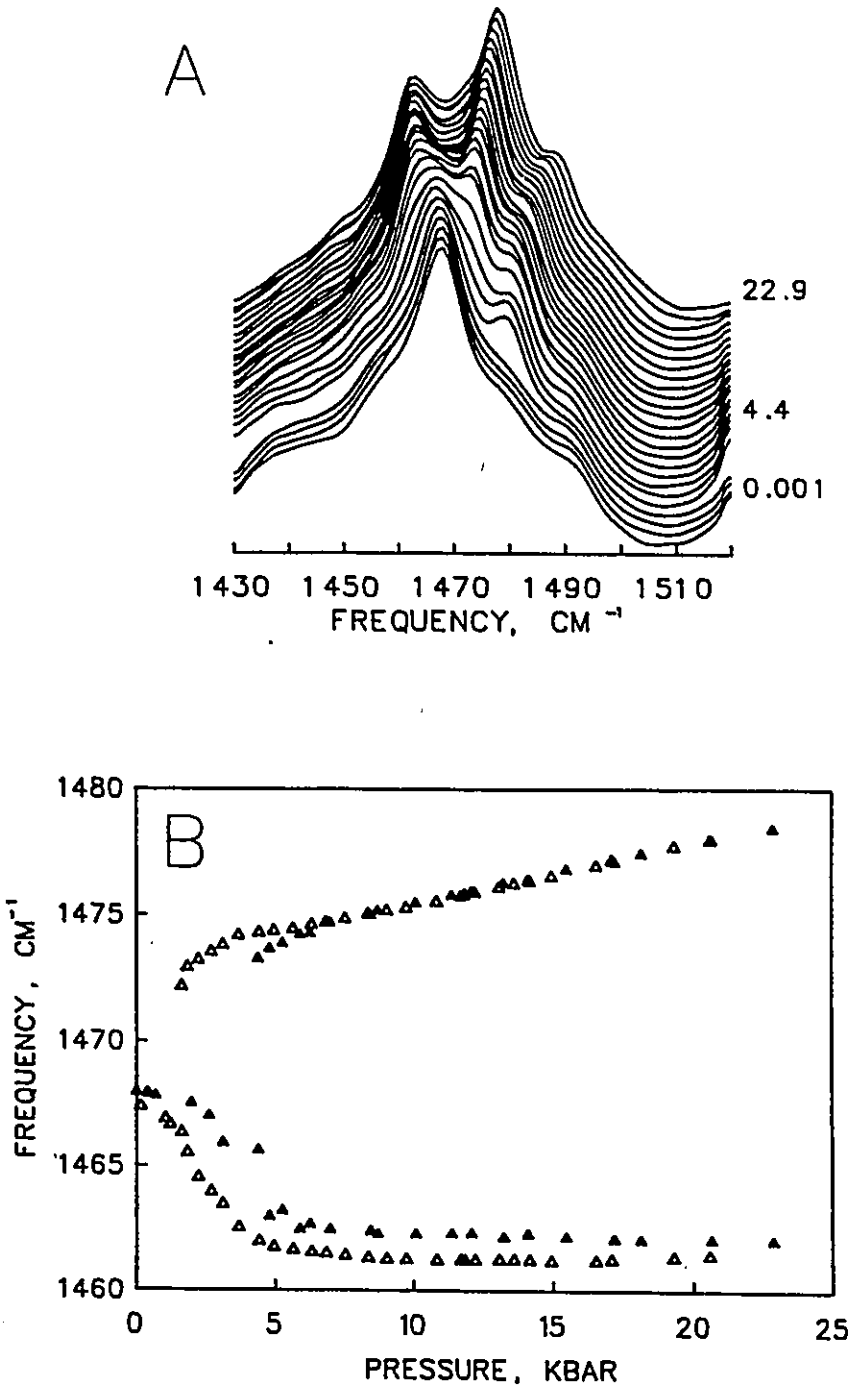

Figure 7.5 A. Stacked plot of the infrared spectra in the CH_2 scissoring region for DHPC:cholesterol+TTC, pH 9.5, and B. Pressure dependence of the frequencies of the δCH_2 mode for (△) DHPC+TTC, pH 9.5 and (▲) DHPC:cholesterol+TTC, pH 9.5.

tetracaine. However, whether or not the interdigitation is totally or only partially prevented cannot be determined from our data. The pressure dependence of the CH_2 scissoring component for DHPC:cholesterol+TTC, pH 9.5 would have to be compared with that obtained for DHPC in the presence of 50 mole% of cholesterol or DPPC, which are known to completely prevent the interdigitation of DHPC alkyl chains (*vide supra*).

7.4 Effects of cholesterol (30 mole%) on pure DMPC bilayers

Many techniques have been used to study the structural and dynamical properties of cholesterol-containing membranes, such as ^2H NMR (Stockton et al, 1976; Oldfield et al., 1978; Taylor et al., 1981, 1982; Dufourc et al., 1984b) and ESR (Schreier-Muccillo et al., 1973; Neal et al., 1976). These studies indicated that cholesterol has a "condensing" effect on the lipid fatty acyl chains at temperatures above that of the gel to liquid-crystalline phase transition, T_m, and a disordering action below T_m. However, little detail is available on the effect of cholesterol on interchain packing of lipids in the gel phase.

A recent high pressure FT-IR study on lipid-cholesterol interactions in the anhydrous solid state (P.T.T. Wong, unpublished results) has demonstrated that the magnitude of the correlation field splitting of δCH_2 is much smaller in dipalmitoyl-phosphoethanolamine (DPPE) containing 20 mole% cholesterol than in pure DPPE and that the splitting is only apparent at higher pressure in the presence of cholesterol. These results suggested that insertion of cholesterol between DPPE molecules causes a reduction in the strong interchain coupling of the CH_2 scissoring modes in pure DPPE.

Prior to a study of the effect of tetracaine on DMPC bilayers containing a physiological concentration of cholesterol (30 mole%), we have monitored the effects of cholesterol on the pure lipid in the gel phase. The pressure dependence of the methylene bands for DMPC in the absence and presence of cholesterol are shown in Figure 7.6A and 7.6B respectively. In the presence of cholesterol, the methylene scissoring mode band and its correlation field component are much broader than for pure DMPC, indicating increased conformational disorder of the acyl chains in the gel state due to the incorporation of cholesterol. Moreover, comparison of the pressure dependence of the frequencies of the CH_2 scissoring mode components for DMPC in the absence and presence of cholesterol (Figure 7.6C) indicates that the magnitude of the correlation field splitting is smaller in the presence of cholesterol, and that this splitting only becomes apparent at higher pressure in this system. These results demonstrate that the intercalation of cholesterol between the lipid acyl chains in the gel state decreases the interchain interactions and increases the chain mobility, as was observed for DPPE in the solid state.

Incorporation of cholesterol (30 mole%) into DMPC bilayers in the gel phase has three main effects: a decrease in interchain interactions as reflected in the smaller correlation field splitting, an increase in reorientational fluctuations of the acyl chains as reflected in the higher pressure required for splitting, and an increased conformational disorder of the chains as reflected in the broadening of the CH_2 scissoring mode bands. These results are in agreement with previous studies (*vide supra*) suggesting that cholesterol "disorders" the lipid acyl chains at temperatures below that of the gel to liquid-crystalline phase transition T_m.

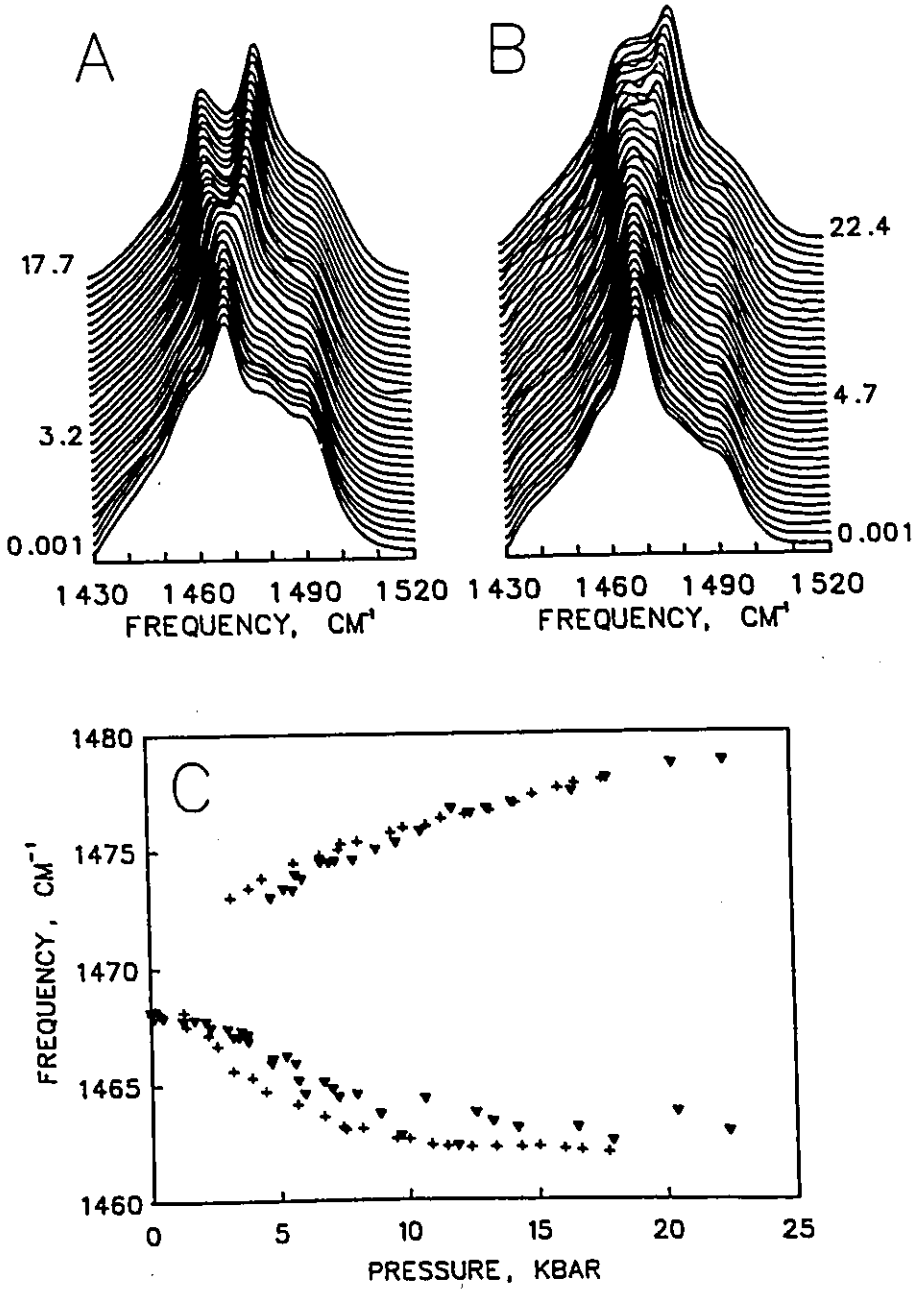

Figure 7.6 Stacked plots of the infrared spectra in the CH_2 scissoring region for A. DMPC, B. DMPC:cholesterol (7:3, molar ratio), and C. Pressure dependence of the frequencies of the δCH_2 mode for (+) DMPC and (▼) DMPC:cholesterol (7:3, molar ratio).

7.5 Effects of tetracaine on DMPC:cholesterol bilayers

Since many plasma membranes and most excitable plasma membranes contain a relatively large amount of cholesterol (≈ 30 mole% of the total lipids), we have investigated the effects of the incorporation of charged and uncharged tetracaine into DMPC bilayers containing a physiological concentration of cholesterol. As mentioned previously, ^2H NMR and high pressure FT-IR studies have shown that the anesthetic is located close to the aqueous interface of cholesterol-containing bilayers (Auger et al., 1987, 1988a, chapters 4 & 6 of this thesis).

The pressure dependences of the methylene scissoring bands for DMPC : cholesterol bilayers in the presence of uncharged and charged anesthetic are shown in Figure 7.7A and 7B respectively. Comparison of these stacked plots with that obtained for DMPC:cholesterol bilayers in the absence of tetracaine (Figure 7.6B) indicates that incorporation of both charged and uncharged tetracaine into cholesterol-containing DMPC bilayers does not induce significant changes in the pressure dependences. The CH_2 scissoring mode band and its correlation field component remain very broad, indicating significant conformational disorder of the lipid acyl chains.

Figure 7.8A compares the pressure dependence of the δCH_2 mode frequencies for DMPC:cholesterol bilayers in the absence and presence of tetracaine. Upon addition of both charged and uncharged tetracaine, the magnitude of the correlation field splitting for DMPC:cholesterol bilayers is not significantly changed while the pressure at which this splitting first occurs is 4.7 kbar in the absence of anesthetic, compared to 6.1 kbar in the presence of uncharged tetracaine and 6.0 kbar in the presence of charged tetracaine.

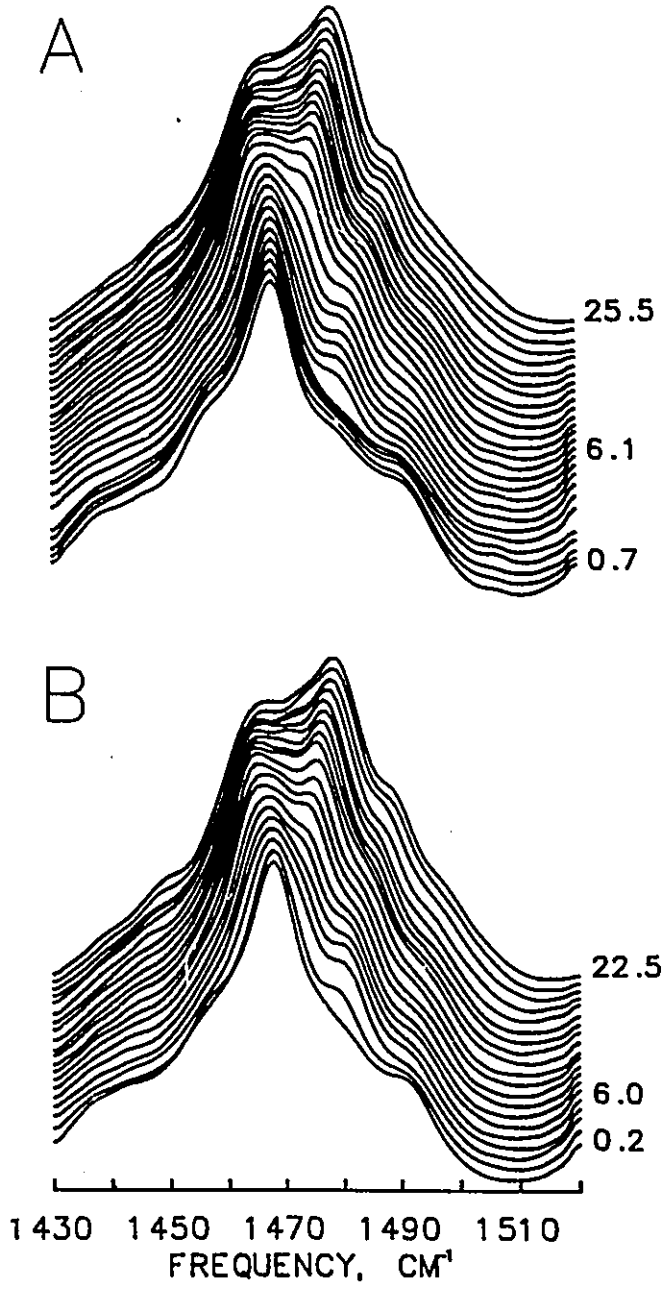

Figure 7.7 Stacked plots of the infrared spectra in the CH_2 scissoring region for **A.** DMPC:cholesterol+TTC, pH 9.5, and **B.** DMPC:cholesterol+TTC, pH 5.5.

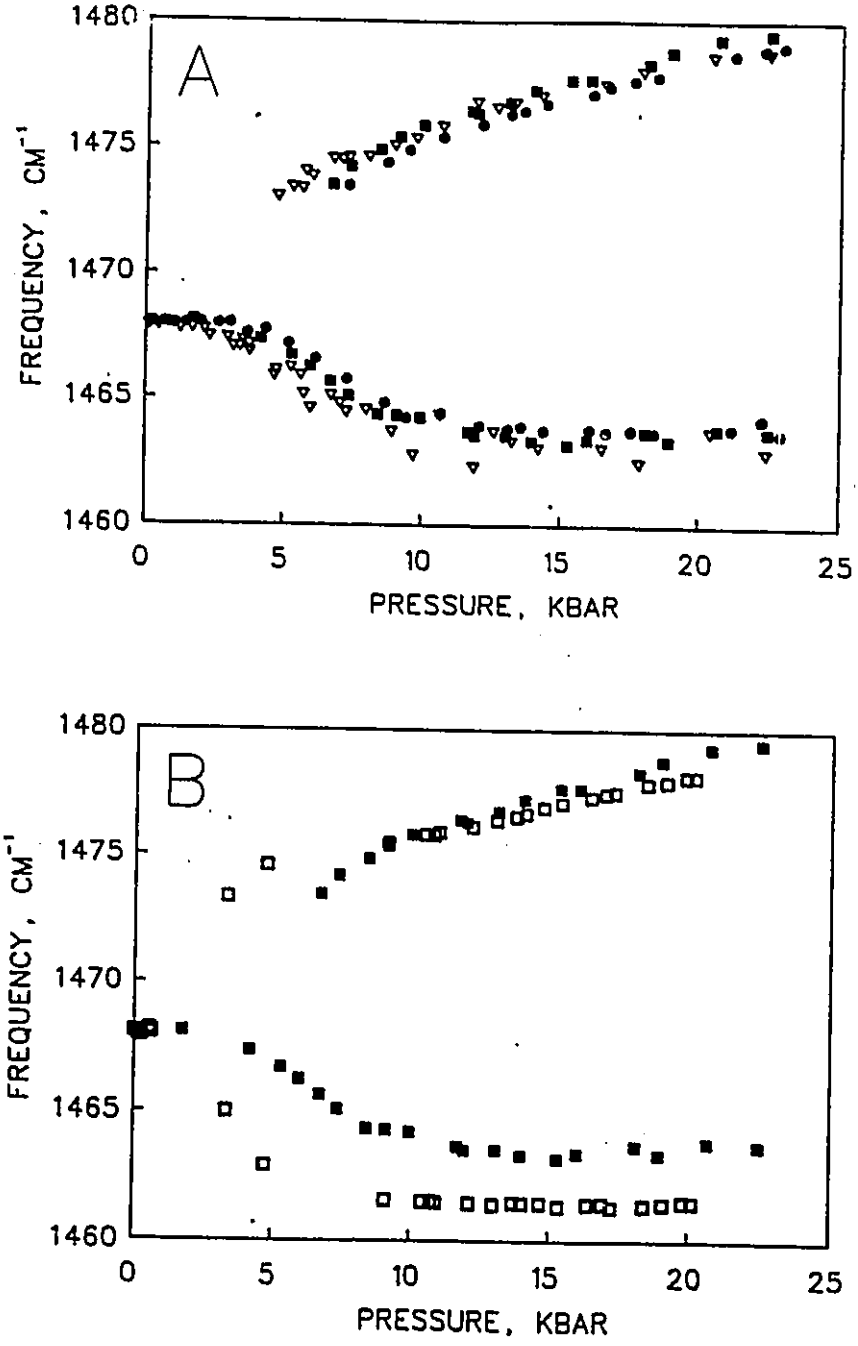

Figure 7.8 A. Pressure dependence of the frequencies of the δCH_2 mode for (▽) DMPC:cholesterol, (●) DMPC:cholesterol+TTC, pH 9.5, and (■) DMPC : cholesterol+TTC, pH 5.5, and **B.** Pressure dependence of the frequencies of the δCH_2 mode for (□) DMPC+TTC, pH 5.5 and (▣) DMPC:cholesterol+TTC, pH 5.5.

These results suggest that the addition of the anesthetic only slightly increases the reorientational fluctuations of the lipid acyl chains in the gel state.

As mentioned previously, the addition of charged tetracaine to pure DMPC bilayers induces the formation of an interdigitated lamellar gel phase. In order to see if the presence of 30 mole% cholesterol in this system prevents the formation of the interdigitated phase, we have compared the pressure dependences of the methylene scissoring mode bands for DMPC+TTC, pH 5.5 (Figure 7.1A) and DMPC : cholesterol+TTC, pH 5.5 (Figure 7.7B). These figures show that the "valley" between the two component bands of the pressure-induced correlation field splitting is less pronounced in the presence of cholesterol. Moreover, the pressure dependence of the frequencies of the CH_2 scissoring bands for these two systems (Figure 7.8B) indicates that the magnitude of the correlation field splitting is smaller in the presence of cholesterol, and that the first manifestation of this splitting in DMPC:cholesterol+TTC, pH 5.5 is at 6.0 kbar compared to 3.3 kbar for DMPC+TTC, pH 5.5. These results suggest that the presence of 30 mole% of cholesterol does, to a large extent, prevent the interdigitation of DMPC acyl chains in the presence of charged tetracaine.

7.6 Conclusions

The present results indicate that high pressure FT-IR spectroscopy is a valuable technique to study the effects of exogeneous agents, such as local anesthetics, on lipid membranes. For all the systems studied, the infrared spectra at atmospheric pressure were

very similar, but the pressure dependence of the methylene scissoring and rocking mode bands contains a great deal of information about the structural and dynamic properties of the lipid hydrocarbon chains. This information is complementary to that obtained by other spectroscopic techniques and demonstrates that high pressure FT-IR is more than simply an alternative approach.

PART FOUR: LIPID DYNAMICS AS VIEWED BY ^2H NMR

CHAPTER 8

Elucidation of motional modes in glycoglycerolipid bilayers: A ^{2}H NMR lineshape and relaxation study

8.1 Introduction

Glycosphingolipids constitute a class of biomolecules which can assume many biological roles (Hannun & Bell, 1989). Of particular importance is their capacity to function as recognition sites (cell-cell recognition (Critchly et al., 1979), immune recognition (Hakamori, 1984) and toxin receptor (Fishman & Brady, 1976)), and as modulators of membrane structure (Sharom & Grant, 1977). In addition to the structure and conformation of the oligosaccharide moiety, molecular recognition at the cell membrane surface will depend on a number of factors such as surface orientation and spatial constraint imposed by the bilayer surface, which will affect "accessibility" of the carbohydrate residues for interaction (Mehlorn et al., 1988; Shichijo & Alving, 1985). In view of the important roles played by the glycolipid head group, it is clear that probing the spatial disposition and dynamics of the carbohydrate moiety can provide valuable insight into cell surface recognition at the molecular level.

Since the systems of interest are inherently spatially anisotropic, solid state ^{2}H NMR spectroscopy is ideally suited to probing such systems (Seelig, 1977; Griffin, 1981; Davis, 1983, 1986; Bloom & Smith, 1985; Smith, 1984). ^{2}H NMR studies of

glycosphingolipids (Skarjune & Oldfield, 1979, 1982) and glycoglycerolipids (Jarrell et al., 1986, 1987a-b; Auger et al., 1989a; Renou et al., 1989; Carrier et al., 1989) have demonstrated that the head group undergoes motion which is spatially restricted (ordered) and that the orientation of the head group relative to the membrane plane can be elucidated. In addition, the conformation of the head group under the influence of the anisotropic interactions present at the membrane surface can be probed.

In addition to probing structural features of systems such as lipid bilayers, ^{2}H NMR provides observation windows in the range where the frequencies of most molecular motions occur (1-10^{10} s^{-1}, for lipid bilayers) (Kimmich et al., 1983). Spin-lattice relaxation data are a source of information about molecular dynamics on time scales near the Larmor frequency. However, the quantitative interpretation of such measurements ultimately requires choosing a motional description which is consistent with experiment. Previous studies have focused on glycoglycerolipids as models of glycosphingolipids in order to elucidate the orientation, conformation and dynamics of the carbohydrate head groups at a bilayer surface and to probe the factors influencing these spatial and motional parameters. During the course of these studies, two observations were common to all systems studied: anisotropic ^{2}H spin-lattice relaxation (dependent on the orientation of the director with respect to the magnetic field direction) in the liquid-crystalline phase, and a dramatic reduction in the ^{2}H quadrupolar echo signal intensity at temperatures just below the gel to liquid-crystalline phase transition temperature (Carrier et al., 1989; Jarrell, unpublished results). The observation of anisotropic relaxation is significant in that it puts severe constraints on the motional descriptions that may be considered to explain relaxation in these systems. Anisotropic spin-lattice relaxation has been used in biomolecular systems to extract details of molecular motion in proteins (Batchelder et al., 1983; Beshah et al.,

1987), DNA (Vold et al., 1986) and lipids (Siminovitch et al., 1988; Jarrell et al., 1988; Bonmatin et al., 1988, 1989). The loss of quadrupolar signal intensity reflects motion on the 10^3-10^6 time scale and is sensitive to the specific details of the motion(s) involved (Griffin, 1981).

In the present study, the glycolipid 1,2,di-*O*-tetradecyl-3-*O*-β-D-glucopyranosyl-*sn*-glycerol is studied in the gel state by ^{2}H spin-lattice relaxation and analysis of quadrupolar echo lineshapes. The principal objective of this study is to probe the lipid dynamics in the highly ordered gel state, where molecular motion is expected to be less complicated, in order to develop a basis for describing molecular motion in the more complex but biologically more relevant liquid-crystalline phase. The results demonstrate the considerable utility of oriented samples in relaxation and lineshape measurements.

8.2 Liquid-crystalline and gel phase powder spectra

The structural and dynamical properties of the glycolipid β-DTGL in the liquid-crystalline phase have been studied by ^{2}H NMR (Jarrell et al., 1986, 1987a-b). Study of β-DTGL labelled in both head group and glycerol regions has allowed the determination of the orientations of these moieties relative to the axis of motional averaging, as shown in Figure 8.1 (left). The ^{2}H NMR spectrum of a multilamellar dispersion of β-DTGL labelled at the C3 position of glycerol is shown in Figure 8.2 (bottom row, column A) at 55°C, at which temperature the lipid is in the liquid-crystalline phase (Jarrell et al., 1986). This spectrum is characteristic of lipids undergoing axially symmetric motion and exhibits two quadrupolar splittings, indicating that the two C-^{2}H bonds at this position make slightly

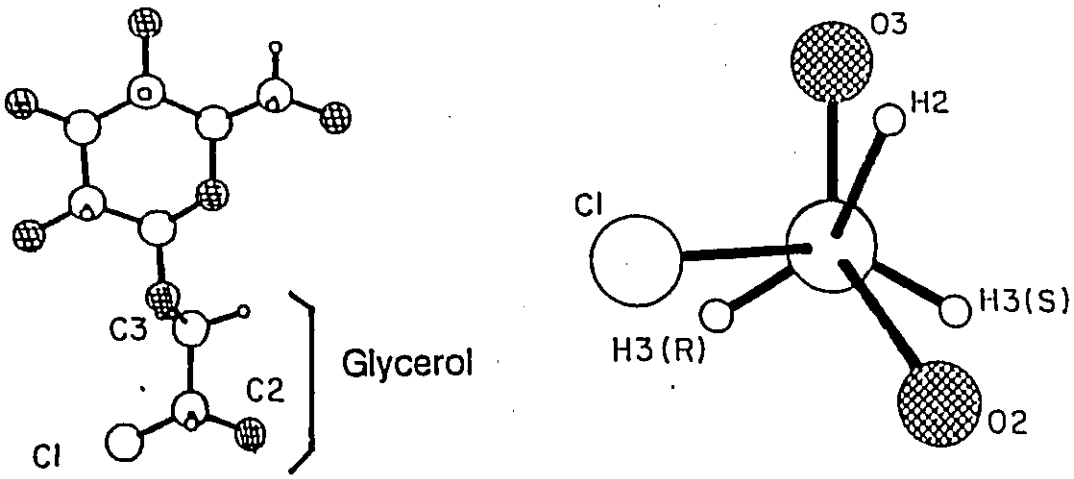

Figure 8.1 **Left:** Head group orientation of β-DTGL relative to the bilayer normal as calculated from ^{2}H NMR data (Jarrell et al., 1986, 1987a). **Right:** Glycerol backbone of β-DTGL. View is along the C2-C3 bond from C2 toward C3. The conformation shown is that calculated from the estimated $^{1}H2$-$^{2}H3(S)$ and $^{1}H2$-$^{2}H3(R)$ dipolar couplings (Jarrell et al., 1987a).

Figure 8.2 **Bottom row:** ^2H NMR spectra of multilamellar dispersions of [3,3-$^2H_2$] β-DTGL. **Four top rows:** Oriented-sample spectra of [3,3-$^2H_2$] β-DTGL:DPPC (4:1, molar ratio) as a function of the angle θ (equation 8.1) between the normal to the plane of the glass plates (taken to be coincident with the bilayer normal) and the magnetic field direction. **A:** Experimental spectra in the liquid-crystalline phase, 55°C. **B:** Experimental spectra in the gel phase, 25°C. **C, D:** Simulated spectra in the gel phase. Spectral simulations were performed using two different three-site jump models with populations 0.50, 0.25, 0.25 (C) and 0.46, 0.34, 0.20 (D). The C-^2H bonds of the 3-carbon of the glycerol backbone are oriented at 69° with respect to the axis of motional averaging and the exchange rate is 5×10^8 rad s^{-1}. A linebroadening of 4 kHz was used in the simulations of gel phase spectra in order to fit the experimental linewidth (8 kHz) of the 0° orientation spectrum in the gel phase.

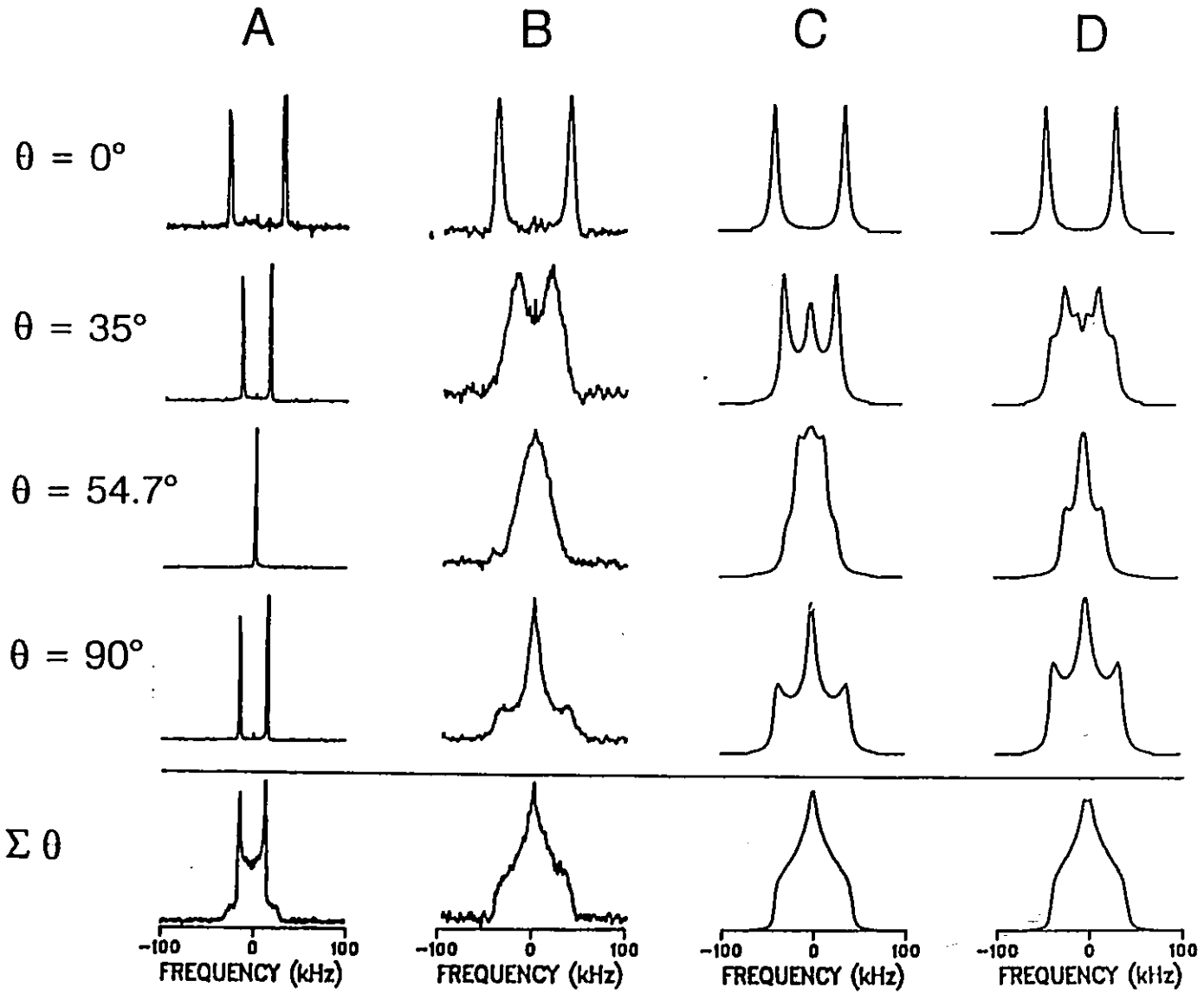
A
B
C
D
θ = 0°
θ = 35°
θ = 54.7°
θ = 90°
Σ θ
-100
0
100
FREQUENCY (kHz)

different angles with respect to the symmetry axis. From the spectra of oriented samples, estimates of the ^2H-^2H dipolar coupling between the deuterons at C3 as well as the ^1H-^2H dipolar couplings between the proton at C2 and the deuterons at C3 of glycerol of β-DTGL were also obtained. From these results, the dihedral angle about the C2-C3 bond, as well as the average conformation of this part of the glycerol backbone, were estimated, as shown in Figure 8.1 (right) (Jarrell et al., 1987a). Moreover, the conformation about the glycosidic bond of the glycolipid is such that the sugar ring is fully extended away from the bilayer surface (Jarrell et al., 1986, 1987a-b). Segmental order parameters S of 0.45, 0.65 and 0.40 were determined for the head group, the glycerol backbone and the hydrophobic core of β-DTGL, respectively.

In contrast to the liquid-crystalline phase, the gel phase of phospholipids and glycolipids has received much less attention. This is in part due to the technical difficulties associated with obtaining gel-state ^2H NMR spectra, which are usually a factor of 2 to 4 times wider, with transverse relaxation times much shorter than those of the liquid-crystalline phase. ^2H NMR studies of phospholipid specifically deuteriated in both the acyl chain and head group regions, suggested that the dominant motion present in these systems is slow axial diffusion with a correlation time τ_c of about 10^{-5} s (Davis, 1979; Blume & Griffin, 1982; Blume et al., 1982a-b). However, lineshape and spin-lattice relaxation studies of acyl chain-labelled N-palmitoylgalactosyl sphingosine (NPGS) in the gel phase (Huang et al., 1980; Siminovitch et al., 1985) indicate that, unlike the phospholipid systems, axial diffusion is very slow on the ^2H NMR time scale ($\tau_c = 1/\Delta\upsilon_Q$) and the gel phase spectra are the result of a simple exchange process of intermediate rate between gauche and trans conformers. To our knowledge, the gel phase ^2H NMR spectra of the glycerol or head group regions of glycolipids have never been investigated. If axial

diffusion is effectively stopped on the ^2H NMR time scale in these systems, the gel phase spectra of the head group region glycolipids should also be solely the result of internal motions. Elucidating these motional modes would provide a strong foundation upon which to examine the dynamics of these head groups in the less ordered liquid-crystalline phase. To this end, we have investigated the ^2H NMR spectral features and relaxation behavior of the glycolipid β-DTGL, labelled at the C3 position of the glycerol backbone, in both the gel and liquid-crystalline phases, in order to elucidate some of the fundamental motions of the lipid in the two phases.

The ^2H NMR spectrum (Figure 8.2 (bottom row, column B)) of glycerol-labelled β-DTGL in the gel phase at 25°C, well below the gel to liquid-crystalline phase transition temperature (52°C) (Jarrell et al., 1986) is very broad (≈ 90 kHz) and characteristic of fast-limit axially asymmetric motion. In such cases, the quadrupolar splitting depends on both Eulerian angles θ and φ defining the orientation of the motionally averaged electric field gradient tensor V_{ii} with respect to the magnetic field direction:

$$\Delta\upsilon_Q(\theta,\phi) = \frac{3}{2}\frac{e^2qQ}{h} S \frac{3\cos^2\beta-1}{2}\left(\frac{3\cos^2\theta-1}{2} + \eta_{eff}\frac{\sin^2\theta\cos 2\phi}{2}\right) \qquad (9.1)$$

In this equation, η_{eff} is the motionally averaged asymmetry parameter defined as $(V_{xx}-V_{yy})/V_{zz}$, where $V_{yy} < V_{xx} < V_{zz}$ are the principal components of the effective electrostatic field gradient tensor in the molecular fixed frame. e^2qQ/h is the quadrupolar coupling constant (170 kHz), θ is the angle between the symmetry axis for the motion and the magnetic field direction, S is the segmental order parameter describing the anisotropic

motion of the molecular unit relative to the bilayer normal (wobbling) and β is the angle between the C-^{2}H bond and the molecular rotation axis.

It has been shown that the observation of spectra indicative of fast-limit axially asymmetric motion requires that the motions have twofold or lower symmetry (Griffin, 1981). This requirement is most simply satisfied with a two-site exchange process, but a mechanism with sites of unequal populations will also satisfy that requirement. Moreover, the spectral lineshapes will depend strongly on the nature of the motion, the populations of the sites and the rates associated with the exchange process (Griffin, 1981).

The lineshape of the [3,3-$^2H_2$] β-DTGL powder spectrum presented in Figure 8.2 is invariant to the spacing, τ, between pulses in the quadrupolar echo sequence for τ values between 40 and 120 μs. In the slow ($\omega_Q\tau_C >> 1$, $\omega_Q = 2\pi \times \Delta\upsilon_Q$) or fast ($\omega_Q\tau_C << 1$) limit motional regimes, the transverse relaxation time T_{2e} is much greater than the delay τ in the quadrupolar echo sequence and the lineshapes are invariant to pulse spacing (Griffin et al., 1988). However, for intermediate exchange ($\omega_Q\tau_C \approx 1$), T_{2e} is anisotropic and smaller or equal to the delay τ for many orientations in the powder, resulting in distorted lineshapes and in a dependence of the lineshapes on the delay τ (Spiess & Sillescu. 1981; Rice et al., 1987). Moreover, the spectral intensity is dramatically decreased when passing through the intermediate exchange region (Wittebort et al., 1987). The absence of a pulse spacing dependence at 25°C for the [3,3-$^2H_2$] β-DTGL spectra therefore indicates that the axially asymmetric motion(s) giving rise to such spectra are in the fast limit relative to the time scale of ^{2}H NMR ($>> 10^5$ sec^{-1}).

8.3 Fast motion

8.3.1 Lineshape study of multilamellar dispersions

While a number of potential motional models may be envisaged to account for the β-DTGL powder spectral lineshape, it is attractive to search for those that are the simplest reasonable descriptions which are consistent with the system under study. A previous study of a phosphatidylcholine suggested that motion about the C2-C3 bond consists of jump between three conformations (Hauser et al., 1980). Using a lineshape simulation program developed by Wittebort et al. (1987) based on the general formalism of Torchia and Szabo (1982), the [3,3-$^2H_2$] β-DTGL powder spectral lineshape in the gel phase presented in Figure 8.2 was simulated with several non-equally populated three-site jump models. In these simulations, the angle β is the angle between the C-^{2}H bond and the axis of motional averaging. As mentioned previously, it has been shown that in the liquid-crystalline phase, the two C-^{2}H bonds of the glycerol backbone C3 make slightly different angles relative to the axis of motional averaging. From the quadrupolar splittings obtained in the liquid-crystalline phase and the value of the segmental order parameter S of 0.65 obtained for the glycerol backbone, the two angles β were calculated to be 73.7 and 71.5°. On the other hand, in the gel phase, only one powder pattern is obtained. This may be due to a larger dipolar contribution to the intrinsic linewidth, which obscures the spectral differences associated with a small difference in the angle β. Alternatively, there may be a small change in the glycerol backbone orientation in the gel phase compared to that in the liquid-crystalline phase which makes the two angles β equivalent. A more exact β value in the gel phase was calculated from the measurement of the doublet separation obtained for the 0° oriented sample spectra (*vide infra*). The doublet separation in this spectrum is 80

kHz. Using equation 8.1 and assuming that the segmental order S is equal to unity in the gel phase (this assumption is reasonable since, as will be shown later, axial diffusion is basically stopped on the ^2H NMR time scale at that temperature; any angular fluctuations of the molecule as a whole can therefore be neglected), an angle β of 69.3° was calculated. This angle is slightly smaller than those obtained for the two C-^2H bonds in the liquid-crystalline phase. However, whether or not this is due to a change in the orientation of the glycerol backbone remains to be confirmed. An angle β of 69° was therefore used for all the gel phase spectral simulations. However, the results of these simulations were not affected significantly when β was varied by $\pm 1°$ about 69°.

The experimental [3,3-$^2H_2$] β-DTGL powder spectrum lineshape was relatively well simulated with a variety of unequally populated three-site jump models. Since the gel phase spectra (Figure 8.2) are in the fast limit relative to the time scale of the ^2H NMR lineshape, simulated spectral lineshapes were relatively insensitive to the jump rate k used in the simulations ($k > 5 \times 10^6$ rad s^{-1}). Two examples are shown in Figure 8.2 (bottom row, columns C and D), for populations of 0.50, 0.25, 0.25 and 0.46, 0.34, 0.20, respectively. It should be mentioned at this point that two main categories of three-site jump models were investigated, the first where one of the populations was much larger than the other two and a second with two approximately equal populations and a third population much smaller than these. Interestingly, the populations of the second set are relatively close to those of the gauche (+), gauche (-) and trans populations about the glycerol C2-C3 bond proposed in phospholipids (0.48, 0.37, 0.15 for dihexadecyl phosphatidylcholine (DHPC) in D_2O) (Hauser et al., 1980). However, from just the powder spectral lineshape simulations (Figure 8.2), it is not possible to unambiguously elucidate the exact motion executed about the C2-C3 bond of the glycerol backbone in the gel phase, since the experimental powder

pattern can be simulated with a variety of motional models.

8.3.2 Lineshape study of oriented samples

In order to accurately determine the asymmetry parameter η_{eff} and therefore the principal components of the motionally averaged electric field gradient tensor V_{xx}, V_{yy} and V_{zz} for glycerol-labelled β-DTGL in the gel phase, measurements of oriented-sample spectra are of great use since this is analogous to a single crystal study. This approach has previously been used in liquid crystals to determine the asymmetry parameter η of biaxial smectic phases (Barbara & Dailey, 1982; Doane, 1985). The ^2H NMR spectra of a macroscopically oriented sample of [3,3-$^2H_2$] β-DTGL 80 mole% in DPPC are shown in Figure 8.2 (column B). For the preparation of oriented samples, β-DTGL was mixed 80 mole% in DPPC in order to achieve a better alignment of the sample. It is important to note that both powder and oriented-sample lineshape and relaxation features are well simulated using the same motional model (*vide infra*). Moreover, the motionally averaged tensor elements extracted from the powder and oriented-sample spectra are very similar and the T_1 values determined from the oriented-sample spectra are in good agreement with the T_1 anisotropy observed in the powder spectra (*vide infra*). Therefore, the presence of 20 mole% DPPC in the oriented sample does not significantly affect the dynamics of β-DTGL. Spectra were measured as a function of the angle θ (equation 8.1) between the normal to the plane of the glass plates (taken to be coincident with the bilayer normal) and the magnetic field direction. The 0° orientation corresponds to the plane of the glass plates orthogonal to the magnetic field direction. The results shown in Figure 8.2 clearly demonstrate that for all but the 0° orientation, powder spectra (over ϕ, (equation 8.1)) are

obtained since η_{eff} = 0. These spectra have lineshapes characteristic of an asymmetry parameter close to unity (simulations not shown). Moreover, the single doublet obtained for the 0° orientation confirms that, as was previously demonstrated in the liquid-crystalline phase (Jarrell et al., 1987a), the bilayer normal is the axis of motional averaging for β-DTGL in the gel phase. For the 0° orientation, the two peaks are much broader than those obtained in the liquid-crystalline phase, due mostly to increased dipolar coupling between the deuterons at C3 and the neighboring protons. It should be noted that the oriented sample used in the gel phase was the same as that from which the oriented spectra in the liquid-crystalline phase were obtained (Figure 8.2, column A). Therefore, the lineshapes obtained for the gel phase spectra are not due to poor orientation of the sample. Moreover, it is important to note that the gel phase oriented-sample spectra are the result of 500 K accumulations, while the corresponding liquid-crystalline phase spectra have been obtained with only 50 K accumulations.

Using a modified version of the lineshape simulation program previously used for the β-DTGL powder spectra (*vide supra*), the oriented-sample spectral lineshapes were now simulated using several three-site jump models distinguished only by the relative populations of the sites. The results for two sets of populations (0.50, 0.25, 0.25 and 0.46, 0.34, 0.20) are shown in Figure 8.2 (columns C an D, respectively) and compared to the experimental spectra for the 0, 35, 54.7 and 90° orientations. It is interesting to note that both descriptions can reproduce relatively well the experimental lineshapes, with the 54.7° orientation being better simulated by the first motional model while the 35° orientation spectrum is better reproduced using the second model. It should be noted at this point that the [3,3-$^2H_2$] β-DTGL powder spectrum lineshape could also be simulated using an equally populated two-site jump model with the two sites separated by an angle of 120°. However,

using this motional model, the simulated and experimental oriented-sample lineshapes differed significantly. It is clear that the use of oriented samples (fixed θ, variable ϕ) can facilitate the discrimination between different motional models that could not be differentiated solely on the basis of powder (variable θ and ϕ) lineshapes.

8.3.3 Spin-lattice relaxation study

8.3.3.1 Introduction

So far, we have demonstrated that a few reasonable three-site exchange models can account for the powder and oriented-sample lineshapes of [3,3-$^2H_2$] β-DTGL in the gel phase at 25°C. However, as discussed previously, the motion giving rise to such spectra appears to be in the fast limit relative to the ^2H NMR lineshape time scale. Therefore, a unique correlation time τ_c for this motion could not be obtained solely from the spectral lineshape simulations. In the slow- or fast-limit motional regimes, other methods are necessary in order to obtain dynamic information. Ultraslow motions in solids and solid polymers, characterized by correlation times $\tau_c >> 1$ s, have been studied by deuteron spin alignment (Spiess, 1980) and more recently by two-dimensional exchange NMR (Schmidt et al., 1986, 1987, 1988; Wefing & Spiess, 1988; Wefing et al., 1988; chapter 10 of this thesis). On the other hand, for phospholipids in the liquid-crystalline phase, where correlation times for C-^2H bond motions are shorter than 10^{-7} s, molecular dynamics of the acyl chains have been widely studied by ^2H spin-lattice relaxation (Brown, 1982; Brown & Davis, 1981; Brown et al., 1983; Williams et al., 1985). For multilamellar dispersions of liquid-crystalline bilayers, the rapid lateral diffusion of lipid molecules over the curved two-

dimensional surface of multilamellar liposomes is frequently sufficiently fast to prevent the observation of orientation-dependent relaxation (Brown & Davis, 1981). However, if the anisotropic relaxation effects are not obscured by lateral diffusion, the measurement of the orientation-dependent ^2H spin-lattice relaxation times (T_{1Z}) can be very useful in the study of molecular dynamics in lipid bilayers. In this regard, the use of macroscopically oriented samples circumvents the orientational averaging effects of rapid lateral diffusion over the curved liposomal surfaces and has proven to be of great value in the study of orientation-dependent relaxation of lipids in the liquid-crystalline phase (Jarrell et al., 1988; Bonmatin et al., 1988, 1989; Pope et al., 1982). On the other hand, the study of ^2H spin-lattice relaxation in the gel phase of lipid bilayers or in the "liquid-gelatin" phase of lipid/cholesterol mixtures is possible since the lipid lateral diffusion rates are about an order of magnitude smaller (Siminovitch et al., 1985, 1988a; Blume & Griffin, 1982; Rubenstein et al., 1979). In particular, the study of the orientation-dependence of ^2H spin-lattice relaxation for the acyl chain labelled glycolipid NPGS (*vide supra*) in the gel phase has allowed the determination of the correlation time for *trans-gauche* isomerization (Siminovitch et al., 1985), information that could not be obtained from the lineshape analysis of fast-limit spectra (Blume & Griffin, 1982).

8.3.3.2 Orientation dependence of spin-lattice relaxation times

Solving the master equation for the time evolution of the density matrix, the Zeeman ^2H spin-lattice relaxation rates is given by:

$$1/T_{1Z} = 1/3\,(\omega_Q^2)\,[J_1(\omega_0) + 4J_2(2\omega_0)] \qquad (8.2)$$

where $\omega_Q = (3/4)e^2qQ/h$ (see section 2.7). The spectral density functions $J_m(\omega)$ are related to the Fourier transform of the autocorrelation functions $G_m(t)$ by the Wiener-Khintchine theorem (Wiener, 1930; Khintchine, 1934):

$$J_m(\omega) = 2 \int G_m(t)\cos\omega t \, dt \tag{8.3}$$

The autocorrelation function expressed in the notation of Torchia and Szabo (1982) is given by:

$$G_m(t) = \sum_{a,a'=-2}^{2} d_{ma}^{(2)}(\theta)\, d_{ma'}^{(2)}(\theta) \exp[i(a-a')\phi]\, G_{aa'}(t) \tag{8.4}$$

where

$$G_{aa'}(t) = \langle D_{0a}^{(2)*}(0,\beta(0),\alpha(0))\, D_{0a'}^{(2)}(0,\beta(t),\alpha(t)) \rangle \tag{8.5}$$

and the brackets indicate an ensemble average. In equation 8.4, the angles θ and ϕ are the spherical polar angles specifying the director (in our case the bilayer normal) orientation with respect to the external magnetic field, and $d_{ma}^{(2)}(\theta)$ are the reduced Wigner rotation matrix elements. The relaxation time anisotropy ($T_{1Z}(\theta,\phi)$) is determined by those terms in equation 8.4 (exclusive of $G_{aa'}(t)$) which are functions of the angles θ and ϕ only. When using oriented samples (*vide supra*), the angle θ is under the control of the experimenter via sample rotation. Since there is no control over the angle ϕ, the experimentally accessible quantities are in fact $T_{1Z}(\theta)=\overline{T_{1Z}(\theta,\phi)}$, where the overbar denotes a powder average over all azimuthal angles ϕ. In equation 8.5, the angles β and α specify the

orientation of the C-^{2}H bond vector with respect to the director, and $D_{0a}^{(2)*}(0,\beta,\alpha)$ are the Wigner rotation matrix elements. Equations 8.4 and 8.5 simplify considerably when we consider a class of model in which C-^{2}H bond reorientation about a symmetry axis does not alter the angle β. Such models, discussed in details by Torchia and Szabo (1982), are appropriate for describing the reorientational motions of the C-^{2}H bond vector for the glycerol-labelled β-DTGL. For these models:

$$G_{aa'}(t) = d_{0a}^{(2)}(\beta)d_{0a'}^{(2)}(\beta)\,\Gamma_{aa'}(t) \qquad (8.6)$$

where, since β is fixed, the ensemble averaging problem is reduced to evaluating the azimuthal autocorrelation function:

$$\Gamma_{aa'}(t) = \langle \exp[ia\alpha(0)]\exp[-ia'\alpha(t)] \rangle \qquad (8.7)$$

8.3.3.3 Experimental results and simulations

In order to discriminate between different three-site exchange models that are able to reproduce the experimental powder and oriented-sample spectra of β-DTGL in the gel phase and to determine the correlation time of the motion in question, we have first performed an inversion recovery experiment on a multilamellar dispersion of [3,3-$^2H_2$] β-DTGL at 25°C. The results shown in Figure 8.3 as a function of the delay T after the inverting pulse clearly demonstrate that there is a significant orientation-dependence of the ^{2}H spin-lattice relaxation times (T_{1Z}) in this system. From this figure, it is clear that the outer edges of the powder spectrum recover faster than does the central part. This effect is

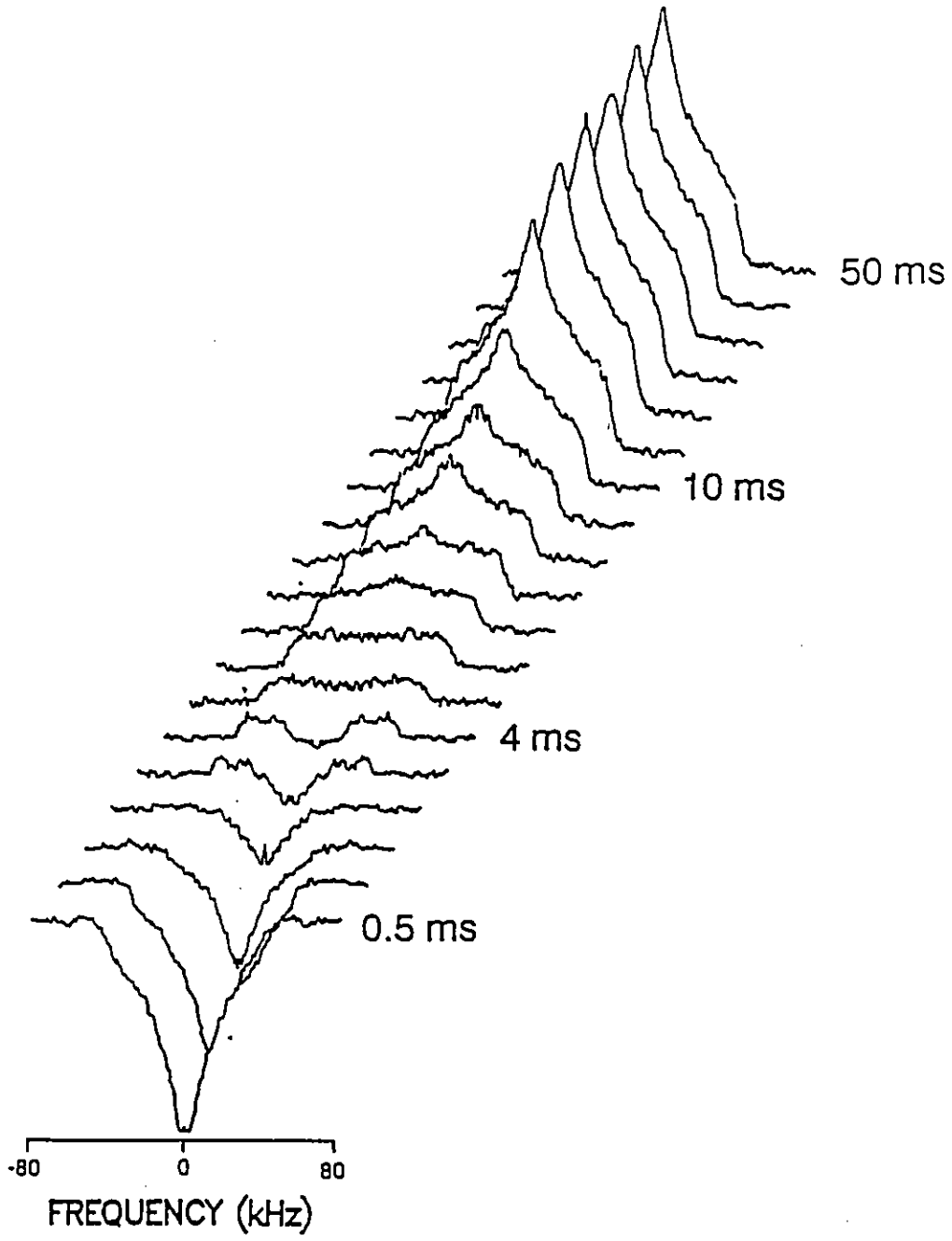

Figure 8.3 Experimental spectra of a multilamellar dispersion of [3,3-$^2H_2$] β-DTGL in the gel phase (25°C) as a function of the delay T in the inversion recovery sequence: 180-T-[90_x-τ-90_y]. Note that near the null point (T= ≈ 4 ms), a θ-dependence of the relaxation times T_{1Z} is observed.

particularly visible near the null point, for T values of about 4 ms. However, since each part of the powder spectrum is not due solely to a unique angle θ describing the orientation of the bilayer normal relative to the magnetic field direction but to a combination of angles (θ, ϕ), it is not possible from the powder spectra to determine the individual spin-lattice relaxation times for each orientation and extract details about the T_1 anisotropy.

In order to determine the T_{1Z} values for a given orientation θ, as well as to examine the T_{1Z} anisotropy, if any, associated with the angle ϕ for this particular orientation, inversion recovery experiments were performed on oriented samples of [3,3-$^2H_2$] β-DTGL at 25°C for θ values of 0, 54.7 and 90°. The experimental T_{1Z} values for these orientations (Table 8.1) exhibit the following angular-dependence of the spin-lattice relaxation times:

$$T_{1Z}(0°) < T_{1Z}(54.7°) < T_{1Z}(90°)$$

It should be noted that for each value of θ, the relaxation time presented in this table is a powder average over all azimuthal angles ϕ. The spin-lattice relaxation times obtained for [3,3-$^2H_2$] β-DTGL are very short, indicating that the correlation time(s) of the motion(s) dominating the relaxation is(are) very close to the T_1 minimum ($\omega_0\tau_C \approx 0.65$).

The experimental T_{1Z} values are compared in Table 8.1 with those calculated using the general formalism developed by Torchia and Szabo (1982). The two categories of three-site exchange model described earlier reproduced the orientation-dependent relaxation times relatively well; calculated values using relative populations of 0.46, 0.34, 0.20 are presented in Table 8.1. Simulations were again performed using an angle β of 69°

Table 8.1

Experimental and calculated ^2H (30.7 MHz) spin-lattice relaxation times (T_{1Z}) for oriented samples of [3,3-$^2H_2$] β-DTGL in the gel phase at 25°C.

	Relaxation times (ms)		
	Experimental	Calculated	
θ		k (rad s^{-1})	
		5×10^8	1.25×10^7
0°	4.04 ± 0.06	3.76	4.22
54.7°	5.23 ± 0.05	5.41	5.50
90°	6.19 ± 0.13	6.92	5.61

The angle θ is the angle between the bilayer normal and the magnetic field direction. The 0° orientation corresponds to the plane of the glass plates orthogonal to the magnetic field direction. Simulations were performed using a three-site jump model with populations 0.46, 0.34, 0.20 and two different jump rates, as indicated in the table.

and the exchange rate k was varied in order to match the experimental T_{1Z} values. The results presented in Table 8.1 indicate that the orientation-dependence of the spin-lattice relaxation times observed experimentally can be reproduced with exchange rates of 1.25×10^7 rad s^{-1} and 5×10^8 rad s^{-1}, corresponding to correlation times τ_c of 2.7×10^{-8} s and 6.7×10^{-10} s, on both sides of the T_{1Z} minimum (where $\tau_c \approx 4 \times 10^{-9}$ s at 30.7 MHz). On the basis of these results alone, it is therefore difficult to determine unambiguously the exact correlation time of the three-site exchange motion.

An additional striking feature of the partially relaxed spectra for the 54.7 and 90°-oriented samples is a dependence of the relaxation times for a given angle θ on the angle ϕ, a ϕ-dependence. Except in very restricted cases, it is generally expected that spin-lattice relaxation times will depend on both angles θ and ϕ (Torchia & Szabo, 1982). However, in powder spectra, the ϕ-dependence is not easily distinguishable from the dependence on the angle θ. To our knowledge, this is the first time that such a ϕ-dependence of relaxation times for axially asymmetric spectra has been observed in lipid bilayers. This ϕ-dependent T_{1Z} for $\theta = 54.7$ is particularly clear in Figure 8.4 (left spectrum) which shows the partially relaxed spectrum of [3,3-$^2H_2$] β-DTGL for a delay T of 3.5 ms in the inversion recovery sequence. A ϕ-dependence was also observed for $\theta = 90°$, in which case the central part of the spectrum relaxes faster than the outer edges.

This ϕ-dependence of the spin-lattice relaxation times observed for the 54.7° orientation serves as an additional feature of the anisotropic relaxation behavior useful in discriminating between the different motional models discussed so far. Simulated partially relaxed spectra for the 54.7° orientation near the null-point, for a T value of 4 ms in the inversion recovery sequence (Figure 8.4) clearly demonstrate that for both sets of relative

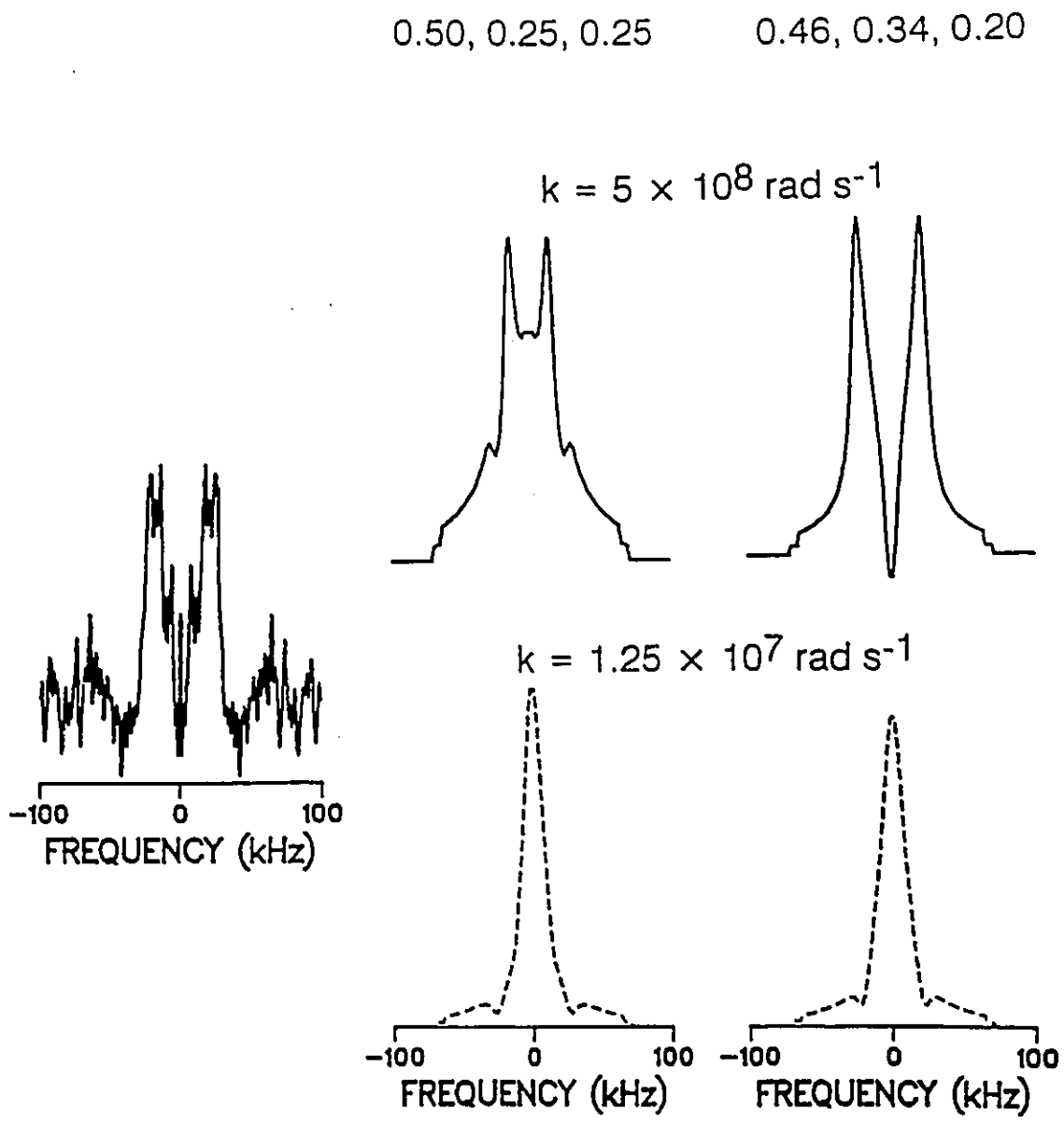

Figure 8.4 **Left:** Experimental inversion recovery spectrum (T=3.5 ms) of [3,3-$^2H_2$] β-DTGL:DPPC (4:1, molar ratio) oriented at θ=54.7°. Note that for this particular θ, a φ-dependence of the relaxation times is observed. **Right:** Corresponding simulated inversion recovery spectra (T=4 ms). Simulations were performed using the two three-site jump models described previously, with exchange rates on both side of the T_1 minimum.

populations, simulations performed using the slower exchange rate (1.25×10^7 rad s^{-1}) give a reversed ϕ-dependence of the relaxation times, even if the average (over ϕ) T_1 value is relatively close to the experimental value. For the faster exchange rate (5×10^8 rad s^{-1}), a ϕ-anisotropy very similar to that observed experimentally is obtained using relative populations of 0.46, 0.34, 0.20.

We can therefore conclude that this ϕ-dependence of the relaxation times for a given value of θ puts severe constraints on both the motional model and exchange rate used to simulate the lineshape and relaxation features observed for glycerol-labelled β-DTGL in the gel phase at 25°C. Taking into account the powder and oriented-sample spectral lineshapes, as well as the θ- and ϕ-dependence of the spin-lattice relaxation times T_{1Z}, the lineshape and relaxation features of [3,3-$^2H_2$] β-DTGL in the gel phase were best simulated using a three-site jump model with relative populations of 0.46, 0.34, 0.20 and an exchange rate k of 5×10^8 rad s^{-1}, which corresponds to a correlation time τ_c ($\tau_c = (3k)^{-1}$) of 6.7×10^{-10} s. Using these parameters, the inversion recovery spectra of multilamellar dispersions of [3,3-$^2H_2$] β-DTGL were simulated near the null-point in the inversion recovery sequence. As shown in Figure 8.5, the agreement between the experimental and simulated partially relaxed spectra is very good. It therefore appears that a combination of ^2H NMR lineshape and relaxation studies of gel phase glycerol-labelled β-DTGL does allow a relatively unambiguous determination of the motions dominating the lineshape and relaxation features in this sytem. Furthermore, the use of aligned samples facilitates the separation of the θ and ϕ contributions to T_1 (θ, ϕ). It is clear that the individual subspectra or partially relaxed subspectra are more sensitive to model parameters than are the corresponding powder spectra.

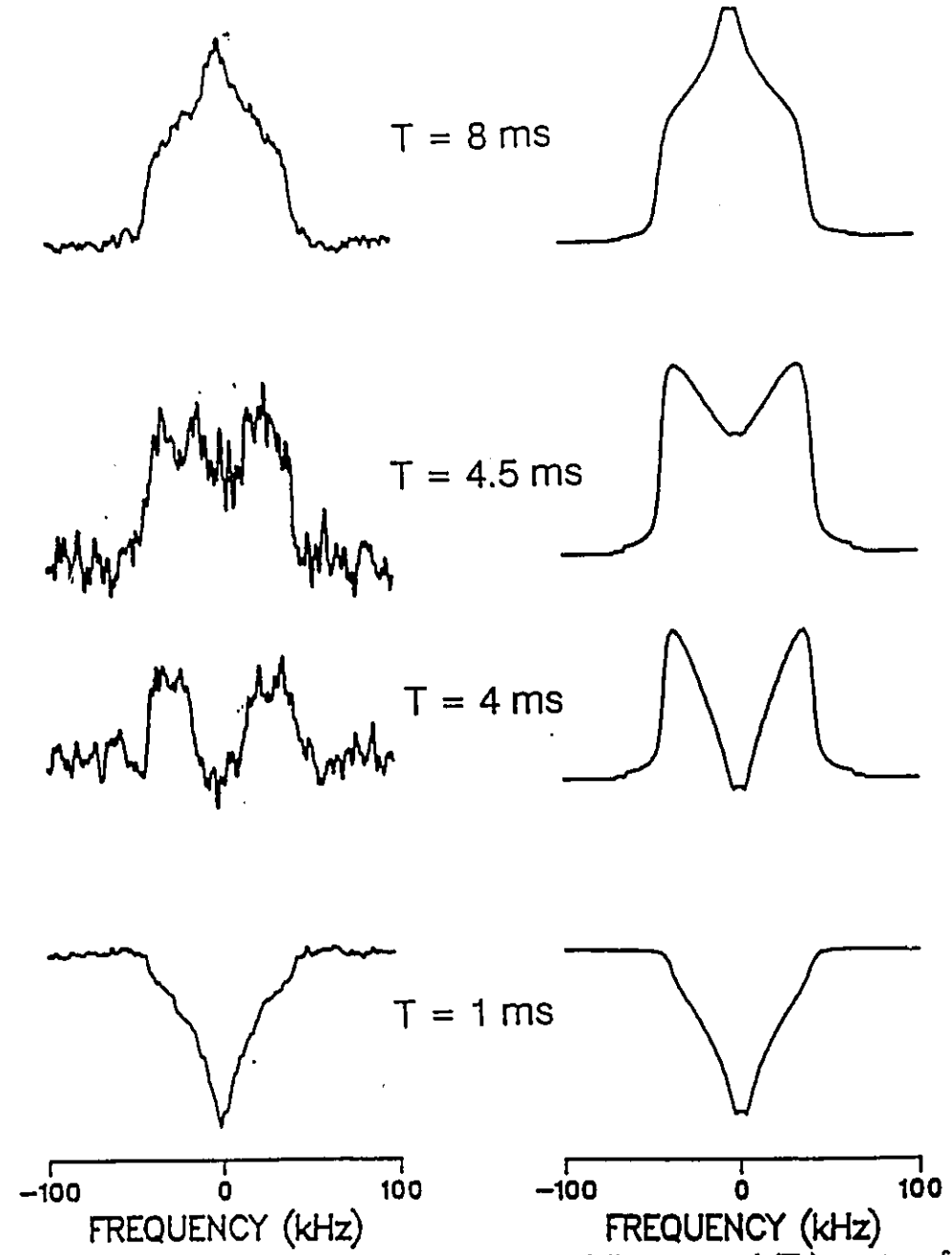

Figure 8.5 Experimental (left) and simulated (right) partially recovered (T_1) spectra of a multilamellar dispersion of [3,3-$^2H_2$] β-DTGL at 25°C as a function of the delay T in the inversion recovery sequence. Simulations were performed using a three-site jump model with an exchange rate of 5×10^8 rad s^{-1} and populations 0.46, 0.34, 0.20.

8.3.4 Nature of the fast motion

Thus far, we have not discussed the detailed nature of the three-site jump motion. Are the features observed for the C3 carbon of the glycerol backbone the result of a motion of the glycolipid molecule as a whole or of an internal motion about the C2-C3 (or C1-C2) bond of the glycerol backbone? The first possibility is unlikely on the basis of previous results obtained with glycolipids in the gel phase (*vide supra*) (Blume & Griffin, 1982; Siminovicth et al., 1985) which have shown that the lineshape and relaxation features in these systems are dominated by internal motions. In addition, the relaxation times for the lipid in the liquid-crystalline phase (52°C) and the gel phase (25°C) are very similar, a surprising result given that the higher temperature phase is less ordered. Internal motion in the glycerol backbone of β-DTGL is therefore a more plausible site of the jumping motion.

The powder lineshape and relaxation features noted for glycerol-labelled β-DTGL were also observed for the head group labelled (C1) glycolipid (results not shown) and for a number of other head group labelled mono- and disaccharide glycolipids in the gel phase (Jarrell et al., unpublished results). Whatever motion is occuring at the glycerol backbone level seems therefore to be reflected in the head group region. Whether this motion takes place about the C2-C3 or the C1-C2 bonds of the glycerol backbone would have to be confirmed by the analysis of β-DTGL specifically deuteriated at the C2 position of the glycerol backbone.

The possibility of an internal motion at the glycerol backbone of β-DTGL seems however in apparent contradiction with previous studies which indicated that the glycerol

backbone in lipids is essentially rigid on the ^{2}H quadrupolar splitting (Strenk et al., 1985) and ^{13}C chemical shift anisotropy (CSA) (Braach-Maksvytis & Cornell, 1988) time scales. The results of these studies suggested that the glycerol conformation is constrained to one which produces motionally inequivalent quadrupolar splittings of the deuterons at C1 and C3 of the glycerol backbone while keeping the same C1 and C3 methylene carbon orientations. Moreover, as mentioned previously, it was shown for β-DTGL that differential ^{1}H-^{2}H dipolar couplings between the two deuterons at C3 and the proton at C2 were obtained, suggesting an inequivalence of these two deuterons (Jarrell et al., 1987a). However, since the correlation time of the proposed internal motion is very short (6.7×10^{-10} s) compared to the time scales of the residual ^{2}H quadrupolar splittings and ^{13}C CSA, the results of the present study may not be in contradiction with the earlier studies described above. If the internal motion is very fast relative to the interaction studied, only an average conformation about the C2-C3 bond will be detected and the glycerol backbone can be treated as effectively rigid relative to the time scale of interest. Additional support for the presence of a fast internal motion at the C2-C3 bond of the glycerol backbone is that the relative populations determined in the present study (0.46, 0.34, 0.20) are in good agreement with those proposed for the gauche (+), gauche (-) and trans conformers about the C2-C3 bond in phospholipids (0.48, 0.37, 0.15) (Hauser et al., 1980). Moreover, relatively small potential energy barriers have been calculated for the rotation about the C1-C2 and C2-C3 bonds of the glycerol backbone in phospholipids (McAlister et al., 1973).

8.4 Slow motion

8.4.1 Temperature dependence of spectral intensity

The results presented so far were obtained at 25°C, well below the gel to liquid-crystalline phase transition temperature (52°C) for β-DTGL. As the temperature of multilamellar dispersions of [3,3-$^2H_2$] β-DTGL was varied from 25°C (gel phase) to 60°C (liquid-crystalline phase), a dramatic decrease in spectral intensity was observed at 50°C, just below the gel to liquid-crystalline phase transition temperature. The results (Figure 8.6 (top, filled circles)), indicate that the relative intensity at 50°C is about 5% of the intensity observed at 55°C, in the liquid-crystalline phase. Moreover, this decrease in intensity is accompanied by a large change in the spectral lineshape at 50°C (Figure 8.6, bottom left). It is also interesting to note that the intensity of the gel phase spectrum at 25°C is about half that observed in the liquid-crystalline phase. This decrease in intensity near a phase transition has been reported for phospholipid systems (Meier et al., 1986). In addition, a similar decrease in spectral intensity has been observed in several mono and disaccharide glycolipid systems (Jarrell et al., unpublished results, chapter 9 of this thesis). Clearly, additional motion(s) is being activated over the temperature range between 25 to 60°C.

The observation of axially symmetric (η_{eff}=0) powder spectra for glycolipid in the liquid-crystalline phase implies that the motions giving rise to such spectra are axially symmetric, i.e. have a threefold or higher symmetry, and are in the fast limit relative to the ^2H NMR lineshape time scale. Generally, it is believed, for both phospholipid and glycolipid systems, that an axial motion of the molecule as a whole is responsible for the

Figure 8.6 **Top:** (●) Temperature dependence of the spectral intensity for a multilamellar dispersion of [3,3-$^2H_2$] β-DTGL. Note that just before the phase transition temperature (52°C), a dramatic decrease in intensity is observed. (□) Calculated spectral intensity as a function of the axial motional rate. Simulations were performed using a 9-site model, in which the axial motion was modelled by an equally populated 3-site jump. A similar decrease in spectral intensity was observed using a 36-site model, in which the axial motion was modelled by an equally populated 12-site jump. For the 9-site model, the lowest intensity occurs for an axial motional rate of 2×10^4 rad s^{-1}, which corresponds to a correlation time τ_c ($\tau_c = (3k)^{-1}$) of 1.7×10^{-5} s for the axial motion. **Bottom:** Comparison between the experimental lineshape at 50°C and that calculated using an axial motion rate of 2×10^4 rad s^{-1}.

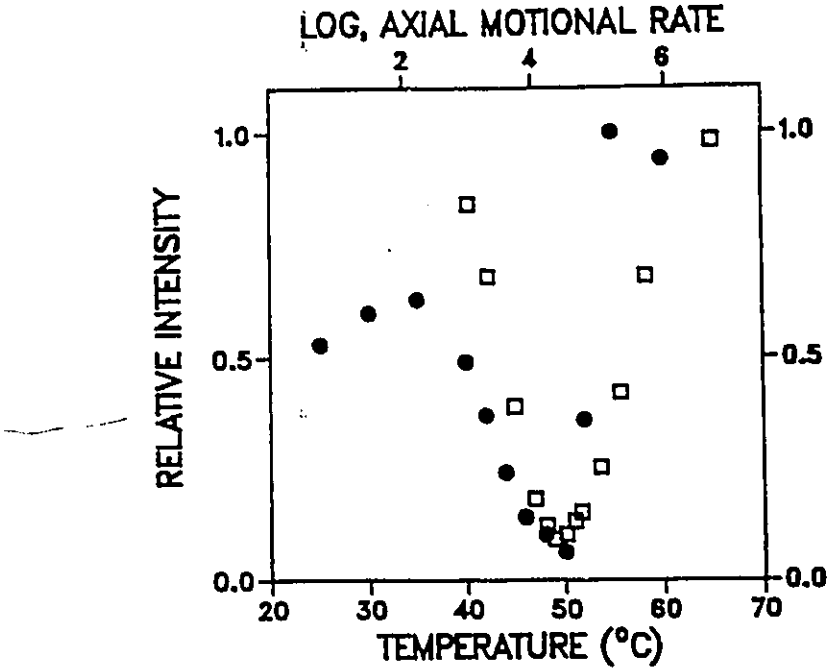

50°C

$k = 2 \times 10^4$ rad s^{-1}

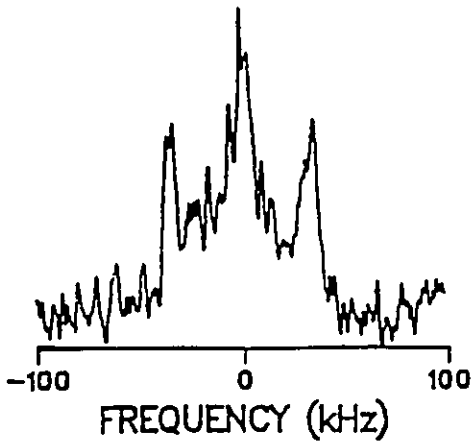

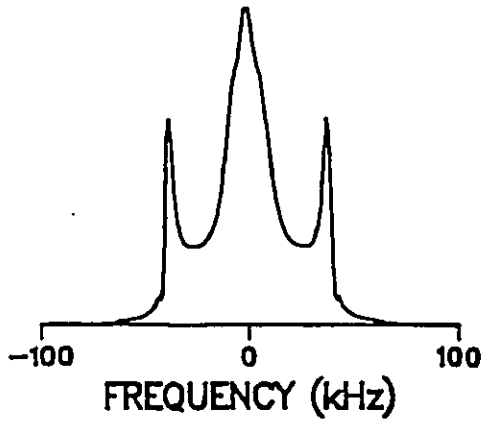

averaging of the electric field gradient tensor to axial symmetry in the liquid-crystalline phase. Additional averaging is also usually observed in the liquid-crystalline phase due to off-axis motion ("wobbling") of the symmetry axis.

If the axial motion of the entire β-DTGL molecule is too slow in the gel phase to influence spectral lineshapes ($\omega_Q\tau_C >> 1$) and fast enough in the liquid-crystalline phase to average the electric field gradient tensor to axial symmetry ($\omega_Q\tau_C << 1$) (for temperatures between 25 and 60°C), the axial motion has to go through an intermediate motional regime ($\omega_Q\tau_C \approx 1$). In such cases, short anisotropic transverse relaxation times T_{2e} will result in a dramatic decrease in spectral intensity and changes in lineshape (*vide supra*). A reasonably simple explanation for the variation in spectral intensity observed for β-DTGL at temperatures between 25 and 60°C is that there is such a change in the rate of axial motion of the glycolipid molecule. To test this hypothesis, simulations of powder and oriented-sample lineshapes were performed using a composite motional model including both the fast rotameric (unequally populated) three-site jump model (internal mode) needed to account for the gel phase lineshape and relaxation features, and an axial motion (whole molecule mode) with exchange rates which were varied from about 1×10^3 rad s^{-1} (slow motional limit) to 5×10^6 rad s^{-1} (fast motional limit). The axial motion was first modelled simply by an equally populated three-site exchange model in which the three sites were coincident with the rotameric jump sites. The relative spectral intensities for powder spectra of glycerol-labelled β-DTGL, simulated using this nine-site model, are presented in Figure 8.6 (top, open squares) as a function of the log of the axial motional rate. It is clear from this figure that varying the axial motion rate in the nine-site model, while keeping the rotameric jump rate constant, can satisfactorily reproduce the experimental temperature dependence of spectral intensity. The smallest simulated spectral intensity, obtained using

an axial motion rate k of 2×10^4 rad s^{-1}, is about 5% that obtained for $k = 5 \times 10^6$ rad s^{-1}. It should be noted, however, that unlike the experimental temperature dependence of spectral intensity, the simulated intensity curve is symmetric since contributions other than chemical exchange were neglected in the simulations. Using the nine-site model, the powder spectrum lineshape obtained for the axial rate giving the smallest simulated spectral intensity (2×10^4 rad s^{-1}) was simulated and compared with the experimental powder spectrum at 50°C (Figure 8.6, bottom). Since the intensity of this powder spectrum is only about 5% that of the liquid-crystalline phase spectrum, the signal-to-noise ratio for the experimental spectrum is rather poor. However, the two powder spectrum lineshapes compare favorably and further support the conclusions made from the temperature dependence of spectral intensities.

The quadrupolar echo amplitude decays with a time constant T_{2e}, which is sensitive to slow motions (Jeffrey, 1981; Bloom & Sternin, 1987). For powder samples, the motion that will most likely dominate transverse relaxation is diffusion of the lipid molecules along the curved membrane surfaces (Bloom & Sternin, 1987; Perly et al., 1985; Rance, 1981; Woessner et al., 1969). By using oriented samples, the orientational averaging effects of rapid lateral diffusion over the curved liposomal surfaces are circumvented. The transverse relaxation time T_{2e} for an oriented sample of [3,3-$^2H_2$] β-DTGL was measured at 52°C, for $\theta = 90°$. The experimental value of 1.2 ms was then compared with that calculated using the nine-site model described previously, in which axial motion is modelled by an equally populated three-site jump. A T_{2e} of 1.13 ms was calculated using an axial motional rate of 3×10^6 rad s^{-1}, which corresponds to the rate estimated for a temperature of ≈ 55°C in the liquid-crystalline phase, as shown in Figure 8.6 (top). The good agreement between the experimental and simulated T_{2e} values confirms the presence

of slow axial motion (on the ^2H spin-lattice relaxation time scale) in the liquid-crystalline phase of β-DTGL and indicates that contributions from any other slow motions to transverse relaxation can most likely be neglected. Note that additional contributions to the transverse decay rate from static and fluctuating dipolar interactions have been neglected in these T_{2e} calculations.

8.4.2 Large angle jump versus diffusive motion

Previous lineshape simulations of phospholipid gel phase spectra (Blume et al., 1982a) and of lipid/cholesterol "liquid-gelatin" phase spectra (Siminovitch et al., 1988) have shown that threefold (120°) rotational jumps about the director would seem to be an appropriate model for rotational diffusion. In the present system, the question remains that while modeling axial motion by large angle jumps (3 sites) is sufficient to explain the data, can a diffusive (small angle) motion be equally satisfactory? Torchia and Szabo (1982) have demonstrated that the correlation function for a N-site nearest-neighbor jump model reduces to that obtained for free diffusion when $N \rightarrow \infty$ and $k \rightarrow \infty$ such that $D = 4\pi^2 k/N^2$ where D is the rotational diffusion rate. In order to investigate this point, we have determined the effect on both T_{1Z} and lineshape intensity of the number of sites used to model axial motion . These simulations were performed using a constant value of the rotational diffusion rate D ($D = 5 \times 10^6$ rad s^{-1}) and the exchange rate k for a particular value of N was calculated from the expression $k = N^2D/4\pi^2$. The results for N varying from 3 to 36 are presented in Figure 8.7. From this figure, it is clear that a large difference in the T_{1Z} values is observed between a three and a six-site jump model and that the T_{1Z} values approach the value calculated for free diffusion (13.4 ms) when the number

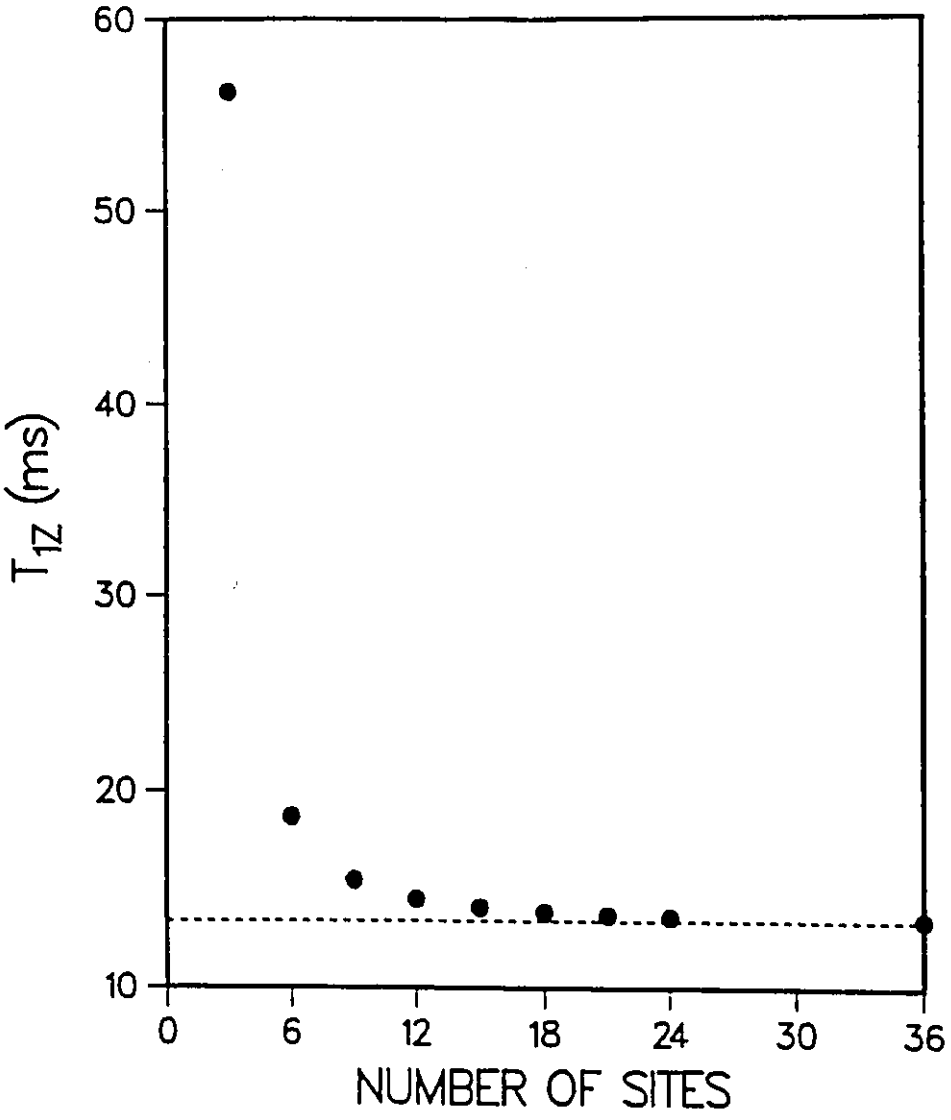

Figure 8.7 Calculated spin-lattice relaxation times T_{1Z} as s a function of the number of sites N in a N-site exchange model. T_{1Z} were calculated using an exchange rate k determined from a constant rotational diffusion rate D of 5×10^6 rad s^{-1}, according to the expression $D = (4\pi^2 k/N^2)$ (Torchi & Szabo, 1982). (----) Free diffusion limit (T_{1Z} = 13.4 ms).

of sites is equal to or greater than 12. Similar results have been obtained by Bonmatin et al. (1989) in a study of the dynamical properties of cholesterol in liquid-crystalline bilayers. In that case, it is found that large (threefold) jumps of cholesterol can best account for the relaxation features in this system, in comparison to small step Brownian diffusion.

The simulations presented in Figure 8.6 were repeated using a 36-site exchange model, representing a three-site fast rotameric jump model with a jump rate of 5×10^8 rad s^{-1} and an axial motion modelled by a 12-site nearest-neighbor jump model. The results of these spectral lineshape simulations are essentially the same as those presented in Figure 8.6; a similar decrease in spectral intensity is observed, the lowest intensity occuring for an axial motion rate of about 5×10^4 rad s^{-1}. The temperature dependence of spectral intensity observed for β-DTGL at temperatures between 25 and 60°C can therefore be simulated by both a 9-site or a 36-site exchange model in which the axial motion of the entire molecule is modelled either by a 3-site or a 12-site jump model. Thus, it is not possible from the present results to determine the exact nature of the axial motion of the β-DTGL molecule. The use of two-dimensional ^2H NMR exchange techniques (Schmidth et al., 1986, 1987 1988; Wefing & Spiess., 1988; Wefing & al., 1988), which are sensitive to the rate and mechanism of very slow motions, could provide a way of distinguishing between a large jump or a free diffusion model of axial motion for β-DTGL, as discussed in chapter 9 of this thesis. It is of interest to note that a recent study suggested that in highly ordered systems, large angle motion may be favoured (Vold & Vold, 1988). Indeed, two recent studies have concluded that large angle jumps occur rather than diffusive motion (Bonmatin et al., 1989; Dammers et al., 1988).

From the comparison between the temperature dependence of spectral intensity

and that obtained from the variation of the axial motional rate (Figure 8.6), an activation energy of about 150 kJ mol^{-1} was estimated for the axial motion of β-DTGL in the gel phase. This value is higher than the value of ≈ 70 kJ mol^{-1} determined by Meier et al. (1986) for phospholipids in the gel phase and could explain why axial motion appears to be slower in the gel phase of glycolipid systems compared to phospholipid systems.

The presence of two motions, a fast internal motion and a slower axial motion, can therefore account quantitatively for the lineshape features of β-DTGL in both the gel and liquid-crystalline phases. As discussed previously, the rates of axial motion (≈ 1×10^6 rad s^{-1}) in the liquid-crystalline phase are in the fast limit relative to the ^2H NMR lineshape time scale and therefore average the spectrum to an axially symmetric powder spectrum. However, these motional rates are relatively far from the T_1 minimum and therefore should not dominate the relaxation features in this system. To verify this point, we have calculated the spin-lattice relaxation times T_{1Z} using either a 9- or 36-site exchange model and varying the axial motional rates from 1×10^2 to 5×10^6 rad s^{-1} while the rotameric jump rate was kept to a constant value of 5×10^8 rad s^{-1}. In all cases, the T_1 values were found to be identical to those presented in Table 8.1 using a three-site rotameric jump model (with $k = 5 \times 10^8$ rad s^{-1}) indicating that the second motion needed to account for the spectral lineshapes observed for β-DTGL does not contribute significantly to spin-lattice relaxation in both the gel and liquid-crystalline phases.

We have demonstrated earlier that the fast internal three-site jump motion at the glycerol backbone provides the dominant spin-lattice relaxation mechanism for β-DTGL in the gel phase at 25°C. Having a reasonable mechanism for spin-lattice relaxation in the gel phase, it is intriguing to test if such a simple description can account for the relaxation in

the less ordered liquid-crystalline phase. Preliminary investigations show that in the liquid-crystalline phase at 52°C, the relaxation times T_{1Z} obtained for [3,3-$^2H_2$] β-DTGL are similar to those obtained in the gel phase. Values of 4.2, 5.7 and 6.7 ms have been obtained respectively for the 0, 54.7 and 90° orientations at 52°C. Comparison of these values with those presented in Table 8.1 clearly indicates similar θ-dependent relaxation times in the gel and liquid-crystalline phases. On the basis of these results, it therefore appears that a fast internal motion could also provide a dominant relaxation mechanism for glycerol-labelled β-DTGL in the liquid-crystalline phase. A more detailed analysis will however be necessary to take into account the effects of other motions present in the liquid-crystalline phase, such as the off-axis motion of the entire glycolipid molecule.

8.5 Comparison with previous studies

It is important to consider the results of the present study in the context of previous descriptions of analogous systems. It has been shown (Brown, 1982; Brown & Davis, 1981; Brown et al., 1983; Williams et al., 1985) that the ^2H relaxation rate T_1^{-1} in the liquid-crystalline phase of saturated lipid bilayers can be written as:

$$T_1^{-1} = T_{1f}^{-1} + T_{1s}^{-1}$$

where T_{1f}^{-1} represents the contribution from relatively fast reorientational motions, including isomerizations, torsional oscillations and long axis rotational diffusion and T_{1s}^{-1} represents the contribution from slower reorientations of the molecule with respect to the bilayer normal (director) due to collective order director fluctuations. ^2H NMR studies of

perdeuteriated 1,2-diacyl-*sn*-glycero-3-phosphocholine (Williams et al., 1985) have shown that the T_{1f}^{-1} contributions from local motions is relatively small and suggested that the dominant contribution to the ^2H spin-lattice relaxation rates arises from collective order director fluctuations (ODF). However, the T_1 anisotropy predicted by this slow collective model was not observed in the partially relaxed powder spectra of unoriented lipid/cholesterol bilayers (Siminovitch et al., 1988) or in the spectra of oriented bilayers of DMPC and DPPC (Jarrell et al., 1988). Therefore, it would appear that isolated rather than collective motions best describe molecular dynamics on time scales $< 10^{-8}$ s in lipid bilayers. The results obtained in this study for the gel and liquid-crystalline phases of the glycolipid β-DTGL further support this hypothesis.

8.6 Conclusions

The present study demonstrates that the lineshape and relaxation features observed for glycerol-labelled β-DTGL can be best reproduced by a fast internal three-site jump motion at the glycerol backbone and that a change in the axial motional rate is observed in going from the gel to the liquid-crystalline phase. It is also interesting to note that the rotameric jump constant ($k = 5 \times 10^8$ rad s^{-1}) is about two orders of magnitude faster than the axial motional rate estimated in the liquid-crystalline phase (5×10^6 rad s^{-1}). Similar results have been obtained by Meier et al. (1986) for phospholipid bilayers where the correlation times for chain rotation and chain fluctuation were of the order of 10^{-8} s, while *trans-gauche* isomerization were significantly faster ($\tau_j \approx 10^{-10}$ s) in the liquid-crystalline phase. Moreover, the activation energies for local motions were determined to be about an order of magnitude smaller than those of the whole molecule motions. On the

other hand, for NPGS/cholesterol bilayers in the liquid-gelatin phase, it was determined that at least two modes of molecular reorientation could contribute to spin-lattice relaxation, namely *trans-gauche* isomerization and long-axis diffusion (Siminovitch et al., 1988). The relative rates of these processes (as determined from the T_1 anisotropy of NPGS powder spectra) were calculated to be of 5×10^8 s^{-1} for rotational diffusion and 5×10^7 s^{-1} for *trans-gauche* isomerization. The relative rates of axial diffusion and local motion determined for NPGS/cholesterol bilayers contrast with those obtained in the present study for β-DTGL, where the axial motion was found to be about two orders of magnitude slower in the liquid-crystalline phase compared to the internal motion. However, there are several experimental observations to support the conclusions obtained in the present study, in particular the ϕ-dependence of the relaxation times observed in gel phase oriented-sample spectra. Moreover, the characteristic powder lineshapes observed for these oriented-sample spectra also provide a way of discriminating between different motional models. The use of oriented samples may therefore prove to be of great value in the study of molecular dynamics of lipid bilayers in the gel phase and may provide a better way of elucidating motional modes than an interpretation based solely on powder spectrum lineshape and relaxation.

A firm basis for the analysis of motional modes in both the gel and liquid-crystalline phases of glycoglycerolipid bilayers has been established in the present study. In effect, dynamics in two well separated motional windows were examined, one in the nanosecond range and the other in the millisecond range. In addition, the internal motion elucidated in this study suggests that similar motion should be considered in the description of the head group motion of other lipid classes.

CHAPTER 9

Glycerolipids: Common Features of Molecular Motion in Bilayers

9.1 Introduction

In the previous chapter, it was demonstrated that a simple motional model involving two motions is sufficient to describe the spectral and relaxation behavior of the glycolipid 1,2-di-*O*-tetradecyl-3-*O*-(β-D-glucopyranosyl)-*sn*-glycerol (β-DTGL). The lineshape and relaxation features of this lipid in the gel phase were best simulated using a three-site jump model with relative site populations of 0.46, 0.34 and 0.20, and a correlation time of 6.7×10^{-10} s. This motion was associated with an internal jump about the C2-C3 bond of the glycerol backbone. A second motion, namely rotation about the long axis of the molecule as a whole, was needed to account for the observed variation in the quadrupolar echo amplitude and the spectral lineshape over the temperature range of 25-60°C. Similar results have been obtained from lineshape and spin-lattice relaxation studies of acyl chain-labelled N-palmitoylgalactosyl sphingosine (NPGS) in the gel phase (Huang et al., 1980; Siminovitch et al., 1985) which indicated that axial diffusion is very slow on the ^{2}H NMR time scale ($\tau_c = 1/\Delta\upsilon_Q$) and that the gel phase spectra are the result of a simple intermediate rate exchange process between gauche and trans conformers.

On the other hand, a recent high resolution NMR study has suggested that there is

a rapid interconversion on the NMR lineshape time scale between two preferred conformations about the glycerol C1-C2 bond in the liquid-crystalline state of phospholipids (Hauser et al., 1988). The coexistence of these two rotamers was found to be consistent with the relatively small potential energy barriers calculated for the rotation about the C1-C2 and C2-C3 bonds of the glycerol backbone in phospholipids (McAlister et al., 1973). Moreover, ^{2}H and ^{13}C NMR studies of phosphatidylcholine and phosphatidylethanolamine bilayers have also suggested the presence of molecular motions in the glycerol backbone (Wittebort et al., 1981; Blume et al., 1982a-b). These results are in apparent contradiction with previous studies which have indicated that the glycerol backbone in phospholipids is essentially rigid on the ^{2}H quadrupolar splitting (Strenk et al., 1985) and ^{13}C chemical shift anisotropy (CSA) (Braach-Maksvytis & Cornell, 1988) time scales.

A comparison of ^{2}H NMR results from previous studies from this laboratory (Jarrell et al., 1986; 1987a-b; Carrier et al., 1989; Renou et al., 1989) and others (Huang et al., 1980; Siminovitch et al., 1985; Blume et al., 1982a-b; Meier et al., 1986) suggested some common features. In the gel phase spectra from the glycerol backbone region, similar axially asymmetric lineshapes were observed. In addition, the echo intensity of the ^{2}H spectra exhibited a minimum as a function of temperature, with the minimum occurring near the gel to liquid-crystalline phase transition. Since the glycerol backbone is a structural feature common to all the lipids involved in these studies, are there also common features in their dynamical description? More specifically, since an adequate motional description for the glycolipid β-DTGL has been elaborated (Auger et al., 1989b; chapter 8 of this thesis), one might speculate that the same simple motional model elucidated for this glycerol-labelled glycolipid could then be generalized to other glycolipids as well as

phospholipid bilayers. Therefore, we have investigated the ^2H lineshape and relaxation features of several lipids in the gel and liquid-crystalline states. Our results demonstrate that dynamics in these lipid bilayers can also be described by a motional model involving fast internal motions and a slower axial motion of the whole molecule. The implications of a common molecular motion in glycerol-containing lipid systems is discussed, and the proposed motional description is compared with previous investigations of molecular dynamics in similar systems.

9.2 Glycolipid bilayers

We first compare the lineshape and relaxation features of the glycolipid 1,2-di-*O*-tetradecyl-3-*O*-(α-D-mannopyranosyl)-*sn*-glycerol (α-DTML) with those previously observed for the glycolipid 1,2-di-*O*-tetradecyl-3-*O*-(β-D-glucopyranosyl)-*sn*-glycerol (β-DTGL) (Auger et al., 1989b; chapter 8 of this thesis) in the gel and liquid-crystalline phases. The ^2H NMR spectra of β-DTGL and α-DTML labelled at the C3 position of the glycerol backbone are shown in Figure 9.1 at 55°C and 25°C, above and below the gel to liquid-crystalline phase transition temperature for both lipids (52°C and 49°C for β-DTGL and α-DTML, respectively) (Jarrell et al., 1986, 1987b). At 55°C, the β-DTGL spectrum is axially symmetric and characteristic of lipids in a lamellar crystalline phase (Figure 9.1A). However, temperature-dependent ^2H NMR spectra of α-DTML reveal a transition from a broad axially asymmetric spectrum to a sharp axially symmetric powder spectrum, with a quadrupolar splitting less than one-half the value obtained for β-DTGL. These results indicate that pure α-DTML undergoes a transition from the gel state directly to a hexagonal liquid-crystalline phase (Jarrell et al., 1987b).

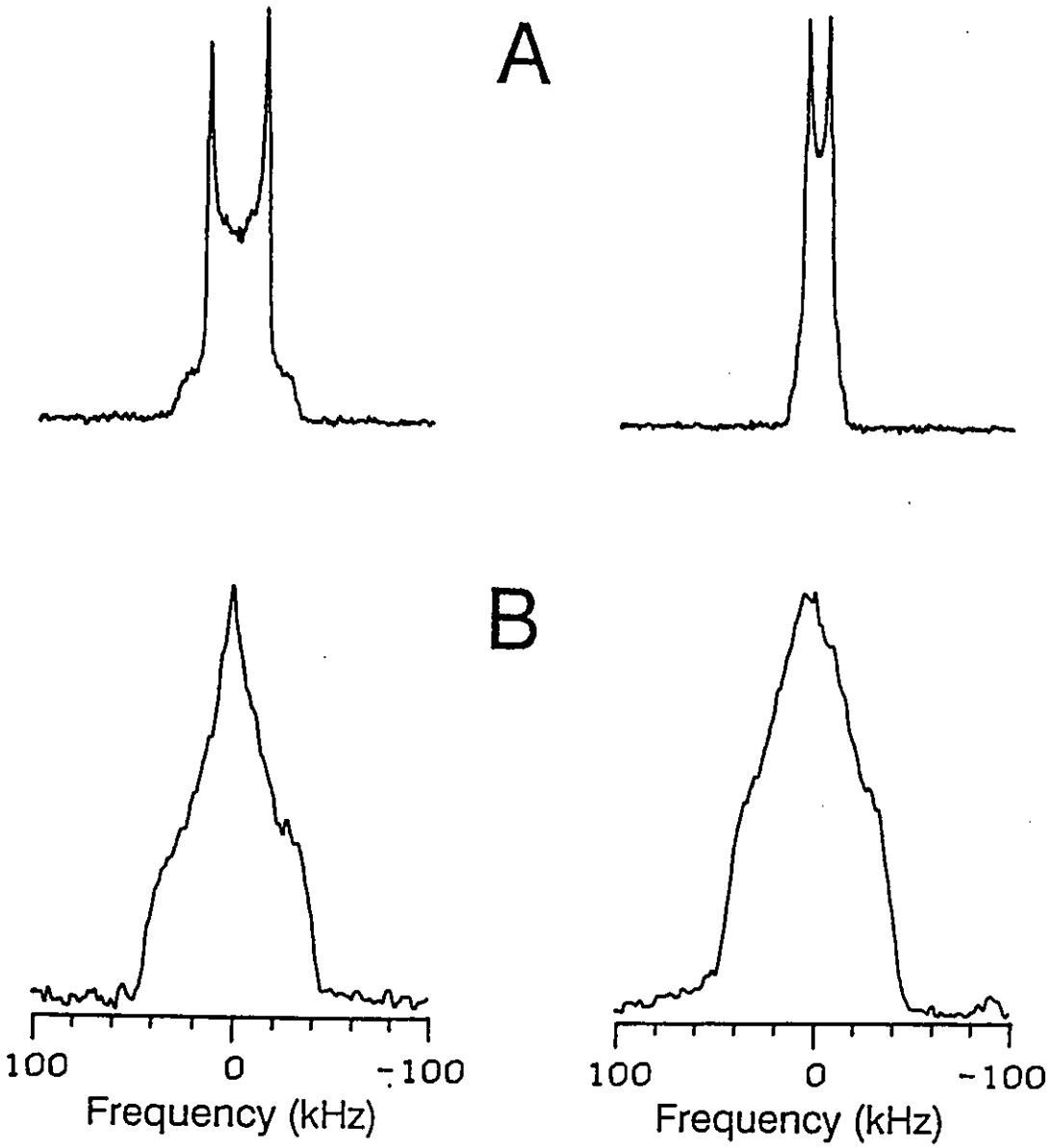

Figure 9.1 Experimental ^2H NMR spectra (30.7 MHz) of multilamellar dispersions of [3,3-$^2H_2$] β-DTGL (left) and [3,3-$^2H_2$] α-DTML (right) at **A.** 55°C and **B.** 25°C.

On the other hand, the ^2H NMR spectra of both β-DTGL and α-DTML below the gel to liquid-crystalline phase transition temperature are strikingly similar (Figure 9.1B). They are broad (≈ 90 kHz) and characteristic of fast-limit axially asymmetric motion. The lineshapes of the gel phase spectra presented in Figure 9.1B are invariant to the spacing, τ, between π/2 pulses in the quadrupolar echo sequence for τ values between 40 and 120 μs, indicating that the axially asymmetric motion(s) giving rise to such spectra are in the fast limit relative to the time scale of ^2H NMR lineshapes (> 10^5 s^{-1}).

While a number of potential motional models may be envisaged to account for the glycolipid powder spectral lineshape in the gel phase, it is attractive to search for the simplest reasonable descriptions consistent with the system under study. A previous study of a phosphatidylcholine suggested that motion about the C2-C3 bond consists of jump between three conformations (Hauser et al., 1980). In the case of [3,3-$^2H_2$] β-DTGL, it was demonstrated in chapter 8 that using a lineshape simulation program developed by Wittebort et al. (1987) based on the general formalism of Torchia and Szabo (1982), the experimental powder spectrum lineshapes were relatively well simulated with a variety of unequally populated three-site jump models. In that study, oriented samples were used to discriminate between the different motional models that were indistinguishable solely on the basis of powder lineshape simulations. The experimental oriented-sample lineshapes were best simulated using a three-site jump model with the C-^2H bonds oriented at 69° with respect to the axis of motional averaging and using relative site populations of 0.46, 0.34, 0.20.

However, since the gel phase spectra of both β-DTGL and α-DTML (Figure 9.1B)

are in the fast limit relative to the time scale of the ^2H NMR lineshape, simulated lineshapes were relatively insensitive to the jump rate k used in the simulations (for $k > 5 \times 10^6$ rad s^{-1}). Therefore, a rate for this motion could not be obtained solely from the lineshape simulations. In the slow- or fast-limit motional regimes, other methods are necessary in order to obtain dynamic information. In order to probe the correlation time of the motion giving rise to the experimental powder spectra of α-DTML in the gel phase, and to compare the results with those of β-DTGL, we have performed inversion recovery experiments on multilamellar dispersions of [3,3-$^2H_2$] α-DTML at 25°C. The results shown in Figures 9.2A and 9.2B as a function of the delay T after the inverting pulse clearly demonstrate that there is a significant orientation-dependence of the ^2H spin-lattice relaxation times (T_{1Z}) in both lipid systems. From this figure, it is clear that the outer edges of the powder spectrum recover faster than does the central part. This effect is particularly visible near the null point, for T values of about 4 ms for β-DTGL and 5 ms for α-DTML. However, since each part of the powder spectrum is not due solely to a unique angle θ describing the orientation of the bilayer normal relative to the magnetic field direction but to a combination of angles (θ, φ), it is not possible from the powder spectra to determine the individual spin-lattice relaxation times for each orientation and extract details about the T_{1Z} anisotropy. However, from inversion recovery experiments on an oriented sample of β-DTGL (Auger et al., 1989b; chapter 8 of this thesis), it has been determined that the spin-lattice relaxation times T_{1Z} have the following angular dependence:

$$T_{1Z}(0°) < T_{1Z}(54.7°) < T_{1Z}(90°)$$

Taking into account the powder and oriented-spectral lineshapes, as well as the θ- and φ-

Figure 9.2 Experimental (left) and simulated (right) spectra of a multilamellar dispersion of A. [3,3-$^2H_2$] β-DTGL and B. [3,3-$^2H_2$] α-DTML in the gel phase (25°C) as a function of the delay T in the inversion recovery sequence: 180-T-[90_x-τ-90_y]. Note that near the null point, a θ-dependence of the relaxation times T_{1Z} is observed. Simulations were performed using a three-site jump model with relative site populations of 0.46, 0.34, 0.20 and exchange rates of A. 5×10^8 rad s^{-1} and B. 6.2×10^8 rad s^{-1}. The C-^{2}H bonds of the 3-carbon of the glycerol backbone are oriented at 69° with respect to the axis of motional averaging.

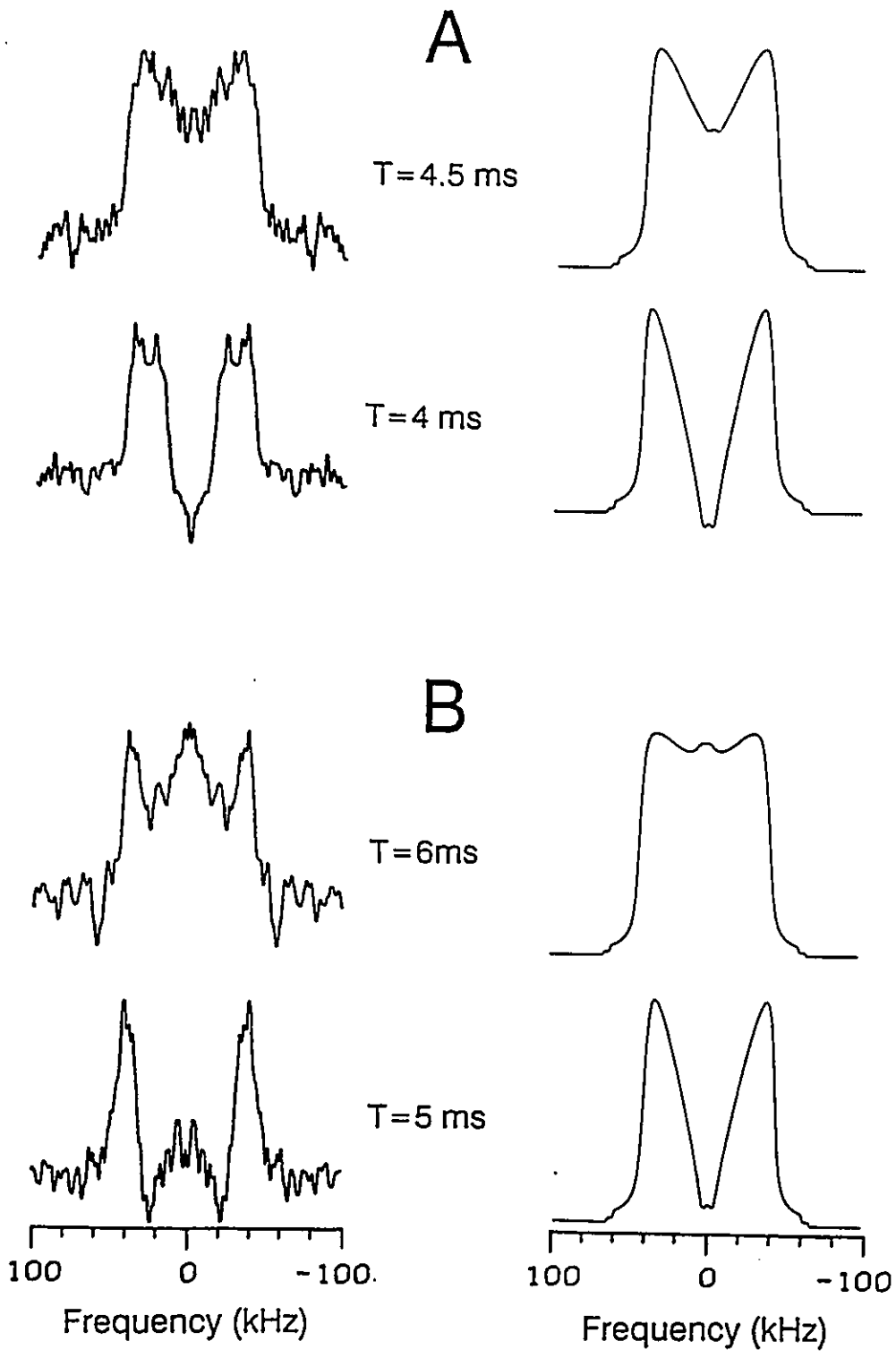
A
T=4.5 ms
T=4 ms
B
T=6ms
T=5 ms
100
0
-100
Frequency (kHz)
100
0
-100
Frequency (kHz)

dependence of the spin-lattice relaxation times T_{1Z}, the most satisfactory simulations of the lineshape and relaxation features of [3,3-$^2H_2$] β-DTGL in the gel phase were accomplished using a three-site jump model with relative populations of 0.46, 0.34, 0.20 and an exchange rate k of 5×10^8 rad s^{-1}, which corresponds to a correlation time τ_c ($\tau_c = (3k)^{-1}$) of 6.7×10^{-10} s (Auger et al., 1989b; chapter 8 of this thesis). Adapting this description to the mannolipid, the orientation-dependence of spin-lattice relaxation times observed for [3,3-$^2H_2$] α-DTML could be equally well simulated using the same motional model with only a slight increase of the exchange rate ($k = 6.2 \times 10^8$ rad s^{-1}), suggesting that similar motions are present in the gel phase of both lipids.

As the temperature of multilamellar dispersions of [3,3-$^2H_2$] β-DTGL and [3,3-$^2H_2$] α-DTML is varied from 25°C (gel phase) to 60°C (liquid-crystalline phase), a dramatic decrease in spectral intensity is observed just below the gel to liquid-crystalline phase transition temperature (Figure 9.3, filled circles). For β-DTGL dynamics, it was determined that a second motion, namely rotation about the long axis of the molecule as a whole, was needed to account for the observed variation in quadrupolar echo amplitude and spectral lineshape over the temperature range of 25-60°C (Auger et al., 1989b). This axial motion was first modelled simply by an equally populated three-site exchange model in which the three sites were coincident with the rotameric jump sites. Spectral simulations indicate that varying the rate of axial motion while keeping the rotameric jump rate constant, can satisfactorily reproduce the experimental temperature dependence of spectral intensity of both β-DTGL and α-DTML and suggested that the axial motion for the two glycolipids in the gel phase at 25°C is very slow on the ^2H NMR lineshape time scale ($\tau_c = 1/\Delta\nu_Q$) (Figure 9.3, open squares). This conclusion has recently been confirmed for β-DTGL (Auger & Jarrell, 1989; chapter 10 of this thesis) by two-

Figure 9.3 (●) Temperature dependence of the spectral intensity for multilamellar dispersions of A. [3,3-$^2H_2$] β-DTGL and B. [3,3-$^2H_2$] α-DTML. Note that just before the phase transition temperature, a dramatic decrease in intensity is observed. (□) Calculated spectral intensity as a function of the axial motional rate. Simulations were performed using a 9-site model, in which the axial motion was modelled by an equally populated 3-site jump.

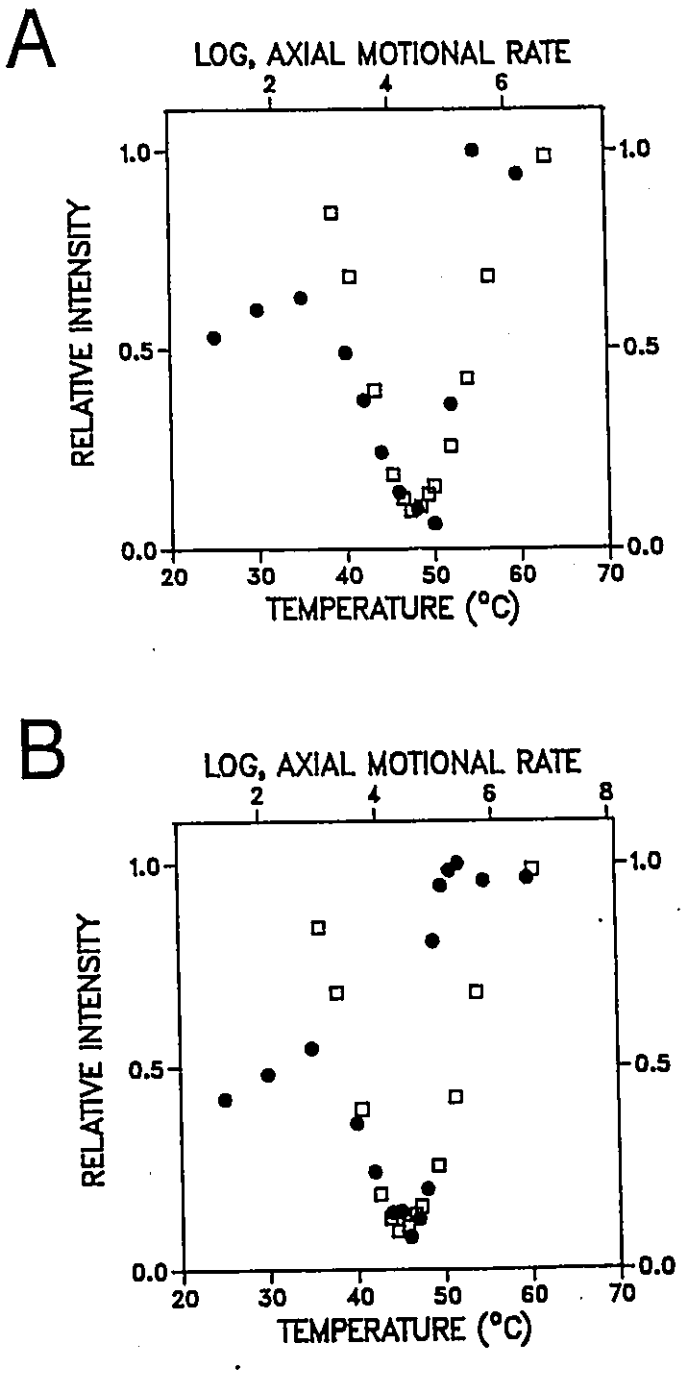
A
LOG, AXIAL MOTIONAL RATE
2
4
6
1.0
0.5
0.0
RELATIVE INTENSITY
20
30
40
50
60
70
TEMPERATURE (°C)
B
LOG, AXIAL MOTIONAL RATE
2
4
6
8
1.0
0.5
0.0
RELATIVE INTENSITY
20
30
40
50
60
70
TEMPERATURE (°C)

dimensional ^2H NMR exchange techniques (Schmidt et al., 1986, 1987, 1988; Wefing & Spiess., 1988; Wefing & al., 1988), which are sensitive to the rate and mechanism of very slow motions.

Comparison of the lineshape and relaxation features of β-DTGL and α-DTML therefore suggests that the gel phase of these two lipids can be described by very similar motional models. This result is somewhat surprising considering that these two lipids form two very different liquid-crystalline phases, lamellar and hexagonal for β-DTGL and α-DTML, respectively (Jarrell et al., 1987b). It is also interesting to note that the relative spectral intensities above the gel to liquid-crystalline phase transition temperature are not significantly affected by the nature (lamellar or hexagonal) of the liquid-crystalline phase.

The characteristic loss of intensity before the gel to liquid-crystalline phase transition has also been observed in two disaccharride glycolipid systems, 1,2-di-*O*-tetradecyl-3-*O*-(6-*O*-β-D-glucopyranosyl-β-D-glucopyranosyl)-*sn*-glycerol (Carrier et al., 1989) and the lactose containing glycolipid 1,2-di-*O*-tetradecyl-3-*O*-(4-*O*-β-D-galactopyranosyl-β-D-glucopyranosyl)-*sn*-glycerol (Renou et al., 1989). Moreover, the spin-lattice relaxation times obtained for both lipids in the liquid-crystalline phase are very short ($\approx$ 3-8ms), which suggests that these systems exhibit motions similar to those observed for the two monosaccharide glycolipids investigated in the present study. Similar conclusions have also been drawn from lineshape and spin-lattice relaxation studies of another glycolipid, the acyl chain-labelled N-palmitoylgalactosyl sphingosine (NPGS) in the gel phase (Huang et al., 1980; Siminovitch et al., 1985, 1988). These studies indicated that axial diffusion in the gel phase is very slow on the ^2H NMR time scale ($\tau_c = 1/\Delta\upsilon_Q$) and that the gel phase spectra are the result of a simple intermediate rate exchange process

between gauche and trans conformers.

Fast internal motions therefore appear to be present in both the gel and liquid-crystalline phases of several glycolipid bilayers. If a similar motion occurs about the C2-C3 bond of the sphingosine residue, it may have considerable importance considering that glycosphingolipids can assume many biological roles (Hannun & Bell, 1989) such as the capacity to function as recognition sites (cell-cell recognition (Critchly et al., 1979), immune recognition (Hakamori, 1984) and toxin receptor (Fishman & Brady, 1976)), and as modulators of membrane structure (Sharom & Grant, 1977). In addition, this aspect must be considered when discussing the average orientation of glycolipid head groups and their conformations. In view of the important roles played by the glycolipid head group, it is clear that a knowledge of the dynamics of the carbohydrate moiety will be a prerequisite for a complete understanding of cell surface recognition at the molecular level.

9.3 Phospholipid bilayers

9.3.1 Introduction

Molecular dynamics of phosphatidylcholine and phosphatidylethanolamine bilayers in the gel and liquid-crystalline phases have been studied by ^{2}H and ^{13}C NMR (Wittebort et al., 1981; Blume et al., 1982a-b). The gel phase lineshapes of these lipids were interpreted in terms of whole molecule axial motion and internal jumps with rates ranging from $\approx 3 \times 10^{4}\ s^{-1}$ to $8 \times 10^{5}\ s^{-1}$, which are intermediate rates on the ^{2}H NMR lineshape time scale. In addition, a loss of spectral intensity was observed just before the gel to

liquid-crystalline phase transition which was interpreted in terms of exchange on an intermediate time scale between gel and liquid-crystalline domains.

However, it is interesting to note that for the glycolipid systems discussed in the previous section, the rotameric jump constant ($k = 5 \times 10^8$ rad s^{-1}) is in the fast-limit relative to the ^2H lineshape time scale and is about two orders of magnitude faster than the axial motional rate estimated in the liquid-crystalline phase (5×10^6 rad s^{-1}). Similar results have been obtained by Meier et al. (1986) for phospholipid bilayers, where the correlation times for chain rotation and chain fluctuation were of the order of 10^{-8} s, while *trans-gauche* isomerization was significantly faster ($\tau_j \approx 10^{-10}$ s) in the liquid-crystalline phase. Moreover, the activation energies for local motions were determined to be about an order of magnitude smaller than those of the whole molecule motions.

It is therefore of interest to investigate if the simple motional model used for the different glycolipid systems can be extrapolated to phospholipid systems. To do so, we have analyzed the lineshape and relaxation features in the gel and liquid-crystalline phases of a phosphonolipid analog of phosphatidylethanolamine, 1,2-di-*O*-hexadecyl-*sn*-glycero-3-(2-aminoethyl)phosphonate (DHAEPn) labelled on both the C2 and C3 positions of the glycerol backbone. Like phosphatidylethanolamine, this lipid exhibits polymorphism, with a gel to lamellar liquid-crystalline phase transition temperature of 70.2°C and a lamellar to hexagonal phase transition at 84.5°C.

9.3.2 C3 labelled DHAEPn

The ^2H NMR spectra of DHAEPn labelled at the C3 position of the glycerol backbone are shown in Figure 9.4 at 75°C and 45°C, above and below the gel to liquid-crystalline phase transition temperature for this lipid (70.2°C). These spectra are very similar to those obtained for the two glycolipids β-DTGL and α-DTML in the gel phase at the same reduced temperature. Inversion recovery experiments were also performed on multilamellar dispersions of DHAEPn, and the partially relaxed spectra shown in Figure 9.5 as a function of the delay T after the inverting pulse clearly demonstrate that (1) there is a significant orientation-dependence of the ^2H spin-lattice relaxation times (T_{1Z}), and (2) this anisotropic relaxation is very similar to that observed in glycolipid systems. The averaged spin-lattice relaxation time value for [3-$^2H_1$] DHAEPn at 45°C is 5.0 ms, which is again very close to that determined in glycolipid systems. These results suggest a common motion for DHAEPn, β-DTGL and α-DTML.

9.3.3 C2 labelled DHAEPn

The gel phase ^2H NMR spectrum of DHAEPn labelled at the C2 position of the glycerol backbone is shown in Figure 9.6 (left spectrum) at 45°C. As was observed for the C3 labelled phosphonolipid, this spectrum is very broad and characteristic of axially asymmetric motion and the corresponding partially relaxed spectra (Figure 9.7) also exhibit a significant orientation-dependence of the spin-lattice relaxation times for DHAEPn labelled at the C2 position of the glycerol backbone. Moreover, the average value of the spin-lattice relaxation time for this labelled position is again very short (8.2 ms), indicating

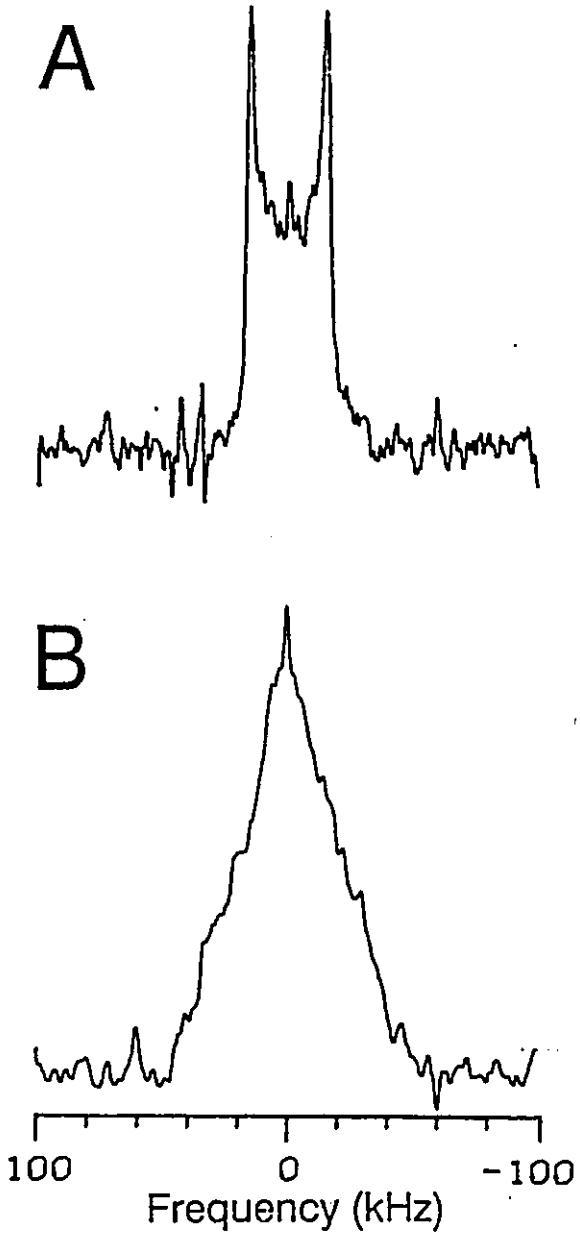

Figure 9.4 Experimental ^2H NMR spectra (30.7 MHz) of a multilamellar dispersion of [3-$^2H_1$] DHAEPn at **A.** 75°C, and **B.** 45°C.

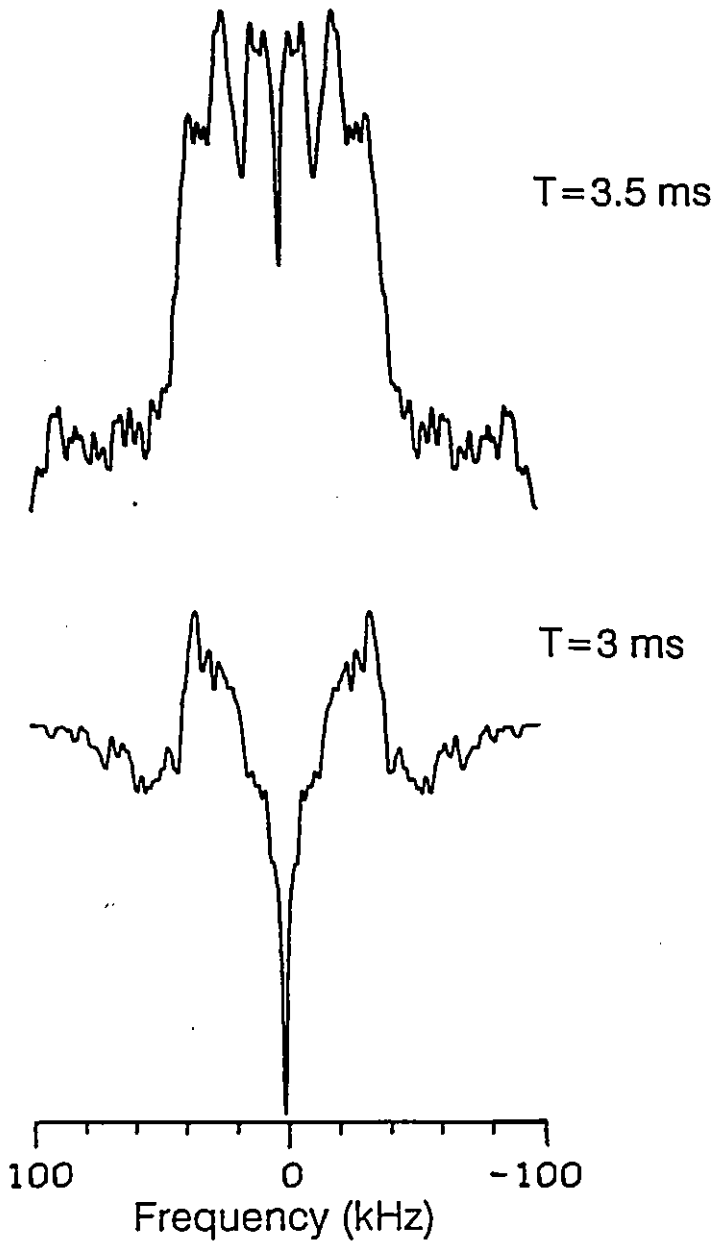

Figure 2.5 Partially recovered (T_{1Z}) spectra of a multilamellar dispersion of [3-$^2H_1$] DHAEPn at 45°C as a function of the delay T in the inversion recovery sequence.

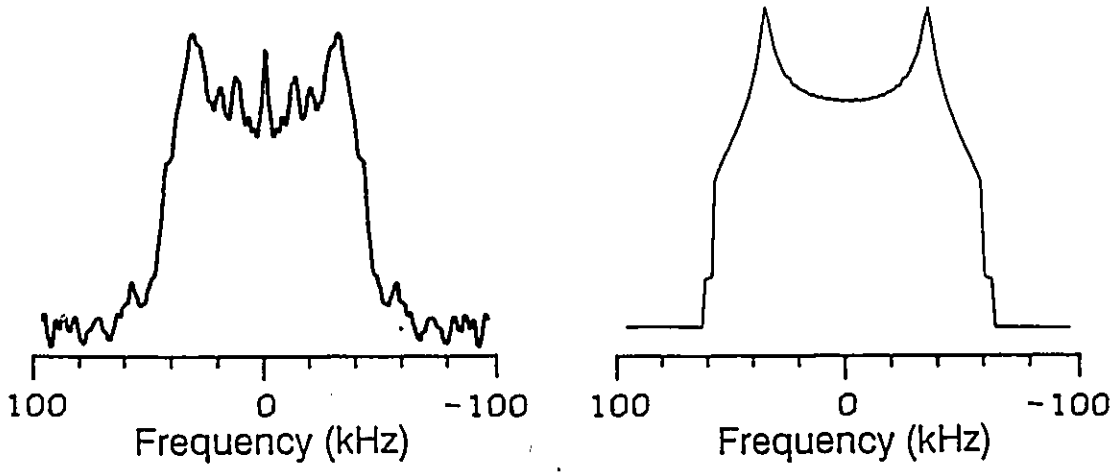

Figure 9.6 Experimental (left) and simulated (right) ^2H NMR spectra of a multilamellar dispersion of [2-$^2H_1$] DHAEPn at 45°C. Simulations were performed using a ±22° two-site jump with equal populations of the sites and a motional rate of 4×10^8 rad s^{-1}.

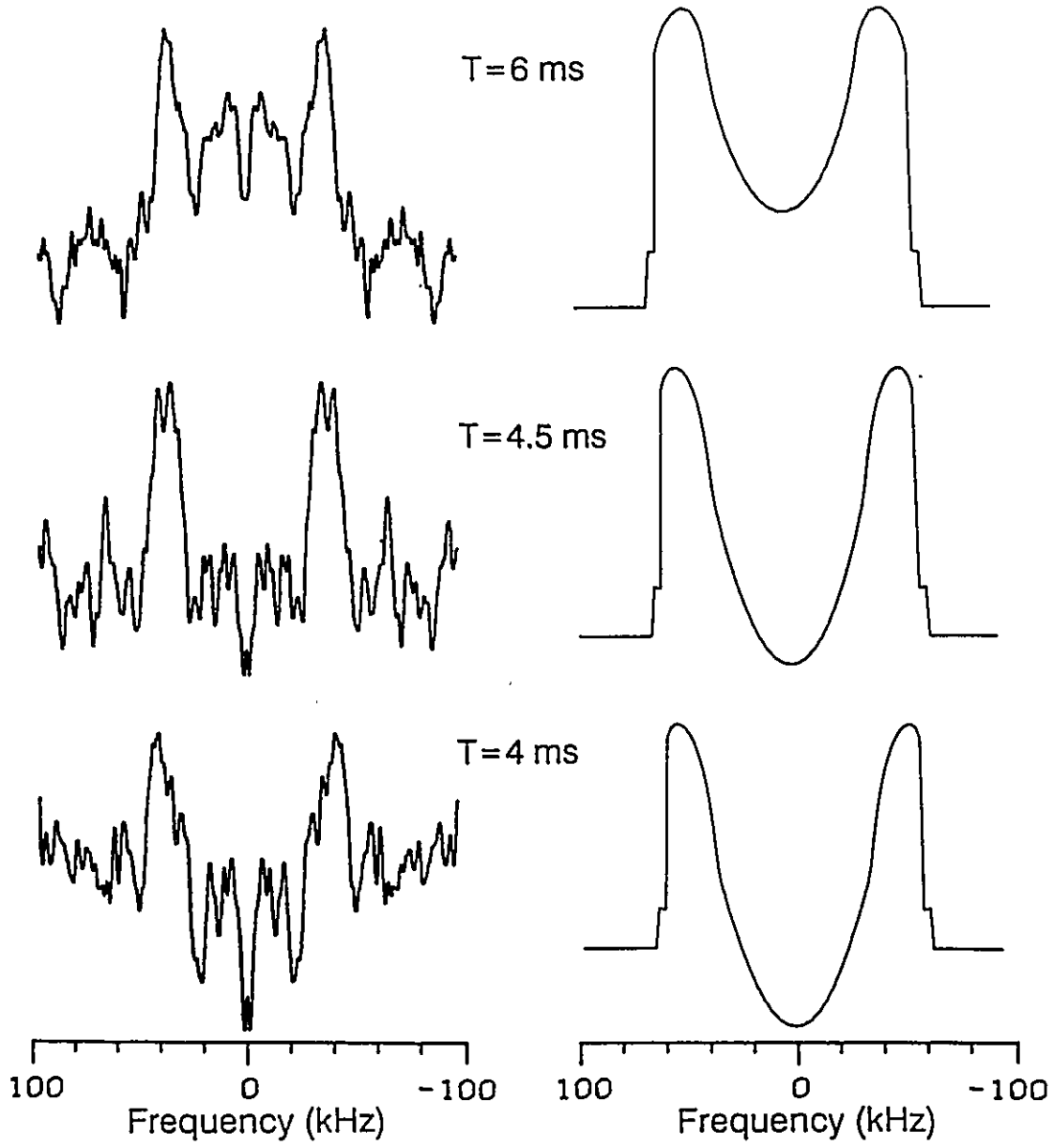

Figure 9.7 Experimental (left) and simulated (right) ^2H NMR spectra of multilamellar dispersions of [2-$^2H_1$] DHAEPn at 45°C as a function of the delay T in the inversion recovery sequence. Simulations were performed using a ±22° two-site jump with equal populations of the sites and a motional rate of 4×10^8 rad s^{-1}.

that the motion dominating relaxation is fast on the ^2H lineshape time scale.

It is interesting to note that the spectrum of C2-labelled DHAEPn in the gel phase is very similar to that obtained by Blume et al. (1982a) for dipalmitoylphosphatidyl-ethanolamine (DPPE) labelled at the same position of the glycerol backbone. In the latter study, the DPPE spectral lineshape was simulated using a six-site jump model including an axial motion modelled by a three-site jump and a slow 20° torsional motion of the C-^2H bond with respect to the axial motion axis. The angle between the director axis and the C2-^2H bond vector was determined to be $\approx$ 24° at 45°C. The lineshape was well simulated using an axial motional rate of $4.5 \times 10^5\ s^{-1}$ and a torsional motional rate of $3.9 \times 10^4\ s^{-1}$. The population of C-^2H bonds oriented at 15° with respect to the diffusion axis was set to 0.6 in order to account for the experimental quadrupolar splitting. Although this motional model can satisfactorily reproduce the experimental spectral lineshapes observed for both C2-labelled DPPE and DHAEPn at the same reduced temperature, it is important to notice that the rates of both motions involved are intermediate, and therefore that neither of the motions in question could provide efficient spin-lattice relaxation. In fact, we have determined that such a motional model would result in spin-lattice relaxation times, T_{1Z}, of about 300 ms, which are two orders of magnitude longer than those observed experimentally for DHAEPn.

The dramatic loss of spectral intensity reported for both the C2 and C3 glycerol-labelled DPPE's (Blume et al., 1982a) has been explained by an exchange between gel and liquid-crystalline domains. We have also observed the variation in quadrupolar echo amplitude and spectral lineshape for both C2 and C3 labelled DHAEPn (results shown in Figure 9.8 for [2-$^2H_1$] DHAEPn, filled circles). However, as for the glycolipid systems

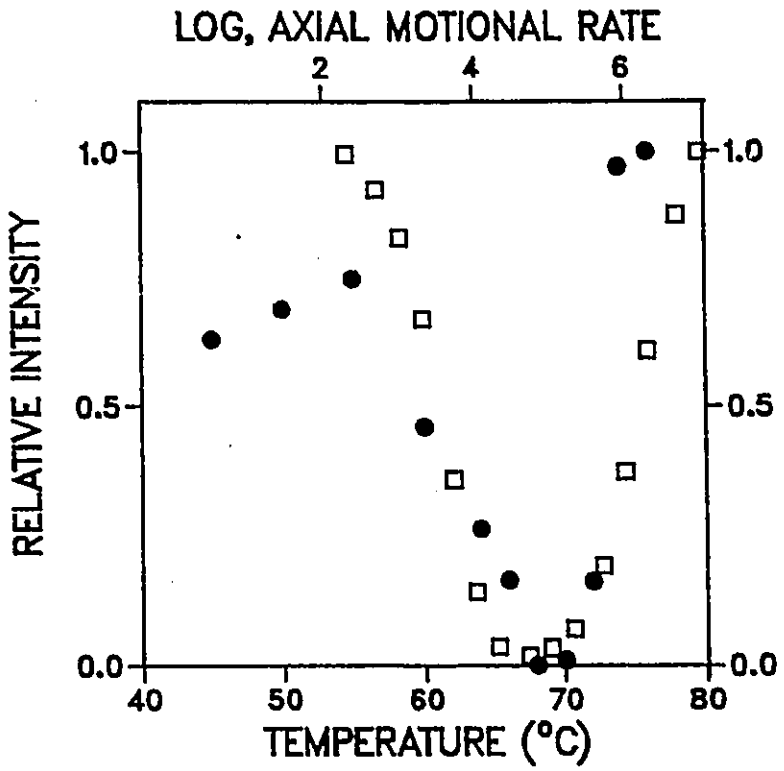

Figure 9.8 (●) Temperature dependence of the spectral intensity for a multilamellar dispersion of [2-$^2H_1$] DHAEPn. Note that just before the gel to liquid-crystalline phase transition temperature (72°C), a dramatic decrease in intensity is observed. (□) Calculated spectral intensity as a function of the axial motional rate. Simulations were performed using a 6-site model, including the two-site jump model described in Figures 9.6 and 9.7 and an axial motion modelled by an equally populated 3-site jump.

discussed previously, this decrease in spectral intensity was relatively well simulated simply by varying the axial motional rate while keeping the internal motional rate constant (Figure 9.8, open squares). These simulations reveal that the axial motional rate in the gel phase at 45°C is about 1×10^3 s^{-1}, which is too slow to influence the ^2H lineshape at that temperature. The spectral lineshape and relaxation features of the C2 labelled DHAEPn were therefore simulated using a two-site jump model in which the libration angle, the relative populations of the sites and the motional rates were varied in order to fit the experimental lineshape and spin-lattice relaxation time. These features were best simulated using a ±22° torsional motion with equal populations of the sites and a motional rate of 4×10^8 rad s^{-1} (Figures 9.6 and 9.7, right spectra). This results in a calculated averaged spin-lattice relaxation time of about 8 ms. It has been suggested that the motion at the C2 position is constrained by the fact that the *sn*-2 chain is attached to this carbon. However, if a fast motion exits at the C3 position of the glycerol, it is not unreasonable to expect some coupling to the 2 position.

9.3.4 Comparison with previous studies

Thus, the lineshape and relaxation features of the phosphonolipid DHAEPn labelled at glycerol C2 and C3 can be described by two motions, a fast internal motion and a slower whole molecule axial motion. This result is in apparent contradiction with previous studies which have treated the glycerol backbone in phospholipids as essentially rigid on the ^2H quadrupolar splitting (Strenk et al., 1985) and ^{13}C chemical shift anisotropy (CSA) (Braach-Maksvytis & Cornell, 1988) time scales. The results of the latter studies suggested that the glycerol conformation is constrained to one which produces motionally

inequivalent quadrupolar splittings of the deuterons at C1 and C3 of the glycerol backbone while keeping the same C1 and C3 methylene carbon orientations. However, since the correlation time of the proposed internal motion is very short ($\approx 10^{-10}$ s) compared to the time scales of the residual ^{2}H quadrupolar splittings and ^{13}C CSA, the results of the present study may not be in contradiction with the earlier studies described above. If the internal motion is very fast relative to the interaction studied, only an average conformation about the C2-C3 bond will be detected and the glycerol backbone can be treated as effectively rigid relative to the time scale of interest.

Additional support for the presence of a fast internal motion at the C2-C3 bond of the glycerol backbone is that the relative populations necessary to simulate the gel phase lineshape and relaxation features of C3 labelled glycolipid and phospholipid bilayers (0.46, 0.34, 0.20) are in good agreement with those proposed for the gauche (+), gauche (-) and trans conformers about the glycerol C2-C3 bond proposed in phospholipids (0.48, 0.37, 0.15 for dihexadecyl phosphatidylcholine (DHPC) in D_2O) (Hauser et al., 1980). Moreover, a recent high resolution NMR study has suggested that there is a rapid interconversion on the NMR lineshape time scale between two preferred conformations about the glycerol C1-C2 bond in the liquid-crystalline state of phospholipids (Hauser et al., 1988). The coexistence of these two rotamers was found to be consistent with the relatively small potential energy barriers calculated for the rotation about the C1-C2 and C2-C3 bonds of the glycerol backbone in phospholipids (McAlister et al., 1973). The results obtained in the present study are in agreement with the hypothesis of rapid equilibrium between different conformations of the glycerol backbone.

9.4 Conclusions

The present study demonstrates that the lineshape and relaxation features observed for two glycerol-labelled glycolipids β-DTGL and α-DTML, as well as for the phosphonolipid DHAEPn, can be well reproduced by a simple motional description in which there is fast internal jump at the glycerol backbone and axial motion whose rate changes by at least a factor of 10^2 on going from the gel to the liquid-crystalline phase. The fast internal motion elucidated in this study suggests that a similar motion should be considered in the description of the head group motion in both glycolipid and phospholipid bilayers. For example, it would be of interest to investigate ^{31}P spin-lattice relaxation in phospholipid bilayers (Milburn & Jeffrey, 1987, 1989) in terms of the motional model discussed in the present study.

The presence of fast internal motions in the glycerol backbone region in both the gel and liquid-crystalline phases of lipid bilayers can have important implications in understanding, for example, the interactions of exogenous molecules with lipid head groups or, in the case of glycolipid bilayers, phenomena such as lectin- or antibody-carbohydrate binding. Investigation of lipid dynamics in simple model systems can therefore be very useful for interpreting the physical properties of these lipids in the more complex environment of biological membranes, and for correlating changes in these physical properties with modulation of membrane function.

CHAPTER 10

Slow Motions in Lipid Bilayers: Direct Detection by Two-Dimensional Solid-State Deuteron NMR

10.1 Introduction

As discussed in the two previous chapters, establishing the time scales and amplitudes of molecular motions in the anisotropic environment of lipid bilayers is a task well suited to solid state ^2H NMR spectroscopy (Seelig, 1977; Griffin, 1981; Davis, 1983, 1986; Bloom & Smith, 1985; Smith, 1984), which provides observation windows in the range where the frequencies of most molecular motions occur (1-10^{10} s^{-1}, for lipid bilayers) (Kimmich et al., 1983). Spin-lattice relaxation measurements are sensitive to motions occurring on the time scale of the Larmor frequency (10^7-10^{10} s^{-1}), while lineshape studies can elucidate motions on the 10^3-10^6 s^{-1} time scale. These techniques can also provide motional discrimination but are not applicable for slower motions ($< 10^3$ s^{-1}).

The quadrupolar echo amplitude decays with a time constant, T_{2e}, which has been shown to be sensitive to slow motions (Jeffrey, 1981). Measurements of transverse relaxation times T_{2e} in lipid bilayers have been used to obtain correlation times of slow motions, in particular those of slow lateral diffusion over curved membrane surfaces (Bloom & Sternin, 1987; Perly et al., 1985). However, in general, such measurements do not necessarily provide information about the nature of the slow motions. An alternative

method of probing the rates and nature of slow molecular motions is the two-dimensional exchange technique, which has been used extensively for structure elucidation of solutions (Bodenhausen et al., 1987). The 2D exchange technique has recently been applied to deuteron NMR and extended the frequency range over which motions may be probed to the ms or longer time scales in simple molecular systems (Schmidt et al., 1986, 1987, 1988; Wefing & Spiess, 1988; Wefing et al., 1988). Moreover, ^{2}H NMR exchange techniques have been shown to be very powerful in distinguishing between motion which is characterized by large angle jumps and free diffusion (Schmidt et al., 1986, 1987; Wefing et al., 1988). Since the quadrupole coupling tensor of deuterons is frequently axially symmetric, the singularities of the 2D exchange signals give rise to simple geometric ridge patterns from which the angles through which the molecules rotate can be read directly. Two-dimensional ^{2}H exchange spectra can therefore yield information about molecular dynamics in a model-independent fashion.

In the present study, we first use two-dimensional deuteron NMR to detect and suggest the nature of a slow whole molecule axial motion in the gel phase of the glycolipid 1,2-di-*O*-tetradecyl-3-*O*-β-D-glucopyranosyl-*sn*-glycerol (β-DTGL). Moreover, it is shown that slow lateral diffusion over a curved membrane surface can be detected in the liquid-crystalline phase of dipalmitoylphosphatidylcholine bilayers, on a time scale of ≈ 100 ms. The implications of this technique for the study of other biological systems will be discussed.

10.2 Two-dimensional exchange NMR in solids

10.2.1 Introduction, two-dimensional NMR

The concept of two-dimensional (2D) Fourier transformation in NMR was first introduced by Jeener (1971). The pulse sequence of a 2D NMR experiment may be divided in general into the following blocks:

$$\text{preparation-evolution } (t_1)\text{-mixing } (t_m)\text{-detection } (t_2)$$

The detection period (t_2) corresponds exactly to that of a normal 1D NMR experiment. The time t_2 provides, after Fourier transformation, the ω_2 frequency axis of a 2D NMR spectrum. The important feature of 2D NMR spectroscopy is that a second time variable, the evolution time t_1, is introduced. The evolution time t_1 is made stepwise longer, i.e. incremented in analogy to the detection time t_2. For each t_1 increment, corresponding to the dwell time in the ω_1 dimension, a separate FID is detected in t_2. Thus, a signal is obtained which is a function of two time variables, t_1 and t_2: $S(t_1,t_2)$. A series of ω_2 spectra is then obtained upon Fourier transformation of each of the FIDs. They differ from one another in the intensities and/or phases of the individual signals, according to the different t_1 increments. A second Fourier transformation over t_1, "perpendicular" to the ω_2 dimension, results in a spectrum as a function of two frequencies $S(\omega_1,\omega_2)$.

Provided that the correlation times of the exchange processes are much longer than the evolution time t_1 and the detection period t_2, the spin Hamiltonian can be assumed to be constant during t_1 and t_2. During the mixing time t_m, however, the Hamiltonian may

change, for example due to a molecular reorientation, which implies that the frequencies during the evolution and detection period may differ. A change in frequency during the mixing time can be directly detected from a 2D exchange spectrum in which the frequencies ω_1 and ω_2 are correlated.

Two-dimensional NMR techniques have been used extensively for several years for the structure elucidation in isotropic solutions (Bodenhausen et al., 1987). The information obtained from these experiments is predominantly coded in the frequency coordinates of cross peaks rather than in lineshape variations. The 2D exchange experiment has also been applied to amorphous solid samples and powders. ^{13}C spectra have been obtained in static (Edzes & Bernards, 1984) and in rotating samples (Harbison et al., 1985). In 2D NMR spectra of static powders, the correlation of two tensorial interactions gives rise to ridges exhibiting characteristic geometrical figures. Two different interactions, for example anisotropic shielding and dipolar coupling, may be correlated (Linder et al., 1980). On the other hand, one interaction may be correlated with itself, providing information on dynamic exchange processes such as rotational motions. In the latter case, the molecular reorientational angles of jump-like motions can be read *directly* from these patterns.

10.2.2 Pulse sequence and phase cycling for deuteron 2D NMR

Figure 10.1 shows a scheme of the deuteron 2D exchange experiment, introduced by Schmidt et al. (1988). The two pulse sequences are needed in order to obtain quadrature in both dimensions. In order to obtain undistorted spectra from the rapidly

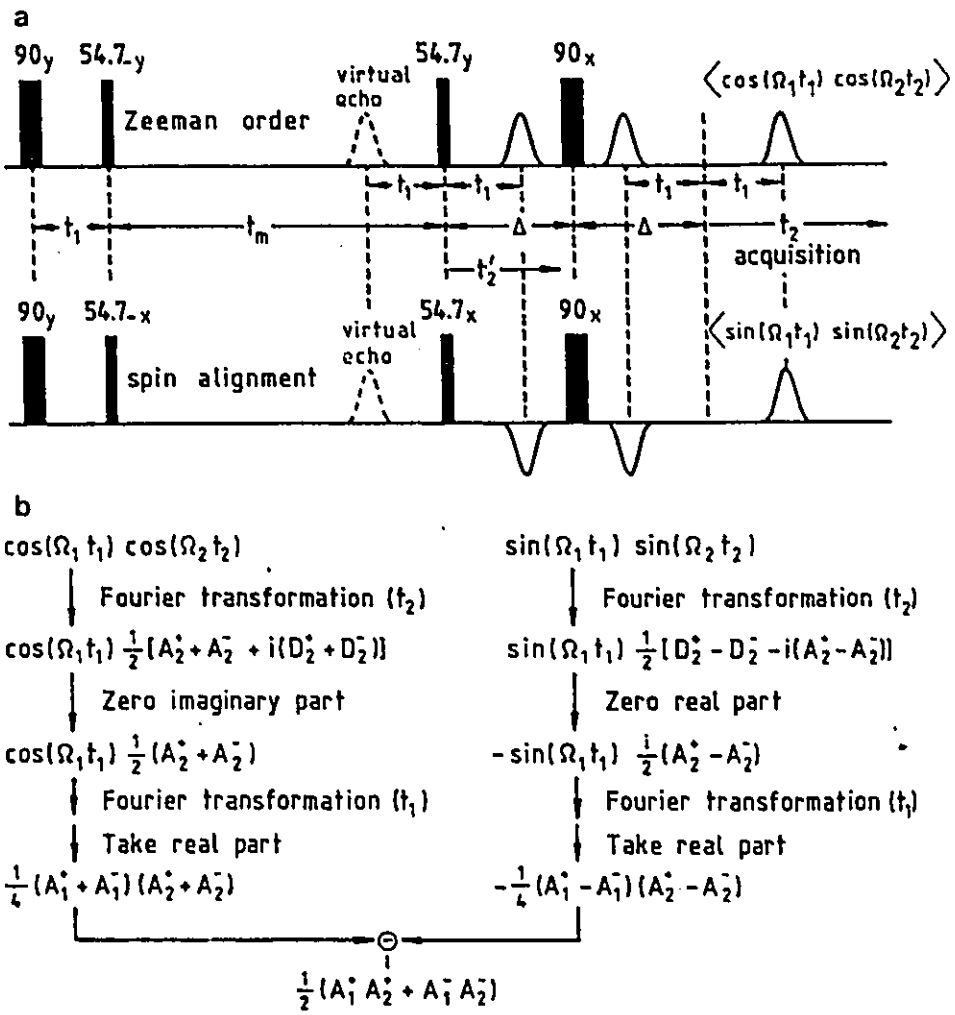

Figure 10.1 **A.** Schemes of the pulse sequences and **B.** of the two-dimensional Fourier transformation for pure absorption mode two-dimensional deuteron spectra. The pulse sequences contain also the echoes created by the last two pulses (detection sequences) in order to illustrate the refocusing character of the fourth pulse. The symbols A and D indicate absorptive and dispersive lineshapes according to $\int f^{\pm}(t_j)\exp(-ix_jt_j)dt_j = A_j^{\pm} + iD_j^{\pm}$ (from Schmidt et al., 1988).

decaying signals of solids, it is necessary to circumvent the dead time of the receiver. Therefore, the third pulse of the classical pulse sequence (Jeener et al., 1979) is substituted by a two-pulse detection sequence, similar to the quadrupolar echo sequence (Davis et al., 1976). Thus, by starting acquisition at a time Δ after the last pulse, the signal is essentially the same as after the third pulse of the corresponding three-pulse sequence.

Figure 10.1 also shows how a pure absorption mode 2D spectrum is obtained from the two data sets acquired with the two pulse sequences. Pure phase spectra are particularly important in the case of powders since overlapping phase-twisted lines may partially cancel because of their dispersive components, thus leading to severe distortions of the powder spectrum. Example of phase twist in powder spectra is given in Schmidt et al. (1988). The spin dynamics of a spin I=1 system during the four-pulse sequences of Figure 10.1 and the resulting observable signals can be calculated in detail using the density operator formalism. The complete derivation will not be given here but can be found in Schmidt et al. (1988).

A minimum phase cycling (Table 10.1) has to be used in order to suppress contributions other than the wanted signals. This phase cycling also eliminates contributions to the final signal which are independent of the evolution time t_1 and would lead to axial peaks on the ω_2 axis of the 2D spectrum. The phase cycles of Table 10.1 have to be further increased by a factor of four by changing the phases of all pulses and the receiver by 90°, 180°, and 270°, in order to suppress quadrature images.

Table 10.i

Minimum phase cycling for the two pulse sequences used to obtain pure absorption mode two-dimensional deuteron spectra

	Pulse phases	Receiver phase
Cosine Signal	y -y y x	x
	y y y x	-x
	y -y y -x	x
	y y y -x	-x
Sine Signal	y -x x x	x
	y x x x	-x
	y -x x -x	x
	y x x -x	-x

10.2.3 Determination of jump angles from 2D exchange spectra

We have first measured the deuteron 2D exchange spectra of a powder of perdeuteriated dimethyl sulfone (DMS) and compare the results with those obtained by Schmidt et al. (1988). The experiment was performed at 37°C, a temperature at which the rotation of the methyl groups is in the rapid exchange limit, resulting in spectra narrowed to about one-third of the static limit. Stacked plots of the 2D exchange spectrum of DMS are shown in Figure 10.2. The two components obtained by the two pulse sequences of Figure 10.1 are shown, together with their difference, the absorption mode spectrum. Along the diagonal, the one-dimensional deuteron powder pattern can be recognized but away from the diagonal, ridges appear in the form of two ellipses intersecting the diagonal and as straight lines parallel to the frequency axes connecting the diagonal to the ellipses. These ridge patterns arise from molecular reorientation during the mixing period t_{mix}. They are the singularities of the 2D exchange cross-powder pattern.

The origin of these exchange singularities have been explained by Schmidt et al. (1988) for axially symmetric coupling tensors by considering the reorientation of an ensemble of molecules for which, during the evolution time t_1, the unique axes of the field-gradient tensors are parallel to the z direction. In the case of dimethyl sulfone, these are the symmetry axes of the rapidly rotating methyl groups, i.e. the S-C bond axes. During the t_1 period, these molecules have all the same NMR frequency. However, for those molecules which have rotated through an angle θ during t_{mix}, the unique axes are located on a cone of angle θ around z during the detection period t_2. The resulting exchange spectrum exhibits two types of singularities. The first arises from the unique axes being perpendicular to the magnetic field after the jump and gives rise to straight ridge parallel

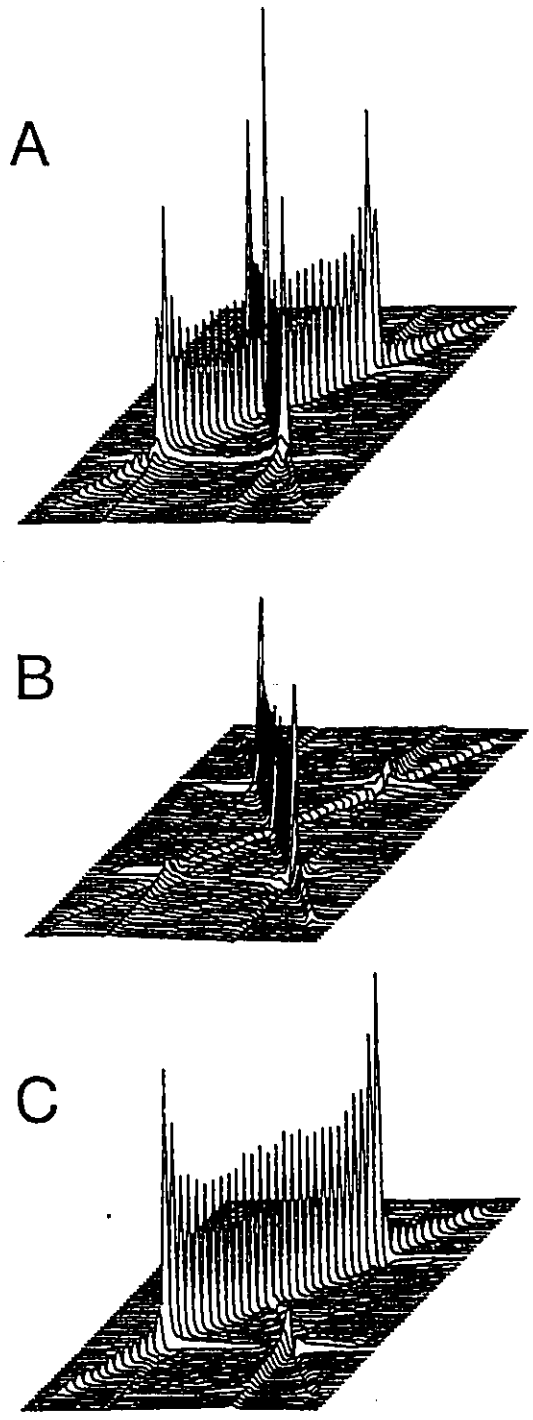

Figure 10.2 Experimental two-dimensional exchange spectra of dimethyl sulfone at 37°C obtained by means of the pulse sequences and Fourier transformations shown in Figure 10.1. A. Cosine spectrum, B. Sine spectrum and C. Absorption mode spectrum.

to the frequency axes. The second type of singularity arises from molecules which have their unique axes inclined at the angle $\beta_o \pm \theta$ with respect to the magnetic field after the jump. The angle between the reorienting molecular axes can be directly related to the geometry of the ellipse as shown in Figure 10.3A for dimethyl sulfone. In this case, the measured data correspond to a jump angle of $\theta = 106°$ (Schmidt et al., 1986). Ridge spectra for two-site deuteron reorientation by different angles are also shown in Figure 10.3B. Straight lines result for jump angles $\theta = 0°$ and 90° while circles are observed for $\theta = 45°$ (Schmidt et al., 1986). The ridge patterns are extremely sensitive to variations in the jump angle, so it can be determined with high accuracy. Different types of molecular motion will also lead to different 2D exchange spectra. For a diffusive motion, for example, only the ridges parallel to the frequency axes will be retained. This is discussed in great details in Schmidt et al. (1986) and Wefing et al. (1988).

10.3 Elucidation of slow motion in the gel phase of β-DTGL

10.3.1 Introduction

In chapter 8, it has been demonstrated that a simple model involving two motions is sufficient to describe the spectral and relaxation behavior of the glycerol-labelled glycolipid 1,2-di-*O*-tetradecyl-3-*O*-(β-D-glucopyranosyl)-*sn*-[3,3-$^2H_2$]-glycerol (β-DTGL). The lineshape and relaxation features of this lipid in the gel phase were best simulated using a three-site jump model with relative site populations of 0.46, 0.34 and 0.20, and a correlation time of 6.7×10^{-10} s. This motion was associated with an internal jump about the C2-C3 bond of the glycerol backbone. A second motion, namely rotation about the long axis of

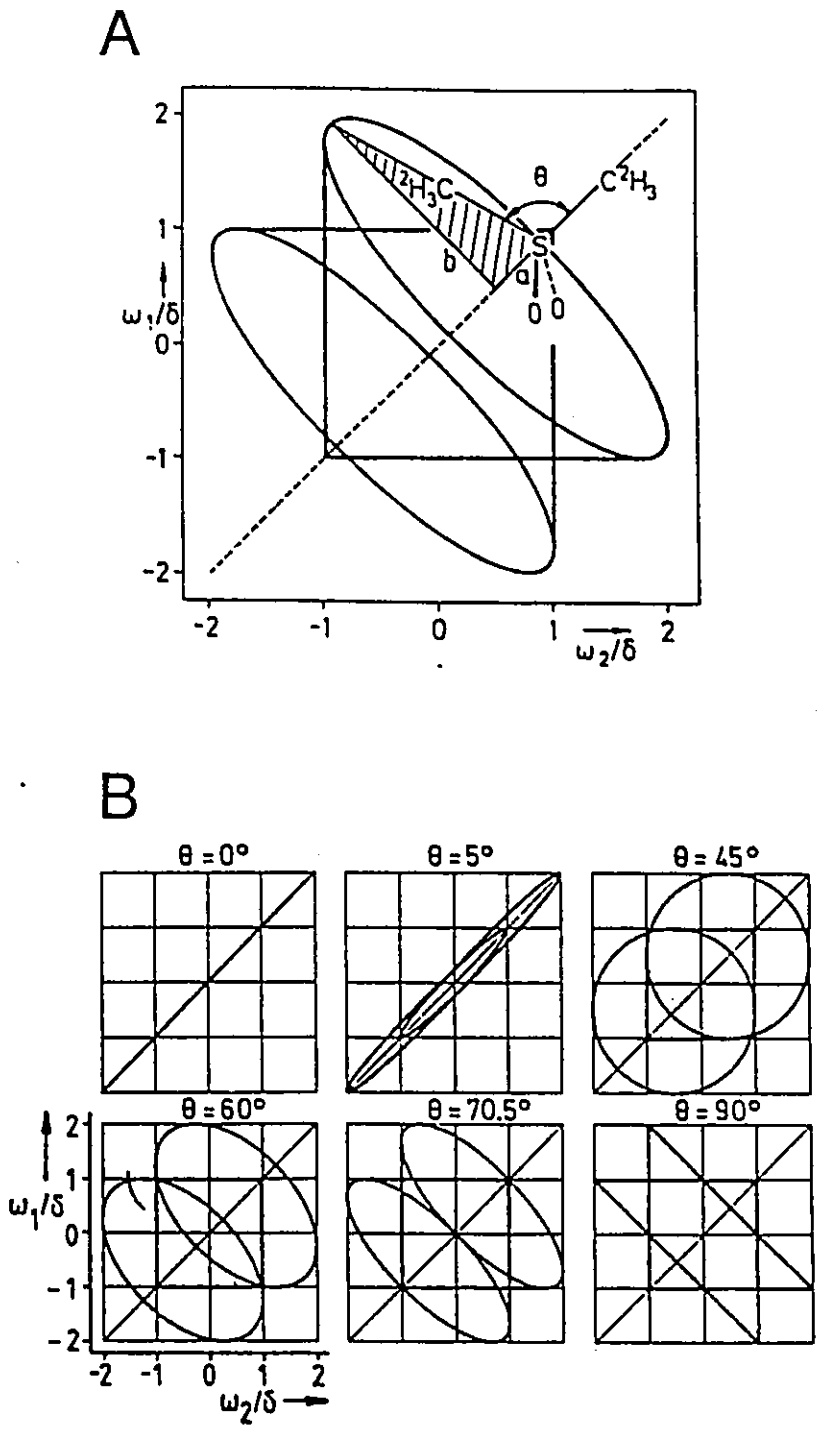

Figure 10.3 **A.** Relation between the exchange ridge pattern and the jump angle for dimethyl sulfone. **B.** Theoretical ridge spectra of powder singularities for deuterons exchanging between two sites by different jump angles (from Schmidt et al., 1986).

the molecule as a whole, was needed to account for the observed variation in the quadrupolar echo amplitude and the spectral lineshape over the temperature range of 25-60°C. Similar results have been obtained from lineshape and spin-lattice relaxation studies of other glycolipids and phospholipids (Auger et al., 1989d; chapter 9 of this thesis) and of acyl chain-labelled N-palmitoylgalactosyl sphingosine (NPGS) in the gel phase (Huang et al., 1980; Siminovitch et al., 1985). All of these studies indicated that axial diffusion is very slow on the ^2H NMR time scale ($\tau_c = 1/\Delta\upsilon_Q$) and that the gel phase spectra are the result of a simple intermediate rate exchange process between gauche and trans conformers. However, these lineshape studies could not provide detailed information about the nature of the slow axial motion.

In the present study, we have investigated in more detail the use of two-dimensional deuteron NMR to confirm the presence of a slow motion in the gel phase of the glycolipid β-DTGL and to get information on the rate and nature of this motion.

10.3.2 Experimental results

The experimental 2D exchange powder spectrum of glycerol-labelled β-DTGL at 25°C and t_{mix}=1 ms is shown in Figure 10.4A. This absorption mode spectrum is a combination of the Zeeman order and quadrupolar order spectra (Figure 10.5) obtained by the pulse sequences and data processing described in section 10.2.2. The lineshape of this diagonal spectrum is very close to that obtained for the normal 1D spectrum of β-DTGL in the gel phase (Figure 8.2) and is characteristic of fast axially asymmetric motion. However, there is no sign of cross peaks or ridge patterns in the 2D spectrum at 25°C. This

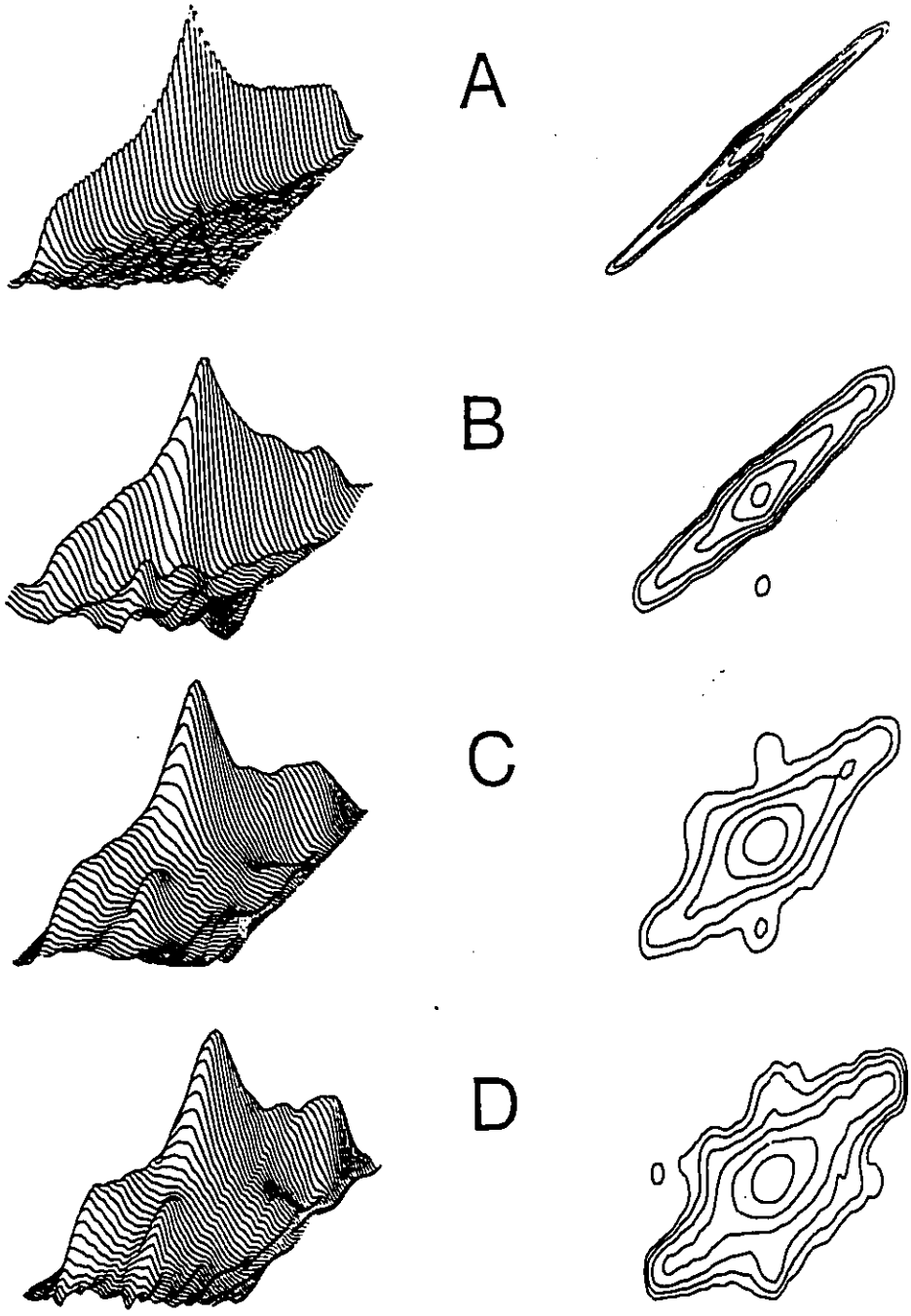

Figure 10.4 Experimental 2D absorption mode exchange spectra and corresponding contour plots of a multilamellar dispersion of [3,3-$^2H_2$] β-DTGL. **A.** 25°C, t_{mix}=1 ms, **B.** 35°C, t_{mix}=0.5 ms, **C.** 35°C, t_{mix}=2 ms and **D.** 40°C, t_{mix}=2 ms.

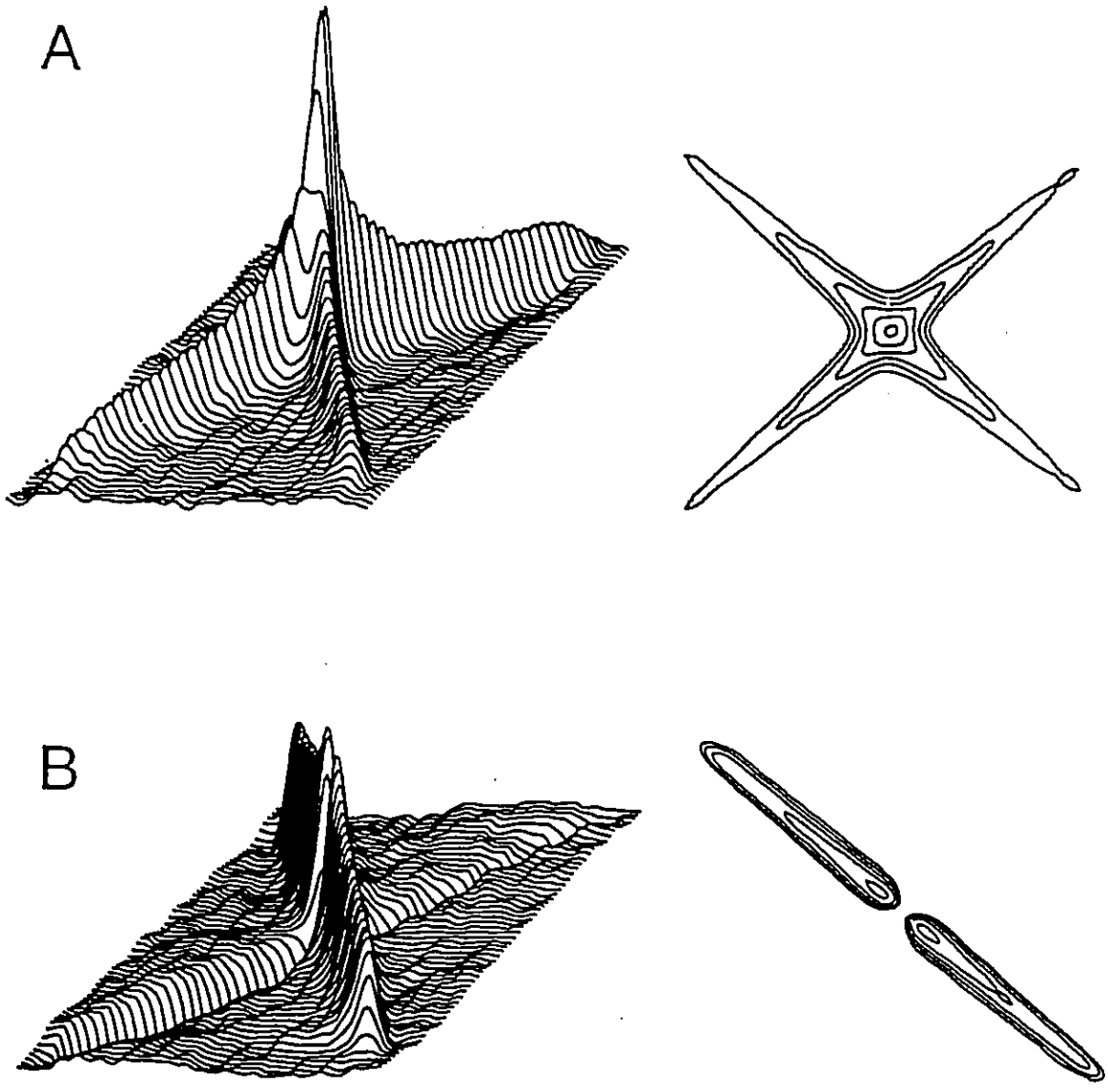

Figure 10.5 A. Cosine spectrum and B. sine spectrum resulting in the absorption mode spectrum of [3,3-$^2H_2$] β-DTGL, 25°C, t_{mix} = 1 ms presented in Figure 10.4A.

indicates that if additional motion(s) is present at this temperature, it is either too slow or too fast relative to the millisecond time scale to be detected by two-dimensional exchange techniques. This result is in agreement with the simulated spectral intensity presented in Figure 8.6, in which it appears that the axial motional rate at 25°C would be of about 10^1-10^2 rad s^{-1}, leading to correlation times of ≈ 10-100 ms.

Inspection of Figure 8.6 suggests that an increase in temperature by about 10°C could activate the axial motion to the millisecond time scale. The 2D exchange spectra of β-DTGL at 35°C are shown in Figures 10.4B and 10.4C, for two different mixing times, t_{mix}=0.5 ms and t_{mix}=2 ms, respectively. Inspection of these spectra indicates that for both mixing times, ridges patterns become distinguishable, the intensity of these patterns being much more significant for the longer mixing time (t_{mix}=2 ms). This is also illustrated on the contour plots (Figures 10.4B and 10.4C, right) in which off-diagonal patterns are clearly distinguishable for t_{mix}=2 ms. If the temperature is further increased to 40°C (Figure 10.4D), the 2D exchange spectrum for a mixing time of 2 ms is similar to that obtained at 35°C for the same mixing time, the relative intensity of the ridge patterns being, however, slightly greater. Similar results were also obtained at 35°C with t_{mix}=4 ms. It is important to note that the choice of mixing time used in these experiments is limited by the Zeeman (T_{1Z}) and quadrupolar (T_{1Q}) spin-lattice relaxation times, which are of the order of 4-6 ms for β-DTGL in the gel phase. An increase of the mixing time above 4 ms would therefore result in a large decrease in signal intensity, due to spin-lattice relaxation effects during the mixing period. The results obtained at 35°C and 40°C for t_{mix}=2 ms suggest that the correlation time for the motion giving rise to the ridge patterns in the 2D spectra is of the order of milliseconds, which is in agreement with the correlation time estimated from the spectral intensity observed for β-DTGL at 35°C (Figure 8.6). Note also that the linewidths

along the diagonal at 40°C are greater than those at 25°C, suggesting that the axial rate is increasing with a corresponding decrease of the transverse relaxation time, as expected.

In addition to providing an estimate of the correlation time, can the 2D spectra observed for β-DTGL also provide information about the nature of the slow motion? It has been demonstrated in the study of β-DTGL dynamics (chapter 8 of this thesis) that the temperature dependence of the spectral intensity observed at temperatures between 25 and 60°C could be equally well reproduced using an axial motion modelled either by a 3-site or a 12-site jump model. Moreover, previous lineshape simulations of phospholipid gel phase spectra (Blume et al., 1982) and of lipid/cholesterol "liquid-gelatin" phase spectra (Siminovitch et al., 1988) have shown that threefold (120°) rotational jumps about the director could provide an adequate model for axial molecular motion in these systems. However, motional models involving small angle jumps (diffusive motion) could not be ruled out from these studies alone.

In the gel phase 2D exchange spectra of β-DTGL at 40°C, the intensity of the diagonal is still significant. This suggests that if the system is at or near equilibrium (which is expected since the relative intensities of the ridge patterns at both 35 and 40°C for t_{mix}=2 ms are very similar), the motion giving rise to the 2D ridge patterns is not diffusive. In fact, it has been demonstrated that diffusive motions give rise to 2D exchange spectra in which all the spectral intensity is distributed in the ridge patterns and the diagonal is absent (Schmidt et al., 1986, 1987; Wefing et al., 1988). In order to elucidate further the nature of the motion giving rise to the ridge patterns observed for β-DTGL in the gel phase at 35 and 40°C, 2D spectral simulations were performed, as discussed in the following section.

10.3.3 Simulations of 2D exchange motionally averaged axially asymmetric spectra

As shown in section 10.2.4, it is possible in the case of axially symmetric powder spectra to obtain information about jump angle from the ridge patterns of the two-dimensional spectra. However, the motionally averaged powder spectrum of β-DTGL in the gel phase is axially asymmetric, as opposed to all the theoretical cases discussed by Schmidt et al. (1986) and Wefing et al. (1988). Moreover, the slow axial motion that we would like to monitor using this two-dimensional technique most likely involves a change in the azimuthal angle α describing the orientation of the C-^{2}H bond relative to the axis of motional averaging, instead of a change in the polar angle β, as in the cases discussed above. In order to determine the nature of the two-dimensional ridge patterns originating from slow "azimuthal jump" in an axially asymmetric powder spectra, spectral simulation has been used. A realistic approach to simulate the β-DTGL two-dimensional spectra involves the simulations of a n-site azimuthal jump. The spectral simulations were performed using a general two-dimensional exchange program (H.C. Jarrell, unpublished results) modified for calculating azimuthal jumps in motionally averaged axially asymmetric spectra. A copy of this program is given in appendix. 2D spectral simulations were performed using a composite motional model including both the fast rotameric three-site jump model (internal mode) needed to account for the gel phase lineshape and relaxation features (Auger et al., 1989b; chapter 8 of this thesis) and a slow axial motion (whole molecule mode), modelled by an n-site equally populated jump, with the jump axis being coincident with the rotameric jump axis. The simulated 2D spectra and contour plots of only the ridge patterns are first shown in Figure 10.6, for different n-site axial motion. It is clear from this figure that different ridge patterns are obtained for the different motional

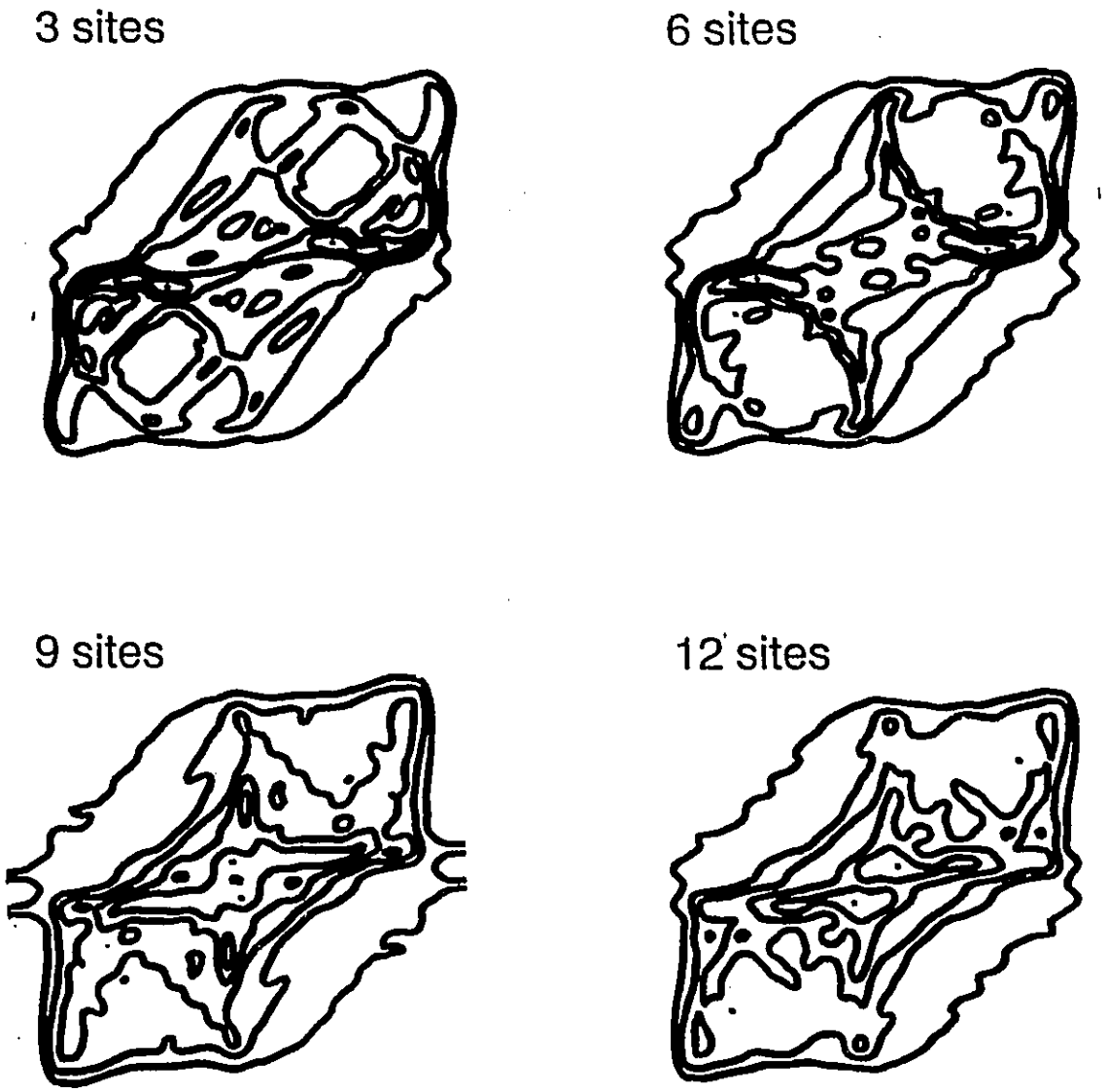

Figure 10.6 Theoretical two-dimensional ridge patterns simulated using a composite motional model including both the fast rotameric three-site jump model (internal mode) needed to account for the gel phase lineshape and relaxation features of [3,3-$^2H_2$] β-DTGL (Auger et al., 1989b; chapter 8 of this thesis) and a slow axial motion (whole molecule mode), modelled by a n-site equally populated jump, with the jump axis being coincident with the rotameric jump axis.

models. In fact, a relatively large difference is observed between a three and a six-site jump model, while the nature of the ridge patterns converge for a higher number of sites. This indicates that two-dimensional NMR techniques could provide discrimination between large and small angle jump models of the slow axial motion of β-DTGL in the gel phase. It is interesting to note in Figure 10.6 that part of the ridge pattern intensity is very close to the diagonal. This suggests that the additional features observed along the diagonal of the experimental β-DTGL spectrum at 40°C are significant and can provide additional means of distinguishing between different motional models.

10.3.4 Comparison between experimental and simulated spectra

The 2D spectral simulations presented so far illustrate the characteristic ridge patterns only, without taking into account the diagonal spectra. Moreover, these spectra were processed using a minimum Gaussian broadening in order to illustrate the cross peak patterns more clearly. However, the experimental two-dimensional spectra obtained for β-DTGL in the gel phase are very broad, due to short transverse relaxation times T_{2e}. The simulated spectra presented in Figure 10.6 were therefore reprocessed using a Gaussian broadening of 9 kHz in both dimensions in order to reproduce the experimental linewidths. Moreover, the spectra were plotted using the proper proportions of diagonal and ridge pattern, as calculated from the site populations. Increasing the number of sites used in modelling the axial motion therefore results in an increase in the intensity of the ridge patterns relative to the diagonal and in a change in the shape of the ridge patterns (Figure 10.7). Comparison of these simulated spectra with the experimental β-DTGL gel phase spectrum at 40°C (Figure 10.4D) indicates that both the relative intensity and the shape of

Figure 10.7 2D spectral simulations performed using a composite motional model including both the fast rotameric three-site jump model (internal mode) needed to account for the gel phase lineshape and relaxation features of [3,3-$^2H_2$] β-DTGL (Auger et al., 1989b; chapter 8 of this thesis) and a slow axial motion (whole molecule mode), modelled by **A.** a three-site or **B.** a twelve-site equally populated jump, with the jump axis being coincident with the rotameric jump axis. A 9 kHz Gaussian multiplication was applied in both dimensions in order to reproduce the linewidths of the experimental 2D spectra. The proportions of diagonal and ridge pattern used in the simulations are calculated from the site populations.

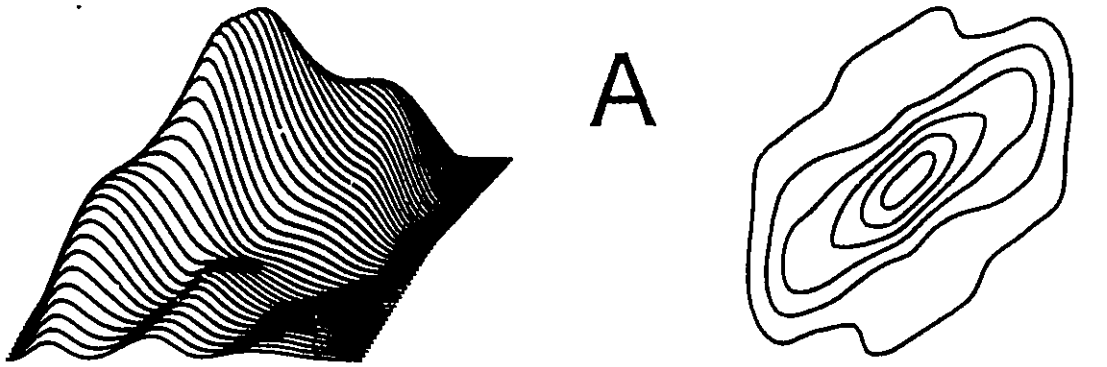
A

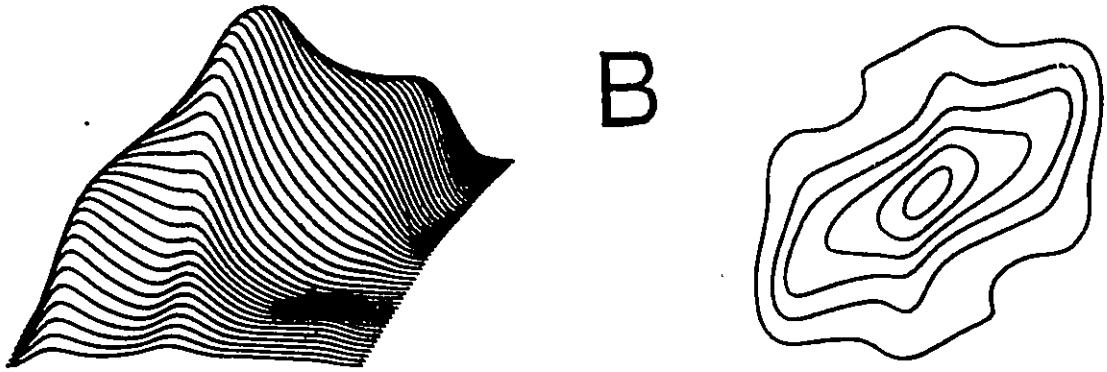
B

the ridge pattern of the experimental 2D exchange spectra are better reproduced by the motional model involving a large angle (three-site) axial motion rather than a small angle motion (< 60°C). This conclusion is in agreement with a recent study of cholesterol dynamics in which it has been shown that the anisotropic spin-lattice relaxation (T_{1Z} and T_{1Q}) behavior of ^2H nuclei on cholesterol in a phospholipid matrix were best simulated using a large angle (three-site) jump model in comparison to small step Brownian diffusion (Bonmatin et al., 1989). It is interesting to note that other studies have also suggested that large angle jumps may be favoured in highly ordered systems (Vold & Vold, 1988; Dammers et al., 1988).

10.4 Elucidation of slow motion in the liquid-crystalline phase of lipid bilayers

10.4.1 Glycolipid bilayers

Since even simple model membranes may be expected to exhibit more than one slow motion, it is important to establish to what extent, if any, such motions can be manifest in the experimental spectra (Figure 10.4). Slow molecular diffusion along the curved liposomal surfaces has been suggested to occur in the liquid-crystalline phase of phospholipid systems (Brown & Davis, 1981; Bloom & Sternin, 1987), preventing the observation of anisotropic spin-lattice relaxation. However, for multilamellar dispersions of glycolipids in the liquid-crystalline phase, anisotropic spin-lattice relaxation has been observed, (Auger et al., 1989b; Renou et al., 1989; Speyer et al., 1989), suggesting slower lateral diffusion or smaller curvature of the multilamellar dispersions. In order to rule out any contribution of slow lateral diffusion to the ridge patterns observed for β-DTGL in the

gel phase, we have measured the 2D exchange spectra of this lipid in the lamellar (55°C) and hexagonal (60°C) liquid-crystalline phases (Figure 10.8). The hexagonal phase is expected to exhibit no effects due to diffusion over curved surfaces and therefore, serves as a control in the present study. In both cases, no ridge patterns are observed for t_{mix}=2 ms, which confirms that diffusion of the lipid molecules along the curved membrane surfaces does not occur on the millisecond time scale for lipid in the liquid-crystalline phase. Since lateral diffusion is slower in the gel phase, it is established that this motion does not contribute to the 2D exchange spectra in the gel phase. However, as mentioned previously, the investigation of slow motions in both the gel and liquid-crystalline phases of the glycolipid β-DTGL is limited by the Zeeman (T_{1Z}) and quadrupolar (T_{1Q}) spin-lattice relaxation times, which are of the order of 4-6 ms in both phases. An increase of the mixing time above 4 ms would therefore result in a large decrease in signal intensity, due to spin-lattice relaxation effects during the mixing period, and therefore, motions with correlation times longer than ≈ 5 ms could not be probed in this glycolipid system. These results establish that the axial motion occurs on a substantially different time scale than that defined by lateral diffusion.

10.4.2 Phospholipid bilayers

As mentioned previously, Brown & Davis (1981) have shown that in the liquid-crystalline phase of DPPC, lateral diffusion is sufficiently rapid that each lipid molecule samples all orientations during times of the order of T_1, thus apparently preventing the observation of the orientation dependence of spin-lattice relaxation. They have estimated from selective inversion recovery experiments that the phospholipid molecules will diffuse

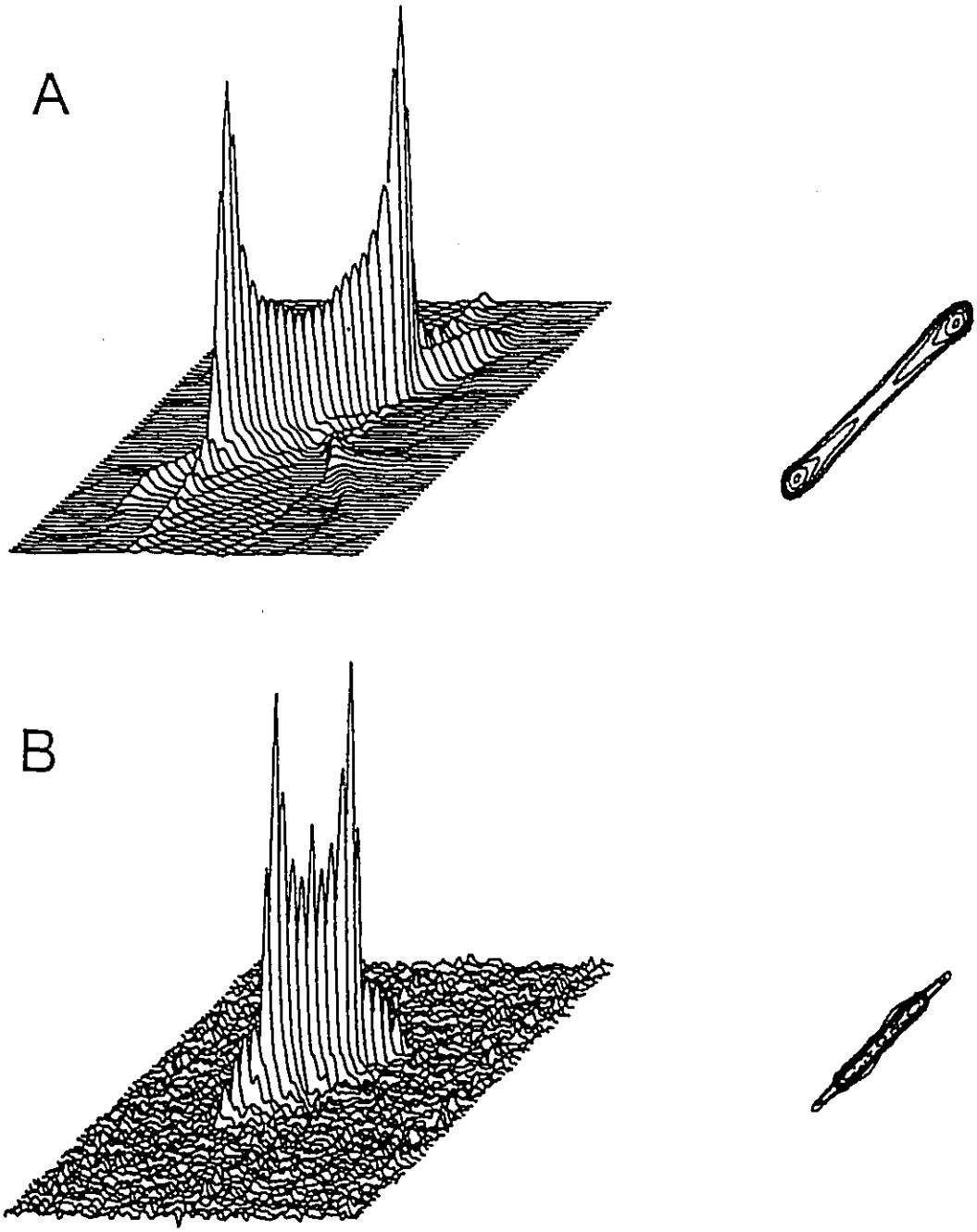

Figure 10.8 Experimental 2D absorption mode exchange spectra and corresponding contour plots of a multilamellar dispersion of [3,3-$^2H_2$] β-DTGL, t_{mix}=2ms at **A.** 55°C, and **B.** 60°C.

through an angular displacement > 1 rad in 5 ms. A similar study involving the selective excitation of ^{31}P NMR lineshapes has suggested a correlation time of 17 ms for lateral diffusion of phospholipids over curved surface (Larsen et al., 1987). On the other hand, using a quadrupolar CPMG pulse train, Bloom & Sternin (1987) have shown that the most plausible mechanism for slow transverse relaxation (T_2) in phospholipid bilayers is lateral diffusion of the phospholipid molecules along curved membrane surfaces and have estimated a correlation time of ≈ 100 ms for that motion. Angular-dependent T_{2e} values have been observed with lipids from the membranes of *A. laidlawii* (Rance, 1981) and Perly et al. (1985) have also observed angular-dependent transverse relaxation in phosphatidylethanolamine bilayers, which they have attributed to lateral diffusion. While such studies have established the presence of a slow motion in the liquid-crystalline phase of lipid bilayers, the correlation times agree less well. It is therefore of interest to investigate if such a motion can be detected and characterized by two-dimensional solid-state deuteron NMR. To do so, we have measured the 2D exchange spectra of a multilamellar dispersion of perdeuteriated DPPC ([$^2H_{62}$] DPPC) in the liquid-crystalline phase at 50°C, as a function of the mixing time t_{mix}. The long spin-lattice relaxation times obtained for the acyl chain-labelled phospholipids (from ≈ 30 ms to 250 ms for the plateau and the tail regions, respectively) allow the use of longer mixing times and therefore permit the investigation of slow motions occurring on longer time scales, compared to the glycerol-labelled glycolipid discussed above.

The 2D exchange spectra and the corresponding contour plots of perdeuteriated DPPC are shown in Figure 10.9 for mixing time t_{mix} of 10, 30 and 100 ms. It is first interesting to note that at a t_{mix} of 10 ms, ridge patterns are almost not distinguishable. This indicates that motions occurring in the liquid-crystalline phase of DPPC bilayers are

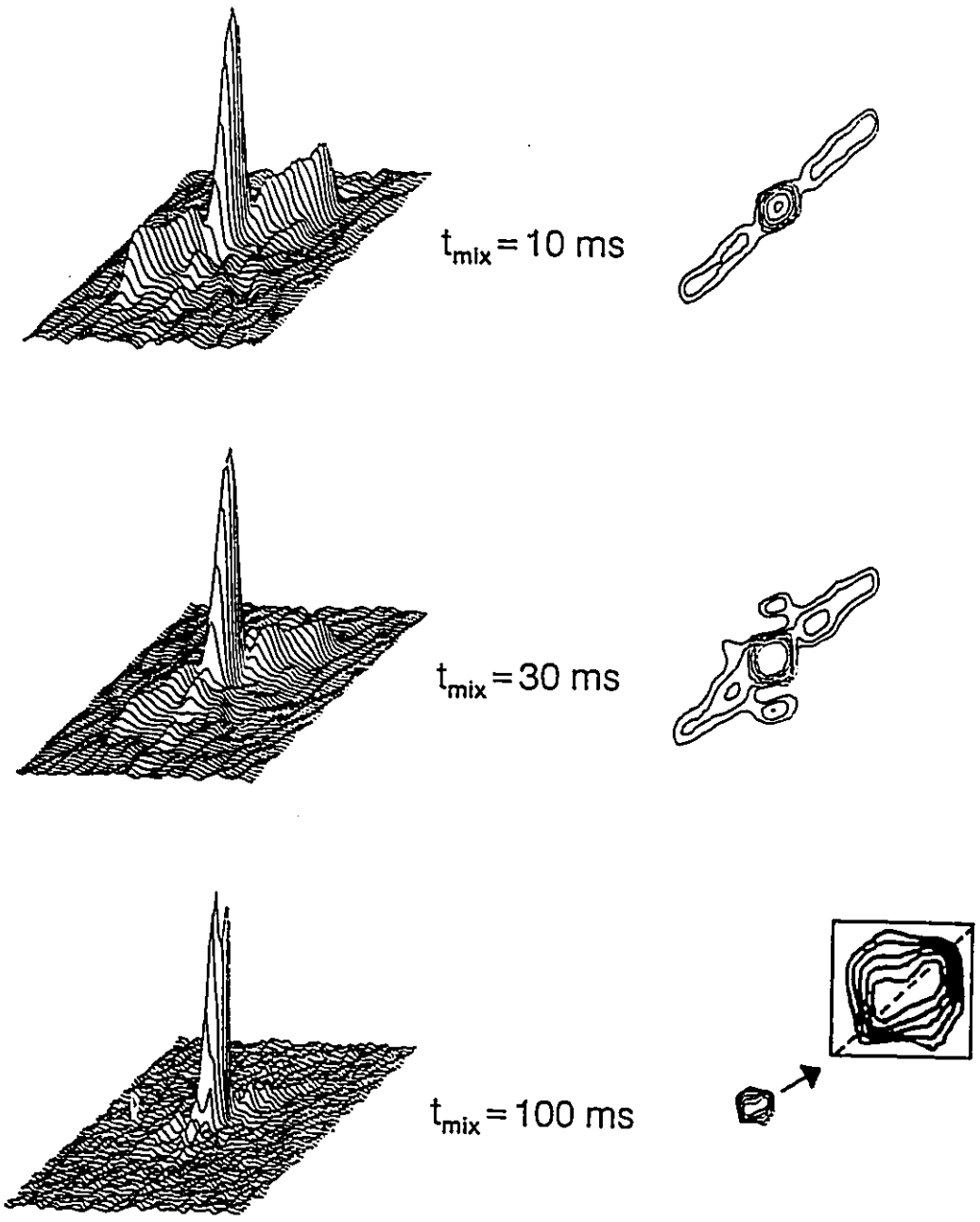

Figure 10.9 2D absorption mode exchange spectra and corresponding contour plots of a multilamellar dispersion of perdeuteriated DPPC at 51°C for different mixing times.

either too fast or too slow to be detected on a time scale of ≈ 10 ms. However, as the mixing time is increased to 30 ms, ridge patterns become distinguishable, while the diagonal element of the 2D spectrum is still significant. For a mixing time of 100 ms, a dramatic loss in signal intensity occurs, due to spin-lattice relaxation, the remaining spectrum being due mostly to the terminal methyl groups of the acyl chains. However, the 2D spectrum of the methyl groups and the corresponding contour plot obtained at t_{mix}=100 ms indicate that little intensity remains along the diagonal, which suggests that the slow motion giving the 2D ridge patterns is most likely of diffusive nature. Since these experiments are again limited by the relatively short ^2H spin-lattice relaxation times, investigation of the solid-state two-dimensional spectra of other nuclei, such as ^{31}P or ^{13}C, for which much longer spin-lattice relaxation times are obtained would extend the time scale (≈ 5 s) over which slow molecular motions could be probed. Such studies are now underway in our laboratory to probe motions on time scales of a second or longer (D.B. Fenske & H.C.Jarrell, unpublished results). Nevertheless, the results presented in Figure 10.9 clearly indicate that a slow motion on a time scale of 100 ms is present in the liquid-crystalline phase of DPPC bilayers and that this motion is most likely diffusion over the curved surface of the multibilayers. It is important to note that lateral diffusion with a comparable correlation time may also be present in the liquid-crystalline phase of the β-DTGL bilayers but can not be probed because of the short T_{1Z} values associated with the ^2H labelled sites of this particular lipid.

10.5 Conclusions

The present study demonstrates that two-dimensional solid-state NMR techniques

can detect the presence and give information about the rate and nature of slow motions in lipid bilayer systems by providing a new observation window in a frequency range ($< 1 \times 10^3\ s^{-1}$) not accessible from lineshape and spin-lattice relaxation study. Two cases have been discussed, the slow whole molecule axial motion in the gel phase of glycolipid bilayers, and lateral diffusion over the curved surface of phospholipid multibilayers in the liquid-crystalline phase. The ability to monitor both the rate and nature of slow molecular motion suggest that two-dimensional NMR techniques could be very useful in probing changes in the properties of membrane surfaces upon binding of exogenous molecules, such as lectin or antibody-carbohydrate binding in the case of glycolipid bilayers.

PART FIVE: GENERAL CONCLUSION

CHAPTER 11

Conclusions and suggestions for future work

11.1 Introduction

Two main problems have been investigated in this thesis. The interactions of the local anesthetic tetracaine with lipid bilayers have first been studied by deuterium NMR spectroscopy and it has been shown that complementary results can be obtained by high-pressure Fourier transform infrared spectroscopy. On the other hand, molecular dynamics have been studied in different lipid systems over a broad range of motional frequencies using deuterium NMR spectroscopy. The main results of each project will now be presented, as well as some suggestions for future work.

11.2 Anesthetic-lipid interactions

The interactions of the local anesthetic tetracaine with pure phospholipid bilayers have been well studied by deuterium NMR spectroscopy (Boulanger et al., 1980, 1981; Kelusky & Smith, 1983, 1984, 1985; Kelusky et al., 1986). In this thesis, these studies have first been extended to the interactions of tetracaine with phosphatidylcholine bilayers containing a physiological concentration of cholesterol, a situation which resembles more closely that encountered in nerve membranes. It has been demonstrated that the location

of the local anesthetic tetracaine is different in cholesterol-containing phosphatidylcholine bilayers, compared to that in the pure lipid system. This conclusion as deduced from deuterium NMR results has been confirmed using high-pressure Fourier transform infrared spectroscopy by monitoring the pressure dependence of the anesthetic carbonyl stretching band in different systems.

Axially asymmetric lineshapes have been observed for deuteriated tetracaine incorporated into cholesterol-containing bilayers, lineshapes similar to those observed in biological membranes. In such cases, it has been shown that lineshape and spin-lattice relaxation analysis can provide information not accessible from an order parameter analysis alone. Preliminary results and simulations have been presented and suggested that a motional model involving both a whole molecule axial rotation and a two-site ring flip could best account for the lineshape and relaxation features of the deuteriated anesthetic ($[^2H_2]$TTC) incorporated into cholesterol-containing phosphatidylcholine bilayers. It would now be interesting to pursue this analysis to the study of deuteriated tetracaine incorporated in nerve membranes, and to monitor the effects of the application of a potential across the nerve membranes on the location and dynamics of the anesthetic. These studies would however be limited by the low sensitivity of deuterium NMR techniques, which require large sample size. An alternative method to get information about the location of local anesthetics in lipid bilayers is neutron diffraction. It would therefore be worthwhile to probe the use of this technique to measure distances between different deuteriated sites in oriented multibilayers.

The interaction of the local anesthetic tetracaine with pure glycolipid bilayers has been shown to lead to the formation of non-lamellar phases but in the mixed

glycolipid:phospholipid system, tetracaine had little or no effect on the lipid aggregate structure or ordering. The formation of non-lamellar phases is itself interesting in that it can give information about some physical properties of the lipids, such as packing, and how the local anesthetic influences these properties, as demonstrated in this thesis.

It has been shown it chapters 6 and 7 that high-pressure FT-IR spectroscopy can give useful information about the location of the anesthetic in different lipid systems and about the effects of the anesthetic on the structural and dynamic properties of the lipid acyl chains, information complementary to that obtained by ^{2}H NMR. Throughout the study of the location of tetracaine in membranes by high-pressure FT-IR, an interesting phenomenon has been observed, namely the pressure-induced expulsion of the local anesthetic from both model membranes and nerve tissues. It was the first time that this new technique was applied to the study of the interactions of local anesthetics with membranes. Moreover, the unity of the pressure-induced phenomenon observed in both model and biological membranes indicates that further experiments using this novel high-pressure vibrational spectroscopic technique on nerve tissues may lead to a better understanding of barotropic phenomena in these systems, and of the mechanism of anesthesia. Extension of this study to systems enriched in channels, such as the acetylcholine receptor membrane, could provide a way to distinguish between lipids and proteins as the primary site for anesthetic action. Preliminary experiments have been attempted in our laboratory but problems with high relative concentrations of water to membrane resulted in very little anesthetic being incorporated into the membrane, and therefore the bound anesthetic infrared spectra were very difficult to monitor.

11.3 Molecular dynamics in lipid bilayers

The surface orientation of carbohydrate head groups in different glycolipid systems has been extensively studied by deuterium NMR spectroscopy (Jarrell et al., 1986, 1987a-b; Carrier et al., 1989; Renou et al., 1989). Although these studies have yielded very valuable information about the effects of carbohydrate structure on surface orientation, little was learned about the details of molecular dynamics in glycolipid bilayers.

The dynamics of the glycerol-labelled glycolipid β-DTGL have been studied in great detail in this thesis. It has been demonstrated that several time windows can be investigated through the analysis of ^2H NMR spin-lattice relaxation times (10^7-10^{10} s^{-1}), lineshape and quadrupolar echo amplitude (10^4-10^6 s^{-1}), and 2D exchange spectra ($< 10^3$ s^{-1}). This study has revealed a great deal of information about lipid dynamics, information that is not accessible from an order parameter analysis. It has been demonstrated that the dynamics of the glycerol-labelled glycolipid β-DTGL can be described in terms of fast internal motions and a slower whole molecule axial motion. It is interesting to note that the order parameter analysis on this lipid was consistent with the glycerol backbone being rigid on the ^2H NMR lineshape time scale (Jarrell et al., 1986; 1987a). This illustrates the need to probe molecular dynamics in lipid systems over a broad motional frequency range. The results presented in chapter 8 also demonstrate the considerable utility of oriented samples in relaxation and lineshape measurements, facilitating the discrimination between different motional models that could not be differentiated solely on the basis of powder lineshapes. A natural extension of this study of β-DTGL dynamics is now to test the model proposed with the data obtained for other labelled positions on the carbohydrate head group, both in the gel and the liquid-crystalline phases. Such studies are now underway in

our laboratory and should also confirm the surface orientation of the carbohydrate head group, as deduced from the order parameter analysis.

It has been shown in chapter 9 that molecular dynamics in several glycerol-labelled lipid systems is also best described by fast internal motions and a slower whole molecule axial motion. This is again in apparent contradiction with studies suggesting a rigid glycerol backbone (Strenk et al., 1985; Braach-Makvytis & Cornell, 1988), but confirms recent investigations of molecular dynamics in lipid bilayers (Hauser et al., 1988; Meier et al., 1986), which have suggested the presence of fast internal motions. It would now be of interest to investigate ^{31}P spin-lattice relaxation in phospholipid bilayers (Milburn & Jeffrey, 1987, 1989), as well as the ^{13}C spectra of the *sn*-2 carbonyl group in different phospholipids (Blume & Griffin, 1982; Blume et al., 1982a-b), in terms of the motional model discussed in the present study. On the other hand, the effects of different exogenous molecules, such as antibiotics and anesthetics, on lipid structure and dynamics have been widely studied by deuterium NMR, mainly by monitoring the variation of the lipid order parameters in the absence and presence of exogenous agents. It would therefore be of interest to investigate how these interactions would affect the dynamic properties of lipids, through lineshape and spin-lattice relaxation analysis.

The first examples of the use of two-dimensional solid-state deuteron NMR for the study of molecular dynamics in lipid bilayers were presented in this thesis. This technique has been shown to be successful in confirming the presence of a slow whole molecule axial motion in the gel phase of the glycolipid β-DTGL. Moreover, comparison between experimental and simulated 2D exchange spectra suggested that this motion is best described by a large angle jump rather than by small step Brownian diffusion, information

that could not be obtained from lineshape analysis alone. Moreover, the 2D exchange technique has been shown to be successful in detecting a slow motion in the liquid-crystalline phase of phosphatidylcholine bilayers, which is most likely associated with the diffusion of lipid over the curved membrane surface. In that case, the experiments were however limited by the short deuterium spin-lattice relaxation times, which restricted the time scale of the motion investigated to rates greater than 10^{-1} s^{-1}. In such cases, the use of nuclei such as ^{31}P, which manifest much longer spin-lattice relaxation times, could provide information on longer time scales, as demonstrated recently in our laboratory (D.B. Fenske & H.C. Jarrell, unpublished results). The demonstration of the validity of the 2D exchange technique for the study of lipid systems now opens new avenues in the study of dynamics in biological systems. For example, this technique may have considerable importance in probing lipid-protein interactions. In such systems, slow motions have been shown to be more sensitive to such perturbations (Meier et al., 1987). This technique may also be useful in the study of surface distortions, such as rippling, which has been suggested to occur before the transition from lamellar to non-lamellar liquid-crystalline phases.

APPENDIX:

Program for 2D exchange spectral simulations: Axial jump

```
C     This program calculates a two dimensional experiment
C     for a deuteron executing a fast three site jump and
C     a slower axial motion.  This slower axial motion is
C     defined by an nsite jump model.
C
C     A normal fid in both dimensions (block decays)
C     is acquired. Data is stored as cosine and sign functions.
C
C     Data to be processed according to Schmidt et al. (1988)
C       J. Mag. Reson. 79, 269-290.
C
C
      double precision dt,sums,decay,big,small
      double precision gr1(256),gr2(256),gr3(256),gr4(256)
      double precision decayt,re(100,100,64),im(100,100,64)
      double precision ddcay,stc,etc,ttc,dtc,btc,atc,ttc
      real fr1(3),fr2(3),gama1(3),cggam1(3),c2ggam1(3)
      real gamat(3), cggamt(3),c2ggamt(3)
      real peq(3)
      real beta,gama,gam2,beta1
      real fdata(512),pbeta(100),freq1(100,100),freq2(100,100,60)
      real rdata(512),idata(512)
C
      character filename*30,filea*30
      character FILE*6,file1*12,file2*12
      character*5 ex1,ex2
      character*1 z1,z2
      filea='proton.001'
      ex1='.fid1'
      ex2='.fid2'
      z1='z'
      z2='q'
C
C
C     read file name
      write(6,1)
    1 format(' input filename a10')
      read(5,2)filename
    2 format(a30)
      open(unit=1,type='old',name=filename)
      write(6,3)
    3 format(' spin-1/2  2d calculation of exchange experiment      ')
    4 format(i1)
      read(1,4)nor
      read(1,4)idiag
      read(1,4)icross
      read(1,6)dvq1
    6 format(f6.2)
      read(1,13)nsite
      read(1,7)rak
    7 format(f7.2)
      read(1,7)sw
      read(1,8)np,na,ng
    8 format(3i4)
      if(na.gt.1)go to 11
      read(1,6)betaa
   11 read(1,6)beta1
      read(1,19)gama1(1),gama1(2),gama1(3)
   19 format(3f6.2)
      read(1,20)peq(1),peq(2),peq(3)
```

```
   20 format(3f5.3)
      read(1,12)file
   12 format(a6)
      read(1,13)nfiles
   13 format(i3)
      read(1,7)pk
C
C
C
      close(1)
      pi=3.1415926
      dwl=pk*1.0e-6
      dwql=(3./2.)*pi*dvql*1000.
      dt=1/(sw*1000.)
      rt2k=1./pi*rak
      ddcay=exp(-dt*rt2k)
      dbeta=pi/(2.*float(na))
      dgama=pi/float(ng)
      dgammn2=2.*pi/float(nsite)
      betal=pi*betal/180.
C
C
      cbetal=cos(betal)
      sbetal=sin(betal)
      c2betl=cos(2.*betal)
      s2betl=sin(2.*betal)
C
C
      do 98 w=1,3
      gamal(w)=pi*gamal(w)/180.
   98 continue

C
C
C
      if(icross.eq.1)then
      nsite=nsite-1
      else
      nsite=nsite
      endif
      ng=ng+1
      if(na.gt.1)then
      na=na+1
      else
      na=1
      endif
      do 32 n=1,na
      if(na.eq.1)then
      beta=betaa*pi/180.
      else
      beta=dbeta*float(n-1)
      endif
      cbeta=cos(beta)
      sbeta=sin(beta)
      c2beta=cos(2.*beta)
      s2beta=sin(2.*beta)
      pbeta(n)=sin(beta)
      do 33 l=1,ng
      gama=dgama*float(l-1)
C
```

```
      fr1(w)=0.
      do 241 w=1,3
      cggam1(w)=cos(gama1(w)+gama)
      c2ggam1(w)=cos(2.*(gama1(w)+gama))
      fr1(w)=(1.5*cbeta**2.-0.5)*(1.5*cbeta1**2.-0.5)
      fr1(w)=fr1(w)-0.75*s2beta*s2bet1*cggam1(w)
      fr1(w)=fr1(w)+0.75*sbeta1**2.*sbeta**2.*c2ggam1(w)
C
      fr1(w)=peq(w)*fr1(w)
      freq1(n,1)=freq1(n,1)+fr1(w)
  241 continue
C
C
      freq1(n,1)=dwq1*freq1(n,1)

C
      do 34 k=1,nsite
      if(icross.eq.1)then
      gam2=dgamma2*float(k)+gama
      else
      gam2=dgamma2*float(k-1)+gama
      endif
C
      fr2(w)=0.
C
      do 242 w=1,3
      gamat(w)=gam2+gama1(w)
      cggamt(w)=cos(gamat(w))
      c2ggamt(w)=cos(2.*(gamat(w)))
      fr2(w)=(1.5*cbeta**2.-0.5)*(1.5*cbeta1**2.-0.5)
      fr2(w)=fr2(w)-0.75*s2beta*s2bet1*cggamt(w)
      fr2(w)=fr2(w)+0.75*sbeta1**2.*sbeta**2.*c2ggamt(w)
C
      fr2(w)=peq(w)*fr2(w)
      freq2(n,1,k)=freq2(n,1,k)+fr2(w)
  242 continue
      freq2(n,1,k)=dwq1*(freq2(n,1,k))
C

C
   34 continue
   33 continue
   32 continue
C
C
C
      do 350 i=1,np
      rdata(i)=0.
      idata(i)=0.
  350 continue
      open(unit=9,access='direct',status='old',recl=512,file=filea)
      read(9,rec=1)(fdata(j),j=1,512)
      close(9)
      fdata(100)=float(np)
      fdata(120)=30.7
      fdata(101)=1.0/dt
      fdata(107)=0.00000000e+00
      fdata(108)=0.00000000e+00
      fdata(99)=dt
```

```
      fdata(220)=float(nfiles)
      fdata(230)=1./dw1
      fdata(221)=0.00000000e+00
      fdata(223)=0.00000000e+00
      fdata(153)=1.000000
      fdata(235)=1.000000
      fdata(222)=0.00000000e+00
      fdata(130)=0.00000000e+00
C
C
      file1=file//z1//ex1
      file2=file//z2//ex2
      lk=128
      krec=0
      nrec=np/lk
      j1=1-lk
      j2=0
C     allow evoution during t1.
      tau=0.
      tau=tau-dw1
      do 66 j=1,nfiles
      tau=tau+dw1
      decay=rt2k*tau
      decayt=exp(-decay)
      do 67 l=1,na
      do 68 k=1,ng
      re(l,k,j)=decayt*pbeta(l)*cos(freq1(l,k)*tau)
      im(l,k,j)=decayt*pbeta(l)*sin(freq1(l,k)*tau)
   68 continue
   67 continue
   66 continue
C     allow exchange w1 - w2(beta)
C     beta starts at 0 and goes to 90
C     calculate Fid(t2) for each t1 period
C     real and imaginary for t1 domain.
      do 760 jj=1,nfiles
      sums=0.
      do 30 i=1,np
      gr1(i)=0.
      gr2(i)=0.
      gr3(i)=0.
      gr4(i)=0.
   30 continue
      do 761 l=1,na
      do 759 m=1,ng
      if(idiag.eq.1)then
      k=l
      kk=m
      decay=1./ddcay
      dtc=freq1(k,kk)*dt
      atc=cos(dtc)
      btc=sin(dtc)
      tc=-dtc
      ctc=cos(tc)
      stc=sin(tc)
      do 764 n=1,np
      decay=decay*ddcay
      ttc=ctc
      ctc=atc*ctc-btc*stc
      stc=atc*stc+btc*ttc
```

```
      gr1(n)=gr1(n)+re(1,m,jj)*ctc*decay
      gr2(n)=0.
      gr4(n)=0.
      gr3(n)=gr3(n)+im(1,m,jj)*stc*decay
  764 continue
      go to 767
      else
      do 773 k3=1,nsite
      decay=1./ddcay
      dtc=freq2(1,m,k3)*dt
      atc=cos(dtc)
      btc=sin(dtc)
      tc=-dtc
      ctc=cos(tc)
      stc=sin(tc)
      do 763 n=1,np
      decay=decay*ddcay
      ttc=ctc
      ctc=atc*ctc-btc*stc
      stc=atc*stc+btc*ttc
      gr1(n)=gr1(n)+re(1,m,jj)*ctc*decay
      gr2(n)=0.
      gr4(n)=0.
      gr3(n)=gr3(n)+im(1,m,jj)*stc*decay
  763 continue
  773 continue
      endif
  767 sums=gr1(1)
  759 continue
  761 continue
      write(6,1070)sums
C
C     normalize spectra so that -50000<data<+50000, and
C     store it as output files.
C
      if(nor.eq.1)then
      big1=1000.
      else
      big=gr1(1)
      small=gr1(1)
      do 50 i=1,np
      if(gr1(i).gt.big)big=gr1(i)
      if(gr1(i).lt.small)small=gr1(i)
   50 continue
      bigs=big
      smalls=small
      if(abs(smalls).gt.abs(bigs))big=small
      write(6,1070)sums
 1070 format('  sums= ',f8.3)
      bigs=big
      big=50000./abs(bigs)
      if(jj.ne.1)goto 1013
      big1=big
      endif
 1013 do 60 i=1,np
      rdata(i)=big1*gr1(i)
      idata(i)=0.
   60 continue
      if(jj.ne.1)goto 333
      open(unit=10,access='direct',status='new',recl=1k,name=file1)
```

```
      open(unit=11,access='direct',status='new',recl=1k,name=file2)
      j1=1-1k
      j2=0
      do 310 i=1,4
      j1=j1+1k
      j2=j2+1k
      krec=krec+1
      kreca=krec
      write(10,rec=krec)(fdata(j),j=j1,j2)
      write(11,rec=krec)(fdata(j),j=j1,j2)
  310 continue
  333 j1=1-1k
      j2=0
      do 334 i=1,nrec
      j1=j1+1k
      krec=krec+1
      j2=j2+1k
      write(10,rec=krec)(rdata(j),j=j1,j2)
  334 continue
      j1=1-1k
      j2=0
      do 335 i=1,nrec
      j1=j1+1k
      krec=krec+1
      j2=j2+1k
      write(10,rec=krec)(idata(j),j=j1,j2)
  335 continue
      do 960 i=1,np
      rdata(i)=big1*gr3(i)
      idata(i)=0.
  960 continue
      krec=kreca
      j1=1-1k
      j2=0
      do 961 i=1,nrec
      j1=j1+1k
      krec=krec+1
      j2=j2+1k
      write(11,rec=krec)(rdata(j),j=j1,j2)
  961 continue
      j1=1-1k
      j2=0
      do 962 i=1,nrec
      j1=j1+1k
      krec=krec+1
      j2=j2+1k
      write(11,rec=krec)(idata(j),j=j1,j2)
  962 continue
      write(6,991)jj,na
  991 format(' spectrum #',i3,'  calculated with # of betas=',i3)
      kreca=krec
  760 continue
      write(6,992)
  992 format(5x,'**********END OF SIMULATION**********')
      close(10)
      close(11)
      call exit
      end
```

REFERENCES

Abragam, A. (1961) *The Principles of Nuclear Magnetism*, Oxford Univ. Press, London.

Akutsu, H., & Seelig, J. (1981) *Biochemistry 20*, 7366-7373.

Arcava, Y., Ikeda, S.R., Daly, J.W., Brookes, N., & Albuquerque, E.T. (1984) *Mol. Pharmacol. 26*, 304-313.

Auger, M., & Jarrell, H.C. (1989) *Chem. Phys. Lett.*, in press.

Auger, M., Jarrell, H.C., Smith, I.C.P., Wong, P.T.T., Siminovitch, D. J., & Mantsch, H.H. (1987) *Biochemistry 26*, 8513-8516.

Auger, M., Jarrell, H.C., & Smith, I.C.P. (1988a) *Biochemistry 27*, 4660-4667.

Auger, M., Jarrell, H.C., Smith, I.C.P., Siminovitch, D.J., Mantsch, H.H., & Wong, P.T.T. (1988b) *Biochemistry 27*, 6086-6093.

Auger, M., Smith, I.C.P., & Jarrell, H.C. (1989a) *Biochim. Biophys. Acta 981*, 351-357.

Auger, M., Carrier, D., Smith, I.C.P., & Jarrell, H.C. (1989b) *J. Am. Chem. Soc.*, in press.

Auger, M., Smith, I.C.P., Mantsch, H.H., & Wong, P.T.T. (1989c) *Biochemistry*, in press.

Auger, M., Van Calsteren, M.-R., Smith, I.C.P., & Jarrell, H.C. (1989d) *Biochemistry*, submitted.

Auger, M., Smith, I.C.P., & Jarrell, H.C. (1989e) *Biochemistry*, submitted.

Barbara, T., & Dailey, B.P. (1982) *Mol. Crys. Liq. Crys. 87*, 239-250.

Barnes, R.G. (1974) *Adv. Quadrupole Res. 15*, 335-355.

Barnes, R.G., & Bloom, J.W. (1973) *Molec. Phys. 25*, 493-494.

Batchelder, L.S., Niu, C.H., & Torchia, D.A. (1983) *J. Am. Chem. Soc. 105*, 2228-2231.

Beshah, K., Olejniczak, E.T., & Griffin, R.G. (1987) *J. Chem. Phys. 86*, 4730-4736.

Bitman, J., & Wood, D.L. (1982) *J. Liq. Chrom. 5*, 1155-1162.

Bloom, M., & Smith, I.C.P. (1985) in *Progress in Protein-Lipid Interactions* (Watts, A., & De Pont, J.J.H.H.M., Eds.) pp 61-88, Elsevier, Amsterdam.

Bloom, M., & Sternin, E. (1987) *Biochemistry 26*, 2101-2105.

Bloom, M., Davis, J.H., & Valic, M.I. (1980) *Can. J. Phys. 58*, 1510-1517.

Bloom, M., Davis, J.H., & MacKay, A.L. (1981) *Chem. Phys. Lett. 80*, 198-202.

Blume, A., & Griffin, R.G. (1982) *Biochemistry 21*, 6230-6242.

Blume, A., Rice, D.M., Wittebort, R.J., & Griffin, R.G. (1982a) *Biochemistry 21*, 6220-6230.

Blume, A., Wittebort, R.J., Das Gupta, S.K., & Griffin, R.G. (1982b) *Biochemistry 21*, 6243-6253.

Bodenhausen, G., Wokaun, A., & Ernst, R.R. (1987) *Principles of NMR in one or two dimensions*, Oxford Univ. Press, Oxford.

Boerio, F.J., & Koenig, J.L. (1970) *J. Chem. Phys. 52*, 3425-33431.

Boggs, J.M., & Moscarello, M.A. (1982) *Biophys. J. 37*,57-59.

Boggs, J.M., Roth, S.M., Yoong, T., Wong, E., & Hsia, J.C. (1976) *Mol. Pharmacol. 12*,136-143.

Bonmatin, J.-M., Smith, I.C.P., Jarrell, H.C., & Siminovitch, D.J. (1988) *J. Am. Chem. Soc. 110*, 8693-8695.

Bonmatin, J.-M., Smith, I.C.P., Jarrell, H.C., & Siminovitch, D.J. (1989) *J. Am. Chem. Soc.*, in press.

Boulanger, Y., Schreier, S., Leitch, L.C., & Smith, I.C.P. (1980) *Can. J. Biochem. 58*, 986-995.

Boulanger, Y., Schreier, S., & Smith, I.C.P. (1981) *Biochemistry 20*, 6824-6830.

Braach-Maksvytis, V.L.B., & Cornell, B.A. (1988) *Biophys. J. 53*, 839-843.

Breckenridge, C., Combos, G., & Morgan, I.G. (1972) *Biochim. Biophys. Acta 266*, 695-707.

Bretscher, M.S. (1985) *Sci. Amer. 253*, 100-109.

Brown, M.F. (1982) *J. Chem. Phys. 77*, 1576-1599.

Brown, M.F., & Davis, J.H. (1981) *Chem. Phys. Lett. 79*, 431-435.

Brown, M.F., & Seelig, J. (1977) *Nature (London) 269*, 721-723.

Brown, M.F., Ribeiro, A.A., & Williams, G.D. (1983) *Proc. Natl. Acad. Sci. USA 80*, 4325-4329.

Brown, M.F., Seelig, J., & Haberlen, U. (1979) *J. Chem. Phys. 70*, 5045-5053.

Browning, J.L., & Akutsu, H. (1982) *Biochim. Biophys. Acta 684*, 172-178.

Burnett, L.J., & Muller, B.H. (1971) *J. Chem. Phys. 55*, 5829-5831.

Butler, K.W., Schneider, H., & Smith, I.C.P. (1973) *Arch. Biochem. Biophys. 154*, 548-555.

Camejo, G., Villegas, G.M., Barnola, F.V., & Villegas, R. (1969) *Biochim. Biophys. Acta 193*, 247-259.

Carrier, D., Giziewicz, J.B., Moir, D.M., Smith, I.C.P., & Jarrell, H.J. (1989) *Biochim. Biophys. Acta 983*, 100-108.

Casal, H.L., Mantsch, H.H., Paltauf, F., & Hauser, H. (1987a) *Biochim. Biophys. Acta 919*, 275-286.

Casal, H.L., Mantsch, H.H., & Hauser, H. (1987b) *Biochemistry 26*, 4408-4416.

Casal, H.L., Martin, A., Mantsch, H.H., Paltauf, F., & Hauser, H. (1987c) *Biochemistry 26*, 7395-7401.

Casal, H.L., & Mantsch, H.H. (1984) *Biochim. Biophys. Acta 779*, 381-401.

Cerbon, J. (1972) *Biochim. Biophys. Acta 290*, 51-57.

Cevc, G., & Marsh, D. (1987) *Phospholipid bilayers: Physical principles and models*, John & Wiley & Sons, New York.

Chacko, G.K., Villegas, G.M., Marnola, F.V., Villegas, R., & Goldman, D.E. (1976) *Biochim. Biophys. Acta 443*, 19-32.

Coster, H.G.L., James, V.J., Berthet, C., & Miller, A. (1981) *Biochim. Biophys. Acta 641*, 281-285.

Critchly, D.R., Ansell, S., & Dill, S. (1979) *Biochem. Soc. Trans. 7*, 314-319.

Cullis, P.R., Verkleij, A.J., & Ververgaert, P.H.J.T. (1978a) *Biochim. Biophys. Acta 513*, 11-20.

Cullis, P.R., van Dijck, P.W.T.M., de Kruijff, B., & de Gier, J. (1978b) *Biochim. Biophys. Acta 513*, 21-30.

Cunningham, B.A., & Lis, L.J. (1986) *Biochim. Biophys. Acta 861*, 237-242.

Dammers, A.J., Levine, Y.K., Balasubramanian, K., & Beth, A.H. (1988) *Chem. Phys. 127*, 149-160.

Danielli, J.F., & Davson, H. (1935) *J. Cell. Physiol. 5*, 495-508.

Davis, J.H. (1979) *Biophys. J. 27*, 339-358.

Davis, J.H. (1983) *Biochim. Biophys. Acta 737*, 117-171.

Davis, J.H. (1986) *Chem. Phys. Lipids 40*, 223-258.

Davis, J.H., Jeffrey, K.R., Bloom, M., Valic, M.I., & Higgs, T.P. (1976) *Chem. Phys. Lett. 42*, 390-394.

Derbyshire, W., Gorvin, T., & Warner, D. (1969) *Molec. Phys. 17*, 401-407.

Doane, J.W. (1985) in *NMR in Liquid Crystals* (J.W. Emsley, Ed.) pp 431-439, Reidel, Dordrecht.

Dufourc, E.J., Smith, I.C.P., & Jarrell, H.C. (1983) *Chem. Phys. Lipids 33*, 153-177.

Dufourc, E.J., Smith, I.C.P., & Jarrell, H.C. (1984a) *Biochemistry 23*, 2300-2309.

Dufourc, E.J., Parish, E.J., Chitrakorn, S., & Smith, I.C.P. (1984b) *Biochemistry 23*, 6062-6071.

Edzes, H.T., & Bernards, J.P.C. (1984) *J. Am. Chem. Soc. 196*, 1515-1517.

Fishman, P., & Brady, R.O. (1976) *Science 194*, 906-915.

Franks, N.O., & Lieb, W.R. (1982) *Nature (London) 300*, 487-493.

Frey, M.H., DiVerdi, J.A., & Opella, S.J. (1985) *J. Am. CHem. SOc. 107*, 7311-7315.

Gall, C.M., DiVerdi, J.A., & Opella, S.J. (1981) *J. Am. Chem. Soc. 103*, 5039-5043.

Giotta, G.I., Chan, D.S., & Wang, H.H. (1974) *Arch. Biochem. Biophys. 163*, 453-458.

Gorter, E., & Grendel, F. (1925) *J. Exp. Med. 41*, 439-443.

Griffin, R.G. (1981) *Methods Enzymol. 72*, 109-174.

Griffin, R.G., Beshab, K., Ebelhäuser, R., Huang, T.H., Olejniczak, E.T., Rice, D.M., Siminovitch, D.J., & Wittebort, R.J. (1988) in *The Time Domain in Surface and Structural Dynamics* (Long, G.J. & Grandjean, F., Eds) pp 81-105, Kluver Academic Publishers.

Gupta, C.M., Radhakishnan, R., & Khorana, H.G. (1977) *Biochemistry 74*, 4315-

Hahn, E.L. (1950) *Phys. Rev. 80*, 580-594.

Hakamori, S. (1984) in *The Cell Membrane* (Haber, E., Ed.) pp 181-201,Plenum Press.

Halsey, M.J., & Wardley-Smith, B. (1975) *Nature (London) 257*, 811-813.

Hannum, Y.A., & Bell, R.M. (1989) *Science 243*, 500-507.

Harbison, G.S., Raleigh, D.P., Herzfeld, J., & Griffin, R.G. (1985) *J. Mag. Reson. 64*, 284-295.

Hauser, H., Guyer, W., Pascher, I., Skrabal, P., & Sundell, S. (1980) *Biochemistry 19*, 366-373.

Hauser, H., Paltauf, F., & Shipley, G.G. (1982) *Biochemistry 21*, 1061-1067.

Hauser, H., Pasher, I., & Sundell, S. (1988) *Biochemistry 27*, 9166-9174.

Hille, B. (1970) *Prog. Biophys. Mol. Biol. 32*, 1-32.

Hille, B. (1980) *Prog. Anesthesiol. 2*, 1-6.

Hiyama, Y., Silverton, J.V., Torchia, D.A., Gerig, J.T., & Hammond, S.J. (1986) *J. Am. Chem. Soc. 108*, 2715-2723.

Hodgins, A.L., & Huxley, A.E. (1952) *J. Physiol. 117*, 500-544.

Hornby, A.P., & Cullis, P.R. (1981) *Biochim. Biophys. Acta 647*, 285-292.

Hoyland, J.R. (1968) *J. Am. Chem. Soc. 90*, 2227-2232.

Huang, T.H., Skarjune, R.P., Wittebort, R.J., Griffin, R.G., & Oldfield, E. (1980) *J. Am. Chem. Soc. 102*, 7377-7379.

Hubbell, W., & McConnell, H. (1969) *Proc. Natl. Acad. Sci. USA 64*, 2--27.

Israelachvili, J.N., Marcelja, S., & Horn, R.G. (1980) *Q. Rev. Biophys. 13*, 121-200.

Jaenicke, R. (1983) *Naturwissenschaften 70*, 332-341.

Janiak, M.J., Small, D.M., & Shipley, G.G. (1979) *J. Biol. Chem. 254*, 6068-6078.

Jarrell, H.C., Giziewicz, J.B., & Smith. I.C.P. (1986) *Biochemistry 25*, 3950-3957.

Jarrell, H.C., Jovall, P.Å., Giziewicz, J.B., Turner, L.A., & Smith, I.C.P. (1987a) *Biochemistry 26*, 1805-1811.

Jarrell, H.C., Wand, A.J., Giziewicz, J.R., & Smith, I.C.P. (1987b) *Biochim. Biophys. Acta 897*, 69-82.

Jarrell, H.C., Jovall, P.Å., Smith, I.C.P., Mantsch, H.H., & Siminovitch, D.J. (1988) *J. Chem. Phys. 88*, 1260-1263.

Jeffrey, K.R. (1981) *Bull. Magn. Reson. 3*, 69-82

Jeener, J. (1971) *Ampere International Summer School II*, Basko Polje, Yugoslavia.

Jeener, J., Meier, B.H., Bachmann, P., & Ernst, R.R. (1979) *J. Chem. Phys. 71*, 4546-4553.

Johansson, L.B.A., & Lindblom, G. (1981) *Biophys. J. 36*, 735-741.

Kelusky, E.C. (1983) *Ph.D. Thesis*, University of Ottawa, Ottawa, Ontario, Canada.

Kelusky, E.C., & Smith, I.C.P. (1983) *Biochemistry 22*, 6011-6017.

Kelusky, E.C., & Smith, I.C.P. (1984) *Can. J. Biochem. Cell Biol. 62*, 178-184.

Kelusky, E.C., & Smith, I.C.P. (1985) *Can. J. Biochem. Cell. Biol. 62*, 178-184.

Kelusky, E.C., Boulanger, Y., Schreier, S., & Smith, I.C.P. (1986) *Biochim. Biophys. Acta*

856, 85-90.

Kendig, J.J., & Cohen, E.N. (1977) *Anesthesiology 47*, 6-10.

Khintchine, A. (1934) *Math. Ann. 109*, 604-615.

Kim, J.T., Mattai, J., & Shipley, G.G. (1987) *Biochemistry 26*, 6599-6603.

Kimmich, R., Schnur, G., & Scheuermann, A. (1983) *Chem. Phys. Lipids 32*, 271-322.

Kirk, G.L., & Gruner, S.M. (1985) *J. Phys. 46*, 761-769.

Larsen, D.W., Boylan, J.G., & Cole, B.R. (1987) *J. Phys. Chem. 91*, 5631-5634.

Lazdunski, M., Balerna, M., Barhanin, J., Chicheportiche, R., Fossett, M., Frelin, C., Jacques, Y., Lombert, A., Pyssegur, J., Renaud, J.F., Romery, G., Schweitz, H., & Vincent, J.P. (1980) *Ann. N.Y. Acd. Sci. 358*, 169-182.

Lever, M.J., Miller, K.W., Paton, W.D., & Smith, E.B. (1971) *Nature (London) 231*, 368-371.

Lindblom, G., & Rilfors, L. (1989) *Biochim. Biophys. Acta 988*, 221-256.

Lindblom, G., Larsson, K., Johansson, L., Fontell, K., & Forsén, S. (1979) *J. Am. Chem. Soc. 101*, 5465-5470.

Linder, M., Höhener, A., & Ernst, R.R. (1980) *J. Chem. Phys. 73*, 4959-4970.

Lohner, K., Schuster, A., Degovics, G., Müller, K., & Laggner, P. (1987) *Chem. Phys. Lipids 44*, 61-70.

Mantsch, H.H., Moffatt, D.J., & Casal, H.L. (1988) *J. Mol. Struct. 173*, 285-298.

Marsh, D. (1981) in *Membrane Spectroscopy*, (Grell, E., Ed.) pp 51-142, Springer-Verlag, Berlin.

McAlister, J., Yathindra, N., & Sundaralingam, M. (1973) *Biochemistry 12*, 1189-1195.

McDaniel, R.V., McIntosh, T.J., & Simon, S.A. (1983) *Biochim. Biophys. Acta 731*, 97-108.

McIntosh, T.J., McDaniel, R.V., & Simon, S.A. (1983) *Biochim. Biophys. Acta 731*, 109-114.

McIntosh, T.J., Simon, S.A., & MacDonald, R.C. (1980) *Biochim. Biophys. Acta 597*, 445-

463.

Mehlorn, I.E., Barber, K.R., & Grant, C.W.M. (1988) *Biochim. Biophys. Acta 943*, 389-404.

Meier, P., Ohmes, E., & Kothe, G. (1986) *J. Chem. Phys. 85*, 3598-3614.

Meier, P., Sachse, J.H., Brophy, P.J., Marsh, P., & Kothe, G. (1987) *Proc. Nat. Acad. Sci. USA 84*, 3704-3708.

Mendelsohn, R., & Mantsch, H.H. (1986) in *Progress in Protein-Lipid Interactions* (Watts, A., & DePont, J.J.H.H.M., Eds.) Vol 2, Ch 4, Elsevier, Amsterdam.

Milburn, M.P., & Jeffrey, K.R. (1987) *Biophys. J. 52*, 791-799.

Milburn, M.P., & Jeffrey, K.R. (1989) *Biophys. J. 56*, 543-549.

Miller, K.W., & Yu, S.C.T. (1977) *Br. J. Pharmacol. 61*, 57-63.

Moffatt, D.J., Kauppinen, J.K., Cameron, D.G., Mantsch, H.H., & Jones, R.N. (1986) *National Research Council Bulletin No.18*, Ottawa, Canada.

Morell, P. (1984) *Myelin*, Plenum, New York.

Mushayakarara, E.C., Wong, P.T.T., & Mantsch, H.H. (1986) *Biochim. Biophys. Acta 857*, 259-264.

Neal, M.J., Butler, K.W., Polnaszek, C.F., & Smith, I.C.P. (1976) *Mol. Pharmacol. 12*, 144-155.

Norton, W.T. (1981) *Adv. Neurol. 31*, 93-121.

Norton, W.T. (1984) *Adv. Neurochem. 5*, 47-75.

Ogawa, I., & Beppu, K. (1982) *Agric. Biol. Chem. 46*, 255-262.

O'Leary, T.J., & Levin, I.W. (1984) *Biochim. Biophys. Acta 776*, 185-189.

Oldfield, E., Meadows, M., Rice, D., & Jacobs, R. (1978) *Biochemistry 17*, 2727-2740.

Papahadjopoulos, D. (1970) *Biochim. Biophys. Acta 211*, 467-477.

Papahadjopoulos, D., Vail, W.J., Newton, C., Nir, S., Jacobson, K., Poste, G., & Lazo, R. (1977) *Biochim. Biophys. Acta 465*, 579-598.

Pearson, R.H., & Pasher, I. (1979) *Nature (London) 281*, 499-501.

Perly, B., Dufourc, E.J., & Jarrell, H.C. (1983) *J. Labelled Compd. Radiopharm. 21*, 1-13.

Perly, B., Smith, I.C.P., & Jarrell, H.C. (1985) *Biochemistry 24*, 4659-4665.

Pethica, B.A. (1955) *Trans. Faraday Soc. 51*, 1402-1411.

Pézolet, M., & Georgescauld, D. (1985) *Biophys. J. 47*, 367-372.

Pope, J.M., Walker, L., Cornell, B.A., & Separovic, F. (1982) *Mol. Cryst. Liq. Cryst. 89*, 137-150.

Rance, M. (1981) *Ph.D. Thesis*, University of Guelph, Guelph, Ontario, Canada.

Rance, M., & Byrd, R.A. (1983) *J. Mag. Reson. 52*, 221-240.

Regnard, P. (1887) *C.R.Seances Soc. Biol.Ses Fil. 39*, 406-409.

Reisse, J. (1983) in *The Multinuclear Approach to NMR Spectroscopy* (Lambert, J.B., & Riddell, F.G., Eds.) pp 63-89, D. Reidel Publishing Company.

Renou, J.P., Giziewicz, J.B., Smith, I.C.P., & Jarrell, H.C. (1989) *Biochemistry 28*, 1804-1814.

Rice, D.M., Meinwald, Y.C., Scherega, H.A., & Griffin, R.G. (1987) *J. Am. Chem. Soc. 109*, 1636-1640.

Rilfors, L., Lindblom, G., Wieslander, Å., & Christiansson, A. (1984) *Biomembranes 12*, 205-245.

Rilfors, L., Eriksson, P.O., Arvidson, G., & Lindbloom, G. (1986) *Biochemistry 25*, 7702-7711.

Ritchie, J.M., & Rogart, R.B. (1977) *Rev. Physiol. Biochem. Pharmacol. 79*, 1-50.

Rose, M.E. (1957) *Elementary Theory of Angular Momentum*, Wiley, New York.

Roth, S.H. (1979) *Adv. Rev. Pharmacol. Toxicol. 19*, 159-178.

Roth, S., & Seeman, P. (1972) *Biochim. Biophys. Acta 255*, 207-219.

Roux, M., Neumann, J.-M., Hodges, R.S., Devaux, P.F., & Bloom, M. (1989) *Biochemistry*

28, 2313-2321.

Rubenstein, J.L.R., Smith, B.A., & McConnell, H.M. (1979) *Proc. Natl. Acad. Sci. USA 76*, 15-18.

Ruocco, M.J., Siminovitch, D.J., & Griffin, R.G. (1985a) *Biochemistry 24*, 2406-2411.

Ruocco, M.J., Makriyannis, A., Siminovitch, D.J., & Griffin, R.G. (1985b) *Biochemistry 24*, 4844-4851.

Saupe, A. (1964) *Z. Naturf. 19a*, 161-171.

Schichijo, S., & Alving, C.R. (1985) *Biochim. Biophys. Acta 820*, 289-294.

Schmidt, C., Wefing, S., Blümich, B., & Spiess, H.W. (1986) *Chem. Phys. Lett. 130*, 84-90.

Schmidt, C., Blümich, B., Wefing, S., Kaufmann, S., & Spiess, H.W. (1987) *Ber. Bunsenges. Phys. Chem. 91*, 1141-1145.

Schmidt, C., Blümich, B., & Spiess, H.W. (1988) *J. Mag. Reson. 79*, 269-290.

Schreier-Muccillo, S., Marsh, D., Dugas, H., Schneider, H., & Smith, I.C.P. (1973) *Chem. Phys. Lipids 10*, 11-27.

Seelig, A. (1987) *Biochim. Biophys. Acta 899*, 196-204.

Seelig, J. (1977) *Q. Rev. Biophys. 10*, 353-418.

Seelig, J., & Neiderberger, W. (1974) *J. Am. Chem. Soc. 96*, 2069-2072.

Seelig, J., Macdonald, P.M., & Scherer, P.G. (1987) *Biochemistry 26*, 7535-7541.

Seeman, P. (1972) *Pharmocol. Rev. 24*, 583-655.

Seeman, P. (1975) in *Molecular Mechanism of Anesthesia, Progress in Anesthesiology* (Fink, B.R., Ed.) 1, pp 243-251, Raven Press, New York.

Selinger, Z., & Lapidot, Y. (1966) *J. Lip. Res. 7*, 174-175.

Shaka, A.J., Keeler, J., & Freeman, R.J. (1983) *J. Mag. Reson. 52*, 335-351.

Sharom, F., & Grant, C.W.M. (1977) *J. Supramol. Struc. 6*, 249-258.

Shichijo, S., & Alving, C.R. (1985) *Biochim. Biophys. Acta 820*, 289-294.

Siegel, D.P. (1986) *Chem. Phys. Lipids 42*, 279-301.

Silvius, J.R. (1982) in *Lipid-Protein Interactions* (Jost, P.C., & Griffiths, O.H., Eds.) 2, pp 239-281, Wiley, New York.

Siminovitch, D.J., Jeffrey, K.R., & Eibl, H. (1983) *Biochim. Biophys. Acta 727*, 122-134.

Siminovitch, D.J., Brown, M.F., & Jeffrey, K.R. (1984) *Biochemistry 23*, 2412-2420.

Siminovitch, D.J., Olejniczak, E.T., Ruoccc, M.J., Das Gupta, S.K., & Griffin, R.G. (1985) *Chem. Phys. Lett. 119*, 251-255.

Siminovitch, D.J., Wong, P.T.T., & Mantsch, H.H. (1987a) *Biophys. J. 51*, 465-473.

Siminovitch, D.J., Wong, P.T.T., & Mantsch, H.H. (1987b) *Biochim. Biophys. Acta 900*, 163-167.

Siminovitch, D.J., Ruocco, M.J., Makriyannis, A., & Griffin, R.G. (1987c) *Biochim. Biophys. Acta 901*, 191-200.

Siminovitch, D.J., Ruocco, M.J., Olejniczak, E.T., Das Gupta, S.K., & Griffin, R.G. (1988) *Biophys. J. 54*, 373-381.

Simon, S.A., McIntosh, T.J., & Hines, M.L. (1986) in *Molecular and Cellular Mechanisms of Anesthetics* (Roth, S.H., & Miller, K.W., Eds.) pp 297-308, Plenum Publishing Corporation, New York.

Singer, S.J., & Nicolson, G.L. (1972) *Science 173*, 720-731.

Skarjune, R., & Oldfield, E. (1979) *Biochim. Biophys. Acta 556*, 208-218.

Skarjune, R., & Oldfield, E. (1982) *Biochemistry 21*, 3154-3160.

Small, D.M. (1977) *J. Colloid Interface Sci. 58*, 581-602.

Smith, I.C.P. (1983) in *NMR of Newly Accessible Nuclei*, pp 1-26, Academic Press Inc.

Smith, I.C.P. (1984) *Biomembranes 12*, 133-163.

Smith, I.C.P., & Butler, K.W. (1985) in *Effects of Anesthesia* (Covino, B.G. et al., eds.), pp. 1-11, Waverly, Baltimore.

Smith, I.C.P., & Mantsch, H.H. (1982) *ACS Symp. Ser. 191*, 97-117.

Snyder, R.G. (1961) *J. Mol. Spectrosc. 7*, 116-141.

Speyer, J.B., Weber, R.T., Das Gupta, S.K., & Griffin, R.G. (1989) *Biochemistry*, in press.

Spiess, H.W. (1980) *J. Chem. Phys. 72*, 6755-6762.

Spiess, H.W., & Sillescu, H. (1981) *J. Mag. Reson. 42*, 381-389.

Stejskal, E.O., & Tanner, J.E. (1965) *J. Chem. Phys. 42*, 288-292.

Stockton, G.W., Polnaszek, C.F., Tulloch, A.P., Hasan, F., & Smith, I.C.P. (1976) *Biochemistry 15*, 954-966.

Strenk, L.M., Westerman, P.W., & Doane, J.W. (1985) *Biophys. J. 48*, 765-773.

Strichartz, G.R. (1973) *J. Gen. Physiol. 62*, 37-57.

Taylor, M.G., Akiyama, T., & Smith, I.C.P. (1981) *Chem. Phys. Lipids 29*, 327-339.

Taylor, M.G., Akiyama, T., Saito, H., & Smith, I.C.P. (1982) *Chem. Phys. Lipids 31*, 359-379.

Torchia, D.A. (1984) *Ann. Rev. Biophys. Bioeng. 13*, 125-144.

Torchia, D.A., & Szabo, A. (1982) *J. Mag. Reson. 49*, 107-121.

Trudell, J.R., Hubbell, W.L., Cohen, E.N., & Kendig, J.J. (1973) *Anesthesiology 38*, 207-211.

Van Calsteren, M.-R. (1989) *Ph.D. Thesis*, University of Ottawa, Ottawa, Ontario, Canada.

Vold, R.R., & Vold, R.L. (1988) *J. Chem. Phys. 88*, 1443-1457.

Vold, R.R., Brandes, R., Tsang, P., Kearns, D.R., & Vold, R.L. (1986) *J. Am. Chem. Soc. 108*, 302-303.

Wann, K.T., & MacDonald, A.G. (1980) *Comp. Biochem. PhysiolA 66A*, 1-12

Wefing, S., & Spiess, H.W. (1988) *J. Chem. Phys. 89*, 1219-1233.

Wefing, S., Kaufmann, S., & Spiess, H.W. (1988) *J. Chem. Phys. 89*, 1234-1244.

Westman, J., Boulanger, Y., Ehrenberg, A., & Smith, I.C.P. (1982) *Biochim. Biophys. Acta 685*, 315-328.

White, S.H., King, G.I., & Cain, J.E. (1981) *Nature (London) 290*, 161-163.

Wiener, N. (1930) *Acta Math. 55*, 117-258.

Wieslander, Å., Rilfors, L., & Lindblom, G. (1986) *Biochemistry 25*, 7511-7517.

Williams, G.D., Beach, J.M., Dodd, S.W., & Brown, M.F. (1985) *J. Am. Chem. Soc. 107*, 6868-6873.

Wittebort, R.J., Schmidt,, C.F., & Griffin, R.G. (1981) *Biochemistry 20*, 4223-4228.

Wittebort, R.J., Olejniczak, E.T., & Griffin, R.G. (1987) J. *Chem. Phys. 36*, 5411-5420.

Woessner, D.E., Snowden, B.S.Jr., & Meyer, G.H. (1969) *J. Chem. Phys. 51*, 2968-2976.

Wong, P.T.T. (1981) *Chem. Phys. Lett. 77*, 291-293.

Wong, P.T.T (1984) *Annu. Rev. Biophys. Bioeng. 13*, 1-24.

Wong, P.T.T. (1985) *Rev. Sci. Instrum 56*, 1417-1419.

Wong, P.T.T. (1986) *Physica B & C 139 & 140*, 847-852.

Wong, P.T.T. (1987a) in *High Pressure Chemistry and Biochemistry* (van Eldick, R., & Jonas, J., Eds.) pp 381-400, D. Reidel, Dordrecht,The Netherlands.

Wong, P.T.T (1987b) in *Vibrational Spectra and Structure* (Durig, G.R., Ed.) pp 357-445, Elsevier, Amsterdam.

Wong, P.T.T. (1987c) in *Current Perspectives of Barobiology* (Jennasch, H.W., Marquis, R.E., & Zimmerman, A.M., Eds.) pp 288-314, Academic Press, New York.

Wong, P.T.T., & Mantsch, H.H. (1985a) *J. Chem. Phys. 83*, 3268-3274.

Wong, P.T.T., & Mantsch, H.H. (1985b) *Biochemistry 24*, 4091-4096.

Wong, P.T.T., Murphy, W.F., & Mantsch, H.H. (1982) *J. Chem. Phys. 76*, 5230-5237

Wong, P.T.T., Moffatt, D.J., & Baudais, F.L. (1985) *Appl. Spectros. 39*, 733-735.

Wong, P.T.T., Weng, S.F., & Mantsch, H.H. (1986) *J. Chem. Phys. 85*, 2315-2319.

Wong, P.T.T., Siminovitch, D.J., & Mantsch, H.H. (1988) *Biochim. Biophys. Acta 947*, 139-171.